

**FATIGUE ESTIMATION OF STAY CABLES  
UNDER THE ACTION OF WIND AND  
RAIN**

Ganesan Vinayaga Murthy  
Tokyo Polytechnic University  
March 2014

# **FATIGUE ESTIMATION OF STAY CABLES UNDER THE ACTION OF WIND AND RAIN**

A dissertation by  
Ganesan Vinayaga Murthy

Submitted to the Graduate School of Engineering  
Tokyo Polytechnic University

In partial fulfillment of the requirements  
for the degree of Doctor of Philosophy

Under the supervision of  
Professor Yukio Tamura  
Professor Masahiro Matsui

Graduate School of Engineering  
Tokyo Polytechnic University  
Atsugi, Kanagawa, Japan

March 2014

## ABSTRACT

The stay cables of the cable stayed bridge were found to exhibit large amplitude vibrations during certain conditions of wind and rain. And since the cable transfers a large amount of forces to the pylon and thus the fatigue life of the cable under such vibration is of concern. Available standards for the fatigue life of the cable didn't consider such vibrations in to account. And also the phenomenon of rain-wind induced vibrations explained in the past was limited to certain conditions. Thus this study focuses on the dynamic characteristics of rain-wind induced vibration as well as the effects of cable inclination angle, wind yaw angle, rainfall intensity and wind speed on the vibration amplitude on the stay cables. A SDOF analytical model was carried to estimate the stay cable vibration. The results of the experiments were used to validate the analytical model. The Joint probability model of wind speed, wind direction and rainfall was found and using the data of the meteorological stations. Stay cables acts as a string due to the large axial force, but because of the sag the cable consists of certain amount of bending stiffness and thus effects of sag and bending stiffness was also studied. Using the experimental results and the Joint probability model, a framework was made to estimate the fatigue damage of the stay cables. A GUI framework was also made to find the fatigue damage of the cable. This work will guide the designers to estimate the fatigue damage of the cable under rain-wind induced vibrations

Chapter I of this dissertation explains the research objective, importance of rain-wind induced vibrations on fatigue life of the stay cables along with a literature review. This chapter also discusses the key points of the oncoming chapters II-V.

Chapter II explains the statistical analysis of the meteorological parameters with a

case study. Three probability models were proposed for the joint action of wind speed, wind direction and rainfall intensity on to the cable, using the data recorded near the bridge site. The first probability model considers the wind speed and direction as dependent event, whereas the rainfall intensity as a independent event and in second model all the three events are considered as dependent event, whereas in the third model the probability of all wind is assumed to blown from the most unfavorable direction. The main theme of the first two models is to study the importance of rainfall intensity or the dependency of rainfall and wind data collected at the megami bridge site. The third model can be used to evaluate a critical condition for fatigue, since the model assumes that all the windblown from the most unfavorable direction. The effects on the modal parameters of the observed meteorological were also studied.

Chapter III deals with an extensive experimental study on the rain-wind induced vibration of stay cable model. In this chapter the experimental setup, procedure and the results of the experiment were discussed. The vibration amplitude of the cable was obtained.

There were two models used in this experiment. The first model with a large diameter explains the effect of wind speed, rainfall intensity, cable inclination angle and wind yaw angle on the vibration amplitude of the stay cable. The phenomenon of rain-wind induced vibration was also explained based on the pictorial observations made during the experiment.

The cross-section of the second cable model is smaller in diameter than the first model. The experiment was carried out for critical conditions of the first model. In addition, this model also explains the effect of Scruton number, diameter ration on the vibration amplitude of the stay cable model. In order to mitigate these vibrations a study was carried out by winding a thin wire around the cable model. The efficiency of the mitigation technique was also tested by varying the spacing between the two successive nodes of the wire.

In Chapter IV a vibration analysis was carried out by following an existing mathematical model. The experiment results were compared and validated with the analytical

results. Some modifications in the mathematical model were achieved, so that the mathematical model can identify the response of the cable for a large number of conditions.

Chapter V explains the importance of bending stiffness and sag in stay cable. A free vibration model was proposed to identify the natural frequency and mode shapes of the stay cable. The relation between displacement and bending stresses were obtained in ANSYS for first 3 symmetric and anti-symmetric modes. This chapter also compares the results obtained in String theory, Analytical and ANSYS solution.

Chapter VI introduces the methodology used to estimate the fatigue damage. Three probability models developed in the chapter II was used for calculating the fatigue. A comparison study was also made between the three probability models. The vibration response obtained using Chapter III and IV was used to estimate the response of the stay cable. Using the results of the Chapter V, the relation between the vibration amplitude and bending moment were derived for every cable and Consequently the Bending and axial stresses. The obtained stresses were then used to estimate the fatigue life of the cables. Six cables in the Megami bridge was considered for the analysis and the methodology for fatigue is explained along with application problem.

Chapter VII discusses the recommendations for the fatigue life design of the stay cables for rain-wind induced cable vibrations. The summary and conclusion of the dissertation is also presented in this chapter.

Ganesan Vinayaga Murthy

Tokyo Polytechnic University, 2014



## ACKNOWLEDGMENTS

First and foremost I offer my sincerest gratitude to my supervisor, Professor Yukio Tamura, who has supported me throughout my thesis with his patience, motivation, enthusiasm, and immense knowledge whilst allowing me the room to work in my own way. His guidance helped me in all the time of research and writing of this thesis. I could not have imagined having a better advisor and mentor for my Ph.D study. His attitude to research inspired me a lot during meetings and discussions. I would like to express my deep gratitude and respect to Professor Masahiro Matsui whose advices and insight was invaluable to me. I have been extremely lucky to have him as my supervisor who cared so much about my work, and responded to my questions and queries so promptly. His help during my study was immense. I would like to thank Prof. Takeshi Ohkuma and Prof. Ryuichiro Yoshie for their suggestions, comments during my presentations.

I would like to offer my thanks to Professor Liu Qingkuan who helped me to carry out the experiments in Shijiazhuang Tiedao University (STDU). I am thankful to Dr. Ma wenyong and Dr. Liu Xiaobing who helped me during my stay in china.

I would like to acknowledge and thank Ministry of Education, Culture, Sports, Science and Technology, Japan, for providing financial support through the Global Center of Excellence Program, 20011-2013. I am happy to acknowledge Shijiazhuang Tiedao University, Shijiazhuang, China for providing the experiment facility to carry out the experiments.

I am happy to be a part of Wind Engineering Research Center, Tokyo Polytechnic University and I also special my thanks to my friends and researchers at Wind Engineering

Research Center, Tokyo Polytechnic University. I would like to offer many thanks to Ms. Shoko Hayama, Ms. Aya Saito, and Ms. Kazuko Ando, and most especially to Prof. Rei Okada for his help during my study. I am really thankful to their own inputs into my work, and for help in my day-to-day needs in Japan.

I would like to offer my thanks to my parents and brothers for their support during my study. Last but not least, I would like to thank god for making the things possible.

Vinayagamurthy Ganesan, Atsugi, Kanagawa, Japan, March 2014

## DEDICATION

To my Professors, family and friends



## TABLE OF CONTENTS

ABSTRACT .....	i
ACKNOWLEDGMENTS .....	v
DEDICATION .....	vii
LIST OF TABLES .....	xv
LIST OF FIGURES .....	xix

### Chapter I

#### INTRODUCTION

1.1	Cable and Cable stayed bridges	1
1.2	Stay cable vibration	3
1.3	Rain-wind induced stay cable vibration	3
1.4	Axial and Bending fatigue of stay cables	4
1.5	Background and Motivation	7
1.6	Details of the present study	9
	1.6.1 Objective	9
	1.6.2 Overview of methodology, and structure of dissertation	10
1.7	References	13

### Chapter II

#### STATISTICAL ANALYSIS OF METEOROLOGICAL PARAMETERS

2.1	Introduction	16
2.2	Selection of the Bridge and the meteorological station	17
	2.2.1 Megami Bridge and Nagasaki Marine Observatory	19
	2.2.2 Statistical analysis of wind data	20
	2.2.3 Turbulent intensity and wind profile at the bridge site	22
	2.2.4 Statistical analysis of rainfall data	23
2.3	Joint probability of wind speed, direction and rainfall	25
	2.3.1 Joint probability model for wind data considering rainfall as a independent event	25
	2.3.1.1 Joint probability model for wind data	25

2.3.1.2	Probability density function for rainfall	27
2.3.1.3	Probability of wind speed, direction and rainfall intensity	29
2.3.1.4.	Application of the Joint probability model for wind speed and direction (rainfall is assumed to be a independent event)	29
2.3.2	Joint probability model for wind data considering rainfall as a dependent event	34
2.3.3	Probability of wind speed in the most unfavorable direction	36
2.4	References	40

## Chapter III

### EXPERIMENT ON RAIN-WIND INDUCED VIBRATION ON THE STAY CABLES

3.1	Introduction	43
3.2	Literature review	43
3.3	Objective of the Experiment	46
3.4	Bridges undergone rain-wind induced vibration on cables	47
3.5	Description about the wind tunnel	48
3.6	Description about the setup for rain-wind induced cable vibrations	49
3.6.1	Cobra 225 probe	51
3.6.2	Rainfall controller	52
3.6.3	Rain gauge	52
3.6.4	S-Type Load cells	53
3.6.5	Vibration recording devices (video)	54
3.7	Wind speed measurement and flow stability	54
3.8	Cable model and testing conditions	55
3.9	Data analysis: Filtering out the noisy signals	58
3.10	Damping in the Cable models	58
3.11	Dynamic characteristics of rain-wind induced vibration	60
3.11.1	General characteristics of rain-wind induced cable vibration of model-I	60
3.11.2	Effect of wind speed and Rainfall Intensity on cable vibration	61
3.11.3	Phenomenon behind rain-wind induced cable vibration	64
3.11.4	Effect of wind yaw angle	66
3.11.4.1	Case $\alpha=25^\circ$ , $\beta=30^\circ, 35^\circ, 40^\circ, 50^\circ$	66
3.11.4.2	Case $\alpha=30^\circ$ , $\beta=30^\circ, 35^\circ, 40^\circ, 50^\circ$	68
3.11.4.3	Case $\alpha=35^\circ$ , $\beta=25^\circ, 30^\circ, 35^\circ, 40^\circ, 50^\circ$	69
3.11.4.4	Case $\alpha=40^\circ$ , $\beta=45^\circ$	71

3.11.5	Effect of wind yaw angles on maximum amplitude	71
3.11.6	Effect of inclination angle	73
3.11.6.1	Case $\beta=30^\circ$ , $\alpha=25^\circ$ , $30^\circ$ , $35^\circ$	73
3.11.6.2	Case $\beta=35^\circ$ , $\alpha=25^\circ$ , $30^\circ$ , $35^\circ$	74
3.11.6.3	Case $\beta=40^\circ$ , $\alpha=25^\circ$ , $30^\circ$ , $35^\circ$	75
3.11.6.4	Case $\beta=45^\circ$ , $\alpha=35^\circ$ , $40^\circ$	76
3.11.6.5	Case $\beta=50^\circ$ , $\alpha=25^\circ$ , $30^\circ$ , $35^\circ$	77
3.11.7	Combined effects of cable inclination ( $\alpha$ ) and wind yaw angles ( $\beta$ )	78
3.11.8	Comparison with past researches	78
3.12	General characteristics of rain-wind induced vibration of the cable model II	79
3.12.1	Effect of wind speed and Rainfall on cable vibration of cable model II	79
3.12.2	Effect of damping ratio on rain-wind induced vibration on cable model II	80
3.12.3	Effect of cable diameter on rain-wind induced cable vibration	82
3.13	Mitigation of rain-wind induced cable vibrations	85
3.14	Evaluation of rivulet position from the experiment	86
3.15	Concluding remarks	89
3.16	References	91

## CHAPTER IV

### SDOF: ANALYTICAL MODEL ON RAIN-WIND INDUCED STAY CABLE VIBRATIONS

4.1	Introduction	95
4.2	Modeling of rain-wind induced stay cable vibration	96
4.3	Horizontal cylinder with fixed rivulet	100
4.4	Application of the model	101
4.5	Inclined cylinder with moving rivulet	102
4.6	Application of the model	105
4.7	Scruton number of the stay cable	107
4.8	Response estimation for the stay cables C12 and D12	108
4.9	GUI for Experimental and Analytical results	111
4.10	Conclusion	112
4.11	References	112

---

## CHAPTER V

### DYNAMIC CHARACTERIZATION AND STRESS EVALUATION ON STAY CABLES

5.1	Introduction	115
5.2	Free-vibration of a taut string	115
	5.2.1 Application of string theory	117
5.3	Free vibration analysis of a stiffened string or stay cable- continuous system	119
	5.3.1. Cable-beam behavior	126
	5.3.2. Importance of sag and Bending in stay cables	127
5.4	Evaluation of Bending stresses	129
	5.4.1 Finite Element modeling of the cable	130
	5.4.2 Free vibration analysis of a stay cable (FEM)	131
	5.4.3 Evaluation of Bending Moment and Bending stresses in the stay cable	134
	5.4.4 Deflected mode shapes, bending moments and stresses	135
5.5	Stresses in symmetric modes	135
5.6	Stresses in Asymmetric modes	140
5.7	Stresses in stay cable C12 and D12 in Megami bridge	144
5.8	Conclusions	150
5.9	References	151

## CHAPTER VI

### FATIGUE ESTIMATION OF STAY CABLES UNDER THE ACTION OF WIND AND RAIN

6.1.	Introduction	154
6.2.	Methodology followed for Fatigue estimation for the probability model I	155
6.3.	Application of the Fatigue methodology for the probability model I	158
	6.3.1. Step 1 Joint occurrence probability of wind speed, direction and rainfall-W matrix	158
	6.3.2. Evaluation of n-matrix	160
	6.3.3. Dimensional Amplitude matrix or (Y-matrix)	163
	6.3.4. Evaluation of Stress matrixes (S-matrix)	167
	6.3.5. Evaluation of N-matrix	171
	6.3.6. Miner's Rule	174
	6.3.7. Fatigue Damage estimation of stay cables using Probability model- I	175
	6.3.7.1. Bending fatigue of stays (C04, Model I)	175
	6.3.7.2. Axial fatigue of stays (C04, Model I)	178

---

6.4.	Fatigue Damage estimation of stay cables using Probability model- II	179
6.4.1.	Bending fatigue of stays (C04, Model II)	181
6.4.2.	Axial fatigue of stays (C04, Model II)	183
6.5.	Fatigue Damage estimation of stay cables using Probability model- III	184
6.5.1.	Bending fatigue of stays (C04, Model III)	186
6.5.2.	Axial fatigue of stays (C04, Model III)	188
6.6.	Fatigue damage comparison between the three probability models (Cables C04, D04)	189
6.7.	Fatigue estimation of stay cable C23, D23	194
6.8.	Fatigue estimation of stay cable using analytical model	196
6.8.1.	Fatigue evaluation of stay cable using the probability model I (Cables -C12, D12, C15 and D15, JPD Model-I)	196
6.8.2.	Fatigue evaluation of stay cable using the probability model II (Cables -C12, D12, C15 and D15, JPD Model-II)	209
6.8.3.	Fatigue evaluation of stay cable using the probability model III (Cables -C12, D12, C15 and D15, JPD Model-III)	210
6.9.	Recommendations and Conclusions	218
6.10.	References	220

## CHAPTER VII

### DISCUSSION, CONCLUSION AND RECOMMENDATIONS

7.1.	Discussion and Conclusions	224
7.2.	Recommendation to the designers	229
Appendix I		231
Appendix II		233
Appendix III		234
Appendix IV		236
Appendix V		241
Appendix VI		247
Appendix VII		248





## LIST OF TABLES

Table 1.1	Bridges subjected Rain-wind induced cable vibrations	9
Table 2.1	Distance between the bridge and the meteorological stations	18
Table 2.2	Relative frequency of wind data (W-matrix) for probability model I	30
Table 2.3	Modal parameters in different wind directions	31
Table 2.4	Distribution of rain events only	33
Table 2.5	Probability density of wind speed in the most unfavorable direction (rainfall is assumed to be independent)	35
Table 2.6	Relative frequency of wind data under R10 rainfall condition	36
Table 2.7	Relative frequency of wind data under R40 rainfall condition	37
Table 2.8	Relative frequency of wind data under R70 rainfall condition	38
Table 3.1	Discharge rate and outlet pressure	53
Table 3.2	Properties of the Cable model I	56
Table 3.3	Non dimensional parameters of the Cable model I	56
Table 3.4	Details of the tests for the cable Model I	57
Table 3.5	Details of the tests for the cable Model II	57
Table 3.6	shows the comparison of Scruton numbers with the other researchers	60
Table 3.7	Comparison of maximum amplitudes (Literature & current study)	72
Table 3.8	Parametric studies on rain-wind induced stay cable vibration– A comparison with the current study (Field measurement)	84
Table 4.1	Aerodynamic co-efficients of a horizontal cylinder with fixed rivulet	101
Table 4.2	Aerodynamic coefficients of an inclined cylinder	105
Table 4.3	Comparison of Scruton number for different bridge cables	107
Table 4.4	Properties of stay cable C12 and D12	108
Table 4.5	Structural properties of stay cable C12 and D12	109
Table 5.1	Properties of stay cable (Aaron, 2005)	117
Table 5.2	Free vibration analysis of the cable #C03–string theory	118
Table 5.3	Axial stress in the stay cable #C03–string theory	118
Table 5.4	Frequency of the stay cable #C03– String theory and Euler Bernoulli (Analytical and ANSYS solution)	125
Table 5.5	Evaluation of stresses in 1 <sup>st</sup> symmetric mode	136
Table 5.6	Evaluation of stresses in 2 <sup>nd</sup> symmetric mode	138
Table 5.7	Evaluation of stresses in 3 <sup>rd</sup> symmetric mode	139
Table 5.8	Evaluation of stresses in 1 <sup>st</sup> Anti-symmetric mode	141
Table 5.9	Evaluation of stresses in 2 <sup>nd</sup> Anti-symmetric mode	142
Table 5.10	Evaluation of stresses in 3 <sup>rd</sup> Anti-symmetric mode	143

Table 5.11	Relationship between vibration amplitude of the cable and Bending moments at the ends (Cable C12 and D12)	144
Table 5.12	Free vibration analysis of the cable (C12 and D12) – string theory	145
Table 5.13	Tension force and axial stresses in stay cable C12 and D12	146
Table 5.14	Evaluation of stresses in 1st symmetric mode (Cable: C12 and D12)	146
Table 5.15	Evaluation of stresses in 1st anti-symmetric mode (Cable: C12 and D12)	147
Table 5.16	Evaluation of stresses in 2nd symmetric mode (Cable: C12 and D12)	147
Table 5.17	Evaluation of stresses in 2nd anti-symmetric mode (Cable: C12 and D12)	148
Table 5.18	Evaluation of stresses in 3rd symmetric mode (Cable: C12 and D12)	149
Table 5.19	Evaluation of stresses in 3rd anti-symmetric mode (Cable: C12 and D12)	149
Table 5.20	Relationship between Peak vibration amplitude and Bending moment (Cable: C12 and D12)	150
Table 6.1	Distribution of rain events	159
Table 6.2	$W_{10}$ -matrix for 0-30 mm/hr rainfall condition	161
Table 6.3	n-matrix for the first symmetric mode under 10 mm/hr rainfall	162
Table 6.4	Y-matrix before transformation	164
Table 6.5	Displacement matrix for the 1 <sup>st</sup> symmetric mode	166
Table 6.6	Relationship between vibration amplitude of the cable and Bending moments at the ends	167
Table 6.7	Bending stresses (in Mpa) at the Pylon end in 1st symmetric mode	168
Table 6.8	Bending stresses (in Mpa) at the Deck end in 1st symmetric mode	169
Table 6.9	Axial stresses (in Mpa) at the Pylon and Deck end in 1st symmetric mode	170
Table 6.10	N-matrix at the Pylon end in 1st symmetric mode	173
Table 6.11	N-matrix at the Deck end in 1st symmetric mode	173
Table 6.12	N-matrix for axial stresses	174
Table 6.13	n-matrix for 1st symmetric mode at Deck end under 10 mm/hr rainfall conditions for 100 years (C04, Model I)	176
Table 6.14	Estimated Fatigue Damage for 1st symmetric mode at Deck end under 10 mm/hr rainfall conditions for 100 years (C04, Model I)	176
Table 6.15	Estimated Bending Fatigue Damage for 1st Symmetric mode at Deck end under three rainfall conditions for 100 years (C04, Model I)	177
Table 6.16	Estimated Cumulative Bending Fatigue Damage at deck end for symmetric and anti-symmetric modes for 100 years(C04, Model I)	177
Table 6.17	Estimated Bending Fatigue life of stay cable (C04, Model I)	178
Table 6.18	Estimated Cumulative Axial Fatigue Damage at deck end for symmetric and anti-symmetric modes for 100 years (C04, Model I)	178
Table 6.19	Estimated Axial Fatigue life of stay cable (C04, Model I)	179
Table 6.20	n-matrix for 1st Symmetric mode under 10 mm/hr rainfall conditions	180

	for 100 year (C04, Model II)	
Table 6.21	Estimated Fatigue Damage for 1st Symmetric mode at Deck end under 10 mm/hr rainfall conditions for 100 years (C04, Model II)	182
Table 6.22	Estimated Bending Fatigue Damage for 1st Symmetric mode at Deck end under three rainfall conditions for 100 years (C04, Model II)	182
Table 6.23	Estimated Cumulative Bending Fatigue Damage at deck end for symmetric and anti-symmetric modes for 100 years (C04, Model II)	183
Table 6.24	Estimated Bending Fatigue life of stay cable (C04, Model II)	183
Table 6.25	Estimated Cumulative Axial Fatigue Damage at deck end for symmetric and anti-symmetric modes for 100 years (C04, Model II)	184
Table 6.26	Estimated Axial Fatigue life of stay cable (C04, Model II)	184
Table 6.27	n-matrix for 1st Symmetric mode under 10 mm/hr rainfall conditions for 100 year (C04, Model III)	185
Table 6.28	Estimated Fatigue Damage for 1st Symmetric mode at Deck end under 10 mm/hr rainfall conditions for 100 years (C04, Model III)	186
Table 6.29	Estimated Bending Fatigue Damage for 1st Symmetric mode at Deck end under three rainfall conditions for 100 years (C04, Model III)	187
Table 6.30	Estimated Cumulative Bending Fatigue Damage at deck end for symmetric and anti-symmetric modes for 100 years (C04, Model III)	187
Table 6.31	Estimated Bending Fatigue life of stay cable (C04, Model III)	188
Table 6.32	Estimated Cumulative Axial Fatigue Damage at deck end for symmetric and anti-symmetric modes for 100 years (C04, Model III)	188
Table 6.33	Estimated Axial Fatigue life of stay cable (C04, Model III)	189
Table 6.34	Accumulated bending fatigue damage in symmetric obtained for 100 years using different probability models (Cables: C04, D04)	191
Table 6.35	Accumulated bending fatigue damage in anti-symmetric obtained for 100 years using different probability models (Cables: C04, D04)	191
Table 6.36	Accumulated axial fatigue damage in symmetric modes for 100 years using different probability models (Cables: C04, D04)	192
Table 6.37	Accumulated axial fatigue damage in anti-symmetric modes for 100 years using different probability models (Cables: C04, D04)	192
Table 6.38	Estimated bending fatigue life (in years) of stay cable using different probability models (Cables: C04, D04)	193
Table 6.39	Estimated axial fatigue life (in years) of stay cable using different probability models (Cables: C04, D04)	193
Table 6.40	Estimated bending fatigue life (in years) of stay cable using different probability models-Symmetric modes (C23, D23)	195
Table 6.41	Estimated bending fatigue life (in years) of stay cable using different probability models-Antisymmetric modes (C23, D23)	195
Table 6.42	Estimated axial fatigue life (in years) of stay cable using different probability models-Symmetric modes (C23, D23)	195
Table 6.43	Estimated axial fatigue life (in years) of stay cable using different probability models-Antisymmetric modes (C23, D23)	196
Table 6.44	n-matrix for the first symmetric mode under 10 mm/hr rainfall ( $\alpha=47$ ,	199

	Sc=4.61, Cables -C12, D12,C15 and D15, JPD model I)	
Table 6.45	n-matrix for the first symmetric mode under 40 mm/hr rainfall ( $\alpha=47$ , Sc=4.61, Cables -C12, D12, C15 and D15, JPD model I)	200
Table 6.46	n-matrix for the first symmetric mode under 70 mm/hr rainfall ( $\alpha=47$ , Sc=4.61, Cables -C12, D12, C15 and D15, JPD model I)	201
Table 6.47	Y-matrix for 1st symmetric mode ( $\alpha=47$ , Sc=4.61, Cables -C12, D12,C15 and D15)	202
Table 6.48	Bending stresses (in Mpa) at the Pylon end in 1st symmetric mode ( $\alpha=47$ , Sc=4.61, Cables -C12, D12,C15 and D15)	202
Table 6.49	Bending stresses (in Mpa) at the Deck end in 1st symmetric mode ( $\alpha=47$ , Sc=4.61, Cables -C12, D12,C15 and D15)	203
Table 6.50	N-matrix at the Pylon end in 1st symmetric mode ( $\alpha=47$ , Sc=4.61, Cables -C12, D12,C15 and D15)	204
Table 6.51	Estimated Fatigue Damage for 1st symmetric mode at Pylon end under R10 conditions (Cables -C12, D12, C15 and D15, JPD Model- I)	206
Table 6.52	Estimated Bending Fatigue Damage for 1st Symmetric mode at Pylon end under three rainfall conditions for (Cables -C12, D12, C15 and D15, JPD Model-I)	207
Table 6.53	Estimated Cumulative Bending Fatigue Damage at Pylon end for symmetric and anti-symmetric modes for 100 years (Cables -C12, D12, JPD Model-I)	207
Table 6.54	Estimated Cumulative Bending Fatigue Damage at Pylon end for symmetric and anti-symmetric modes for 100 years (Cables -C15, D15, JPD Model-I)	208
Table 6.55	Bending Fatigue life of stays (Cables -C12, D12, C15 and D15, JPD Model-I)	208
Table 6.56	n-matrix for the first symmetric mode under 10 mm/hr rainfall ( $\alpha=47$ , Sc=4.61, Cables -C12, D12, C15 and D15, JPD Model-II)	209
Table 6.57	n-matrix for the first symmetric mode under 40 mm/hr rainfall ( $\alpha=47$ , Sc=4.61, Cables -C12, D12, C15 and D15, JPD Model-II)	209
Table 6.58	n-matrix for the first symmetric mode under 70 mm/hr rainfall ( $\alpha=47$ , Sc=4.61, Cables -C12, D12, C15 and D15, JPD Model-II)	212
Table 6.59	Estimated Fatigue Damage for 1st symmetric mode at Pylon end under R10 conditions (Cables -C12, D12, C15 and D15, JPD Model-II)	213
Table 6.60	Estimated Bending Fatigue Damage for 1st Symmetric mode at Pylon end under three rainfall conditions (Cables -C12, D12, C15 and D15, JPD Model-II)	214
Table 6.61	Estimated Cumulative Bending Fatigue Damage at Pylon end for symmetric and anti-symmetric modes for 100 years (Cables -C12, D12, JPD Model-II)	215
Table 6.62	Estimated Cumulative Bending Fatigue Damage at Pylon end for symmetric and anti-symmetric modes (Cables -C15, D15, JPD Model-II)	216

---

Table 6.63	Bending Fatigue life of stays (Cables -C12, D12, C15 and D15, JPD Model-II)	216
Table 6.64	Estimated Cumulative Bending Fatigue Damage at Pylon end for symmetric and anti-symmetric modes (Cables –C12, D12, C15, D15, JPD Model-III)	217
Table 6.65	Bending Fatigue life of stays (Cables -C12, D12, C15 and D15, JPD Model-III)	217
Table 7.1	Bending Fatigue life of stay cables under three different probability models- 1st Symmetric and anti-symmetric mode	229
Table 7.2	Axial Fatigue life of stay cables under three different probability models- 1st Symmetric and anti-symmetric mode	229

## LIST OF FIGURES

Figure 1.1	Parallel attachment design and Radial attachment design	2
Figure 1.2	Parallel stranded cable of a cable-stayed bridge	2
Figure 1.3	Damaged stay cable at the lower anchorage	5
Figure 1.4	Broken wire locations in the section of the strand: 0 shape wires, O cylindrical wires, broken wires	6
Figure 1.5	Surface fracture of an inter-wire fretting fatigue wire breakage	6
Figure 1.6	Distribution of wire breaks	7
Figure 1.7	Recorded Rain-wind induced vibrations on cable stays: Fred Hartman Bridge	8
Figure 1.8	Broken Guide Pipe – Fred Hartman Bridge	8
Figure 1.9	Flow-chart of the thesis	12
Figure 2.1	Overview of the Statistical analysis of Meteorological parameters	17
Figure 2.2	Selected bridges and their locations along its latitudes and longitudes.	19
Figure 2.3	Megami Bridge and Nagasaki Marine Observatory (32.73° N, 129.86° E, 26.9m High)	20
Figure 2.4	Megami Bridge and Nagasaki Marine Observatory	21
Figure 2.5	Position of the bridge axis and the wind direction sectors	21
Figure 2.6	Wind profile and turbulent intensity profile at bridge site	23
Figure 2.7	wind profile of the stay cables at the bridge site	23
Figure 2.8	Monthly rainfall for 15 years	24
Figure 2.9	Annual rainfall for 15 years	24
Figure 2.10	Gamma distribution for rainfall intensity (mm/hr)	28
Figure 2.11	Weibull distribution for rainfall intensity (mm/hr)	28
Figure 2.12	Weibull distributions and relative frequency of 10 minute mean wind speed for 15 years data	32
Figure 2.13	Relative frequency and assumed frequency of wind speed	34
Figure 2.14	Relative frequency of wind direction $f(\theta)$ under different rainfall conditions	39

Figure 3.1	Limitations of the past research on rain-wind induced stay cable vibration	46
Figure 3.2	Schematic view of the wind tunnel in Shijiazhuang Tiedao University	48
Figure 3.3	Setup for the experiment on the rain-wind induced cable vibration.	50
Figure 3.4	Cable hanged on to the Rain vibration setup with rainfall system installed	50
Figure 3.5	The schematic view of the total experimental setup	51
Figure 3.6	View of the rain gauge to calibrate rainfall intensity	53
Figure 3.7	S-type Load cell	53
Figure 3.8	Setup, approaching flow, inclination and yaw angles	54
Figure 3.9	Flow stability of the approaching wind towards the stay cable	55
Figure 3.10	Relation between the wind at the exit of the wind tunnel and on the cable	55
Figure 3.11	Damping in stay cables	58
Figure 3.12	Free decay of vibration amplitude of the cable model I	59
Figure 3.13	Comparison of amplitude of vibration with and without rain ( $\alpha=30^\circ$ , $\beta=30^\circ$ )	61
Figure 3.14	Filed investigation on 29 April 2003 Ni et. al, 2007	62
Figure 3.15	Effect of rainfall intensity	63
Figure 3.16	Effect of wind speed and rainfall intensity ( $\alpha=30^\circ$ , $\beta=35^\circ$ )	63
Figure 3.17	Upper and lower rivulets on the stay cable ( $\alpha=35^\circ$ , $\beta=35^\circ$ )	65
Figure 3.18	Effect of wind yaw angle on vibration amplitude of the cable ( $\alpha=25^\circ$ )	68
Figure 3.19	Effect of wind yaw angle vibration amplitude ( $\alpha=30^\circ$ )	69
Figure 3.20	Effect of wind yaw angle vibration amplitude of the cable ( $\alpha=35^\circ$ )	70
Figure 3.21	Effect of wind yaw angle vibration amplitude of cable ( $\alpha=40^\circ$ , $\beta=45^\circ$ )	71
Figure 3.22	Effect of wind yaw angle on maximum amplitude ( $\alpha=25^\circ, 30^\circ, 35^\circ$ ) at different rainfall conditions	72
Figure 3.23	Effect of inclination angle on vibration amplitude ( $\beta=30^\circ$ )	73
Figure 3.24	Effect of inclination angle on vibration amplitude ( $\beta=35^\circ$ )	75
Figure 3.25	Effect of inclination angle on vibration amplitude ( $\beta=40^\circ$ )	76
Figure 3.26	Effect of inclination angle on vibration amplitude ( $\beta=45^\circ$ )	76
Figure 3.27	Effect of inclination angle on vibration amplitude ( $\beta=50^\circ$ )	77
Figure 3.28	Comparison of test results with the past studies	79

Figure 3.29	Effect of rainfall intensity and wind speed on vibration amplitude of the Stay cable ( $\alpha=25^\circ, \beta=35^\circ$ ) - Cable model II	80
Figure 3.30	Effect of damping ratio and scruton number on stay cable vibration ( $\alpha=30^\circ, \beta=30^\circ$ )	81
Figure 3.31	Effect of damping ratio on stay cable vibration ( $\alpha=25^\circ, \beta=30^\circ$ and $\alpha=30^\circ, \beta=35^\circ$ )	82
Figure 3.32	Effect of diameter on vibration amplitude of the cable ( $\alpha=30^\circ, \beta=35^\circ$ ) for different rainfall intensities	83
Figure 3.33	Cable with a thin wire of $L_c=8D$	85
Figure 3.34	Breakdown of continuous rivulet ( $\alpha=25^\circ, \beta=35^\circ$ )	85
Figure 3.35	Comparison of vibration amplitudes with and without mitigation at 10 mm/hr rainfall condition ( $\alpha=25^\circ, \beta=35^\circ$ )	86
Figure 3.36	Evaluation of static position of the Experimental cable model	86
Figure 3.37	Mean wind speed versus position of the rivulet ( $\alpha=35^\circ, \beta=30^\circ, R=10, 40$ mm/hr)	87
Figure 3.38	Mean wind speed versus position of the rivulet ( $\alpha=35^\circ, \beta=30^\circ$ and $35^\circ$ )	88
Figure 3.39	Mean wind speed versus position of the rivulet ( $\alpha=35^\circ, \beta=35^\circ, R=40, 70$ m/hr)	88
Figure 3.40	Mean wind speed versus position of the rivulet ( $\beta=45^\circ$ )	89
Figure 4.1	Modeling of rain-wind induced cable vibration (a) orientation of the cable and (b) relative velocity of the cable with moving rivulet	96
Figure 4.2	Aerodynamic co-efficients of a horizontal cylinder	98
Figure 4.3	Horizontal cylinder with fixed rivulet	100
Figure 4.4	Position of the rivulet vs Maximum vibration amplitude of the stay cable	101
Figure 4.5	Wind speed vs normalized vibration amplitude of the stay cable	102
Figure 4.6	Position of the rivulet $\theta_0$ vs Maximum vibration amplitude $A_{max}$ of the stay cable	102
Figure 4.7	Inclined stay cable model	103
Figure 4.8	Aerodynamic co-efficient of a inclined cylinder (Hikami and shiraishi, 1988)	103
Figure 4.9	Mean wind speed vs. static position of the upper rivulet on an inclined	104

	cylinder	
Figure 4.10	Mean wind speed vs. static position of the lower rivulet on an inclined cylinder	104
Figure 4.11	Motion of the upper rivulet on an inclined stay cable	105
Figure 4.12	Comparison of vibration amplitudes for different rivulet amplitudes	106
Figure 4.13	Comparison of experimental and analytical response	106
Figure 4.14	mean wind speed Vs. vibration amplitude of the cable ( $\alpha=45^\circ$ , $\beta=30^\circ$ )	109
Figure 4.15	mean wind speed Vs. vibration amplitude of the cable ( $\alpha=45^\circ$ , $\beta=35^\circ$ )	109
Figure 4.16	mean wind speed Vs. vibration amplitude of the cable ( $\alpha=45^\circ$ , $\beta=40^\circ$ )	110
Figure 4.17	mean wind speed Vs. vibration amplitude of the cable ( $\alpha=45^\circ$ , $\beta=45^\circ$ )	110
Figure 5.1	Discredited element of a string	116
Figure 5.2	Forces acting on a Stay cable - Equations of Motion of a stay cable	119
Figure 5.3	3-Dimensional plot of equation 5.24	124
Figure 5.4	Contour plot of $\alpha$ and $\beta$ (Equation 5.24)	125
Figure 5.5	Mode shapes of the Euler-Bernoulli beam with $T/EI=0$	126
Figure 5.6	Mode shapes of the Euler-Bernoulli beam with $T/EI=42637$	126
Figure 5.7	Effect of Tension force on Tension-Bending parameter	129
Figure 5.8	Effect of Axial tension force on sag parameter	129
Figure 5.9	Boundary conditions and forces acting on the stay cable	130
Figure 5.10	1 <sup>st</sup> Symmetric mode of the stay cable	131
Figure 5.11	1 <sup>st</sup> Anti-Symmetric of the stay cable	132
Figure 5.12	2 <sup>nd</sup> Symmetric mode of the stay cable	132
Figure 5.13	2 <sup>nd</sup> Anti-symmetric mode of the stay cable	133
Figure 5.14	3 <sup>rd</sup> Symmetric mode of the stay cable	133
Figure 5.15	3 <sup>rd</sup> Anti-Symmetric mode of the stay cable	134
Figure 5.16	Bending stress in 1 <sup>st</sup> symmetric mode for 0.5 m peak displacement	136
Figure 5.17	Bending stress in 2 <sup>nd</sup> symmetric mode for 0.5 m peak displacement	137
Figure 5.18	Bending stress in 2 <sup>nd</sup> symmetric mode for 0.5 m peak displacement	139
Figure 5.19	Bending stress in 1 <sup>st</sup> asymmetric mode for 0.5 m peak displacement	140
Figure 5.20	Bending stress in 2 <sup>nd</sup> Asymmetric mode for 0.5 m peak displacement	142
Figure 5.21	Bending stress in 3 <sup>rd</sup> Asymmetric mode for 0.5 m peak displacement	143
Figure 5.22	Boundary conditions of the stay cable inclined at $47^\circ$ - C12 and D12	145

Figure 6.1	Bridge axis and the wind directions	163
Figure 6.2	Preliminary bending spectrum for monostrand	172
Figure 6.3	Stay cable positions on the Megami bridge	195

## **CHAPTER I**

### **INTRODUCTION**

#### **1.1. Cable and Cable stayed bridges**

Cables of the cable-stayed bridges are made of steel with higher strength acts as main tension elements in transferring loads from the bridge decks to the standing pylons and thus fatigue life of the cable is of greater concern in cable-stayed bridges. Any cable stayed bridge is supported by several cables which are inclined at certain angles such that the cables can carry the loads of the bridge deck to the pylon. Figure 1.1 shows two different kinds of cable stayed bridges based on method of attaching the cables from the bridge deck to the pylon. Since the cables plays a main role in the cable stayed bridge and carries live loads from traffic, earthquake, wind, rain, snow, heat etc. and thus fatigue in stay cables is of major concern in design life of the stay cables. It can be seen from figure 1.1 that the stay cables acts as a tension elements between the bridge deck and the pylon.

Cables are made up of high strength steel wire of diameters typically from 3-7 mm wound together either in a parallel or helical. The cables of the cable stayed bridges are made of multiple number of steel wires with diameter 3-7 mm are combined together either in a parallel or helical or interlocked. Locked-coil cables have been used in Germany, while spiral type cables were used in UK and parallel wire strands are widely used in Japan and US. The

seven wire strands usually consist of a single straight core surrounded by a six layers of six wires [1].

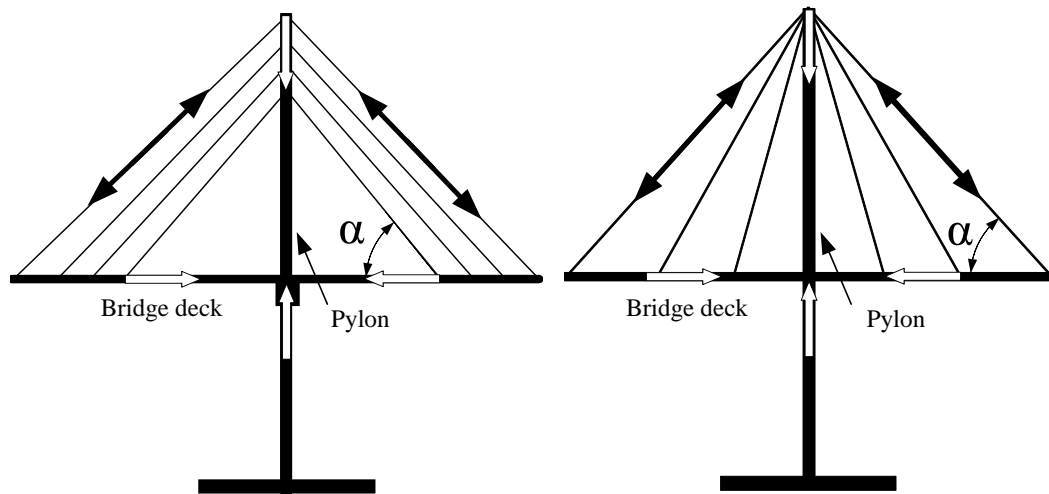


Figure 1.1 Parallel attachment design and Radial attachment design

Figure 1.2 shows the parallel wire strand. The cables usually vary from 100 mm to 200 mm in diameter and length may vary from few meters to 200 m or even more. Usually the  $L/D$  ratio's of the large cables stayed bridges is of the order of 0.001, with a very small damping ratio which varies from 0.05-0.3 %. The chemical composition of the cable steel contains high carbon content which is of five times that of structural steel [1]. The high carbon content makes the cable unsuited for welding.

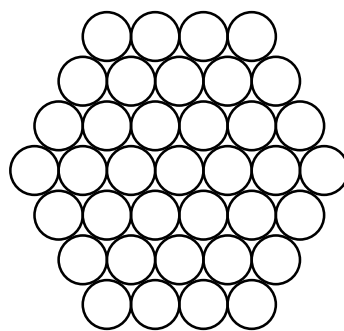


Figure 1.2 Parallel stranded cable of a cable-stayed bridge [2]

## 1.2. Stay cable vibration

The low-damping ratio and its slenderness of the stay cables makes it to vulnerable to variety of vibrations such as vortex shedding, buffeting, galloping, traffic induced vibrations, earth-quake induced vibrations and rain-vibrations etc and these vibrations may induce stresses in the stay cables and which may have a greater influence on the life of the stay cables. Since, the rain-wind induced vibrations exhibits a very large amplitude vibration and it becomes the major concern in determining the fatigue of the stay cables. Hikami[3] and Matsumoto[4] had also stated that the rain-wind induced vibrations can take a major part in determining the bending fatigue, whereas the contribution of rain-vibration over the years was not found. The present work is not only focused on the fatigue life estimation due to rain-wind induced vibrations, but also it considers three different possible probabilities.

For the past decade, rain-wind induced vibration is of greater threat to the existing stay cables. These vibrations severe and the amplitude of vibration are quite large in comparison with any other kind of cable vibrations such as vortex shedding [3,5], buffeting, galloping, traffic induced vibrations etc and these vibrations may induce fatigue in the stay cables. And thus it became necessary to study the effects of rain-wind induced vibration on the fatigue life of the stay cables.

## 1.3. Rain-wind induced stay cable vibration

In certain conditions of wind and rain, the stay cables of the cable stayed bridges exhibits a kind of large-amplitude vibration which is also characterized by a frequency lower than the vortex induced vibration but with a higher amplitude, and later on it is turned to be called as rain-wind/wind-rain induced vibrations. These vibrations were first observed on Meikonishi Bridge and reported by Y. Hikami [3], when the wind speed was around 14 m/s,

the cable showed peak to peak amplitude of about 550 mm. Since, then there were lot of field investigations [6] and experiments [3,6,7] were carried out to study the characteristics of rain-wind induced vibrations which also confirmed that these vibrations are quite large and thus may affect the fatigue life of the stay cables of the cable stayed bridge.

The phenomenon behind rain-wind induced vibration was explained in Chapter III of the thesis. During conditions of rain and wind, stay cable exhibits a large amount of vibration which is of twice the diameter. And thus it is necessary to consider such vibrations for bending fatigue.

#### **1.4. Axial and Bending fatigue of stay cables**

Generally stay cables were subjected to a large amount of tension forces leading to axial stresses, whereas across wind effects causes bending fatigue on stay cables. And the codes [8], doesn't resemble the importance of bending fatigue due to assumption that the stay cables acts as strings (due to less bending stiffness) in which bending is not predominant. But later on there were few field investigations and lot of experimental test on bending fatigue of stay cables, which proven that cable cannot be considered as a taut string due to the bending stiffness and the existing sag in the stay cables. Figure 1.3 shows one of the damaged cables at the lower anchorage of a stay cable in western France. There were mainly three places where the maximum failures occur i.e., at the anchorage (near the bridge deck), at the mid span of the cable, and at the other end of the cable (near saddle) either by fretting or wedge failure which can be seen from figures 1.4 and 1.6.



Figure 1.3 Damaged stay cable at the lower anchorage [9]

Figure 1.4 shows the cross-section of the damaged stay cable at the anchorage end, whereas figure 1.5 (a), (b) and (c) shows the experimental results of a damaged stay cable at different positions on the cable i.e., at the live end, the mid-span and the rear end of the cable. From the figures 1.4 and 1.5, it can be said that the possible axial stress distribution would be maximum at its ends rather than at the center of the cross-section and is approximately plotted in figure 1.9.

Siegert [9] reported bending fatigue in stay cables as shown in figures 1.3, 1.5 and 1.6. And also the monitoring reports revealed the occurrence of large amplitude vibrations but it is important to note that there is no correlation between heavy traffic or tower and deck vibrations, whereas there were correlations between the winds at the east direction of the bridge (which is nearly perpendicular to the plane of the stay cable). Due to large-amplitude vibrations induced by wind-and rain-wind induced vibrations, it is necessary to consider those vibrations in a higher priority than the other kinds of vibrations.

Sharon L. Wood [10] considered two series of tests to identify the axial and bending fatigue damage to the parallel, seven-wire, prestressing strand in the grouted stay cables with the length of the stay was less than one-sixth the length of the shortest of the prototype stays. The first one with 12 specimens with the cross section of the stay-cable nominally identical to

that of the smallest diameter stays on the Fred Hartman Bridge. And the second one with 3 specimens, number of strands in these specimens was much smaller than the prototype stays and the cross-sectional properties did not vary along the length of the specimen. Their test results indicate that fatigue damage is concentrated in the regions of the highest bending stress: the ends of the stays and locations where a damper or restrainer induces local bending in the stay. The risk of fatigue damage was considered to be low at the tension ring, along the free length of the stay, and in the vicinity of unintentionally crossed strands.

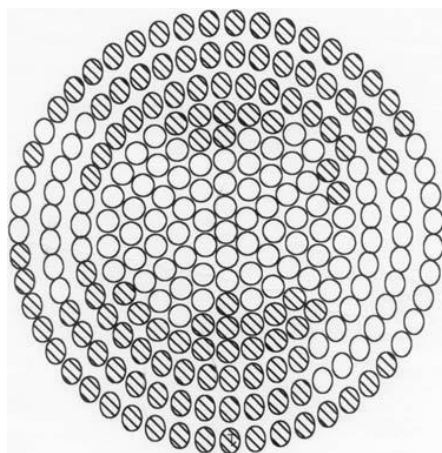


Figure 1.4 Broken wire locations in the section of the strand: 0 shape wires, O cylindrical wires, broken wires [10] Broken wire

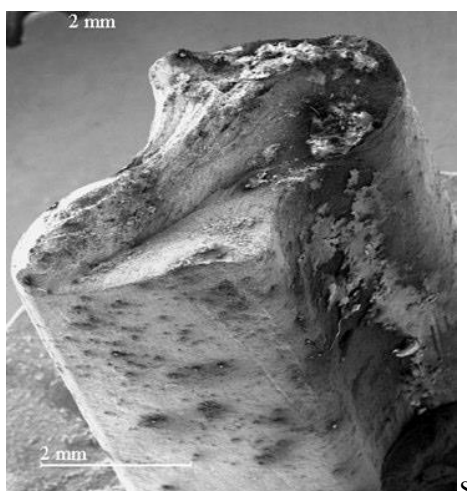


Figure 1.5 Surface fracture of an inter-wire fretting fatigue wire breakage [10]

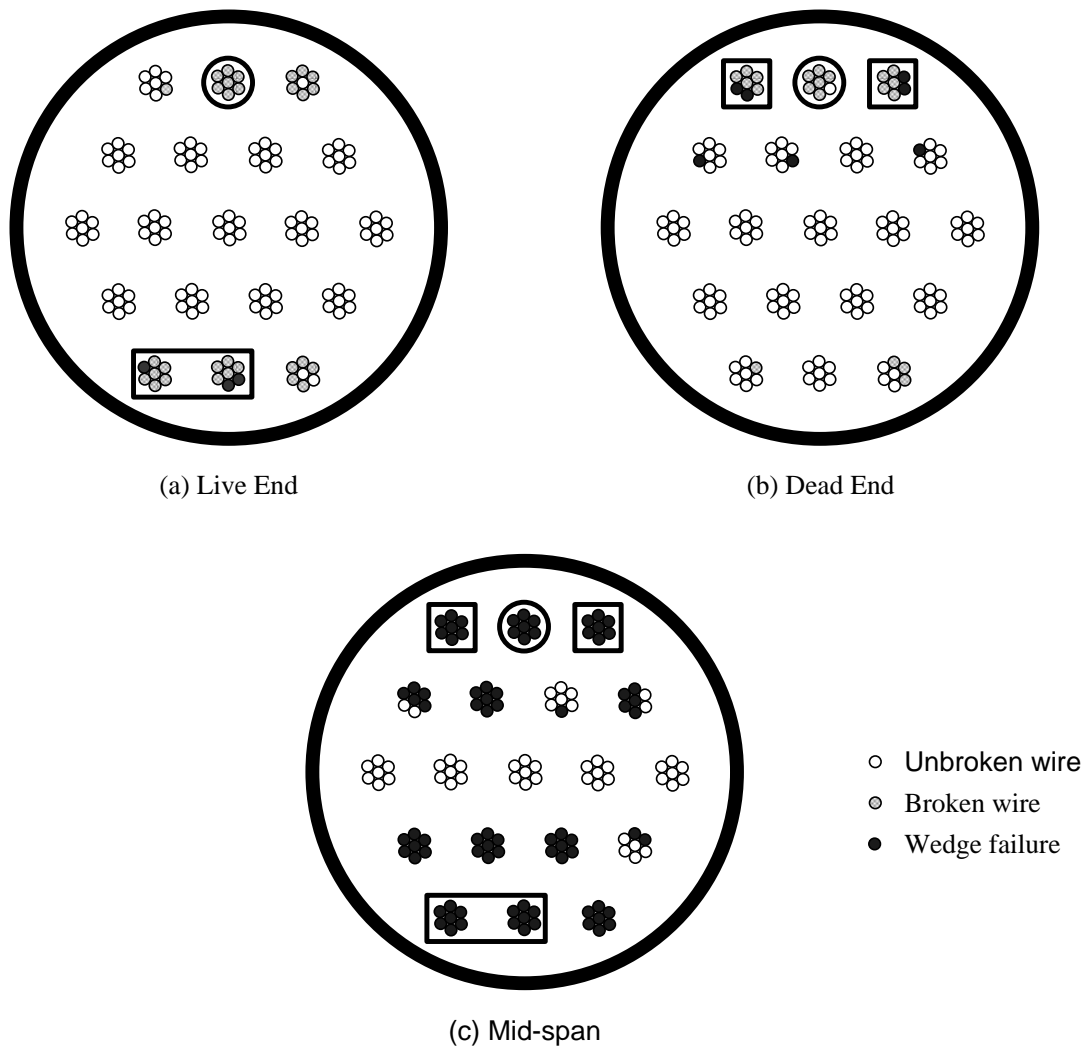


Figure 1.6. Distribution of wire breaks [10]

## 1.5. Background and Motivation

The above section explains the bending and axial fatigue. The main cause for such fatigue is believed to be rain-wind induced vibrations, as the vibrations are large in amplitude. Figure 1.7 shows the rain-wind induced vibration of the stay cable occurred in the Fred-Hartman Bridge [12]. The cables of the Fred-Hartman bridge exhibited large amplitude vibrations under the normal conditions of wind and rain, and the amplitudes of vibration were on second mode and more than a diameter. Figure 1.7 shows the fatigue damage caused due to rain-wind induced vibrations. The figure 1.8 shows the broken pipe of the cable in Fred

Hartman's bridge, which was suffered heavily by rain-wind induced vibration.

And considering all these facts explained in section, it's a must to consider bending stresses to estimate the fatigue life of the stay cable. Similarly vibrations had been found widely all over the world and are listed in table 1.



Figure 1.7 Recorded Rain-wind induced vibrations on cable stays: Fred Hartman Bridge [11]



Figure 1.8 Broken Guide Pipe – Fred Hartman Bridge [11]

And thus it is a must for the designers to consider the rain-wind induced vibration for fatigue life estimation. And also the bending fatigue must be considered for fatigue life calculations.

Table 1.1 Bridges subjected Rain-wind induced cable vibrations

Name of the Bridge	Country
Meiko-Nishi cable-stayed bridge [Hikami, 1988]	Japan
Fred Hartman Bridge in Texas [Aaron James Pebley, 2005]	US
Sidney Lanier Bridge , Talmadge Memorial Bridge in Georgia	US
Cochrane Bridge	Alabama
Faroe Bridge	Denmark
Aratsu Bridge Tempohzan Bridge	Japan
Erasmus Bridge	Holland
the Nanpu and Yangpu Bridges	China

## 1.6. Details of the present study

The following section explains the details of the present study. The detailed description is explained below.

### 1.6.1. Objective

The primary aim of the thesis is to evaluate the fatigue damage and life due to tensile and bending stresses caused by rain-wind induced vibrations. The secondary outcomes of the thesis are the studies made to understand the phenomenon of the rain-wind induced vibration, effect of different parameters on vibration amplitude of the stay cable, mitigation of rain-wind induced vibration and its efficiency, validation of an analytical model using the experimental data, studies to understand the behavior of strings and cable-beam action,

methodology to evaluate the stresses, modal contribution on fatigue and the procedure or methodology considered for the fatigue analysis.

### **1.6.2. Overview of methodology, and structure of dissertation**

The overview of the thesis is shown in figure 1.9. The flow chart explains the procedure followed for estimating the fatigue life of the stay cables. The structure is arranged in such a manner that the first chapter gives an introduction about the problem.

The second chapter deals with the statistical analysis of the meteorological parameters concerning the rain-wind induced vibration. The joint probability of three parameters concerning the rain-wind induced vibration. i.e., wind speed, wind direction and rainfall. The wind data collected at the meteorological station were used to find the joint probability models. From the collected data, three joint probability models were made; the first one is to estimate the joint probability of wind speed and wind direction considering the rainfall as independent event, and the second model assumes that all wind comes from the most unfavorable direction whereas the third model is a robust one considering wind speed, direction and rainfall as dependent events. The Chapter III of the thesis deals with the design of the frame made for mounting the stay cable, experimental models used to evaluate the response of the stay cable. This chapter also explains the effects of different parameters such as inclination angle, wind yaw angle, cable diameter, frequency and damping on vibration amplitude of the stay cable. As an extension of the study, tests were conducted to mitigate the rain-wind induced cable vibration by means of adding spires over the surface of the cable. The mitigation efficiency was also studied by varying the number of spires wound over the cable.

Chapter IV of the thesis discusses the analytical model for rain-wind induced vibration. This chapter also discusses the analytical model for horizontal cable, effect of static

rivulet position on the stay cable and further the analytical model is evaluated and is validated by comparing the analytical response results with the experimental results.

The stay cable consists of certain amount of bending stiffness and thus cannot be assumed as string. The boundary conditions of a string and a beam implies the effect of bending at the edges. Using the tension-bending parameter, the effects of cable-beam behavior was studied. The equation of motion was derived for a stay cable fixed at the ends and the analytical solution was found and later compared with the ANSYS results. The displacement obtained using modal analysis was normalized to unity and then multiplied with a factor equivalent to the peak displacement (in Chapter III) of the cable and a static analysis was carried out to find the bending moments at the ends of the cable.

Using the stresses, the fatigue life was calculated for different joint probability models in Chapter VI of the thesis. The contribution of modes on fatigue life of the stay cable was also studied. This chapter also gives recommendations for the different joint probability models and also explains the worst case scenario. A recommendation for the designers was made based on the results obtained for the fatigue analysis.

Chapter VII of the thesis discusses the outcome of the each chapter and the conclusions that were made in the design point of view. Recommendations to the designers were also made for fatigue estimation of the stay cables.

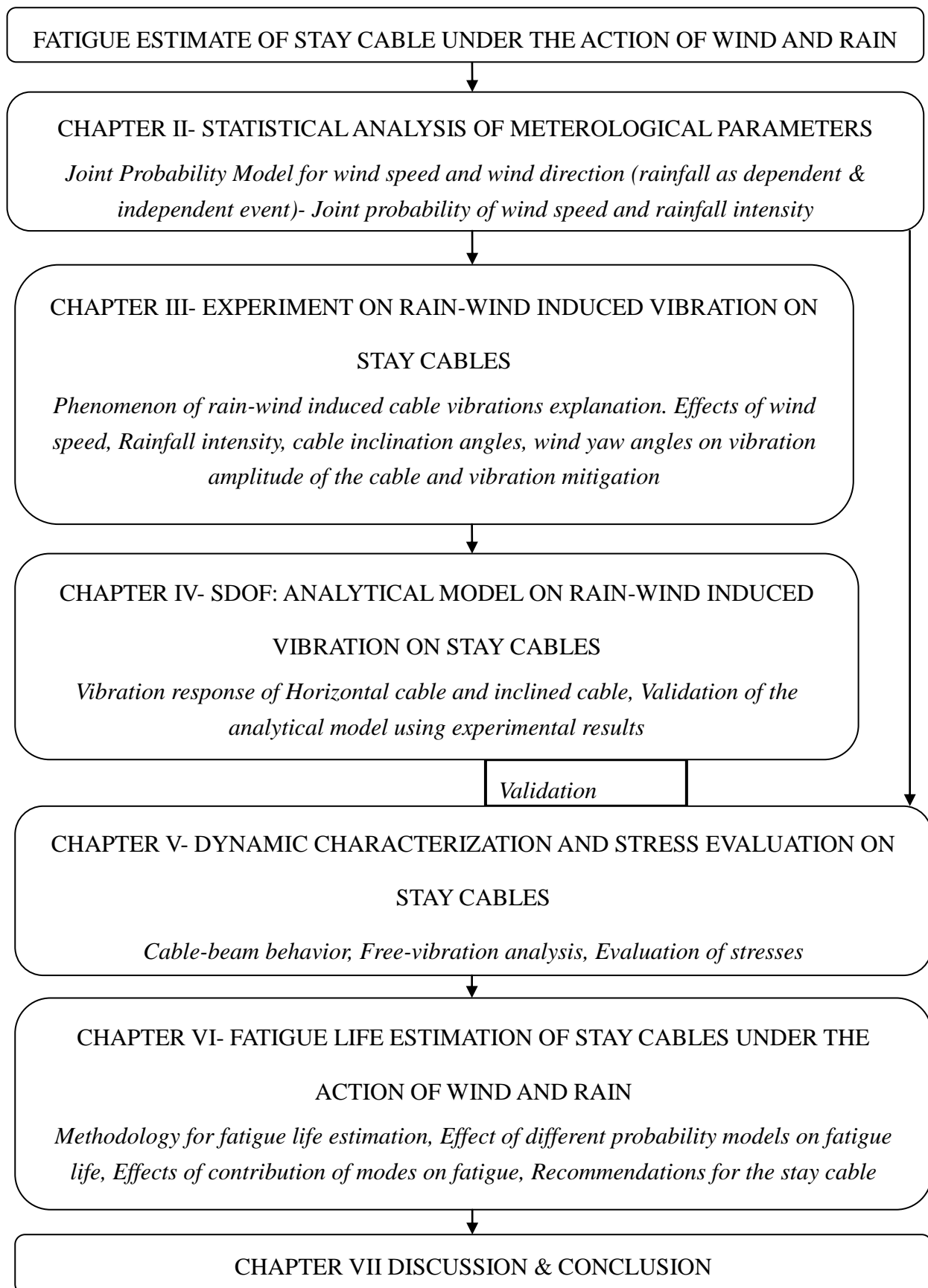


Figure 1.9 Flow-chart of the thesis

## 1.7. References

1. NCHRP synthesis 353, Inspection and Maintenance of Bridge Stay Cable Systems: A Synthesis of Highway Practice, 2003, ISSN 0547-5570, ISBN 0-309-09760-6.
2. Niels J. Gimsing, Cable supported bridges-concept and design (1983), John Wiley and sons, New York
3. Y. Hikami, N. Shiraishi, 1988, Rain-wind induced vibrations of cables in cable stayed bridges, *J. Wind Eng. & Ind. Aerodyn.*, 29, pp. 409-418.
4. M. Matsumoto, T. Yagi, Y. Shigemura and D. Tsusgima, 2001, Vortex-induced cable vibration of the cable-stayed bridges at high reduced wind velocity, *J. Wind Eng. & Ind. Aerodyn.*, 89 pp. 633-647.
5. M. Matsumoto, N. Shirashi and H. Shirato, Rain-wind induced vibration of cables of cable-stayed bridges, *J. Wind Eng. & Ind. Aerodyn.*, 41-42(1992) 2011-2012.
6. M. Gu, S. Y. Li and X.Q. Du, Experimental and theoretical simulations on wind-rain induced vibration of 3-D rigid stay cables, *J. Sound & Vibration*,
7. H. J. Zhou, Y. L. Xu, Wind-rain-induced vibration and control of stay cables in a cable-stayed bridge”, (2007, *Journal of Structural Control and Health Monitoring*, 14,pp. 1013-1033.
8. Acceptance of Stay Cable Systems Using Prestressing Steels, 2005, *International Federation for Structural Concrete (fib)*
9. Siegert, D., Brevet P., 2003, Fatigue of stay cables inside end fittings: High frequencies of wind induced vibrations, *In: Proc. OIPEEC technical meeting*.
10. Sharon L. Wood, Marcel Poser, Karl H. Frank, Matthew J. Bean, Joseph A. Dowd, 2008, ‘Bending Fatigue Response of Grouted Stay Cables’, Texas department of Transportation, Report No. FHWA/TX-0-1401-1

11. Aaron James Pebley, B.S., Bending Stresses in Stay-Cables During Large-Amplitude Vibrations - A Fred Hartman Bridge Case Study, August 2005, The University of Texas at Austin



## **CHAPTER II**

### **STATISTICAL ANALYSIS OF METEOROLOGICAL PARAMETERS**

#### **2.1 Introduction**

Generally built-in structures undergo several kinds of environmental loads and thus a designer has to ensure that the structure can withstand such loads during the design phase of the structure. Since the rain-wind induced vibration was influenced by wind speed, wind direction and rainfall and it's a must to study the Joint Probability of these three events in order to study the vibration characteristics and also to obtain the fatigue life of the stay cables.

Statistical methods are used to build probability or Joint probability models that can represent the statistical quantities of one or more independent parameters. Here in this chapter the Joint probability of the meteorological parameters such as wind speed, wind direction and rainfall that contributes to the rain-wind induced vibration of the stay cable is studied. Figure 2.1 shows the flowchart of chapter II. The first part of this chapter discusses about the selection of meteorological station and data processing. The second part of this chapter deals with the Joint probability models of wind speed, wind direction and rainfall intensity.

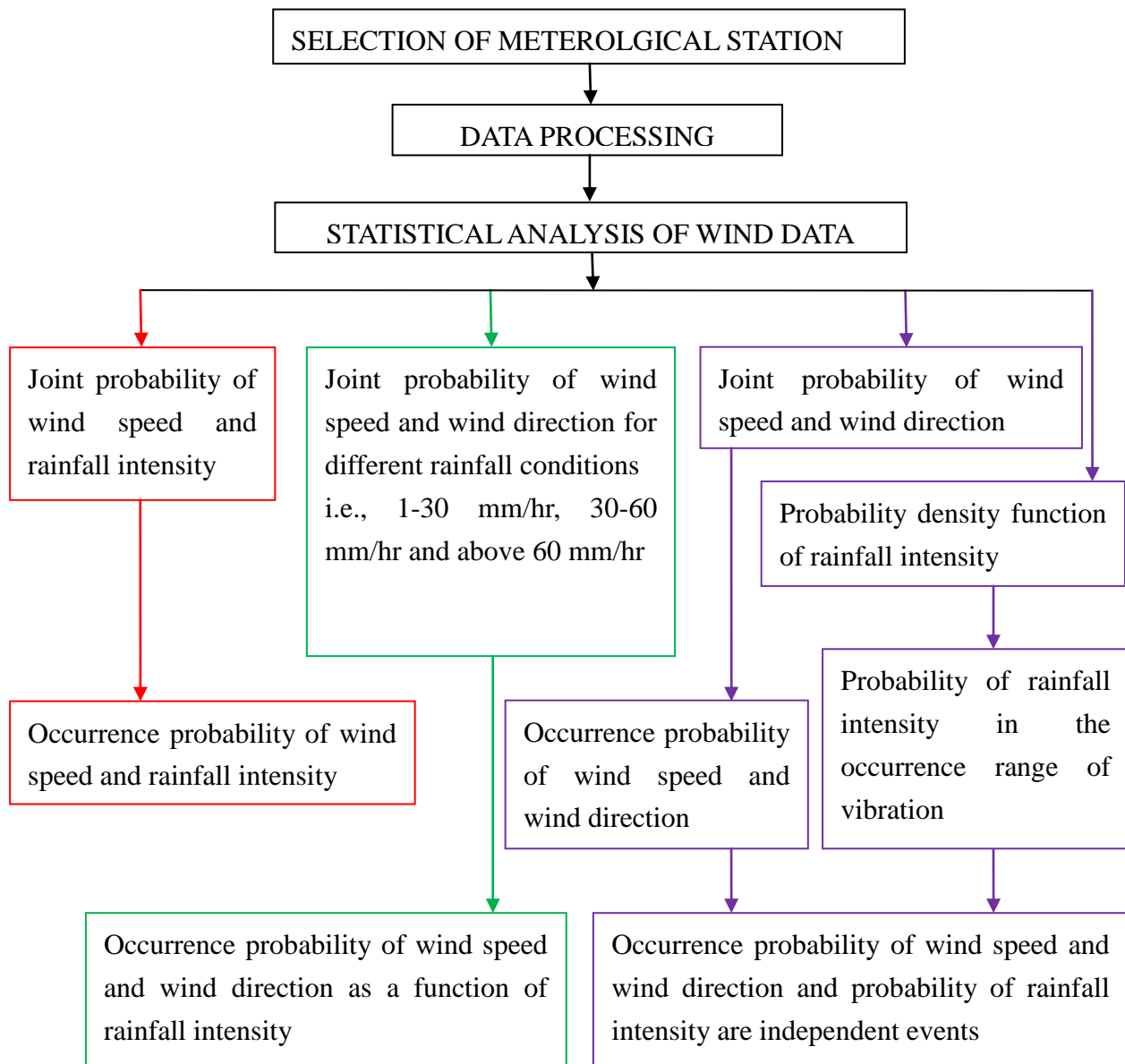


Figure 2.1 Overview of the Statistical analysis of Meteorological parameters

## 2.2 Selection of the Bridge and the meteorological station

The first step deals with the selection of meteorological station, collection of daily records, and availability of the data. The second one is to find the occurrence probability of two independent parameters such as wind speed and wind direction for each condition of rainfall or by assuming the rainfall intensity as an independent variable. The following section explains the steps involved in the selection of the bridge site, turbulent intensity

profile at the bridge, mean wind profile at the cable, data processing for the statistical analysis, and then the Joint probability models for the meteorological data.

Every place has its own meteorological stations and in this study meteorological stations which exists near the bridge is taken. And also the distance between the bridge and the meteorological stations, terrain features were also considered for analysis. So, the meteorological station which is near by the bridge is selected. The selected bridges fall in different areas widely over Japan. Fig. 2.2 shows the selected bridges and their locations along its latitudes and longitudes. The position of the bridge can be seen along its latitudes and longitudes of the map.

In the preliminary stage of the analysis the distance between the bridge and the meteorological stations and the terrain conditions of the bridge and the observatory stations were first considered and were tabulated in the table 2.1.

Table 2.1 Distance between the bridge and the meteorological stations

Id	Bridge	Meteorological Observatory	Distance between Bridge and Observatory (km)	Length of the bridge (m)
1	*Megami	Nagasaki Marine Obs.	2.2	880
2	Tatara	Ohmishima	5.8	1480
		Ikuchijima	5.3	
3	**MeikoNishi	Tokai	7.0	758
4	Yokohoma Bay	Yokohama Local Met. obs.	2	860
5	Mihara	EbetsuAmedas	2.6	340
*Bridge selected for analysis				

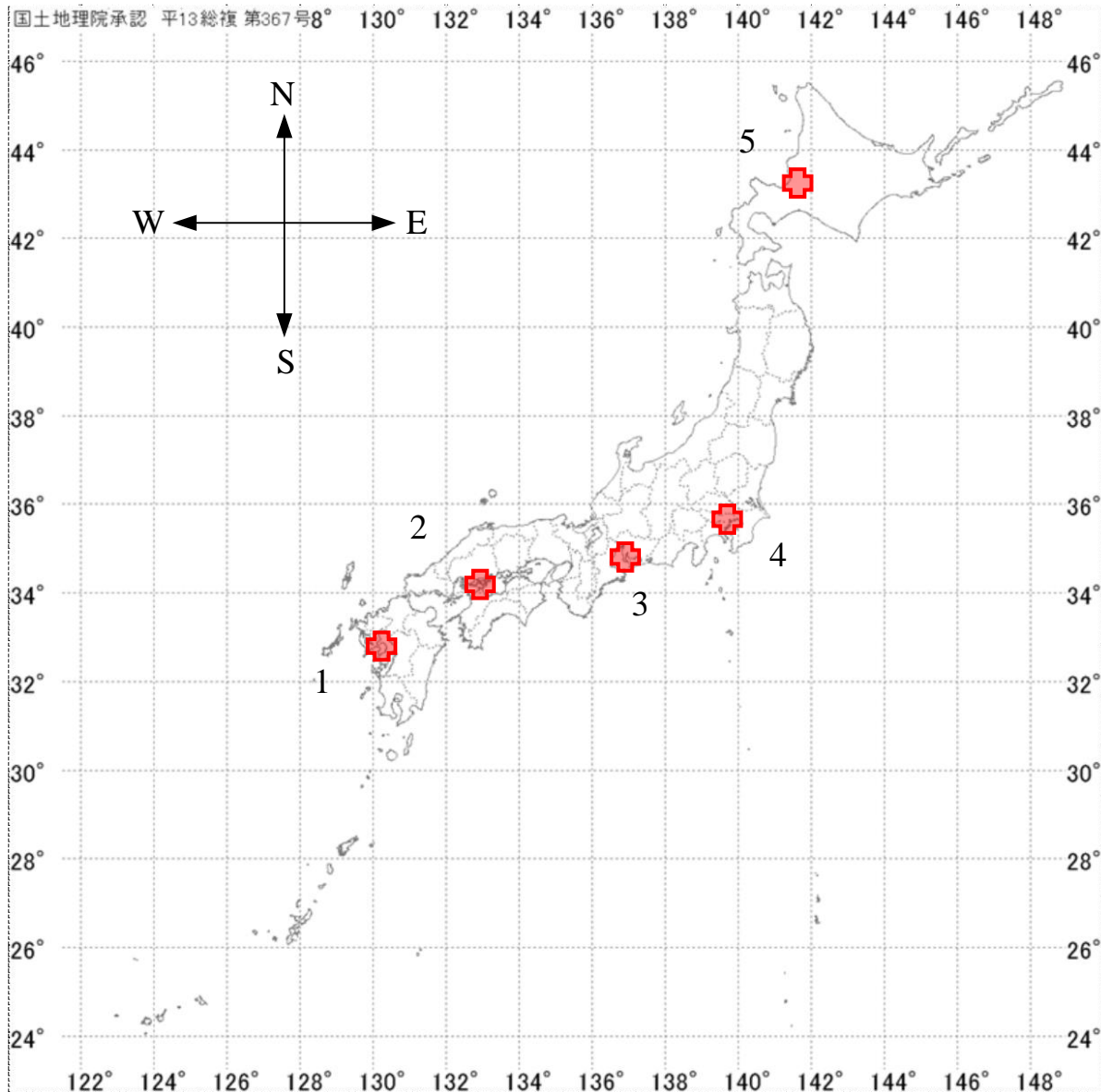


Figure 2.2 selected bridges and their locations along its latitudes and longitudes.

### 2.2.1. Megami Bridge and Nagasaki Marine Observatory

Megami Bridge was first considered for analysis based on its terrain conditions and the availability of qualitative meteorological data. The terrain conditions, locations of the meteorological stations and the bridges which are listed in the table 2.1 are shown in Appendix I of the thesis. More details about the stay cables are provided in Appendix II.



Figure 2.3 Megami Bridge and Nagasaki Marine Observatory

(32.73° N, 129.86° E, 26.9m High)

### 2.2.2. Statistical analysis of wind data

The following section explains the Statistical analysis of meteorological data which is measured at the Nagasaki Meteorological Observatory. And the main assumption is that the Megami cable stayed bridge is assumed to exist neat the Nagasaki marine observatory. Figure 2.3 shows the locations of Megami Bridge and Nagasaki observatory. It is a must to note the height at which the wind speeds are measured, so that the wind profile at the bridge site can be simulated. Here at Nagasaki Observatory the wind data is measured at 26.9 meters above the sea level, where as the bridge deck is about 65 meters above the sea level as shown in figure 2.4.

The Processed data are characterized by wind velocity, wind direction and rainfall count. The wind direction is discredited in to 16 directions of the directional circle with 22.5 degree interval as shown in figure 2.5. The Rainfall is categorized by three main groups i.e., 1-30 mm/hr, 30-60 mm/hr and rainfall above 60 mm/hr rainfall condition. Due to the effect of environmental factors, the original data lacks adequate representation and consistency. The collection of daily records for every 10 minutes data of wind speed, wind direction and

rainfall is collected at the Nagasaki Marine Observatory(NMO) for a period of 15 years ranging from 1 June 1994 until 1 June 2009 and is processed by separating it by season wise namely i.e., seasons of Japan-Spring, summer, autumn and winter. The measured wind speed below 1 m/s is eliminated in this study. The maximum wind speed at the NMO is found to be 23 m/s.

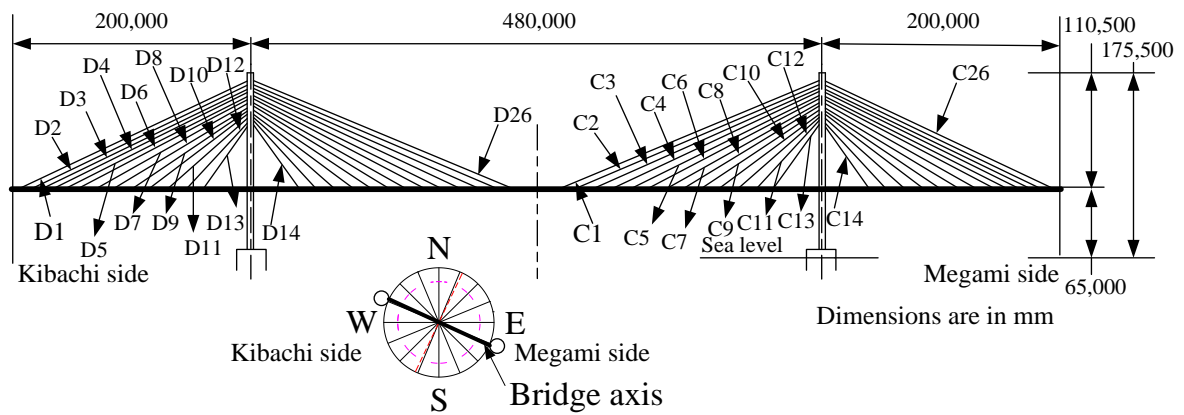


Figure 2.4 Megami Bridge and Nagasaki Marine Observatory

$$\beta = \theta + 64.7^\circ \tag{2.1}$$

The relation between wind direction ( $\theta$ ) observed from the site is related to the wind yaw angle ( $\beta$ ) through equation 2.1.

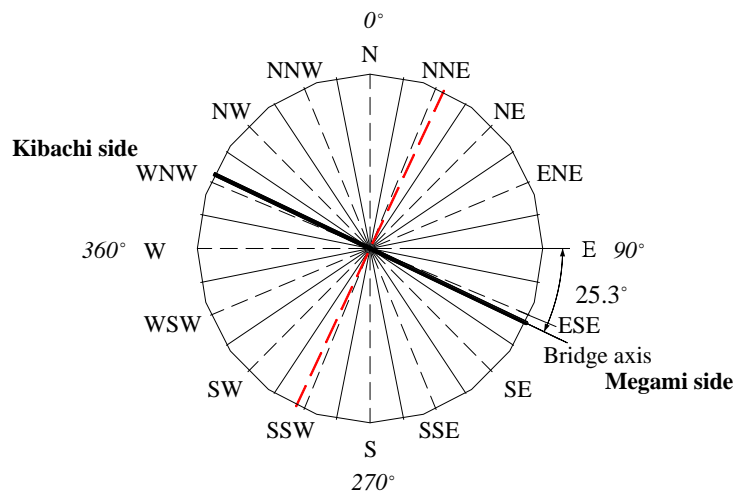


Figure 2.5 Position of the bridge axis and the wind direction sectors

### 2.2.3. Turbulent intensity and wind profile at the bridge site

Since, the study focuses on the simultaneous effects of wind and rain on the cable. Thus the turbulent intensity profile and mean wind profile was simulated at the bridge site assuming that the bridge is located at the Nagasaki observatory. The turbulent intensity along the height can be estimated from the equation 2.2 [Jim Hay, 1992].

$$I(z) = I(10) \left[ 1 - 0.00109 (z - 10) \right] \left( 10 / z \right)^{0.17} \quad 2.2$$

And the terrain shown in figure 2.3 can be classified as open country and the roughness parameter  $z$  can be taken as 0.18 (Jim Hay, 1992). Figure 2.6 shows the wind profile and turbulent intensity profile variation with the height at the bridge site. The vertical wind profile can be expressed by the equation 2.3 in which 0.17 is the power-law exponent.

$$U(z) = U_r \left( \frac{z}{z_r} \right)^{0.17} \quad 2.3$$

Since the stay cables are inclined at certain angles and vary up to 300 m. Thus its necessary to find the wind profile considering the slant height. And the wind profile for any inclined cable can be estimated by equation 2.4 in which  $x$  is the length along the cable,  $\alpha$  is the inclination angle of the cable.

$$U(l) = U(z(x)) = U_r \left( \frac{z_0 + \frac{(x) \sin \alpha}{z_r}}{z_r} \right) \quad 2.4$$

Usually the length of the stay cable may vary from few meters to 300 or even more depending on the span of the bridge and thus the unidirectional wind profile may not be suitable for the analysis. Thus a bi-directional wind profile was simulated along the slant height of the cable using the equation 2.4. It can be seen from figure 2.7 the variation of the  $U(z_0)/U_r$  varies from 1.27 to 1.32 at the center of the cable and thus it can assumed that  $U(z_0)/U_r$  as 1.3 for the sake of simplicity. The wind data obtained at the bridge site is

transformed to the wind on to the deck end of cable using wind profile equation.

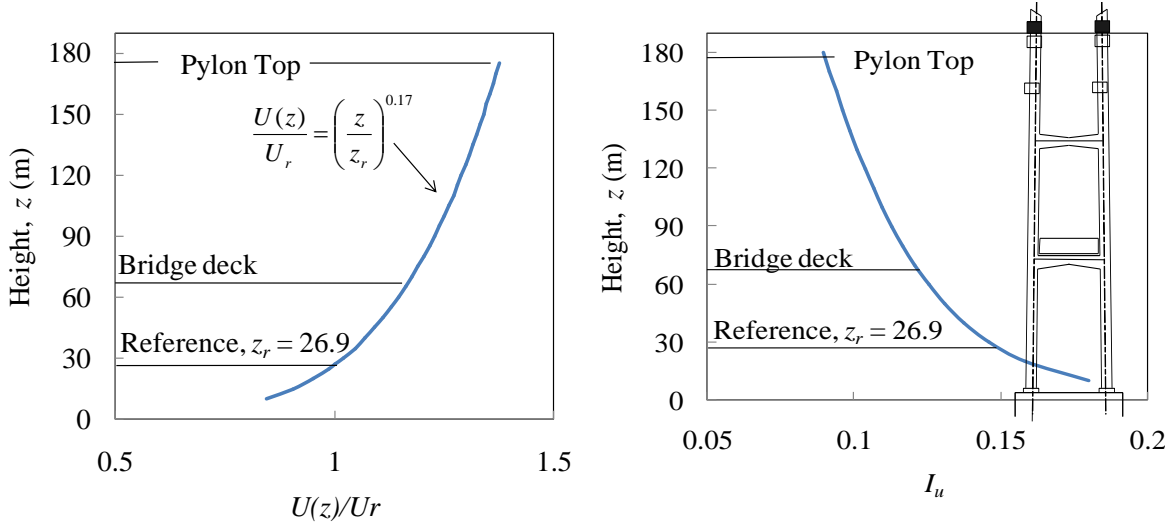


Figure 2.6 Wind profile and turbulent intensity profile at bridge site

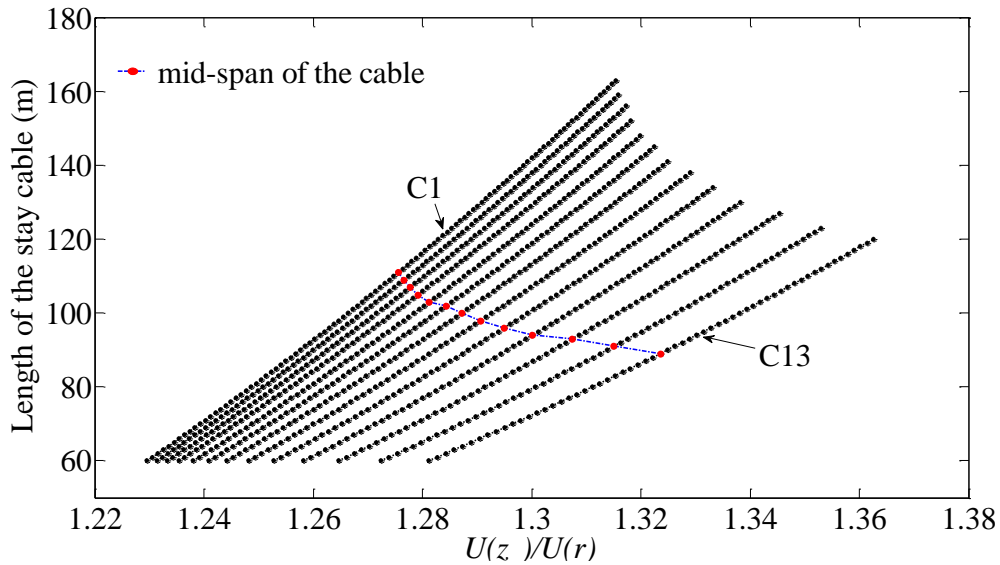


Figure 2.7 Wind profile of the stay cables at the bridge site

#### 2.2.4. Statistical analysis of rainfall data

After analyzing the 15 year wind data, it was decided to consider the large rainfall region. The rainfall intensity was also measured simultaneously with the wind data at the Nagasaki Marine Observatory from 1<sup>st</sup> June 1994 until 1<sup>st</sup> June 2009 and there are some missing data's which are eliminated in the analysis.

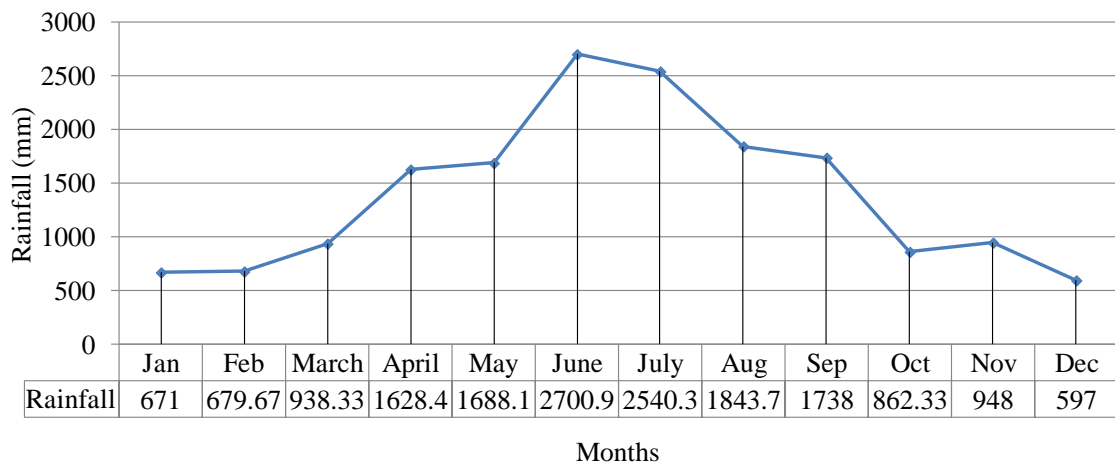


Figure 2.8 Monthly rainfall for 15 years

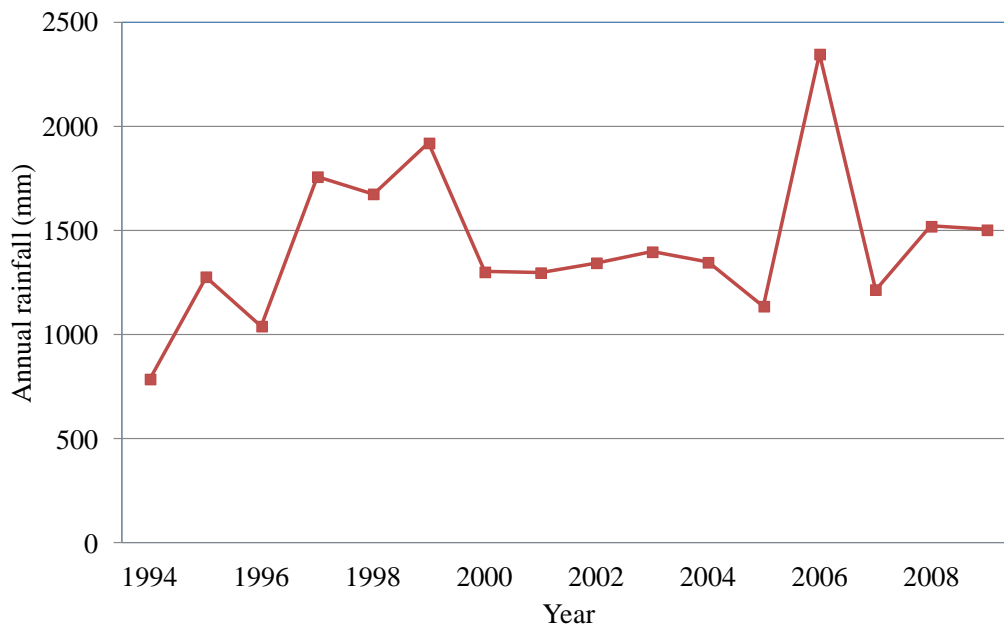


Figure 2.9 Annual rainfall for 15 years

Figure 2.8 shows the monthly rainfall for every month. And it can be seen that June and July can produce large amount of rain, whereas January, February and December lies in a very low raining season. Figure 2.9 shows the annual rainfall for 15 years from June 1994 till June 2009. It can also be seen in 2006 heavy rainfall had occurred which is quite different from other years. And from figure it can be seen that large number of rainy events were recorded during the year 1997, 1998, 1999, 2006 and 2008.

## **2.3 Joint probability of wind speed, direction and rainfall**

In order to study the fatigue damage due to rain-wind induced vibrations, it is necessary to study the simultaneous action of wind and rain on the cable. So, the joint occurrence probability of wind speed, wind direction and rainfall has to be considered. And in this chapter three kinds of Joint probability models were studied i.e.,

- (i) Joint probability of wind speed, wind direction and rainfall intensity in which the probability of rainfall intensity is considered as an independent event.
- (ii) Probability of relative wind blows in the most unfavorable direction to the cable.

The following will elaborate the probability models in detail.

- (iii) Joint probability of wind speed, wind direction and rainfall intensity in which rainfall is a dependent or a control event

### **2.3.1 Joint probability model for wind data considering rainfall as an independent event**

In this model the joint probability of wind speed and wind direction was obtained using weibull distribution function considering both as dependent events and the probability density of rainfall data was considered as an independent one. The following explains the Joint probability of wind speed and wind direction considering rainfall as independent one.

#### **2.3.1.1. Joint probability model for wind data**

Rain-wind induced vibrations is a kind of velocity-restricted vibration (Hikami, 1988) and also found to occur in low-and-moderate wind speeds (Hikami,1988, Ming Gu, 2005) and thus a complete population of wind speed has to be considered rather than an extreme distribution (Shan et al, 2008). And most often weibull or normal distributions were

used to fit the wind speed data as it is concerned about the complete population (Corotis et. al, 1974). And thus in this study a two-parameter weibull distribution function has been used. The probability density functions (PDF) and cumulative density functions (CDF) of the weibull distribution are given in equation 2.1 and 2.2.

$$f_U(U) = \frac{b}{a} \left[ \frac{U}{a} \right]^{b-1} \exp \left[ - \left[ \frac{U}{a} \right]^b \right] \quad 2.5$$

$$P_u(U) = \left( 1 - \exp \left[ - \left( \frac{U}{a} \right)^b \right] \right) \quad 2.6$$

in which a and b are shape and scale parameters and are bound to be positive values. i.e., whereas U is the mean wind speed in m/s.

Studies also revealed that amplitude of rain-wind induced vibrations were not only a function of wind speed but also a function of wind direction (Hikami 1988, M.Gu 2005, Zhan et al. 2008, Lin-Shan Xu 1996) and thus it is mandatory to consider the joint distribution of wind speed and wind direction. Thus a Joint probability model is must to study the occurrence conditions of rain-wind induced cable vibrations. A similar probability models have been developed in the past (Xu et. al 2008, Yaojun Ge 2002, Jun Chen 2009) and the following model considers the rainfall intensity as an independent event. The joint probability distribution of wind speed and wind direction based on two assumptions (Zhan et al. 2008) and the same assumption is applicable in this part of the study.

- i) The distribution of the component of wind speed for any given wind direction follows the Weibull distribution and
- ii) The interdependence of wind distribution in different wind directions can be reflected by the relative frequency of occurrence of wind.

The Joint probability density and cumulative distribution function of the wind speed (U) and wind direction ( $\theta$ ) can be given by,

$$f_{U,\theta}(U, b(\theta), a(\theta)) = \frac{b(\theta)}{a(\theta)} \left[ \frac{U}{a(\theta)} \right]^{b(\theta)-1} \exp \left[ - \left[ \frac{U}{a(\theta)} \right]^{b(\theta)} \right] \quad 2.7$$

$$P_{\theta}(\theta) = \int_0^{\theta} f_{\theta}(\theta) d\theta \quad 2.8$$

$$P_{u,\theta}(U, \theta) = P_{\theta}(\theta) \left( 1 - \exp \left[ - \left( \frac{U}{a(\theta)} \right)^{b(\theta)} \right] \right) \quad 2.9$$

$$= \iint f_{\theta}(\theta) f_{u,\theta}(U, a(\theta), b(\theta)) du d\theta \quad 2.10$$

in which  $\theta$  is the wind direction from  $0^{\circ}$  to  $360^{\circ}$ .

### 2.3.1.2. Probability density function of rainfall

Zhan et al. (2008) have reported the influence of rainfall on the vibration amplitude of the stay cable vibration. And Ni et. al.(2007) reported that the very low and moderate rainfall intensities may cause a very large amplitude vibrations and thus the probability density of rainfall has to be considered, in order to figure out the vibration response of the cable. Xu et. al (2008) showed that the probability of occurrence of vibration during rain events can be extracted from the total rain events by,

$$P_r(B) = P_r(A \cap B) = P_r(A)P_r(B|A) \quad 2.11$$

The Gamma distribution function and weibull function is opted for the rainfall intensity, R are given in equations 2.12 and 2.13.

$$f_r(R) = \frac{1}{b^a \Gamma(a)} R^{a-1} e^{-\frac{R}{b}} \quad 2.12$$

where  $\Gamma(a) = \int_0^{\infty} y^{a-1} e^{-y} dy$ ,  $a$  and  $b$  are shape and scale parameters for gamma distribution.

The weibull distribution may also be used,

$$f_r(R) = \frac{d}{c} \left(\frac{R}{c}\right)^{d-1} e^{-\left(\frac{R}{c}\right)^d} \quad 2.13$$

in which  $c$  and  $d$  are shapes and scale parameter for the weibull distribution.

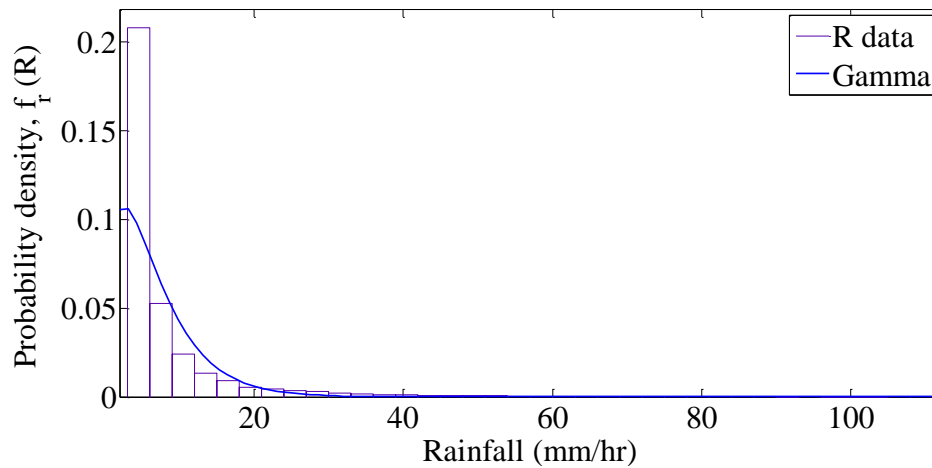


Figure 2.10 Gamma distribution for rainfall intensity (mm/hr)

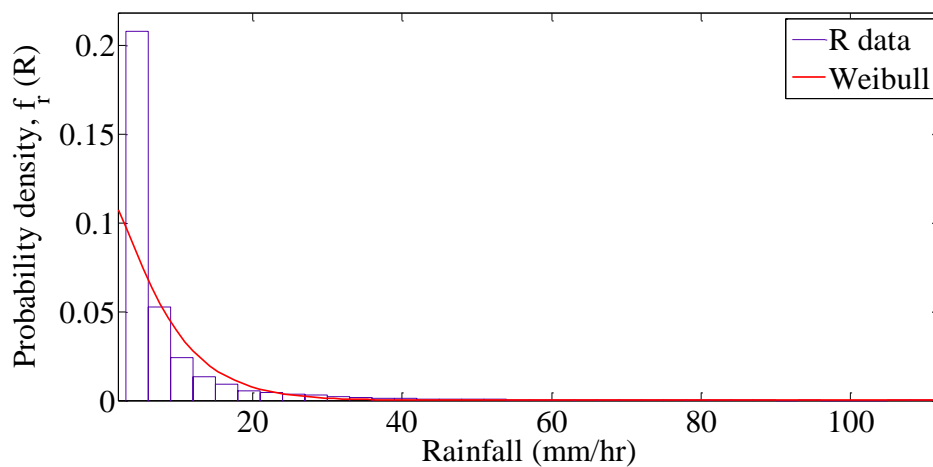


Figure 2.11 Weibull distribution for rainfall intensity (mm/hr)

The R-square of the fitting can be compared and final decision can be made to use either weibull or Gamma. Figures 2.9 and 2.10 show the probability density of rainfall fitted to weibull and gamma distributions.

### 2.3.1.3. Probability of wind speed, direction and rainfall intensity

The probability of wind speed, direction and rainfall can be found from the following equation 2.10. in which  $f_r(R)$  is the frequency of the rainfall intensity,  $\Omega_r$  occurrence probability of the rain-wind induced vibration level.

$$\begin{aligned}
 P_{(u,\theta)}\{(U, \theta) \in \Omega_{u,\theta}^{A_s}\} &= \int_{\Omega_{u,\theta}} \int_{A_s} f_{\theta}(\theta) f_{u,\theta}(U, k(\theta), c(\theta)) du d\theta \\
 P_r(B|A) &= P_r(B \in \Omega_r) = \int_{\Omega_r} f_r(R) dR \\
 P_{(u,\theta)}\{(U, \theta) \in \Omega_{u,\theta}^{A_s} \cap (B \in \Omega_r)\} \\
 &= P_r(A) \int_{\Omega_r} f_r(R) dR \int_{\Omega_{u,\theta}} \int_{A_s} f_{\theta}(\theta) f_{u,\theta}(U, k(\theta), c(\theta)) du d\theta
 \end{aligned}
 \tag{2.14}$$

### 2.3.1.4. Application of the Joint probability model for wind speed and direction (rainfall is assumed to be a independent event)

The wind speed falling on each direction is counted based on the rainfall count and occurrence probability distribution was calculated according to the equation. The occurrence table is shown in table 2.2.

$$(P_{U,\theta}) = \left( \frac{N_{U,\theta}}{N * \Delta U * \Delta \theta} \right) \tag{2.15}$$

Where U=wind velocity,  $\theta$  is the wind direction,  $N_{v,\theta}$ =Number of count of wind data (occurrence of wind speed and direction), N is the total number of wind data. The joint

occurrence probability of wind speed and direction  $P_{U,\theta}$  was obtained from equation 2.15 and is shown in table 2.2. The wind data was fitted using the weibull distribution and the modal parameters are obtained. The modal parameters such as shape parameter, scale parameter, mean and variance are shown in table 2.3. These modal parameters in other words define the shape and size of distribution. The relative frequency, shape and scale parameter are again plotted and shown in the figure 2.12. It can be seen that from figure 2.12 (b), the scale parameter is large for South South West and West directions and which means that the distribution width is large or these two occupies more wind speeds ranges than other directions.

Table 2.2 Relative frequency of wind data (W-matrix) for probability model I

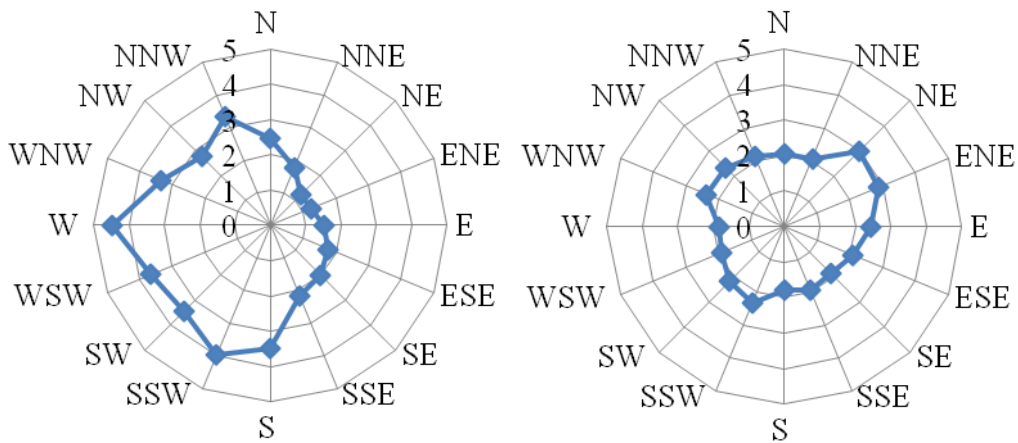
$\theta$	U (m/s)								
	0-3	3-6	6-9	9-12	12-15	15-18	18-21	>21	Total
N	3.9E-2	4.9E-2	2.7E-2	9.6E-3	3.8E-3	2.9E-4	1.4E-4	1.6E-4	1.3E-1
NNE	5.1E-2	2.5E-2	6.9E-3	1.7E-3	6.0E-4	3.2E-5	1.4E-5	8.3E-6	8.6E-2
NE	5.6E-2	6.9E-3	3.2E-4	3.7E-5	1.4E-6	0.0E+0	0.0E+0	0.0E+0	6.4E-2
ENE	5.4E-2	7.4E-3	3.9E-4	4.9E-5	1.4E-5	0.0E+0	0.0E+0	0.0E+0	6.2E-2
E	2.7E-2	1.0E-2	1.3E-3	2.1E-4	2.6E-5	1.4E-6	0.0E+0	0.0E+0	3.9E-2
ESE	1.4E-2	8.1E-3	1.6E-3	4.5E-4	1.9E-4	9.7E-6	5.5E-6	2.8E-6	2.5E-2
SE	9.5E-3	5.7E-3	2.0E-3	8.4E-4	4.4E-4	2.1E-5	1.4E-6	1.1E-5	1.9E-2
SSE	1.0E-2	7.4E-3	3.4E-3	1.2E-3	5.5E-4	3.9E-5	5.5E-6	2.8E-6	2.3E-2
S	9.8E-3	9.6E-3	7.7E-3	6.1E-3	6.7E-3	1.4E-3	6.1E-4	2.8E-4	4.2E-2
SSW	1.0E-2	1.8E-2	3.4E-2	2.9E-2	1.9E-2	3.3E-3	1.5E-3	9.4E-4	1.2E-1
SW	7.2E-3	1.4E-2	2.0E-2	1.1E-2	5.1E-3	9.7E-4	5.0E-4	3.2E-4	5.8E-2
WSW	8.4E-3	1.2E-2	1.2E-2	8.3E-3	7.2E-3	1.7E-3	7.5E-4	5.9E-4	5.1E-2

W	1.2E-2	1.0E-2	1.2E-2	1.2E-2	1.8E-2	4.5E-3	2.7E-3	2.8E-3	7.4E-2
WNW	8.1E-3	1.3E-2	1.6E-2	1.1E-2	6.3E-3	4.0E-4	6.5E-5	3.5E-5	5.5E-2
NW	8.8E-3	1.3E-2	1.1E-2	5.1E-3	1.6E-3	3.5E-5	2.8E-6	4.2E-6	4.0E-2
NNW	2.0E-2	3.1E-2	2.9E-2	2.0E-2	1.6E-2	1.4E-3	3.5E-4	2.1E-4	1.2E-1
Total	3.5E-1	2.4E-1	1.9E-1	1.2E-1	8.5E-2	1.4E-2	6.7E-3	5.4E-3	1

Table 2.3 Modal parameters in different wind directions

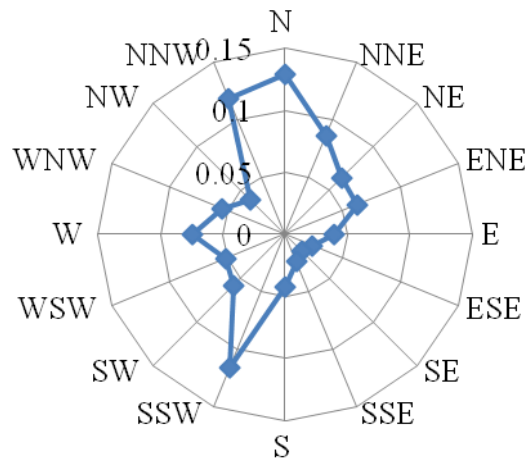
Wind direction $\theta$ degrees	Relative frequency $f(\theta)$	Weibull distribution				
		Modal Parameters		Mean	Variance	Coefficient of determination
		$a(\theta)$ (scale)	$b(\theta)$ (shape)	$\mu$	$\sigma^2$	
N	1.3E-1	2.48	2.06	2.19	1.24	1.00
NNE	8.6E-2	1.76	2.06	1.56	0.63	0.99
NE	6.4E-2	1.24	2.99	1.11	0.16	0.98
ENE	6.2E-2	1.26	2.86	1.13	0.18	0.99
E	3.9E-2	1.53	2.42	1.36	0.36	0.99
ESE	2.5E-2	1.76	2.07	1.56	0.62	0.98
SE	1.9E-2	2.01	1.86	1.79	1.00	0.99
SSE	2.3E-2	2.16	1.94	1.91	1.05	0.99
S	4.2E-2	3.48	1.77	3.10	3.26	0.98
SSW	1.2E-1	3.99	2.32	3.53	2.62	0.99
SW	5.8E-2	3.45	2.18	3.05	2.19	0.99
WSW	5.1E-2	3.65	1.90	3.24	3.14	1.00
W	7.4E-2	4.48	1.84	3.98	5.03	0.99

WNW	5.5E-2	3.37	2.36	2.98	1.80	1.00
NW	4.0E-2	2.76	2.34	2.44	1.23	1.00
NNW	1.2E-1	3.34	2.12	2.96	2.15	1.00
Total	1.00	42.70	35.09	37.88	26.67	15.83
Average		2.67	2.19	2.37	1.67	0.99



(a) Weibull Scale parameter  $a(\theta)$

(b) Weibull Shape parameter  $b(\theta)$



(c) Relative frequency of wind direction  $f(\theta)$

Figure 2.12 Weibull distributions and relative frequency of 10 minute mean wind speed for 15 years data

Table 2.4 shows the distribution of rainy events from the collected rainfall data, whereas the total probability of rainy events can be found by dividing the probability of rainy events to the probability of total events.

Table 2.4 Distribution of rain events only

	Events without rain $P_r(WR)$	Total rainy events $(P_r(R))$	0-30 mm/hr $P_r(R10)$	30-60 mm/hr $P_r(R40)$	>60 mm/hr $P_r(R70)$
Events	695552	24017	23526	419	72
$P_r(R)$	0.97	0.03	0.03	0	0

Since the vibration amplitude of the stay cable under rain-wind induced vibration is not only velocity restricted but also dependent on rainfall intensity (Vinayagamurthy et. al, 2013, S. Zhan, 2008) and thus it is necessary to include the effect of rainfall intensity in to the relative frequency of wind. Table 10 shows the distribution of rainy events from the collected rainfall data, whereas the total probability of rainy events can be found by dividing the probability of rainy events to the probability of total events.

$$P_r(T) = \text{Total number of rainy events} = 24017$$

$$P_r(R10) = \text{Probability of 10 mm/hr rainfall} = 0.03$$

Similarly  $P_r(R40)$  and  $P_r(R70)$  were obtained. The vibration amplitude obtained for three different categories of rainfall conditions namely 10, 40 and 70 mm/hr. And thus it is assumed that 1-30 mm/hr rainfall can be grouped to 10 mm/hr, 30-60 mm/hr to 40 mm/hr and anything above 60 mm/hr to 70 mm/hr rainfall intensity of the experimental conditions and this will be dealt in the sections of chapter VII. The probability of wind in 10 mm/hr condition can be obtained by multiplying the  $P_r(R10)$  with the relative frequency of wind data, which is also called as  $W_{10}$ \*matrix or the relative frequency of wind in different

direction in 10 mm/hr rainfall condition. Similarly,  $W_{40}^*$  and  $W_{70}^*$  can be found. The  $W_{10}^*$ ,  $W_{40}^*$  and  $W_{70}^*$  matrix will be further used in chapter VII to evaluate the fatigue life.

### 2.3.2 Probability of wind speed in the most unfavorable direction

It is then decided to consider the probability of relative wind speed in most unfavorable direction (figure 2.13). One dimensional wind speed is considered as multivariate weibull distributions. The joint distributions of the two parameters can be obtained by 2.18. In other words it can be said that the relative frequency of all wind comes from the most critical direction.

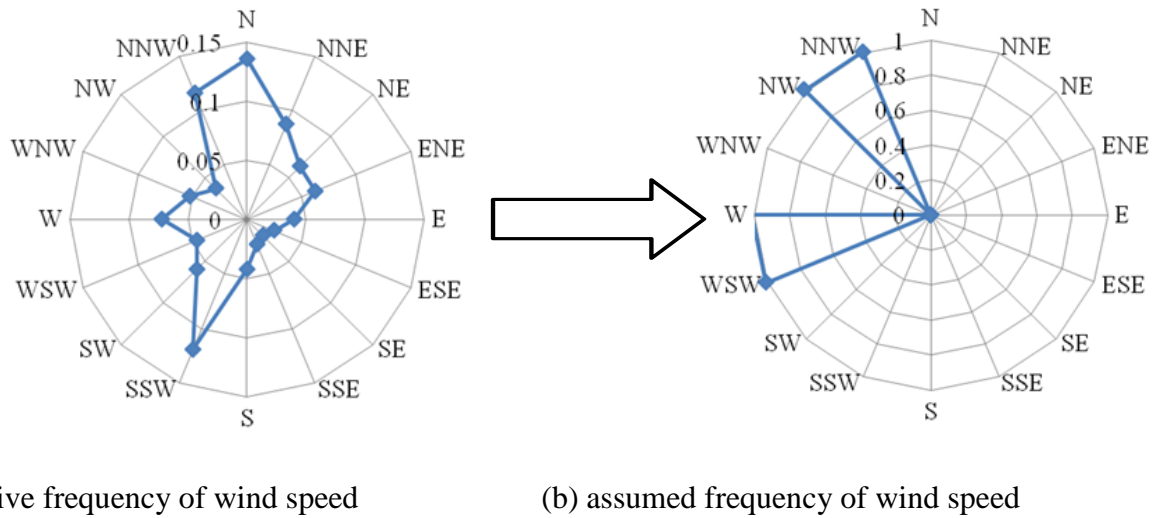


Figure 2.13 Relative frequency and assumed frequency of wind speed

The Joint probability density and cumulative distribution function of the wind speed ( $U$ ) and wind direction ( $\theta$ ) can be given by,

$$f_{U,\theta}(U, b(\theta_{critical}), a(\theta_{critical})) = \frac{b(\theta)}{a(\theta)} \left[ \frac{U}{a(\theta)} \right]^{b(\theta_{critical})-1} \exp \left[ - \left[ \frac{U}{a(\theta)} \right]^{b(\theta_{critical})} \right] \quad 2.16$$

$$P_{\theta}(\theta_{critical}) = \int_0^{\theta} f_{\theta}(\theta) d\theta \quad 2.17$$

$$P_{u,\theta}(U, \theta_{critical}) = P_{\theta}(\theta) \left( 1 - \exp \left[ - \left( \frac{U}{a(\theta)} \right)^{b(\theta)} \right] \right) \quad 2.18$$

$$P_{(u,\theta_{critical})} \{ (U, \theta) \in \Omega_{u,\theta}^{A_s} \cap (B \in \Omega_r) \} \quad 2.19$$

$$= P_r(A) \int_{\Omega_r} f_r(R) dR \int_{\Omega_{u,\theta}} \int_{A_s} f_{\theta}(\theta) f_{u,\theta}(U, k(\theta), c(\theta)) du d\theta$$

in which  $\theta$  is the wind direction from  $0^\circ$  to  $360^\circ$ .

Since it can be seen from chapter VII, that the most unfavorable wind direction for the stay cable is from West South West to North West West and thus a portion of the matrix is displayed in table 2.5.

Table 2.5 Probability density of wind speed in the most unfavorable direction (rainfall is assumed to be independent)

$\theta$	U (m/s)								Sum
	0-3	3-6	6-9	9-12	12-15	15-18	18-21	>21	
WSW	3.5E-1	2.4E-1	1.9E-1	1.2E-1	8.5E-2	1.40E-02	6.70E-03	5.40E-3	1
W	3.5E-1	2.4E-1	1.9E-1	1.2E-1	8.5E-2	1.40E-02	6.70E-03	5.40E-3	1
WNW	0	0	0	0	0	0	0	0	0
NW	3.5E-1	2.4E-1	1.9E-1	1.2E-1	8.5E-2	1.40E-02	6.70E-03	5.40E-3	1
NNW	3.5E-1	2.4E-1	1.9E-1	1.2E-1	8.5E-2	1.40E-02	6.70E-03	5.40E-3	1
Sum	1.4	9.6E-1	7.6E-1	4.8E-1	3.4E-1	5.60E-02	2.68E-02	2.16E-2	4

Similar to section 2.3.1.4, the probability of wind in each rainfall condition can be obtained by multiplying the  $P_r(R)$  (Probability of rainy event) with the relative frequency of wind. The obtained  $W_{10}^*$ ,  $W_{40}^*$  and  $W_{70}^*$  matrix will be further used in chapter VII to

evaluate the fatigue life.

### 2.3.3 Joint probability model for wind data considering rainfall as a dependent event

The probability distributions explained in sections 2.3.1.1, 2.3.1.2, and 2.3.1.3 are again applied in this model for different rainfall conditions. The Joint probability of wind speed and wind direction was obtained separately grouped under three different rainfall conditions. i.e., R10 (10-30 mm/hr) representing the low-rainfall condition, R40 (30-60 mm/hr) representing the medium-rainfall condition and R70 (above 60 mm/hr) representing the heavy-rainfall condition. The joint occurrence of wind speed and direction for different rainfall conditions i.e., R10, R40 and R70 is obtained and are shown in table 2.6, 2.7 and 2.8. The relative frequency of wind speeds in different direction under three different rainfall conditions are shown in figure 2.13. In the previous section 2.3.1.4, the probability of wind is multiplied with the probability of rainfall to obtain the joint probability of wind speed, direction and rainfall, whereas in this section, it can be seen that the rainfall is a dependent event and thus the obtained relative frequency itself gives the joint probability of wind speed, direction and rainfall. Table 2.6, 2.7 and 2.8 are also called as  $W_{10}^*$ ,  $W_{40}^*$  and  $W_{70}^*$  matrix, and these matrices will be further used in chapter VII to evaluate the fatigue life considering the rainfall as a dependent event.

Table 2.6 Relative frequency of wind data under R10 rainfall condition

$\theta$	U (m/s)								
	0-3	3-6	6-9	9-12	12-15	15-18	18-21	>21	Sum
N	4.9E-02	7.9E-02	4.4E-02	1.5E-02	4.3E-03	2.6E-03	4.2E-03	2.8E-03	1.2E-02
NNE	4.7E-02	4.0E-02	1.7E-02	7.1E-03	2.7E-03	1.1E-03	1.0E-03	2.6E-04	1.2E-01

NE	2.6E-02	9.0E-03	1.4E-03	4.3E-04	4.3E-05	0.0E+00	0.0E+00	0.0E+00	3.7E-02
ENE	2.1E-02	9.7E-03	2.4E-03	3.4E-04	1.3E-04	0.0E+00	0.0E+00	0.0E+00	3.3E-02
E	2.0E-02	1.4E-02	6.2E-03	1.3E-03	3.4E-04	0.0E+00	4.3E-05	0.0E+00	4.3E-02
ESE	1.5E-02	1.4E-02	6.6E-03	2.7E-03	1.3E-03	7.2E-04	2.1E-04	0.0E+00	4.0E-02
SE	1.0E-02	1.1E-02	8.7E-03	6.1E-03	3.2E-03	8.5E-04	1.3E-04	0.0E+00	4.0E-02
SSE	1.0E-02	1.1E-02	1.0E-02	6.2E-03	3.7E-03	1.2E-03	5.1E-04	0.0E+00	4.3E-02
S	9.0E-03	1.1E-02	1.2E-02	9.3E-03	9.7E-03	7.5E-03	1.0E-02	1.9E-03	7.0E-02
SSW	1.1E-02	1.5E-02	2.0E-02	2.1E-02	2.1E-02	1.5E-02	1.9E-02	6.3E-03	1.3E-01
SW	7.4E-03	8.2E-03	8.2E-03	5.1E-03	4.9E-03	3.9E-03	4.8E-03	1.0E-03	4.3E-02
WSW	6.0E-03	6.4E-03	5.7E-03	5.1E-03	3.5E-03	2.6E-03	3.1E-03	1.7E-03	3.4E-02
W	7.4E-03	4.8E-03	4.1E-03	4.2E-03	4.3E-03	3.4E-03	4.9E-03	2.6E-03	3.6E-02
WNW	6.9E-03	5.4E-03	4.0E-03	3.1E-03	1.7E-03	1.3E-03	5.5E-04	5.5E-04	2.4E-02
NW	9.2E-03	6.8E-03	3.1E-03	1.3E-03	5.1E-04	2.1E-04	2.1E-04	4.3E-05	2.1E-02
NNW	2.1E-02	2.7E-02	2.1E-02	9.0E-03	4.3E-03	1.7E-03	3.9E-03	1.7E-03	8.9E-02
Sum	2.8E-01	2.7E-01	1.8E-01	9.7E-02	6.6E-02	4.2E-02	5.3E-02	1.9E-02	1.0E+00

Table 2.7 Relative frequency of wind data under R40 rainfall condition

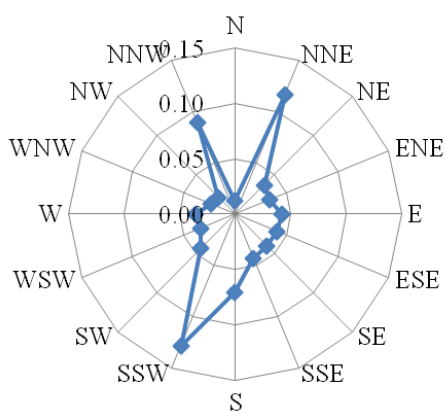
$\theta$	U (m/s)								Total
	0-3	3-6	6-9	9-12	12-15	15-18	18-21	>21	
N	1.7E-2	3.3E-2	4.8E-3	2.4E-3	7.2E-3	0.0E+0	0.0E+0	2.4E-3	6.7E-02
NNE	1.9E-2	1.4E-2	4.8E-3	0.0E+0	0.0E+0	0.0E+0	0.0E+0	0.0E+0	3.8E-02
NE	1.4E-2	1.2E-2	0.0E+0	2.4E-3	0.0E+0	0.0E+0	0.0E+0	0.0E+0	2.9E-02
ENE	4.8E-3	1.4E-2	0.0E+0	0.0E+0	0.0E+0	0.0E+0	0.0E+0	0.0E+0	1.9E-02
E	7.2E-3	7.2E-3	2.4E-3	2.4E-3	0.0E+0	0.0E+0	0.0E+0	0.0E+0	1.9E-02

ESE	9.5E-3	1.7E-2	1.2E-2	0.0E+0	0.0E+0	0.0E+0	2.4E-3	2.4E-3	4.3E-02
SE	1.4E-2	9.5E-3	1.7E-2	0.0E+0	2.4E-3	0.0E+0	0.0E+0	4.8E-3	4.8E-02
SSE	2.4E-3	1.7E-2	1.2E-2	9.5E-3	4.8E-3	4.8E-0	0.0E+0	0.0E+0	5.0E-02
S	9.5E-3	2.4E-2	9.5E-3	1.7E-2	7.2E-3	1.2E-2	1.2E-2	7.2E-3	9.8E-02
SSW	2.4E-3	2.6E-2	3.8E-2	2.4E-2	3.6E-2	5.0E-2	3.8E-2	1.7E-2	2.3E-01
SW	2.4E-3	1.7E-2	1.2E-2	1.9E-2	7.2E-3	1.2E-2	2.4E-2	4.8E-3	9.8E-02
WSW	4.8E-3	9.5E-3	1.2E-2	1.4E-2	1.2E-2	9.5E-3	1.4E-2	4.8E-3	8.1E-02
W	9.5E-3	9.5E-3	2.4E-3	4.8E-3	7.2E-3	7.2E-3	1.2E-2	2.4E-3	5.5E-02
WNW	7.2E-3	2.4E-3	2.4E-3	0.0E+0	0.0E+0	0.0E+0	0.0E+0	2.4E-3	1.4E-02
NW	9.5E-3	2.4E-3	7.2E-3	2.4E-3	0.0E+0	2.4E-3	0.0E+0	2.4E-3	2.6E-02
NNW	7.2E-3	1.7E-2	1.7E-2	9.5E-3	4.8E-3	2.4E-3	9.5E-3	1.7E-2	8.4E-02
Total	1.4E-1	2.3E-1	1.5E-1	1.1E-1	8.8E-2	1.0E-1	1.1E-1	6.7E-2	1

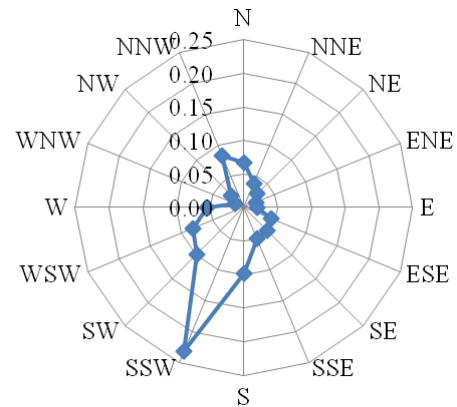
Table 2.8 Relative frequency of wind data under R70 rainfall condition

$\theta$	U (m/s)								
	0-3	3-6	6-9	9-12	12-15	15-18	18-21	>21	Total
N	5.6E-2	2.8E-2	1.4E-2	1.4E-2	0.0E+0	0.0E+0	0.0E+0	0.0E+0	1.1E-1
NNE	0.0E+0	1.4E-2	0.0E+0	0.0E+0	0.0E+0	0.0E+0	0.0E+0	0.0E+0	1.4E-2
NE	2.8E-2	1.4E-2	1.4E-2	0.0E+0	0.0E+0	0.0E+0	0.0E+0	0.0E+0	5.6E-2
ENE	1.4E-2	0.0E+0	1.4E-2						
E	1.4E-2	2.8E-2	0.0E+0	1.4E-2	0.0E+0	0.0E+0	0.0E+0	0.0E+0	5.6E-2
ESE	1.4E-2	2.8E-2	0.0E+0	0.0E+0	0.0E+0	0.0E+0	0.0E+0	0.0E+0	4.2E-2
SE	1.4E-2	1.4E-2	2.8E-2	0.0E+0	0.0E+0	0.0E+0	0.0E+0	1.4E-2	6.9E-2
SSE	0.0E+0	1.4E-2	2.8E-2	1.4E-2	2.8E-2	1.4E-2	0.0E+0	0.0E+0	9.7E-2

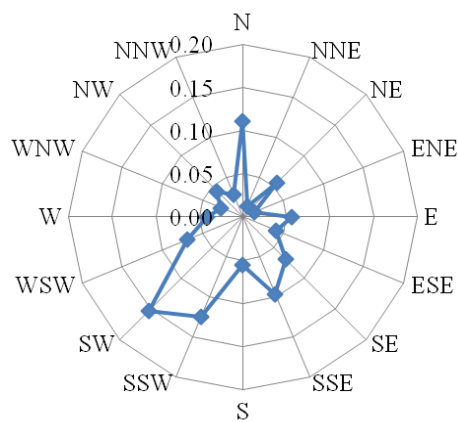
S	0.0E+0	1.4E-2	0.0E+0	0.0E+0	0.0E+0	1.4E-2	1.4E-2	1.4E-2	5.6E-2
SSW	0.0E+0	0.0E+0	1.4E-2	1.4E-2	1.4E-2	6.9E-2	0.0E+0	1.4E-2	1.3E-1
SW	0.0E+0	0.0E+0	2.8E-2	2.8E-2	2.8E-2	5.6E-2	0.0E+0	1.4E-2	1.5E-1
WSW	0.0E+0	1.4E-2	1.4E-2	0.0E+0	1.4E-2	1.4E-2	0.0E+0	1.4E-2	6.9E-2
W	0.0E+0	0.0E+0	1.4E-2	0.0E+0	1.4E-2	1.4E-2	0.0E+0	0.0E+0	4.2E-2
WNW	0.0E+0	1.4E-2	1.4E-2	0.0E+0	0.0E+0	0.0E+0	0.0E+0	0.0E+0	2.8E-2
NW	1.4E-2	1.4E-2	1.4E-2	0.0E+0	0.0E+0	0.0E+0	0.0E+0	0.0E+0	4.2E-2
NNW	0.0E+0	1.4E-2	1.4E-2	0.0E+0	0.0E+0	0.0E+0	0.0E+0	0.0E+0	2.8E-2
Total	1.5E-1	2.1E-1	1.9E-1	8.3E-2	9.7E-2	1.8E-1	1.4E-2	6.9E-2	1



(a) R10 rainfall condition



(b) R40 rainfall condition



(c) R70 rainfall condition

Figure 2.14 Relative frequency of wind direction  $f(\theta)$  under different rainfall conditions

## 2.4 References

1. Y. Hikami, N. Shiraishi, 1988, Rain-wind induced vibrations of cables in cable stayed bridges, *Journal of Wind Engineering and Industrial Aerodynamics*, 29, pp. 409-418.
2. Ming Gu, Xiaoqin Du, 2005 'Experimental investigation on rain-wind-induced vibration of cables in cable-stayed bridges and its mitigation', *Journal of Wind Engineering and Industrial Aerodynamics*, 93, pp. 79-95.
3. S. Zhan, Y.L. Xu, H.J. Zhou, K.M. Shum, 2008 'Experimental study of wind-rain-induced vibration using a new model setup scheme', *Journal of Wind Engineering and Industrial Aerodynamics*, 96. pp. 2438-2451.
4. Lin-Shan Xu, Yao-Jun Ge, Lin Zhao, 2009 , 'Experimental Investigation on Rain-Wind-Induced Vibration of Stay Cables based on High precision raining machine', *7<sup>th</sup> Asia Pacific Conference on Wind Engineering*, November 8-12, Taipei, Taiwan.
5. Cosentino, N., Flamand, O. and Ceccoli, C., 2003, "Rain-wind induced oscillations of inclined stay cables Part I: Experimental investigation and physical explanation", *Wind and Structures*, Vol. 6, No. 6, pp 471-484.
6. Cosentino, N., Flamand, O. and Ceccoli, C., 2003, "Rain-wind induced oscillations of inclined stay cables Part I: Mechanical modeling and parameter Characterization", *Wind and Structures*, Vol. 18, No. 6, pp 485-498.
7. Y.L.Xu., J.Chen, C.L. Ng., H.J.Zhou, No.1/Feb 2008, Occurrence probability of wind rain induced stay cable vibration, *Advances in structural Engineering*, 1369-4332, volume 11, pp. 53-69
8. Yaojun Ge, Haifan Xiang, 2002, Statistical study of mean wind velocity in shanghai

- area, *Journal of wind Engineering and Industrial Aerodynamics*, 91,pp.1585-1599
9. Jun Chen, Xiaoqin Zhang, 2009, An Empirical Joint Probability Density function of wind speed and direction, *7th Asia Pacific Conference on Wind Engineering*, Nov., 8-12, Taipei, Taiwan
  10. Y.Q. Ni, X.Y. Wang, Z.Q. Chen, J.M. Ko, 2007, Field observations of rain-wind-induced cable vibration in cable-stayed Dongting Lake Bridge, *Journal of Wind Engineering and Industrial Aerodynamics*, 95, 303-328.
  11. Response of Bridges to wind, by Jim Hay, State of the Art review/5, 1992
  12. McWilliams B., Newmann M.M., and Sprevak D., 1979, "The Probability Distribution of Wind Velocity and Direction", *Wind Engineering*, Vol. 3, No. 4. pp 269-273.



## **CHAPTER III**

# **EXPERIMENT ON RAIN-WIND INDUCED VIBRATION ON THE STAY CABLES**

### **3.1 Introduction**

There are series of tests conducted on rain-wind induced vibrations and these tests were conducted for specific number of parameters concerning rain-wind induced vibrations. Since most of the stay cable fatigue damage is believed to be caused by rain-wind induced vibration as it causes large amplitude vibrations. Thus a study was carried out to study the response of the stay cable under the action of wind and rain. The following chapter explains the experimental setup, phenomenon behind rain-wind induced vibrations, results of rain-vibration test carried out for a large number of cases.

### **3.2 Literature review**

The researchers used three main ways to study the characteristics of rain-wind induced vibrations. The first one is by simulating the real rain environment (Y. Hikami 1988, M.Matsumoto 1990, Olivier Flamand 1995, Akihiro HONDA 1995, C.Verwiebe 1998, Ming Gu 2005, S.Zhan 2008, Yong-le Li, Lin-Shan Xu 2009) and the second is by sticking the artificial rivulets to the cable surface (Bosdogianni 2005, Ming Gu 2008, Ming Gu 2009) and

the third way is to pouring water at one end of the cable. And lot more researchers tried to suppress these vibrations by modifying the surface of the cable (Phelan S., 2006, M.Gu., 2005). The author perceives that the simulating rain will be more reliable than fixing an artificial rivulet to understand the phenomenon. Researchers tried to understand the phenomenon of rain-wind induced vibrations using variety of techniques. Some of the researchers studied the phenomenon using analytical models, semi-analytical and even more they relayed on computational methods. Some of the literatures were listed in this section.

Hikami (1988) conducted a test on a prototype model inclined and yawed at  $45^\circ$ , found very large amplitude vibration under the condition of wind and rain and he coined that the motion of the upper rivulet (formed over the cable) due to the wind is the reason for such vibrations, Matsumoto (1990) conducted his experiment on a cylinder yawed at  $45^\circ$  and put forth his view stating that the vibration is due to the existence of the secondary axial flow. Some of the notable remarks made by the researchers in the past were that the Rain-wind induced stay cable vibration occurs during a short period which involves the action of both wind and rain, which are characterized by a much lower frequency than vortex induced vibration and by a much higher amplitude. Motion of the rivulet is responsible for the aerodynamic instability of the cable causing such large amplitude vibrations, and further it also confirms the existence of an intense axial flow along the cylinder axis, which plays a role of disturbing the regular vortex shedding Hikami (1988).

And much further Matsumoto (1990) conducted a flow-visualization to confirm the flow characteristics of a yawed cylinder. And further it is pointed that the excited mechanism of yawed cylinder can be attributed to the existence of the secondary axial flow. Flamand (1995) says that the dirt formed because of the dust coating over the cable allows the movement of the upper rivulet and consequently the excitation. When the researchers were keep on searching for the background reason for the rain-wind induced cable vibration, lot of

them started studying about the conditions or the effect of parameters influencing or contributing the vibration.

Ming Gu (2005) studied about the effect of wind speed, damping, inclination angle, wind yaw angle, and frequency by maintaining the rainfall at 340-390ml/ (min. m<sup>2</sup>) and the ways to suppress such vibrations. Out of his experiment, he concluded that rain-wind induced vibration is most severe when the inclination angle is 30° and wind yaw angles are 30° and 35°.

Later on very few researchers focused on the influence of rainfall intensity on the cable vibration, the one among them is Lin-Shan Xu (2009) studied the effects of inclination, yaw angles, damping, rainfall intensity (0-80 mm/hr), frequency for wind speeds up to 11 m/s. Out of his experimental results, he observed that rain-wind induced vibration occurs under the combination of light rain with higher wind speed (8.7 m/s) and heavy rain with lower wind speed (4.1 m/s).

Chen Wen-Li (2010) conducted an experiment and studied the aerodynamic forces on cables under rain-wind induced conditions. During the tests he captured and published few pictures in his papers and which shows the rivulet distribution over the cable surface.

S.Zhan, Y.L.Xu, (2008) studied the effects of rainfall intensity on stay cable inclined at 30° and yawed at 35° for different wind speeds and rainfall conditions. The observation showed that the amplitude decreases with increasing rainfall for a moderate wind speed.

Y.Q.Ni, (2008) carried out a field measurements continuously for 45 days on the cable stayed Dongting Lake Bridge to measure the vibrations due to rain-wind and traffic loading. The measurements show that cable vibrates when the wind speed at the deck is 6-14 m/s and the critical wind yaw angle is about 10° to 50°.

Flamand (1995) conducted his experiments on the cable inclined at 25° and varied the yaw angles from 0 to 90° (with an interval of 15°). For each cable inclination angle i.e.,

$\alpha=25^\circ, 30^\circ, 35^\circ, 40^\circ-50^\circ$  the wind yaw angle and rainfall intensity used by the previous researchers were plotted in figure 3.1, which also elucidates the limitations of the previous work and also the cases carried out in the present paper by fulfilling those limitations. From figure 3.1 it can be seen the present work in this paper covers a wide range of testing parameters such as rainfall intensity (R:0-70 mm/hr), wind speed(U:1-18 m/s), cable inclination angle( $\alpha:25^\circ-45^\circ$ ) and wind yaw angle ( $\beta:25^\circ-45^\circ$ ).

### 3.3 Objective of the Experiment

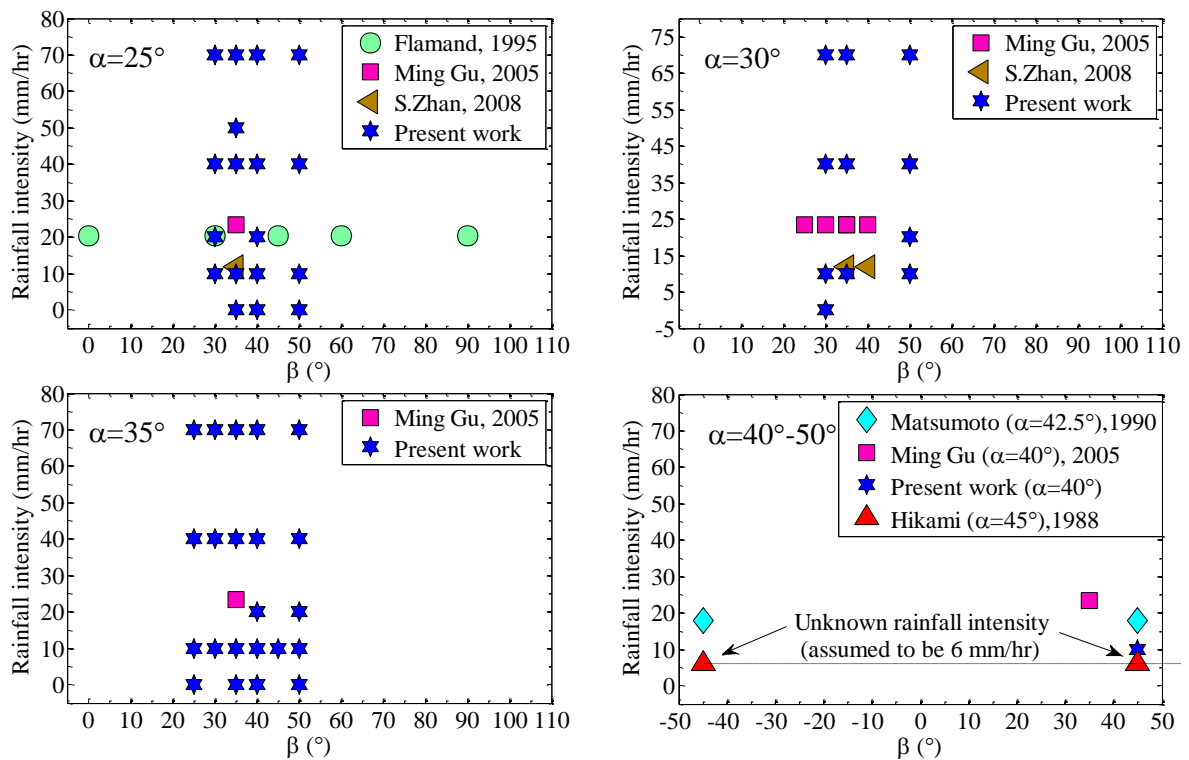


Figure 3.1 Limitations of the past research on rain-wind induced stay cable vibration

While compiling all the views of the past researchers explained in section 3.2, the interesting facts were revealed that cable vibration are limited to wind yaw angles are around  $30^\circ-45^\circ$ , inclination angles are from  $25^\circ-50^\circ$ , damping ratio's were around 0.08-0.15 %, and then it was decided to carry out an experiment to study the effect of rainfall intensity, wind

speed, position of the rivulet, inclination angles, wind yaw angles and damping ratio in a broad manner. Since, the large amplitude oscillations causes higher fluctuating stresses at the anchorage, which may reduce the life of the cables leading to fatigue and it is a must to consider damages due to such oscillations in to the design. And also for the safety it is necessary to evaluate the fatigue life of a cable due to such large amplitude vibrations induced by wind and rain.

In this chapter, the experimental results of the stay cable with diameters 155 mm and 128 mm were explained in detail. This chapter also focuses on the effects of variety of parameters concerning the positioning of the cable (inclination angle, wind yaw angle), environmental parameters (rain, wind speed) and the structural parameters like damping and frequency.

This chapter also discusses the mechanism behind of rain-wind induced vibration using the pictorial images (out of the experiment), and a deep study was carried out on the effects of various parameters such as inclination angle, yaw angle, rainfall intensity and diameter, concerning rain-wind induced vibration. And apart from that, the response curves were plotted and these results will be further used in the next chapters for estimating the fatigue life of the stay cable. The following section will briefly discuss about the wind tunnel and its setup for cable vibration, cable models and its parameters, and later on each of the parameters will be elaborately discussed to study its effects on amplitude.

### **3.4 Bridges undergone rain-wind induced vibration on cables**

Before introducing the experiment, it is necessary for us to know the bridges which were suffered by rain-wind induced vibrations and few of them are reported below for the reference.

1. Fred Hartman Bridge in Texas (US),
2. Sidney Lanier Bridge , Talmadge Memorial Bridge in Georgia (US),
3. Cochrane Bridge in Alabama,
4. Faroe Bridge in Denmark,
5. Aratsu Bridge , Tempohzan Bridge in Japan,
6. The Erasmus Bridge in Holland, and
7. The Nanpu and Yangpu Bridges in China.

### 3.5 Description about the wind tunnel

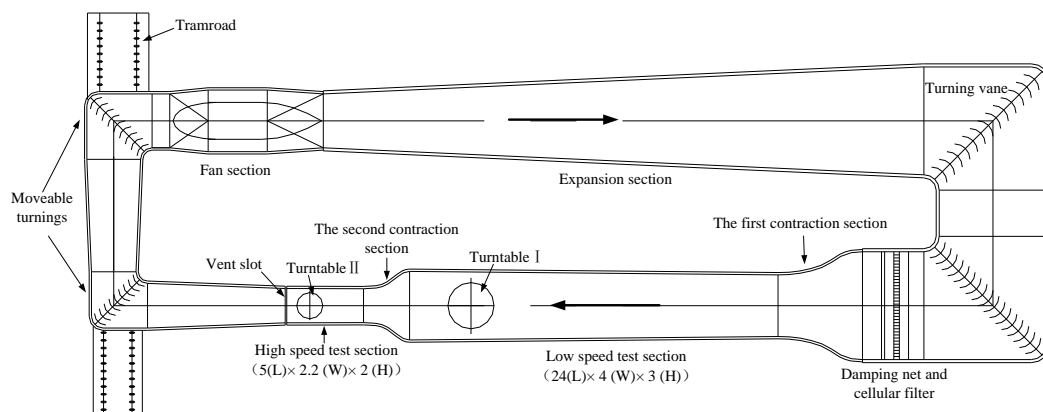


Figure 3.2 Schematic view of the wind tunnel in Shijiazhuang Tiedao University

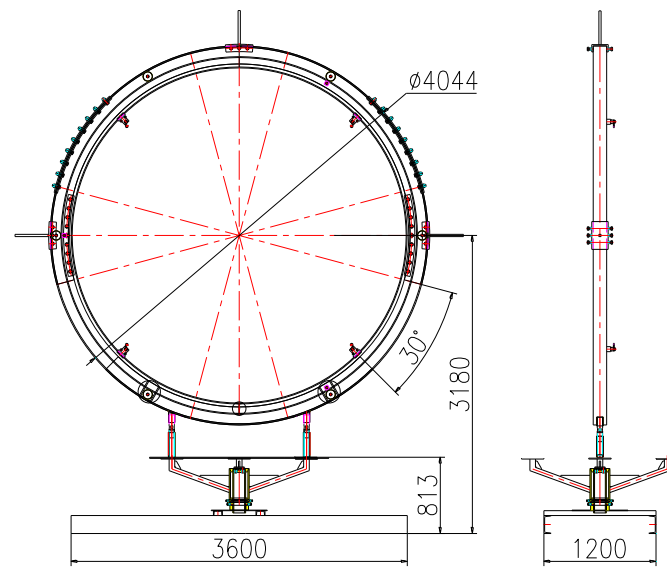
Since, rain-wind induced vibration is a non-conventional testing in the wind tunnel which requires rain-spraying unit in addition to the wind. The experiment tests were conducted at the multi-functional closed/open circuit type wind tunnel (Liu Qingkuan, 2011) at Shijiazhuang Tiedao University, which was built especially to deal with wind and rain-wind effects on structures. The closed wind tunnel was made to open at one of its exits and the exit cross-section of the wind tunnel is about 3 m (width) x 1.75 m (height) and the models were tested up for wind speeds varying from 1 – 18 m/s. The maximum wind speed at

the exit may go up to 20m/s with a turbulent intensity of 15%.

### **3.6 Description about the setup for rain-wind induced cable vibrations**

A rigid setup for mounting the stay was designed and manufactured to carry the large amount of forces that is expected to be produced from the prototype section of the stay cable. The setup consists two main parts viz. the upper structure and the lower turn table. The one is the upper structure which is made of four rims, four rollers, ball bearings etc. to rotate the rim to change the inclination angle ( $\alpha$ ) of the stay cable, and hooks were provided to hang the springs and the cable. The rigid setup was first fitted and moved by a heavy crane and made to sit over the lower turn table, which is heavy and rigid to support the vertical structure and the cable. The bottom structure or the turn table is used to change the yaw angle ( $\beta$ ) of the stay cable. This setup helps in rotating the inclination and yaw angles of the model in both clockwise and in the anticlockwise direction. And thus, the setup saves a lot of time for changing the angles with ease. And figure 3.2 shows the CAD model of the setup made for mounting the stay cable. Figure 3.4, shows the schematic view of the manufactured model with a cable hanged on to the rain-vibration setup with rainfall system installed. The rain-simulation unit is setup just above the experimental setup, and adjusted so that the rain-simulation unit sprinkles rain over the cable model. The submersible pump delivers water to the rain-simulating unit, which then sprinkles the water through their sprinkling heads.

There were 4 sprinkling nozzles at each end and comprises of 12 heads in total, is as shown in figure 3.4. The rain-water simulation unit can provide rain from 10 mm/hr to 180 mm/hr. This was done by precisely controlling the unit at a constant pressure.



All dimensions are in mm

Figure 3.3 Setup for the experiment on the rain-wind induced cable vibration.

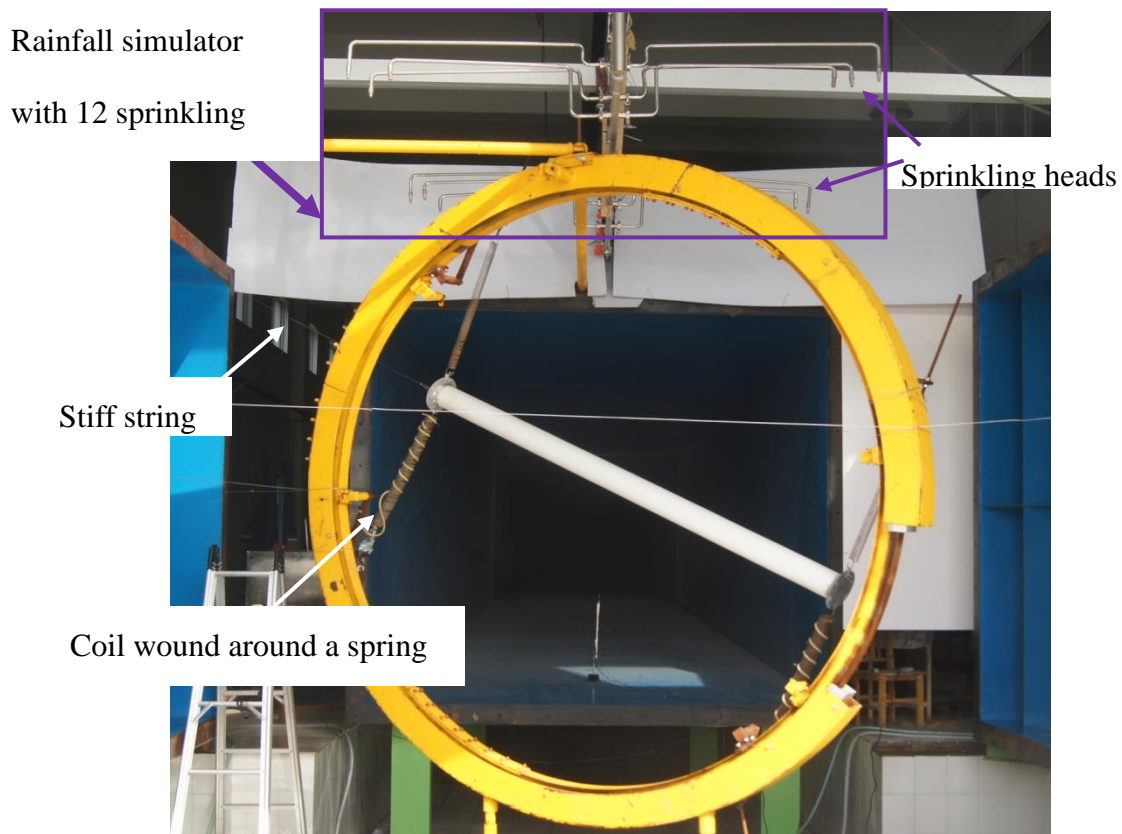


Figure 3.4 Cable hanged on to the Rain vibration setup with rainfall system installed

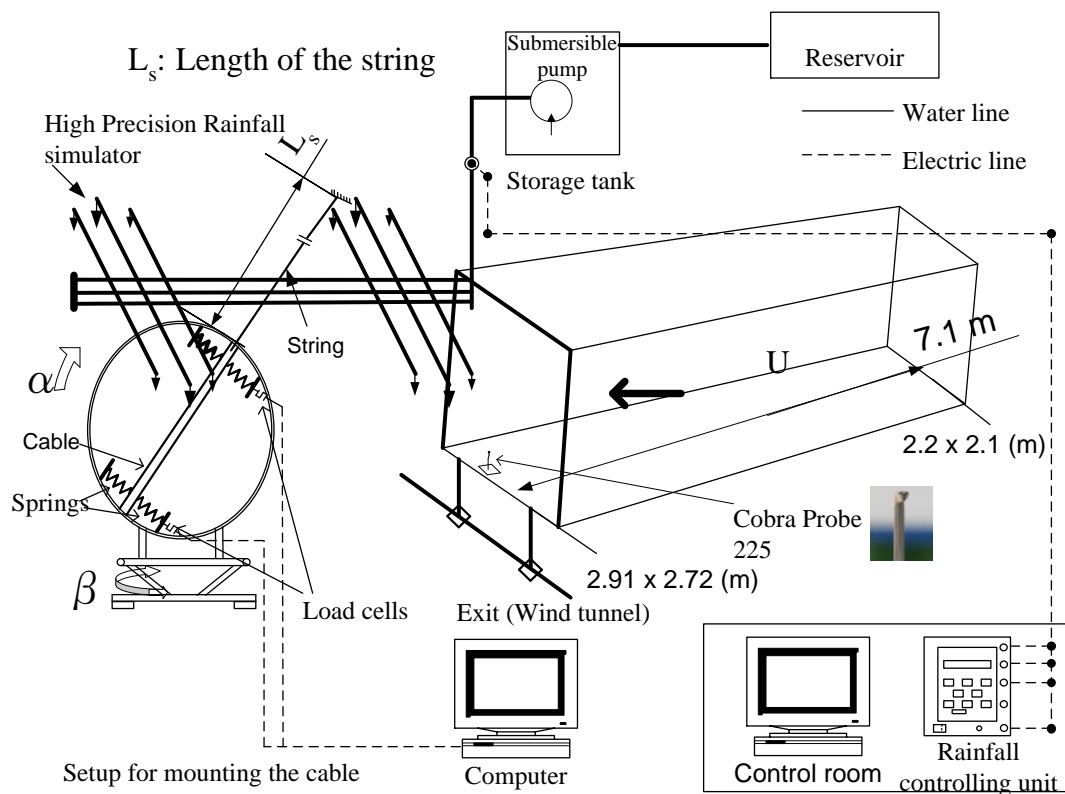


Figure 3.5 The schematic view of the total experimental setup

There were two load cells fitted to the bottom ends of the springs, which reads the forces and in turn the displacement of the cable was found at each of the springs. Figure 3, shows the schematic view of the total experimental setup. The cable model is hanged to the ceiling by means of a stiff string whose length ( $L_s > 4$  m) may vary according to the cable inclination and wind yaw angles. The main drawback of this setup is that it is strongly affected by the outside climatic conditions i.e., while carrying out the rain-tunnel experiments during winter, the rain may turn to ice.

The measurement system and other control devices used in the experiment, which is shown in figure 3.5 is as explained below.

### 3.6.1 Cobra 225 probe

The cobra probe is used to measure the velocity in space (for the three directions) at

the exit of the wind tunnel. It also gives the Turbulence intensities, Reynolds stresses for the three directions at that point.

### 3.6.2 Rainfall controller

The rainfall simulated in the raining machine is controlled by the rainfall controller. The rainfall controller controls the amount of water discharged at a given pressure. The rainfall simulator consists of three nozzles of different diameters to control the volume of water being discharged. The Pressure and intensity of rainfall are shown in the following table 3.1.

Table 3.1 Discharge rate and outlet pressure

Pressure (Mpa)	Rainfall (mm/hr)
0.08	40.5
0.10	41.4
0.12	43.4
0.14	45.0
0.16	49.5
0.18	60.1
0.20	72.4

### 3.6.3 Rain gauge

The rain gauge is kept just below rainfall simulator near the cable, which can precisely estimate the rain being simulated. The top open section (20x20 cm) will collect the vertical rain droplets and the side open section (20x20 cm) at the side will collect the rain droplets washes away by the wind.



Figure. 3.6 View of the rain gauge to calibrate rainfall intensity

A scale was fitted to the rain gauge to measure the amount of water collected over a period of time. Finally the collected rain water and controlled rain water was then calibrated. The distribution of water is not the same all over the ground. However the central part of the setup gives almost a considerable result.

#### 3.6.4 S-Type Load cells

The vibrations on the cable were measured in terms of force using these S-type load cells, as shown in figure 3.7. Later on, forces are changed to displacements. Each end of the spring carries a load cell, so there are two load cells connected at each end of the bottom springs.



Figure 3.7 S-type Load cell

### 3.6.5 Vibration recording devices (video):

In order to study the size and motion of the rivulet, the response of the cable with rivulet was precisely captured (Sony Alpha 55, Canon 14 Megapixels camera) for different combination of wind speeds and rainfall.

### 3.7 Wind speed measurement and flow stability

The longitudinal uniformity of the wind was tested ahead of the cable by placing the cobra probe at a distance of 161 cm, 171 cm, and 181 cm from the exit of the wind tunnel and also at the center of the cable. Figure 3.8 shows the uniformity of the wind measured at different places ahead of the cable and 3.9 shows the position of the cable with respect to the approaching flow.

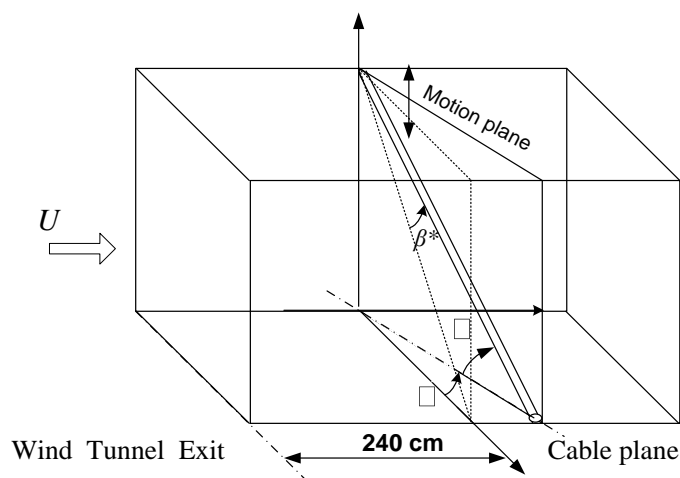


Figure 3.8 Setup, approaching flow, inclination and yaw angles

The wind at the exit of the wind tunnel and at the center of the cable was also obtained and plotted in figure 3.10, which shows a linear relation between them and is shown in equation (1).

$$U_{cable} = 1.058 U_{exit} + 0.932 \quad 3.1$$

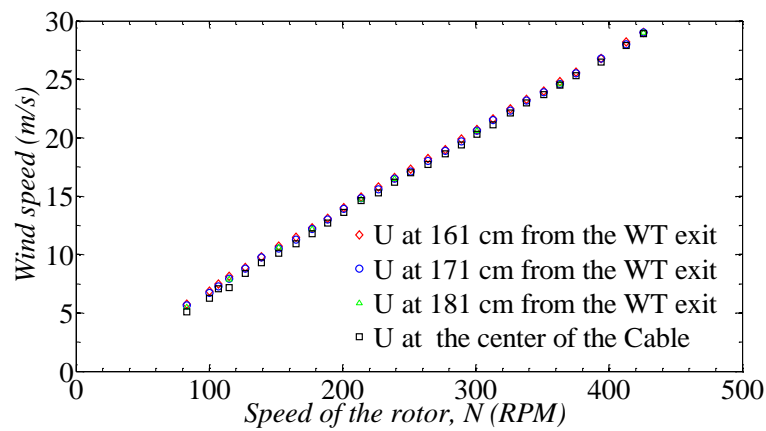


Figure 3.9 flow stability of the approaching wind towards the stay cable

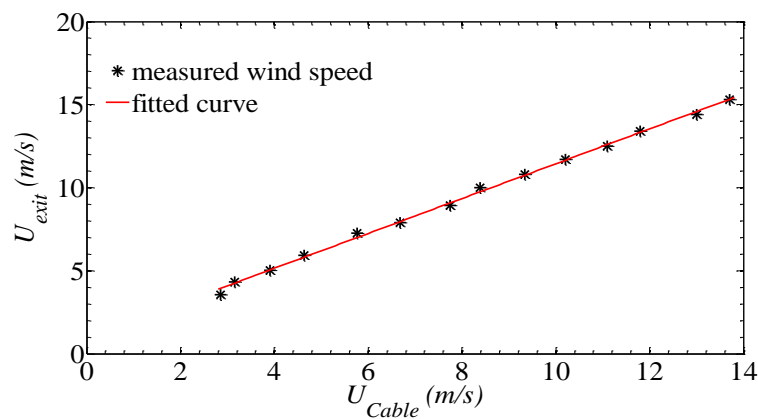


Figure 3.10 Relation between the wind at the exit of the wind tunnel and on the cable

### 3.8 Cable model and testing conditions

In this experiment, two cable models were used. Both the models were wrapped with polyethylene, which is usually used in the existing stay cables of the cable-stayed bridges. The first model is of 155 mm in diameter with a mass of 17.76 kg/m, whereas the second model is of 128 mm in diameter with a mass of 13.96 kg/m and was tested for the wind speeds from 1-18 m/s. The damping in the cable model was achieved by winding a coil around both the springs as shown in figure 3.11 and it is found by logarithmic decrement technique which is explained in the section of this chapter. The Scruton number for the

prototype cable models are 6.86 (M.Gu 2005) which is 11.37 times than that of the model I and 10.96 times than that of the model II) and 5.31 (Ni 2007) which is 8.81 times than that of the model I and 8.5 times than that of the model II).

The properties of the cable models were listed in Table 3.2 and the non-dimensional parameters are shown in Table 3.3. There were two labels made at either end of the cable to read the position of the rivulet with respect to the cable axis. The detail of the tests on the cable model I is shown in Table 3.4, and the test details of the cable model II is listed in Table 3.5.

Table 3.2 Properties of the Cable model I

		Model I	Model II	Unit
Diameter of the cable	$D$	0.155	0.128	m
Length of the cable	$L$	2.5	2.2	m
Mass of the cable	$M$	17.76	13.96	Kg/m
Damping ratio	$\xi$	0.1%	0.04%, 0.1%	
Natural frequency	$f_n$	1.02 and 1.07	0.88	Hz
Wind speed	$U$	1-18	1-18	m/s
Air density	$P$	1.225	1.225	Kg/m <sup>3</sup>
Kinematic viscosity	$N$	$15.1 \times 10^{-6}$	$15.1 \times 10^{-6}$	m <sup>2</sup> /s

Table 3.3 Non dimensional parameters of the Cable model I

			Model I	Model II
Reynolds number	$Re$	$\frac{UD}{\nu}$	10264.9-195033.11	8476.8-161059.6
Mass ratio	$m^*$	$\frac{m}{\rho D^2 L}$	603.45	488.09

Scruton number	$S_c$	$\frac{m\xi}{\rho D^2}$	0.6	0.27, 0.7
Reduced wind speed	$U_R$	$\frac{U}{fD}$	6.32-113.85 ( $f_n=1.02\text{Hz}$ ) 6.02-108.53 ( $f_n=1.07\text{Hz}$ )	8.8-168.6

Table 3.4 Details of the tests for the cable Model I

		$\alpha$			
		25°	30°	35°	40°
$\beta$	25°	-	-	R0, R10, R40, R70	-
	30°	R10, R20, R40, R70	R0, R10, R40, R70	R10, R40, R70	-
	35°	R0, R10, R40, R50, R70	R10, R40, R70	R0, R10, R40, R70	-
	40°	R0, R10, R20, R40, R70	R10, R40, R70	R0, R10, R20, R40, R70	-
	45°	-	-	R10	R10
	50°	R0, R10, R40, R70	R10, R20, R40, R70	R0, R10, R20, R40, R70	-
	Frequency, $f_n=1.02$ Hz			Frequency, $f_n=1.07$ Hz	
Note: R0: without rain; R10- R80-Represents the amount of Rainfall from 10 to 80 mm/hr.					

Table 3.5 Details of the tests for the cable Model II

		$\alpha$	
		25	30
B	30	R10, R40, R70	R10, R40, R70
	35	R10, R20, R30, R40, R50, R60, R70, R80	R10, R40, R70
Note: R-Represents Rainfall Intensity, whereas the number followed by R represents the intensity of rain in mm/hr.			

### 3.9 Data analysis: Filtering out the noisy signals

Data contains small and large time history and the low amplitude history carries large amount of noise. Since the experiment was carried out at the exit of the wind tunnel the data recorded is noisy and thus two kinds of filters were used to remove the noise i.e., Smoothing rloess and Savitzky-Golay filtering. Any one technique of both of them will be used based on the noise level of the signal.

### 3.10 Damping in the Cable models

Damping is simulated by winding a coil around the bottom springs as shown figure. In this method, the free vibration displacement amplitude history of the cable to an impulse (by means of hand) is measured and recorded. A free decay curve was obtained is shown in figure. Logarithmic decrement is the natural logarithmic value of the ratio of two adjacent peak values of displacement in free decay vibration.

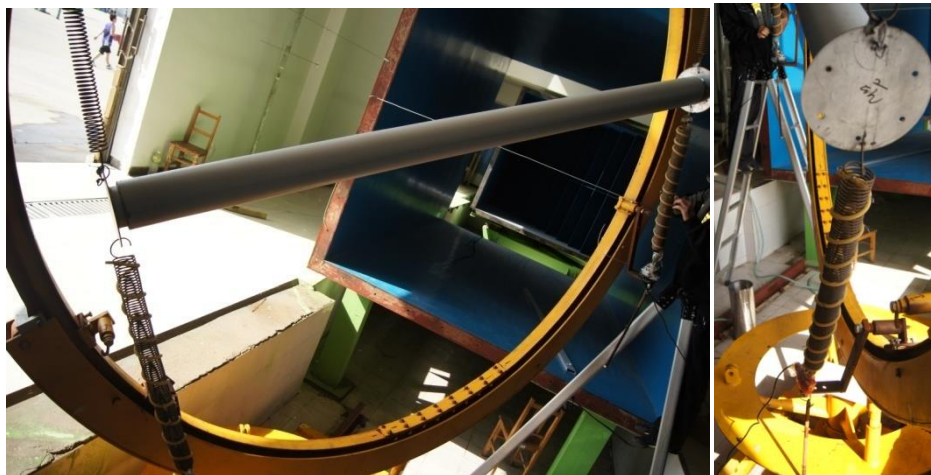


Figure 3.11 Damping in stay cables

The figure 3.12 shows the free decay of vibration amplitude and the fitted curve for the cable model I. The logarithmic decrement technique was applied to obtain the damping in the cable model.

$$f(t) = A e^{-\xi\omega t}$$

$$\xi\omega = 0.006586$$

$$\xi = \frac{0.006586}{2\pi f_n} = 0.1\%$$

Similarly for stay cable model II(a) and II(b), the damping is found to be 0.04 % and 0.09%

The Scruton number is an important parameter when considering vortex excitation, rain/wind-induced vibrations, wake galloping, and dry inclined cable galloping [U.S. Department of Transportation-Federal Highway Administration, Publication No. FHWA-HRT-05-083 Date: August 2007].

$$S_c = \frac{M \xi}{\rho D^2}$$

Where,  $\xi$ =damping ratio,  $M$ =Mass of the cable,  $\rho$ =density of air ( $1.225 \text{ kg/m}^3$ ) and  $D$ =Diameter of the cable. The Scruton number of the models are tabulated in the table 3.6.

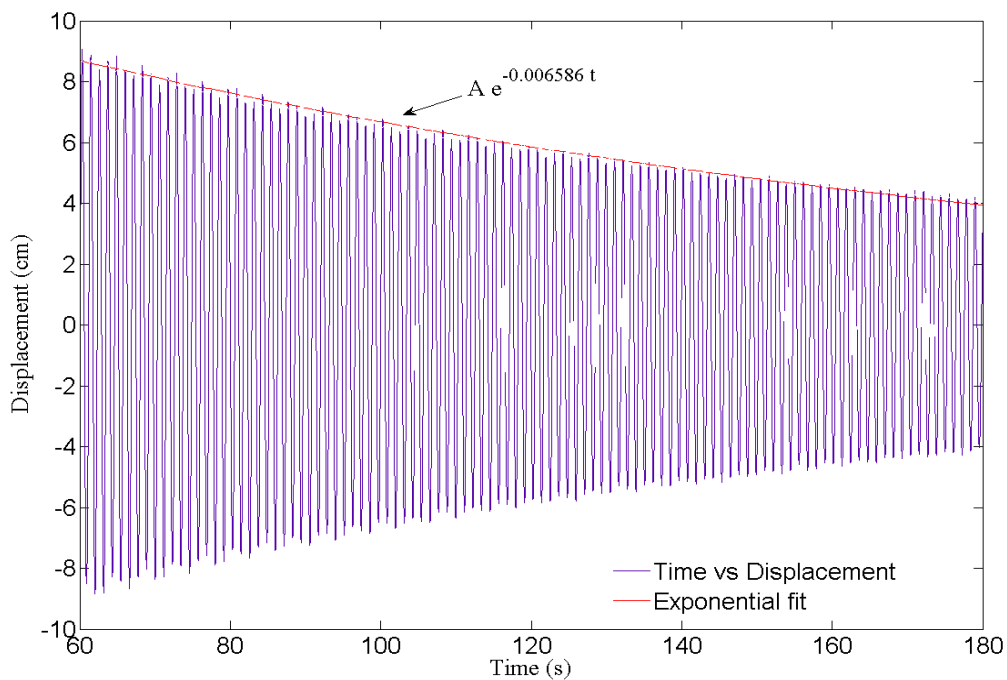


Figure 3.12 Free decay of vibration amplitude of the cable model I

Table –3.6 Comparison of Scruton numbers with the other researchers

Cable model		Experiment & Prototype		Experiment		
		Exp.	Prototype/ Exp.	Gu (2005)	Zhan et al. (2008)	Bosdogianni (1996)
I	D=0.155 m, ( $\xi=0.1\%$ )	0.6	11.36 times	0.46-0.77	0.24-2.5	2.2-6.44
II (a)	D=0.128 m, ( $\xi=0.04\%$ )	0.27	24.6 times			
II (b)	D=0.128 m, ( $\xi=0.1\%$ )	0.69	9.86 times			

The structural density of the prototype cables are  $7800 \text{ kg/m}^3$  and thus the Scruton number is about 6.86, which is 11.37 times as large as that of model compared with the model I. (Ming Gu, 2005). The Scruton number used by various researchers are 0.46 (Ming GU, 2005), 0.24-2.5 (Zhan et al., 2008).

### 3.11 Dynamic characteristics of rain-wind induced vibration

The experimental results are arranged in such a form that the model I is explained in section 3.11.1 and results of the second model is explained in the next section. The dynamic characteristics of rain-wind induced cable vibration and the various parameters influencing the vibration were studied in detail and discussed below.

#### 3.11.1 General characteristics of rain-wind induced cable vibration of model I

The amplitude of the stay cable was influenced by wind speed, rainfall, inclination angle of the cable and the wind yaw angle. So, each factor concerning the rain-wind induced vibration is considered in this study. The high precision rain-simulating unit is used to

simulate the rain precisely over the stay cable.

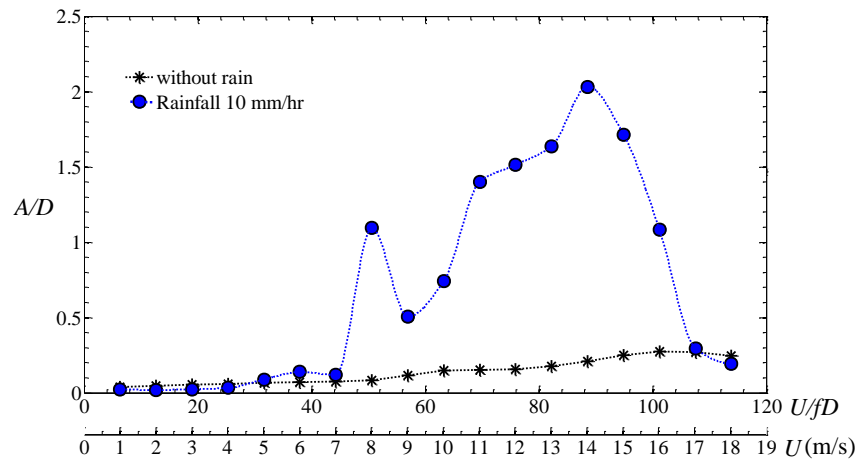


Figure 3.13 Comparison of amplitude of vibration with and without rain ( $\alpha=30^\circ$ ,  $\beta=30^\circ$ )

Figure 3.13, shows a basic case for the comparison of vibration amplitudes of the cable with and without rain conditions when the cable is inclined and yawed at  $30^\circ$ . It can be seen that the amplitude of cable vibration is much larger during rainfall condition when compared without rainfall condition.

### 3.11.2 Effect of wind speed and Rainfall Intensity on cable vibration

Ni (2007) reported about the field observations on rain-wind induced vibrations on cables in Dongting Lake Bridge. The results of his observations showed that the stay cable showed violent large amplitude vibration under very small rainfall intensity with a moderate wind. One of the observations was taken for a short time and projected in the figure 3.14. From Figure 3.14, It can be seen that the large-amplitude vibrations were recorded when the mean wind speeds are from 10-14 m/s blowing at mean wind yaw angles from  $38^\circ$ - $42^\circ$  and the very small rainfall condition of about 5 mm/hr

Figure 3.15, shows the effect of rainfall intensity on rain-wind induced vibration at a wind speed of 14 m/s for the cable inclined at  $30^\circ$  and yawed at  $35^\circ$ . Considering the results

reported in figure 3.14, it was decided to extrapolate the results from 10 mm/hr to a very small rainfall intensity that may cause violent vibrations and then interpolated till the without rainfall condition and is shown in figure 3.15.

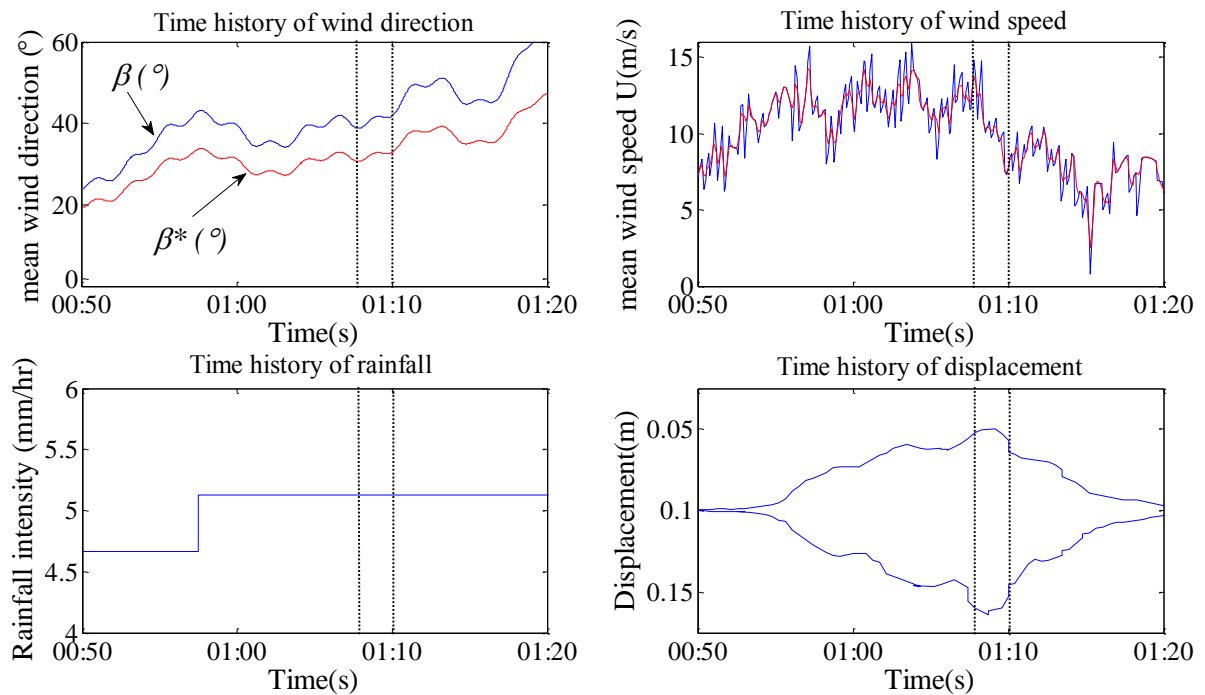


Figure 3.14 Filed investigation on 29 April 2003 Ni et. al, 2007

It can be seen that the lower rainfall condition shows a very large amplitude of about 2.01 D (D-Diameter of the cable) which is of 1.35 times the amplitude of vibration in 20mm/hr rainfall condition, 1.758 times the amplitude of vibration of the 40 mm/hr rainfall condition and 1.85 times that of 80 mm/hr, and thus the rainfall intensity have a much larger effect on amplitude of the cable vibration. It is also seen that the amplitude ceases down drastically from 10 mm/hr to 40 mm/hr rainfall and decreases further with a small amplitude change as the intensity of rain increases. Considering the limitations of the experiments that the rainfall simulator cannot simulate rain precisely for less than 10 mm/hr and from the results shown in figures 3.15 and 3.16, it was decided to carry out the experiment for three different rainfall

conditions namely 10 mm/hr, 40 mm/hr and 70 mm/hr. i.e., Low, medium and High rainfall condition.

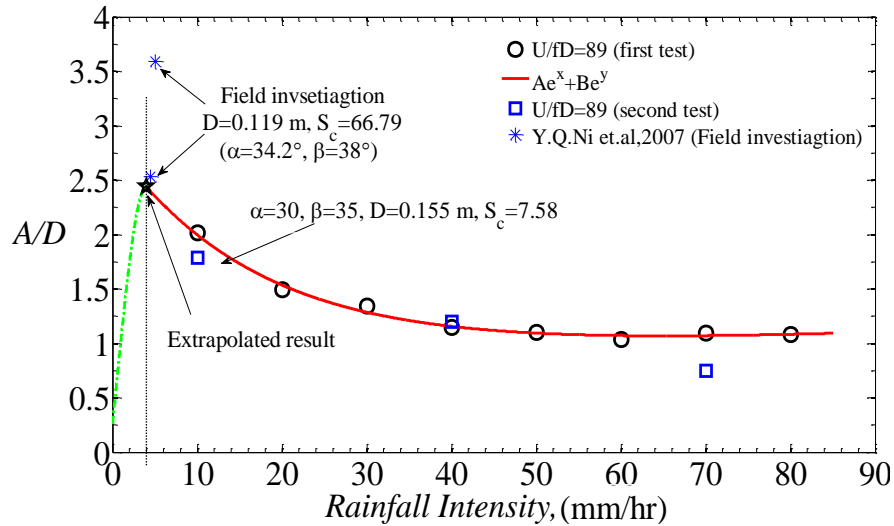


Figure 3.15 Effect of rainfall intensity

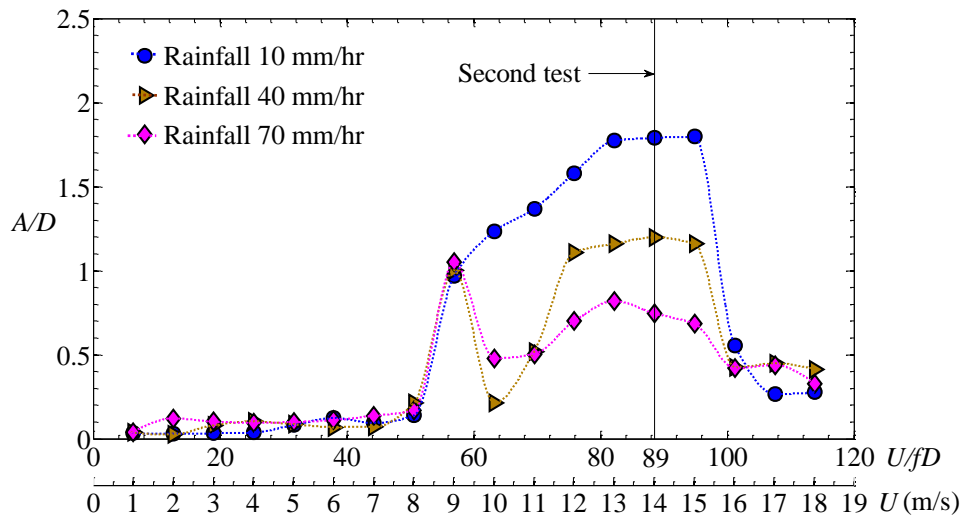


Figure 3.16 Effect of wind speed and rainfall intensity ( $\alpha=30^\circ, \beta=35^\circ$ )

The prototype cable model was further tested for most of the conditions from 10 mm/hr to 70 mm/hr, prioritizing the three main rainfall conditions as shown in Table 1, in which R10 (10 mm/hr) condition in the table represents the low rainfall condition, R40 (40 mm/hr) represents the medium and R70 (10 mm/hr) represents the heavy rainfall conditions. From figures 3.13, 3.15 and 3.16 it can be said that the rain-wind induced vibration is a velocity-

and amplitude- restricted vibration which was guided by the intensity of rain or can be called as velocity-amplitude-rainfall restricted vibration.

### **3.11.3 Phenomenon behind rain-wind induced cable vibration**

In general, this vibration is characterized by vortex shedding for a range of wind speeds from 1 m/s to 6 m/s (reduced wind speed: 6.3-37.9), and then followed by the formation of a rivulet causing rain-wind-induced vibration, which is characterized by amplitudes higher than vortex shedding with an oscillating rivulet. The observations show that, in most cases, the lowest rainfall causes large vibrations over a wide range of wind speeds (7-18 m/s, as shown in Figure 3.16), whereas medium and higher rainfalls cause medium vibrations over a narrow range of wind speeds (11-16 m/s, as shown in Figure 6(b)). The reason behind these variations lies with the formation and motion of the rivulet.

The general tendency of the rain-wind-induced vibration is the formation of a rivulet and its meandering motion over the upper surface of the cable, which in turn is a function of cable inclination angle, wind yaw angle, rainfall intensity and wind speed. During the experiment, the formation and motion of the rivulet was continuously observed. When the simulated rain water was sprinkled over the inclined cable, the cable's inclination caused small droplets of water to slide over the curved surface of the cable due to the inertial force of the rivulet and the surface traction force between the cable and rivulet, which in turn created a number of very thin water strips on the windward side of the cable which slid circumferentially over the curved surface of the circular cross-section. Due to the action of wind, the tiny strips of water were pushed further towards the top of the cable, thus forming an upper rivulet. Figure 3.17(a) shows a snapshot of the upper rivulet formed under 10 mm/hr rainfall, whereas Figure 3.17(b) shows that under 70 mm/hr rainfall. It is also found that there existed two rivulets: one on the windward side and the other on the leeward side [1, 2, 6, 8].

Visuals of the experiment show that the formation and motion of the rivulet was influenced by the inclination and yaw angles. The upper rivulet formed on the windward side seems to be meandering over the upper surface of the cable section and the leeward side rivulet was almost static and its position varied with a small angular displacement in the lower surface. The positions of the upper and lower rivulets are shown in Figure 3.17(c). The interesting fact is that for every rainfall condition for each inclination and yaw angle, the size of the rivulet and its mean position varied according to rainfall intensity and wind speed.

Under the 10 mm/hr rainfall condition, the water droplets were too thin, leading to the formation of a thin rivulet (about 0.1 - 0.3 mm thick), and thus the lower wind speeds overcame the circumferential force of the rivulet, making the rivulet oscillate over the cable surface, which in turn caused a disturbance in the flow field and induced large-amplitude motion in the cable. Further, the cable motion by itself caused additional motion in the rivulet, leading to very high-amplitude vibration in the stay cables. Thus, cables are much more vulnerable to low rainfall, which causes large-amplitude oscillations over a wide range of wind speeds.

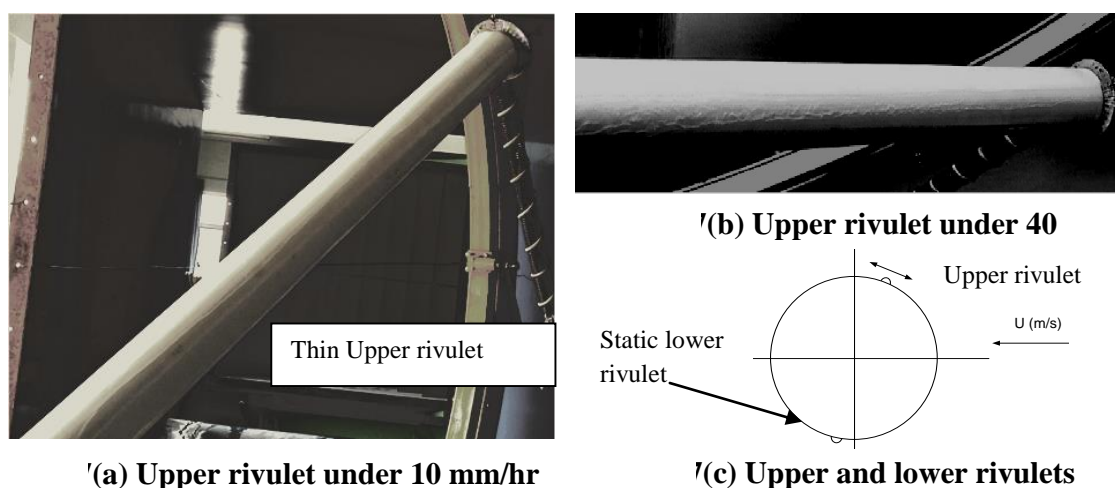


Fig. 3.17 Upper and lower rivulets on the stay cable ( $\alpha=35^\circ$ ,  $\beta=35^\circ$ )

In the case of moderate or higher rainfall, the rivulet thickness was around 1-1.5 mm

and it broke down under moderate wind and restricted the cable vibration to a limited range of wind speeds.

### 3.11.4 Effect of wind yaw angle

At first a basic rain-vibration test was conducted on a cable positioned at  $\alpha=25^\circ$  and  $\beta=35^\circ$  and a large variation in amplitude was found under rain conditions. For ease of testing at a large number of wind yaw angles and considering the convenience of changing yaw angle in the setup, it was decided to fix the inclination angle to study the effect of yaw angle. The effect of wind yaw angle ( $\beta$ ) on the vibration amplitude of the cable model was studied by fixing the inclination angles and varying the wind yaw angles for different rainfall conditions. The effects of wind speed and rainfall intensity on the wind yaw angle, and the effect of maximum amplitude on the cable, are discussed.

The effect of wind yaw angles ( $25^\circ$ - $50^\circ$ ) on cable vibration amplitude was tested by fixing the inclination angles at  $25^\circ$ ,  $30^\circ$ ,  $35^\circ$ , and  $40^\circ$  and rainfall intensities to 10 mm/hr, 40 mm/hr, and 70 mm/hr. The observed results are explained below.

#### 3.11.4.1 Case $\alpha=25^\circ$ , $\beta = 30^\circ, 35^\circ, 40^\circ, 50^\circ$

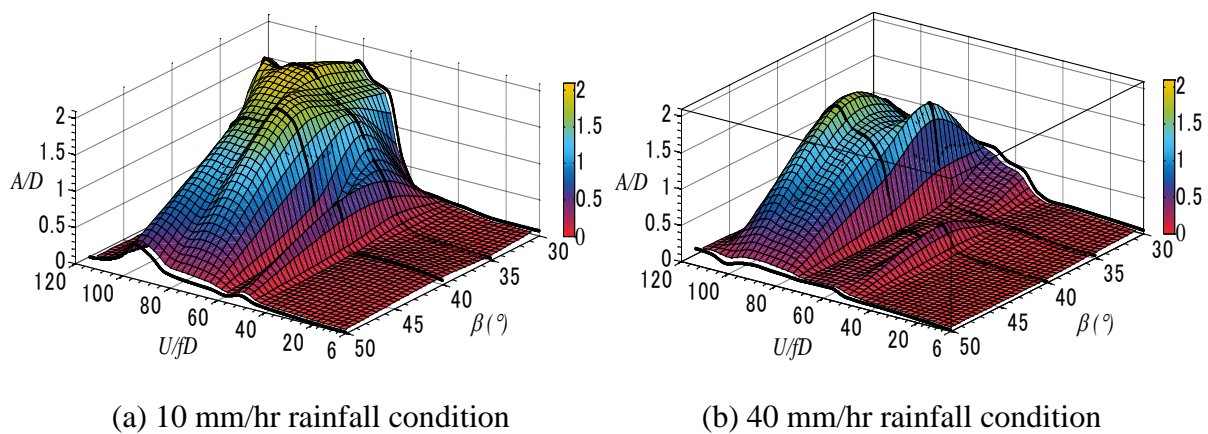
When the cable was inclined at  $25^\circ$ , the effect of wind yaw angle on cable vibration amplitude was studied during the different rainfall conditions and the result is plotted in Figure 3.18. Figure 3.18(a), 3.18(b) and 3.18(c) show the effects of wind yaw angle on stay cable vibration amplitude under different rainfall intensities. These results show that the cable is subjected to large-amplitude vibrations in the range of yaw angles ( $\beta$ ) from  $25^\circ$ - $40^\circ$ , and for  $35^\circ$  wind yaw angle it vibrates over a wider range of wind speeds, whereas increasing the yaw angle ( $\beta$ ) from  $35^\circ$  to  $40^\circ$  decreases the maximum vibration amplitude and also the range of wind speeds causing vibrations. Further increasing it to  $50^\circ$  results in very small-amplitude

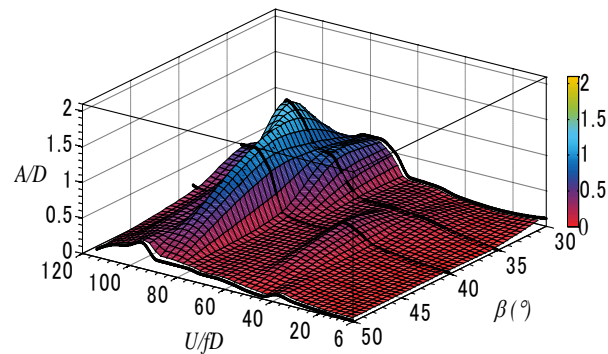
vibrations. For 40 and 70 mm/hr rainfall conditions, a similar trend was observed, as shown in Figures 3.18(b) and 3.18 (c), but with much lower maximum amplitudes than for 10 mm/hr.

From Figures 3.18 (a), 3.18 (b) and 3.18 (c), it can be said that:

- i) As the wind yaw angle increases from  $30^\circ$  to  $50^\circ$ , maximum cable vibration amplitude and the range of wind speeds causing vibration decreases.
- ii) As the rainfall intensity increases from 10 to 40 mm/hr, the maximum vibration amplitude and range of wind speeds causing vibration drops and as the rainfall intensity increases from 40 mm/hr to 70 mm/hr, the maximum vibration amplitude and range of wind speeds causing vibration decreases.
- iii) When the cable is inclined at  $25^\circ$  and the wind yaw angles are increased beyond  $40^\circ$ , ie.,  $45^\circ$  and  $50^\circ$ , there is a very small vibration amplitude for 10 mm/hr rainfall and the cable vibration disappears when the rainfall intensity is increased to 70 mm/hr.

A similar result was found when the cable was inclined at 30, 35, and 40 degrees, as shown in Figures 3.19, 3.20 and 3.21.





(c) 70 mm/hr rainfall condition

Figure 3.18 Effect of wind yaw angle on vibration amplitude of the cable ( $\alpha=25^\circ$ )

#### 3.11.4.2 Case $\alpha=30^\circ$ , $\beta=30^\circ, 35^\circ, 40^\circ, 50^\circ$

Figure 3.19 shows the effect of yaw angle on cable vibration amplitude when the cable is inclined at  $30^\circ$ . It can be seen that the maximum amplitude of more than 2D (D-Diameter of the cable) was observed for  $\alpha=30^\circ$ , and  $\beta=30^\circ$  and  $35^\circ$  under 10 mm/hr rainfall conditions. A trend similar to the previous case ( $\alpha=25^\circ$ ) was found to happen. The amplitude was large when the yaw angle was  $30^\circ$  and started decreasing as the yaw angle increased to 35 and  $40^\circ$ . When  $\beta$  was further increased to  $50^\circ$ , the maximum amplitude reduced from 2D to 1D (D-Diameter of the cable) under 10 mm/hr rainfall.

When the rainfall intensity was set to 40 mm/hr, the overall maximum amplitude decreased to 1.47 D and when the wind yaw angle was increased, the vibration amplitude and the severity of the wind speeds causing the vibration was limited. When the rainfall was further increased to 70 mm/hr, the maximum amplitude was further reduced to 1.13 D, and the range of wind speeds causing vibration also decreased, and the vibration disappeared when the yaw angle was increased to  $50^\circ$ .

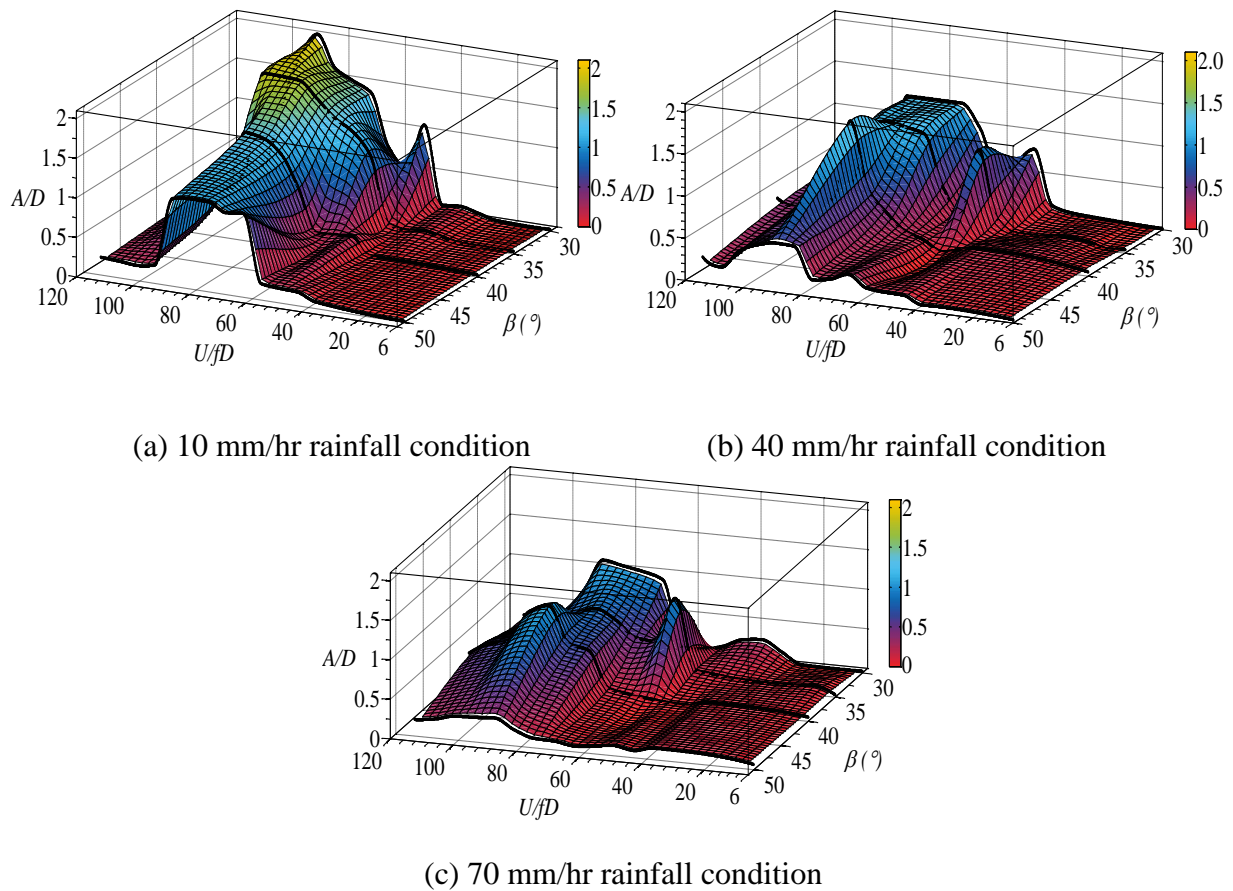


Figure 3.19 Effect of wind yaw angle vibration amplitude ( $\alpha=30^\circ$ )

#### 3.11.4.3 Case $\alpha=35^\circ$ , $\beta=25^\circ, 30^\circ, 35^\circ, 40^\circ, 50^\circ$

Figure 3.20 (a) clearly shows that the cable vibration was highly influenced by its yaw angle. Under 10 mm/hr rainfall and  $25^\circ$  wind yaw angle, a maximum amplitude of 1.39 D was observed and when the yaw angle was increased from  $25^\circ$  to  $30^\circ$ , the amplitude increased to 1.68 D, and when the yaw angle was further increased to  $35^\circ$ , the maximum amplitude increased to 1.71 D and started decreasing as the yaw angle increased from  $35^\circ$  to  $40^\circ$  and  $50^\circ$ . When the yaw angle was  $45^\circ$  and  $50^\circ$ , the vibration amplitude was less than 1D and vibration occurred over a very narrow range of wind speeds. Figure 3.20(b) shows the effect of yaw angle on cable vibration amplitude under 20 mm/hr rainfall. The maximum amplitude was found to be 1.12 D for  $\beta=40^\circ$  and 0.45 D for  $\beta=50^\circ$ .

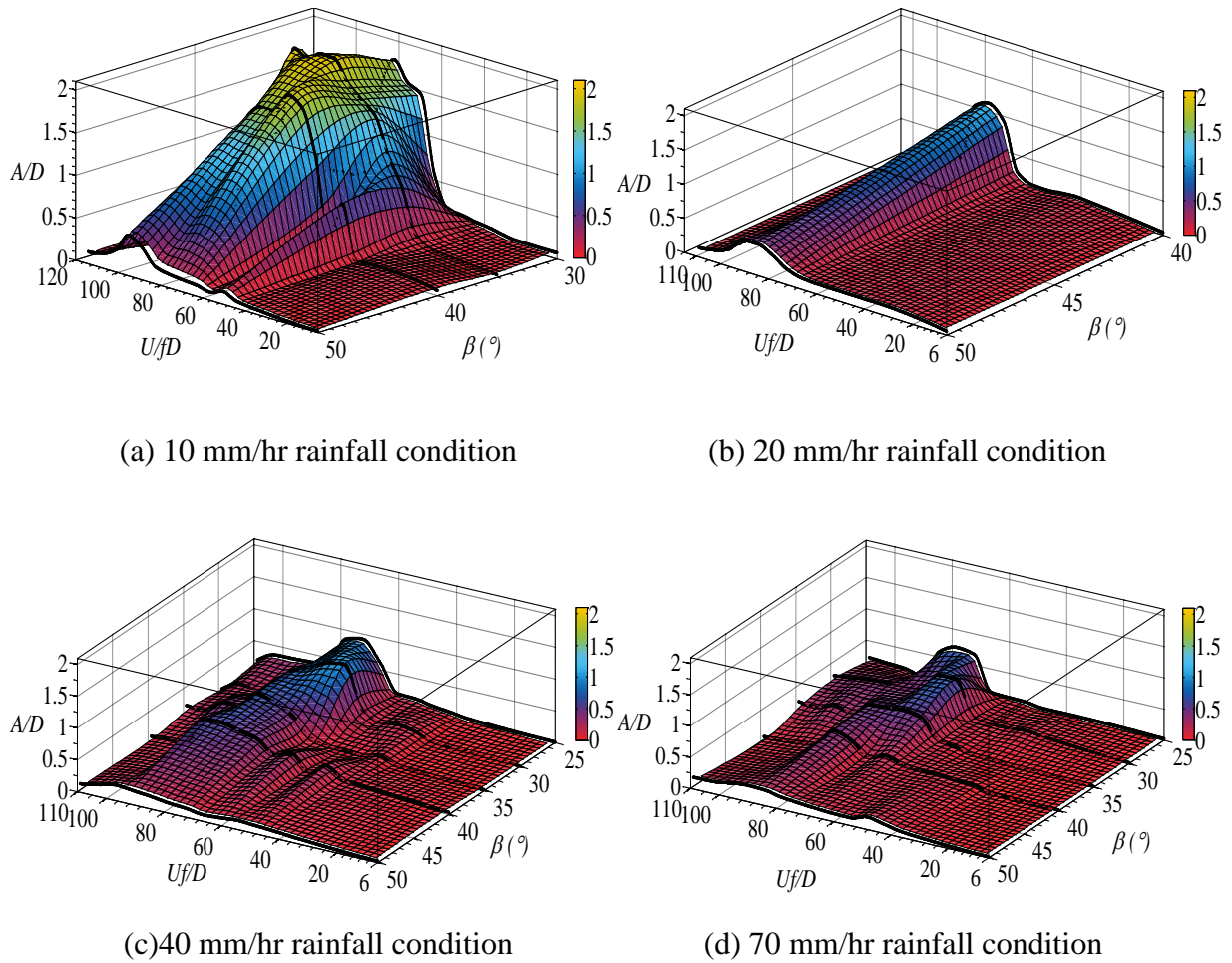


Figure 3.20 Effect of wind yaw angle vibration amplitude of the cable ( $\alpha=35^\circ$ )

For rainfall intensities of 40 mm/hr and 70 mm/hr, the effects of wind yaw angle were as shown in Figures 3.20(c) and 3.20(d), showing similar tendencies to the previous cases. For wind yaw angles of  $25^\circ$  and  $30^\circ$ , there was a maximum amplitude of about  $0.922D$  for the 40 mm/hr rainfall, and when the rainfall was increased to 70 mm/hr, the maximum amplitude decreased to  $0.72 D$ , as shown in Figure 3.20(d), whereas the vibration disappeared when the yaw angle was  $50^\circ$  for both 40 mm/hr and 70 mm/hr rainfall conditions

#### 3.11.4.4 Case $\alpha=40^\circ$ , $\beta=45^\circ$

From the above results, it was found that the vibration decreases with increase in yaw angle. Thus, in order to find out the vibration boundary (the angles through which a cable can vibrate), the cable was tested only for wind yaw angle  $45^\circ$ . The result is shown in Figure 3.21.

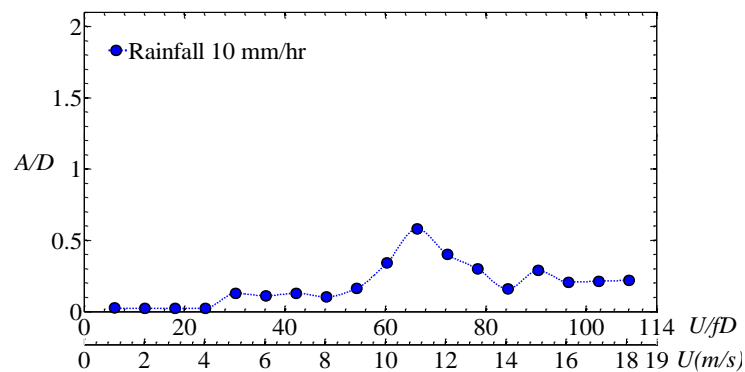


Figure 3.21 Effect of wind yaw angle vibration amplitude of cable ( $\alpha=40^\circ$ ,  $\beta=45^\circ$ )

#### 3.11.5 Effect of wind yaw angles on maximum amplitude

It was found that for all cases the maximum amplitude occurred when the rainfall was about 10 mm/hr, medium maximum vibrations for 40 mm/hr and very small amplitude for 70 mm/hr. Figures 3.22(a), 3.22(b), and 3.22(c) show the effect of yaw angle on maximum cable vibration amplitude for different inclination angles. Under the 10 mm/hr rainfall conditions the cables were prone to large-amplitude vibrations, provided the wind yaw angles ranged from  $25^\circ$  to  $40^\circ$  and the inclination angles ranged from  $25^\circ$  to  $35^\circ$ . A peak amplitude of 2.03 D occurred when the cable was positioned at  $\alpha=30^\circ$  and  $\beta=30^\circ$ , and a peak amplitude of 2.01 D occurred for the case of  $\alpha=25^\circ$  and  $\beta=35^\circ$ . For  $\alpha=35^\circ$  and  $\beta=35^\circ$ , the peak amplitude was about 1.71D. When the wind yaw/inclination angles were further increased, the vibration amplitudes started decreasing. The region of maximum vibration

amplitudes are compared with the literature as shown in Table 4. A similar tendency was observed when the rainfall was varied to 40 mm/hr and 70 mm/hr (with a maximum

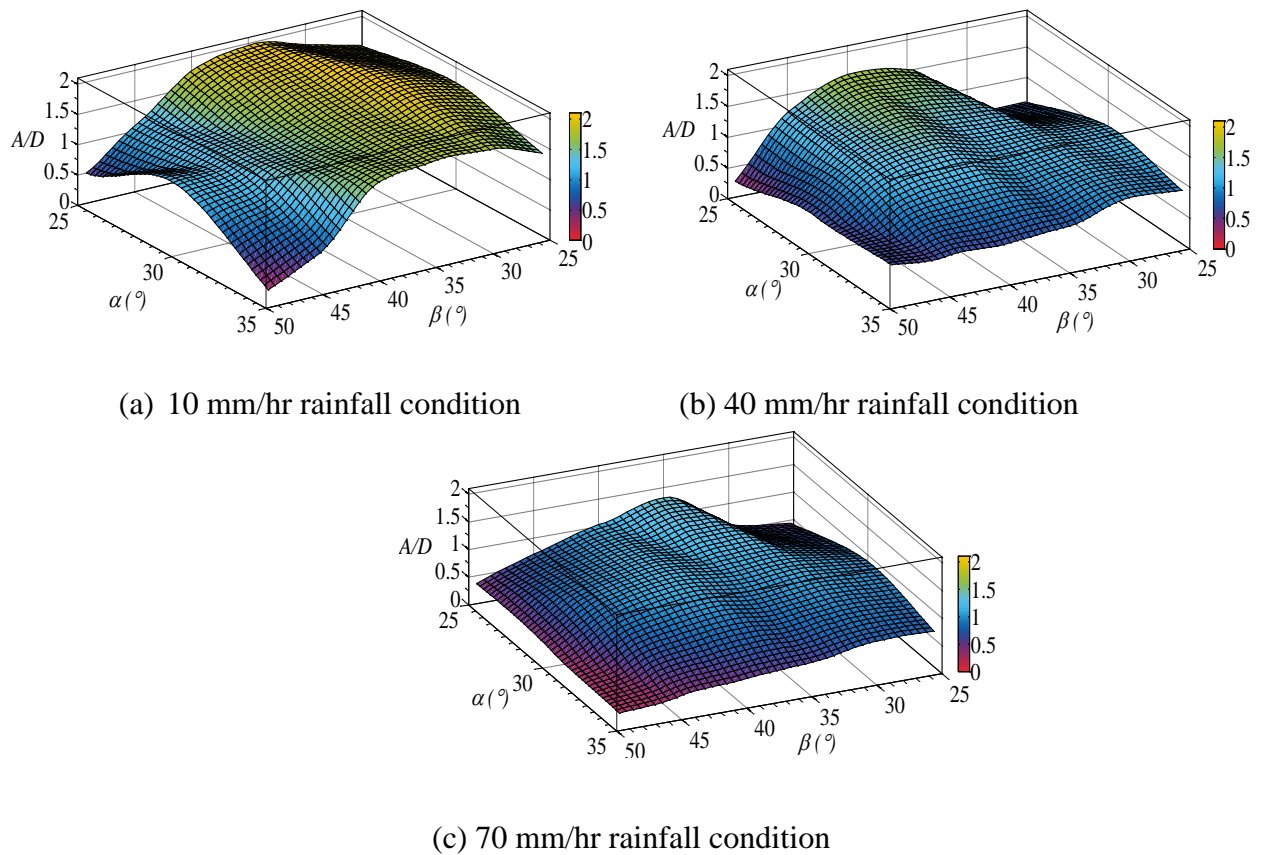


Figure 3.22 Effect of wind yaw angle on maximum amplitude ( $\alpha=25^\circ, 30^\circ, 35^\circ$ ) at different rainfall conditions

amplitude much less than that for the 10 mm/hr rainfall condition, as shown in Figure 3.22(b) and 3.22 (c)).

Table 3.7 Comparison of maximum amplitudes (Literature & current study)

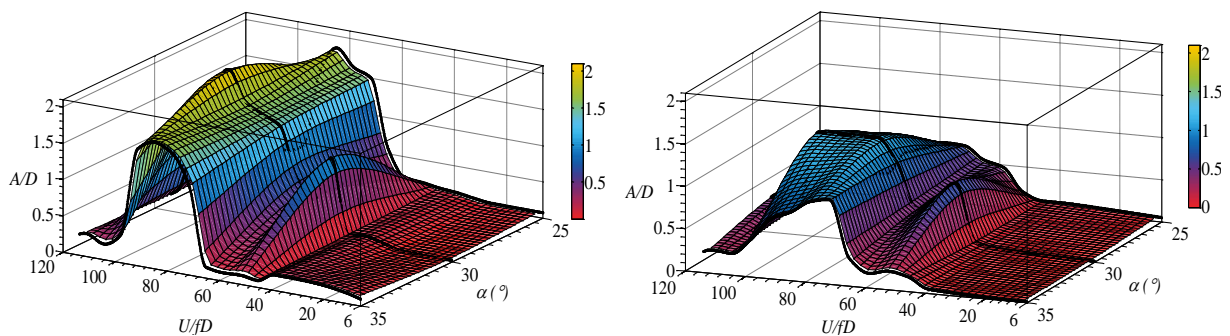
Authors	Rainfall condition	Cable inclination and wind yaw angles at which maximum amplitude occurred
Flamand [5]	0-300 mm/hr	$\alpha=25^\circ, \beta=30^\circ$
Gu [8]	20.4-23.4 mm/hr	$\alpha=30^\circ, \beta=35^\circ$

Xu [10]	12 mm/hr	$\alpha=30^\circ, \beta=35^\circ$
Present work	10 mm/hr	$\alpha=25^\circ, 30^\circ; \beta=30^\circ, 35^\circ;$

### 3.11.6 Effect of inclination angle

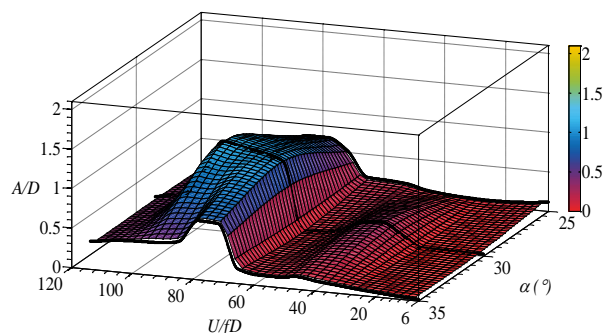
The effect of inclination angle was studied by keeping the yaw angle fixed and changing the inclination angles and the rainfall intensities. The wind yaw angles were fixed at  $30^\circ, 35^\circ, 40^\circ, 45^\circ$  and  $50^\circ$ , and the effects of the inclination angles ( $25^\circ$ - $35^\circ$ ) on the cable vibration were tested for different rainfall intensities (10-70 mm/hr). For different wind yaw angles, the effects of inclination angles ( $25^\circ$ - $35^\circ$ ) on cable vibration are explained as follows.

#### 3.11.6.1 Case $\beta=30^\circ, \alpha=25^\circ, 30^\circ, 35^\circ$



(a) 10 mm/hr rainfall condition

(b) 40 mm/hr rainfall condition



(c) 70 mm/hr rainfall condition

Figure 3.23 Effect of inclination angle on vibration amplitude ( $\beta=30^\circ$ )

Figures 3.23(a), 3.23(b) and 3.23(c) show the effects of inclination angle on cable vibration when the wind yaw angle is fixed at  $30^\circ$  under 10 mm/hr, 40 mm/hr, and 70 mm/hr rainfalls. From Figure 3.23 (a) it can be seen that a large-amplitude vibration occurred during 10 mm/hr rainfall intensity in wind speeds ranges from 8 m/s to 17 m/s. The interesting fact is that the vibration amplitude decreases with increase in cable inclination angle and accordingly the range of wind speeds causing rain-wind vibration is also limited. It can be seen that the cable at  $\alpha=25^\circ$  under 10 mm/hr rainfall vibrates from 8 m/s to 17 m/s covering a wide envelope of wind speeds, whereas for  $\alpha=30^\circ$ , vibration is limited to wind speeds from 9 m/s to 16 m/s, and for  $\alpha=35^\circ$ , the cable vibrates when the wind speeds are from 10.5 m/s to 15 m/s. This decreasing tendency of cable vibration amplitude is also seen in Figures 3.23(b) and 3.23(c) for 40 mm/hr and 70 mm/hr rainfall conditions. For all three rainfall conditions, the maximum amplitude occurs when the cable is inclined at  $\alpha=30^\circ$ .

#### 3.11.6.2 Case $\beta=35^\circ$ , $\alpha=25^\circ$ , $30^\circ$ , $35^\circ$

The most critical case is when the wind yaw angle is  $35^\circ$ , where the cable is inclined at  $25^\circ$  and  $30^\circ$ . It can be seen clearly from Figure 3.24(a) that 10 mm/hr rainfall causes large-amplitude vibrations over a wide range of wind speeds for  $\alpha=25^\circ$  and  $30^\circ$ . When  $\alpha=25^\circ$ , vibration occurs over a wide range of reduced wind speeds from 37.9 to 113.85 (6-18 m/s) with a peak amplitude of 2.01 D, and for  $\alpha=30^\circ$  and  $35^\circ$  the vibration period decreases from 50.6 to 101.2 (8-16 m/s) and from 56.9 to 101.2 (9-16 m/s). A similar tendency is seen for 40 mm/hr and 70 mm/hr but with smaller amplitudes, as shown in Figures 3.24(b) and 3.24 (c).

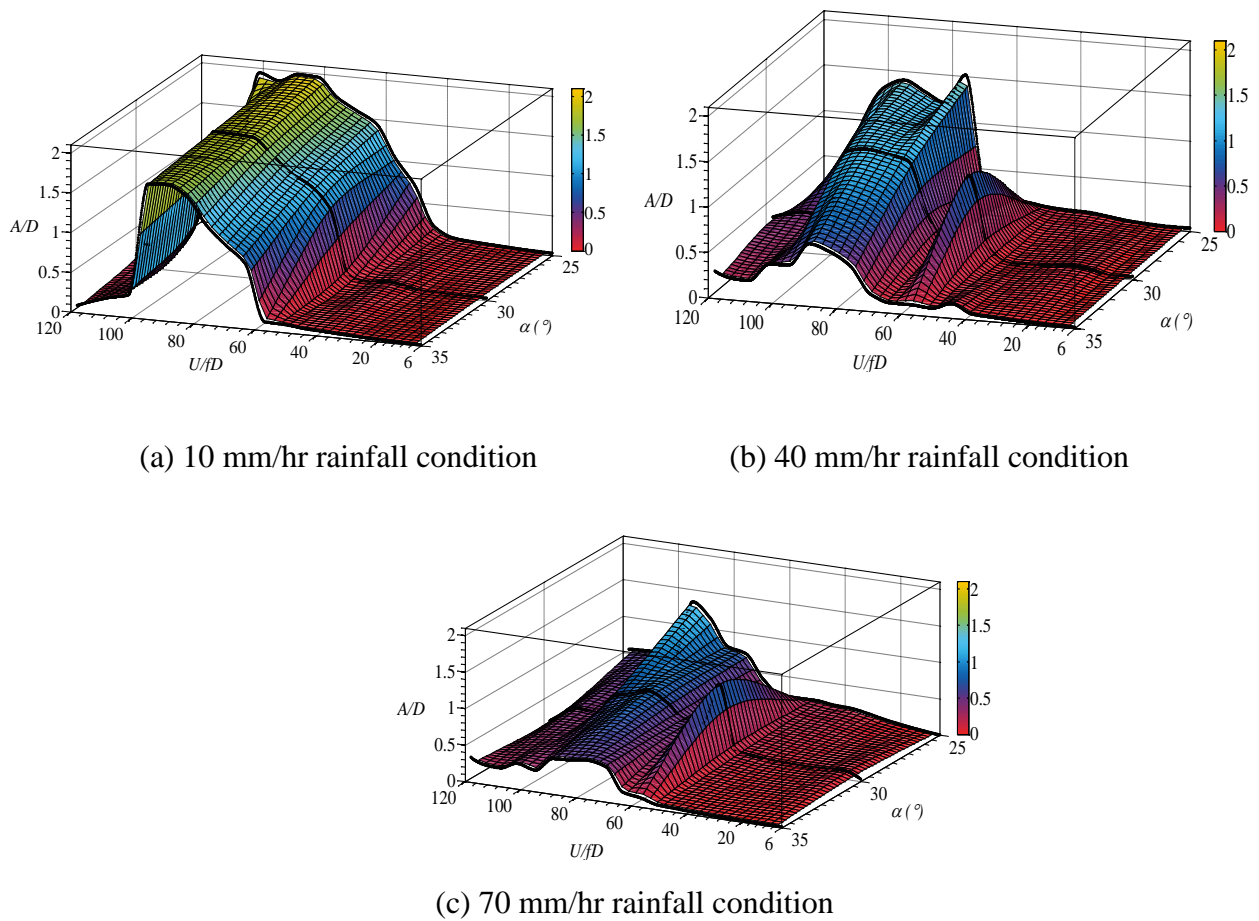


Fig. 3.24 Effect of inclination angle on vibration amplitude ( $\beta=35^\circ$ )

### 3.11.6.3 Case $\beta=40^\circ$ , $\alpha=25^\circ$ , $30^\circ$ , $35^\circ$

The effects of inclination angle on vibration amplitude of the cable fixed at  $\beta=40^\circ$  are shown in Figures 3.25(a), 3.25(b) and 3.25(c) for different rainfall intensities i.e., 10 mm/hr, 40 mm/hr and 70 mm/hr. The results show a maximum amplitude of 1.84 D for  $\alpha=25^\circ$  (10 mm/hr rainfall,  $U_{crit} = 9-16$  m/s), whereas the range of reduced wind speeds causing vibration for  $\alpha=30^\circ$  and  $35^\circ$  is limited to 63.25-101.2 ( $U_{crit} : 10-16$  m/s) in 10 mm/hr rainfall condition. From Figures 3.25(b) and 3.25(c), it can be seen that the maximum vibration amplitude for 40 mm/hr and 70 mm/hr rainfall condition is much less than that of 10 mm/hr rainfall.

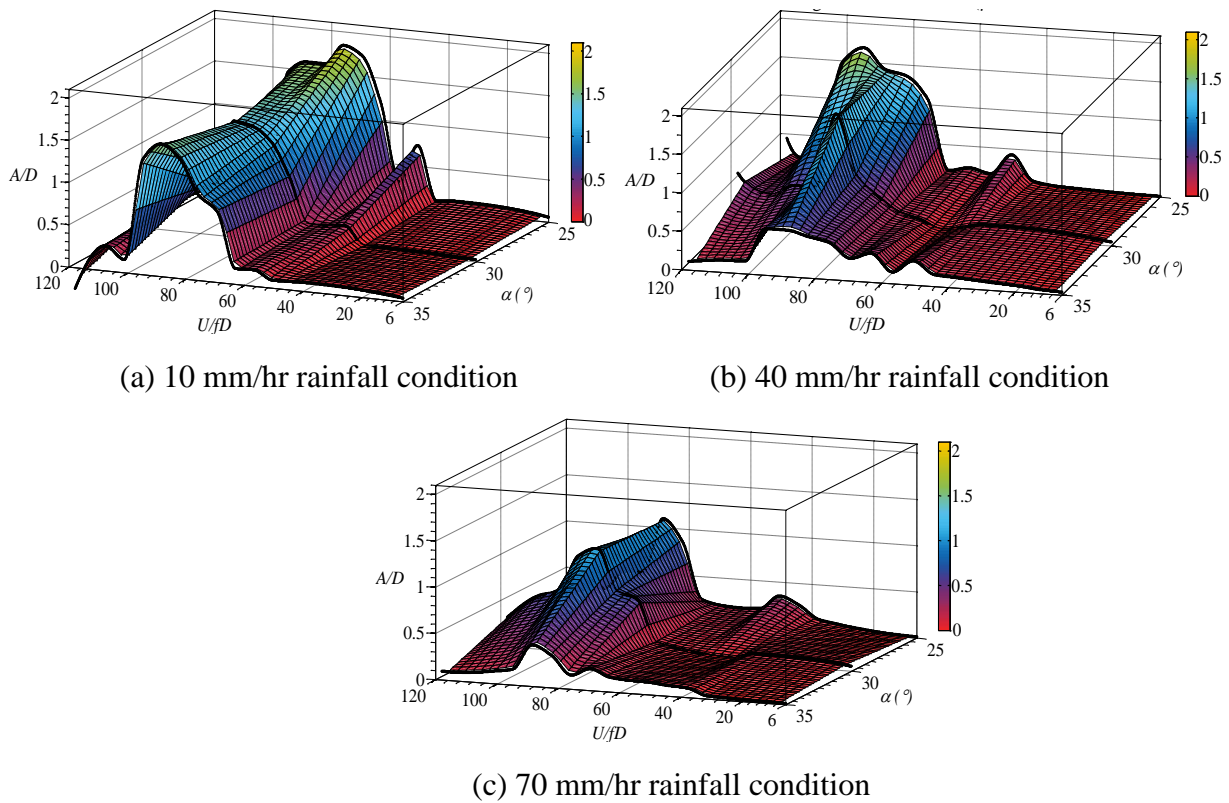


Fig. 3.25 Effect of inclination angle on vibration amplitude ( $\beta=40^\circ$ )

#### 3.11.6.4 Case $\beta=45^\circ$ , $\alpha=35^\circ, 40^\circ$

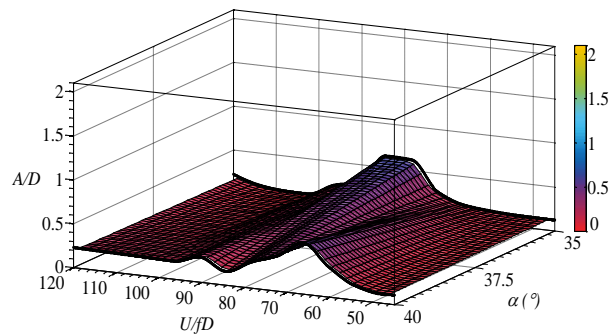


Fig. 3.26 Effect of inclination angle on vibration amplitude ( $\beta=45^\circ$ )

For the cable inclined at  $35^\circ$  and  $40^\circ$  and yawed at  $45^\circ$ , the vibration amplitude is found to be around  $0.58 D$  for 10 mm/hr rainfall, as shown in Figure 3.26. It can be seen from Figures 6-16 that the vibration amplitude decreases not only with increase in rainfall intensity but also with increase in cable inclination angle or wind yaw angle. The authors perceive that

for  $\beta=45^\circ$ , and by increasing the cable inclination angle ( $\alpha$ ) to  $50^\circ$  or increasing rainfall intensity may not produce large-vibration amplitudes.

### 3.11.6.5 Case $\beta=50^\circ$ , $\alpha=25^\circ$ , $30^\circ$ , $35^\circ$

With the wind yaw angle fixed at  $50^\circ$ , the effect of inclination angles  $25^\circ$ ,  $30^\circ$ , and  $35^\circ$  on cable vibration for different rainfall intensities is plotted in Figures 3.27(a), 3.27(b), 3.27(c) and 3.27(d). Figure 3.27(a) shows that for 10 mm/hr rainfall,  $\alpha=25^\circ$  causes peak amplitude of about 0.98 D, whereas other wind yaw angles did not show much vibration.

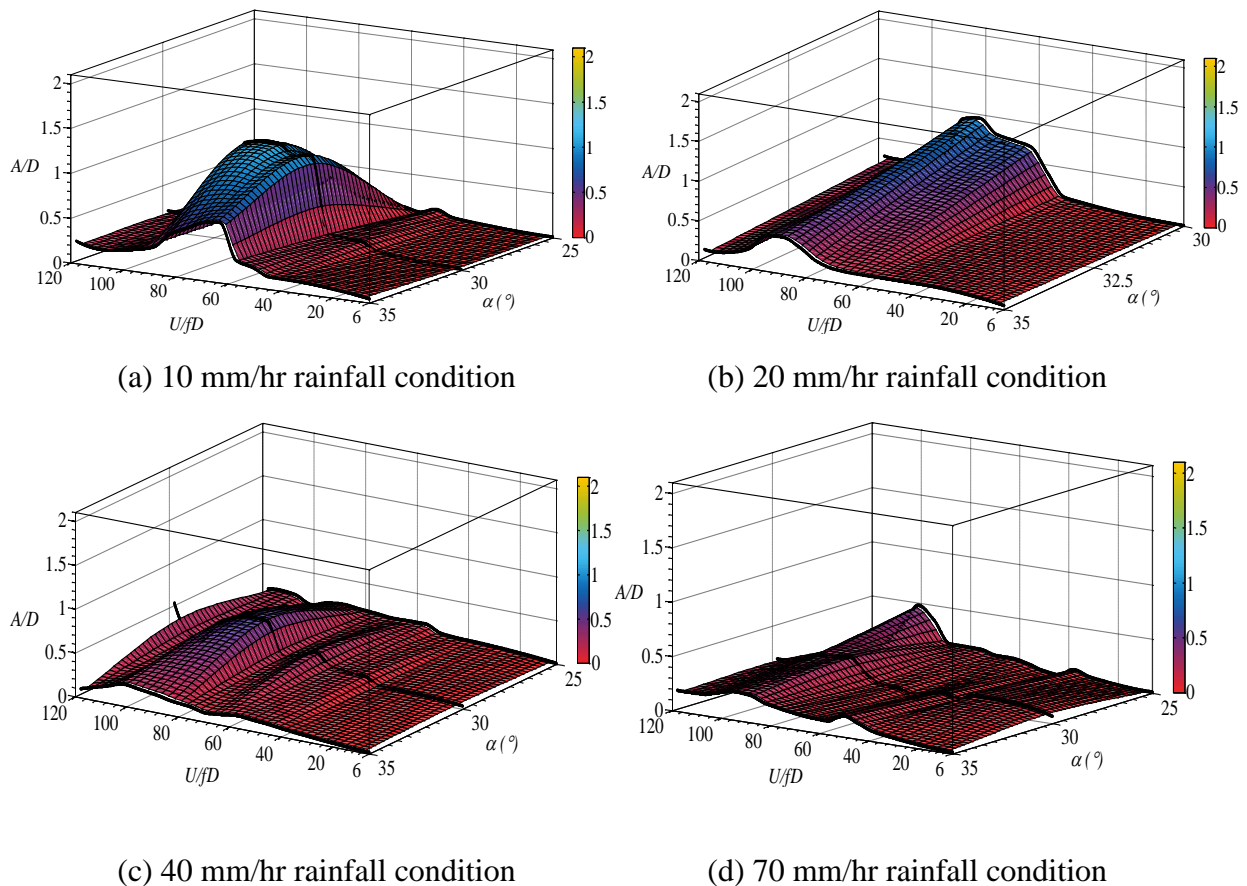


Fig. 3.27 Effect of inclination angle on vibration amplitude ( $\beta=50^\circ$ )

Increasing rainfall makes the rain-wind-induced vibration disappear, whereas the cable was subjected to buffeting when the reduced wind speeds were 107.5 (17 m/s) or

higher.

### 3.11.7 Combined effects of cable inclination ( $\alpha$ ) and wind yaw angles ( $\beta$ )

From the results shown in Figures 3.18-3.27, it is easy to identify the range of cable inclination angles, wind yaw angles, rainfall intensities and wind speeds that cause severe vibrations.

For the combination of inclination and yaw angles, i.e.,  $\alpha = 25^\circ, 30^\circ$  and  $\beta = 30^\circ, 35^\circ$ , the cable shows a very large-amplitude vibration and the results of the present work are compared with field investigations, as shown in Table 5. Increasing yaw angles ( $35^\circ$ - $50^\circ$ ) or cable inclination angles ( $30^\circ$ - $45^\circ$ ) show a decreasing tendency of maximum amplitude and severity range of the vibration. The following cases, i.e.,  $\alpha = 30^\circ, 35^\circ$  and  $\beta = 40^\circ, 45^\circ, 50^\circ$ , show very small-amplitude vibration.

### 3.11.8 Comparison with past researches

Since past studies have been limited to certain wind yaw and cable inclination angles, comparison is made for available results, as shown in Figure 3.28. Figure 3.28(a) compares the vibration amplitudes of cables ( $\alpha = 25^\circ, \beta = 35^\circ$ ) with different Scruton numbers under different rainfall conditions. The vibration amplitude for 10 mm/hr rainfall is compared with that for 20 mm/hr rainfall of Gu (M.Gu,2005). This shows that the cable vibration amplitude is very sensitive to Scruton number. Figure 3.28(b) compares the cable vibration amplitudes of the cable ( $\alpha = 30^\circ, \beta = 35^\circ$ ) of the present study with those of Gu [8] and Zhan [10]. Figure 3.28 (c) compares the cable vibration amplitudes of the cable ( $\alpha = 25^\circ, \beta = 40^\circ$ ) under different rainfall conditions with the results of Flamand [5]. Figure 3.28 (d) compares the vibration amplitudes of cables with different Scruton numbers when the cable is inclined and yawed at  $45^\circ$ . The parameters given to estimate the Scruton number are as given by Hikami [1] and is

found to be less than 3.71. Figure 3.28 elucidates the importance of rainfall intensity, wind speed, damping and frequency with respect to cable vibration amplitude for different Scruton numbers.

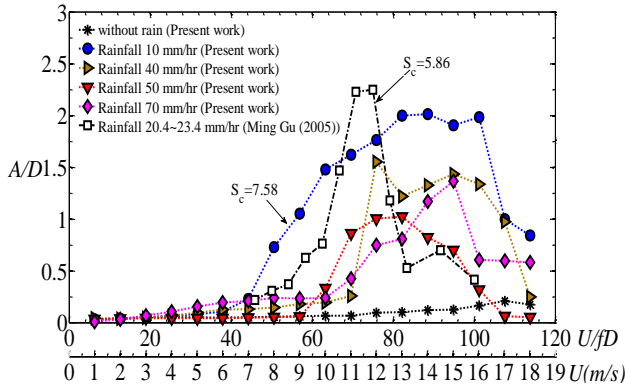


Fig. 8(a)  $\alpha=25^\circ, \beta=35^\circ$

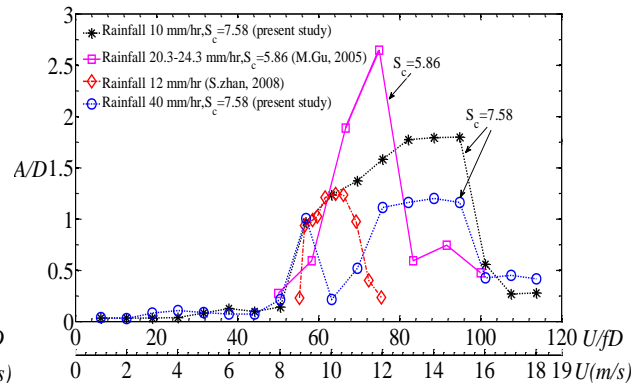


Fig. 8(b)  $\alpha=30^\circ, \beta=35^\circ$

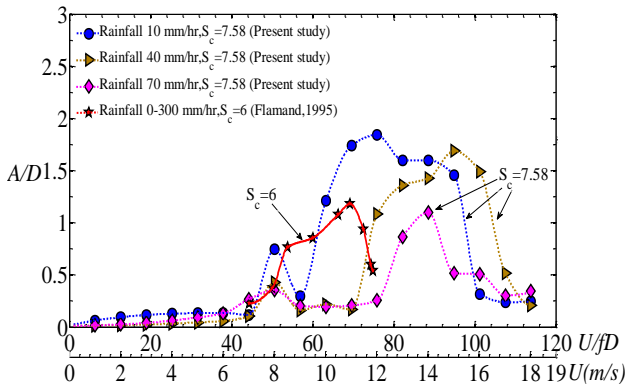


Fig. 8(c)  $\alpha=25^\circ, \beta=40^\circ$

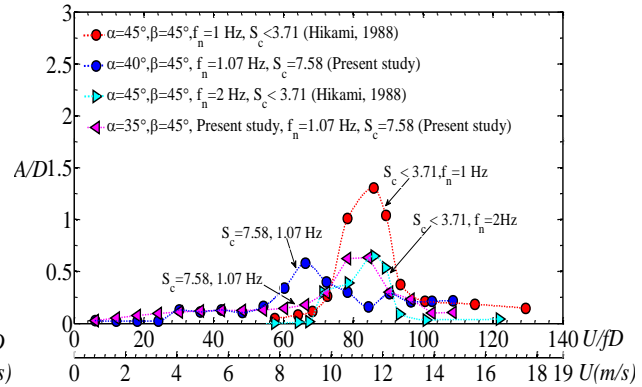


Fig. 8(d)  $\beta=45^\circ$

Figure 3.28 Comparison of test results with the past studies

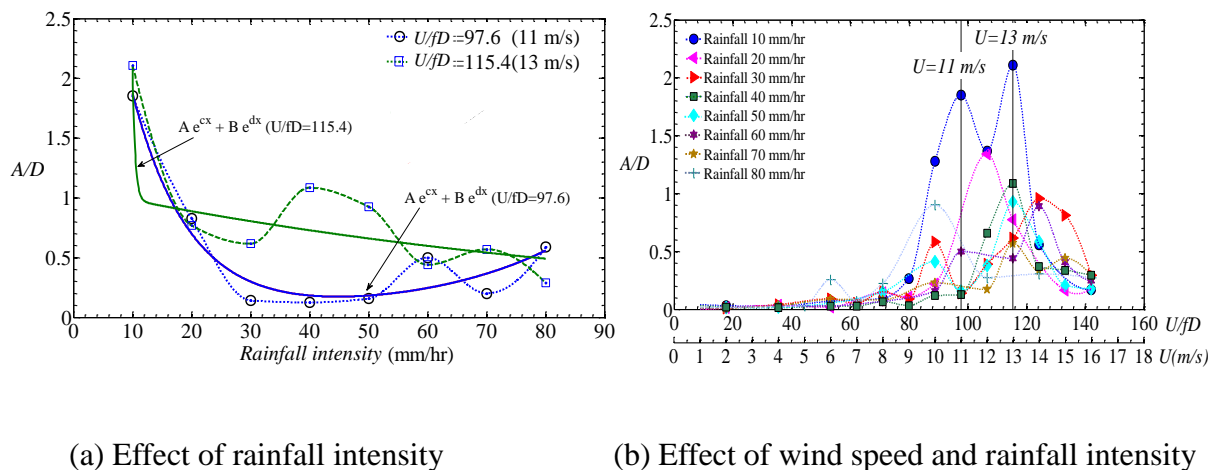
### 3.12 General characteristics of rain-wind induced vibration of the cable model II

The experimental results of the cable model II is discussed below.

#### 3.12.1 Effect of wind speed and Rainfall on cable vibration of cable model II

Figure 3.29 and 3.30 shows the vibration amplitude of cable models I and II. Figure 3.29(a) shows the effect of rainfall intensity on stay cable vibration ( $\alpha=30^\circ, \beta=35^\circ$ ) for the first test. The increase in rainfall intensity shows a decrease tendency of vibration amplitude.

Figure 3.29(b) shows the second test carried out for three rainfall conditions namely 10 mm/hr, 40 mm/hr and 70 mm/hr. It can be seen that for model I, increase in rainfall intensity decreases the vibration amplitude of rain-wind induced vibration. Whereas figure 3.29 (a) and 3.29(b) shows the effect of rainfall intensity and wind speed on vibration amplitude of the cable ( $\alpha=25^\circ$ ,  $\beta=35^\circ$ ) under different rainfall conditions. In both the figures 5 and 6, the largest amplitude occurs under 10 mm/hr rainfall condition. A similar phenomenon was also observed for several combination of inclination and wind yaw angles i.e.,  $\alpha = 25^\circ - 45^\circ$  and  $\beta = 25^\circ - 50^\circ$ . The cables are subjected to large amplitude vibrations under 10-30 mm/hr rainfall condition and also the range of reduced wind speeds causing rain-vibration is more for larger diameter cable than the smaller diameter.



(a) Effect of rainfall intensity

(b) Effect of wind speed and rainfall intensity

Figure 3.29 Effect of rainfall intensity and wind speed on vibration amplitude of the Stay cable ( $\alpha=25^\circ$ ,  $\beta=35^\circ$ ) - Cable model II

### 3.12.2 Effect of damping ratio on rain-wind induced vibration on cable model II

Figure 3.30 and 3.31 shows the comparison of damping ratio's and Scruton number for the cable positioned to  $\alpha=25^\circ$ ,  $30^\circ$  and  $\beta=30^\circ$ ,  $35^\circ$ . Figure 3.30(a) and 3.30(c) shows vibration amplitude of the cable model II with damping ratio's,  $\xi=0.04\%$  and  $0.1\%$  for cable

positioned to  $\alpha=30^\circ$  and  $\beta=30^\circ$ . And figure 3.30 shows the effect of damping ratio on cable positioned to  $\alpha=30^\circ$  and  $\beta=35^\circ$ .

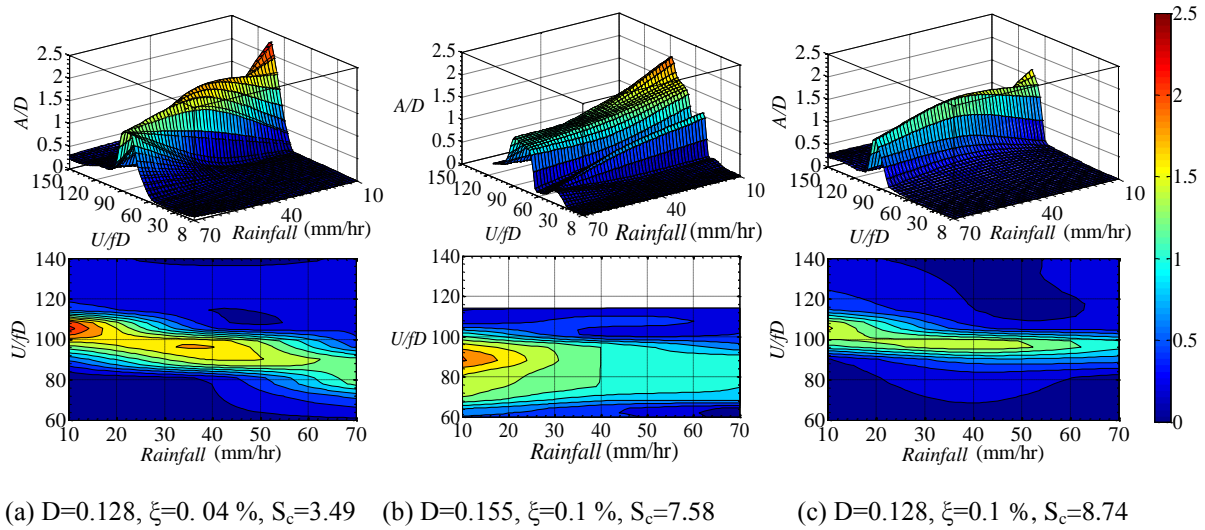
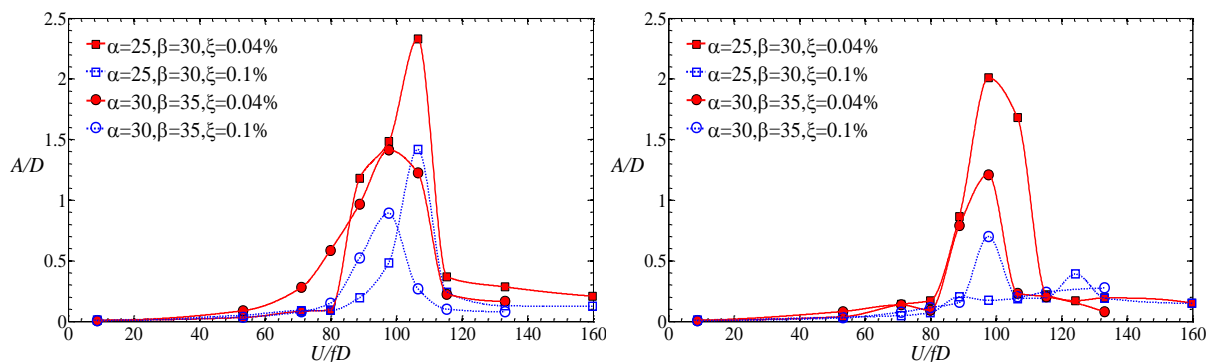


Figure 3.30 Effect of damping ratio and Scruton number on stay cable vibration

( $\alpha=30^\circ, \beta=30^\circ$ )

Figures 3.30(a), 3.30(b) and 3.30(c) show the peak vibration amplitude and the range of reduced wind speeds ( $U/fD_{crit}$ ) causing rain-wind induced vibrations decreases with increase in damping. The Scruton number of the cable model II with 0.04 % and 0.1% damping are 3.49, 8.74 whereas the Scruton number of cable model I is 7.58. Figure 3.31 shows the effect of Scruton number on the vibration amplitude of stay cable under rain-wind induced cable vibration. A similar phenomenon was observed for the cable with  $\alpha=25^\circ, 30^\circ$  and  $\beta=30^\circ, 35^\circ$ .



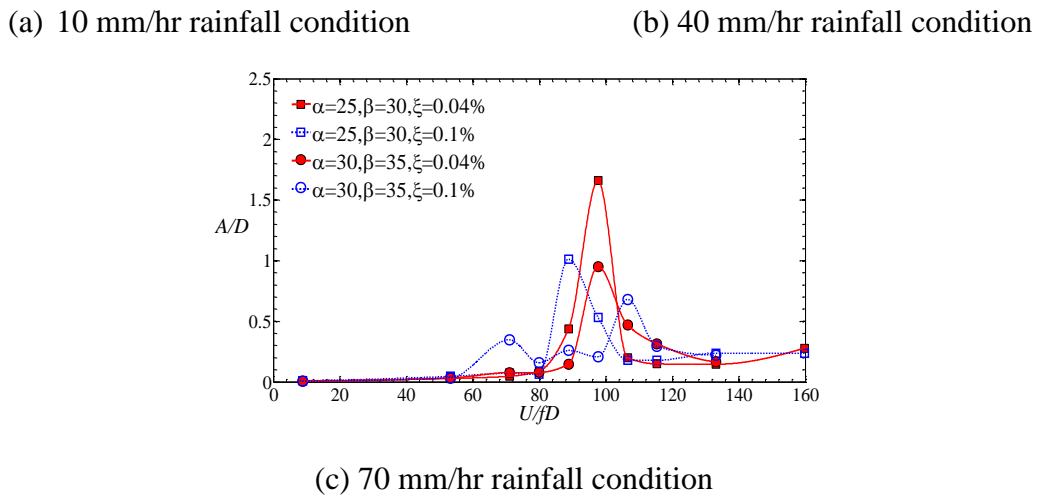
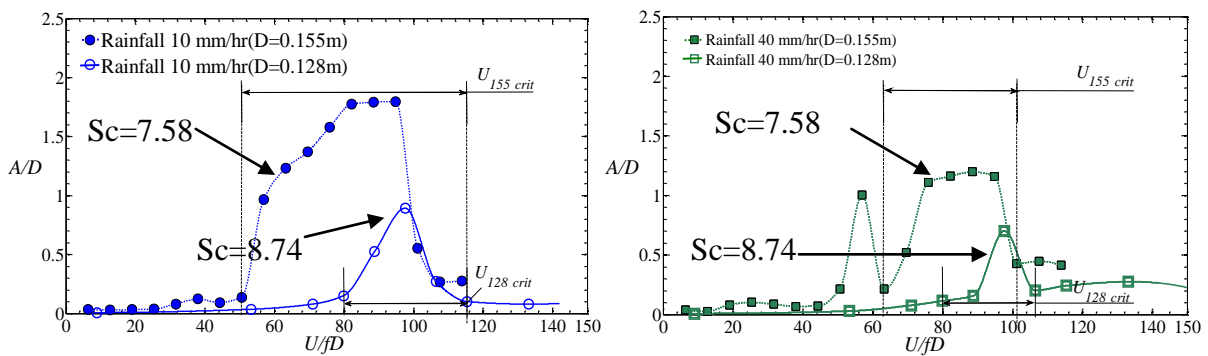


Figure 3.31 Effect of damping ratio on stay cable vibration ( $\alpha=25^\circ, \beta=30^\circ$  and  $\alpha=30^\circ, \beta=35^\circ$ )

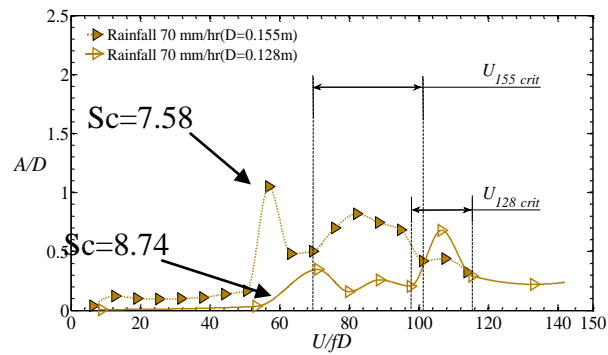
**3.12.3 Effect of cable diameter on rain-wind induced cable vibration**

Figure 3.32 shows the effect of vibration amplitude of the cable ( $\alpha=30^\circ, \beta=35^\circ$ ) of diameters 0.155m and 0.128m for different rainfall intensities i.e., 10, 40 and 70 mm/hr. Under 10 mm/hr rainfall condition, the cable model I ( $D=0.155$  m) vibrates for a long range of wind speeds ( $U_{155}$  crit), whereas the cable model II ( $D=0.128$ ,  $\xi=0.1\%$ ) vibrates for a short period of wind speeds ( $U_{128}$  crit). It is also important to notice that the cable model-II (i.e.,  $D=0.128$  m) vibrates at lower wind speeds, whereas the cable model-I vibrates for a longer range of wind speeds. The peak amplitude of vibration decreases with increase in rainfall intensity for both the cable models I and II. The cable model II exhibits much smaller amplitude of vibration than that of model I for all the three rainfall intensities.



(a) Rainfall 10 mm/hr

(b) Rainfall 10 mm/hr



(c) Rainfall 70 mm/hr

Figure 3.32 Effect of diameter on vibration amplitude of the cable ( $\alpha=30^\circ, \beta=35^\circ$ ) for different rainfall intensities

A similar phenomenon was also found in cables which are inclined at  $25^\circ$  and wind yaw angles are from  $30^\circ$  and  $35^\circ$ .

Table 3.8 Parametric studies on rain-wind induced stay cable vibration– A comparison with the current study (Field measurement)

Author	Dia. × Length (m)	weight (kg/m)	$f_n$ (Hz)	$\xi$ (%)	$\alpha$ (°)	$\beta$ (°)	Wind speed (m/s)	Rainfall (mm/hr)	Peak –Peak amplitude (mm)	Critical conditions	$S_c$
Hikami [1]	0.14 × (65-200)	51	1-3	0.11-0. 44	25-65	30-45 (NNW & SSE)	5-18		550 (U:14 m/s)	$\alpha$ : 33°-64° $\beta$ : 30°-45° U : 7-17 m/s	39.9-159. 8
Ni [13]	0.119 × 121.9	51.8	1.07,2.4, 3.2,4.23	0.178 -0.086	35.2	0-90	2-18		10 g	$\beta$ : 10°-50° U: 6-14 m/s Rainfall $\leq$ 8 mm/hr	
Present work	0.155 × 2.5	17.76	1.02 & 1.07	0.12	25-45	25-50	4-18	10, 40, 70	600	$\alpha$ =25°, 30° and $\beta$ =30°, 35°	7.58

 $\alpha$ : inclination angle of the cable; $\beta$ : wind yaw angle;  $\xi$ : damping ratio; $f_n$ : frequency;  $S_c$ : Scruton number

(based on vibration modes)

### 3.13 Mitigation of rain-wind induced cable vibrations

There were many kind of modification over the cable surface was done to mitigate the rain-vibration by breaking the continuous rivulet formed over the cable [8, 5, 15]. In order to study the efficient way to mitigate such vibrations, the surface of the cable model was modified by means of winding a thin wire around the cable as shown in the figure 3.33. From the experimental results explained in section 3.11.4.1 and 3.11.6.2 of this paper, it is known that the cable positioned at  $\alpha=25^\circ$  and  $\beta=35^\circ$  shows very large amplitude and thin wire was twined around the cable. These thin wire serves the cable from vibrating, as it breaks down the rivulet formed over the upper and bottom surface of the cable as showin in figure 3.34. Figure 3.34 shows the break down of rivulet when  $U/fD = 75.9$  and  $82.22$  under  $10 \text{ mm/hr}$  rainfall condition.

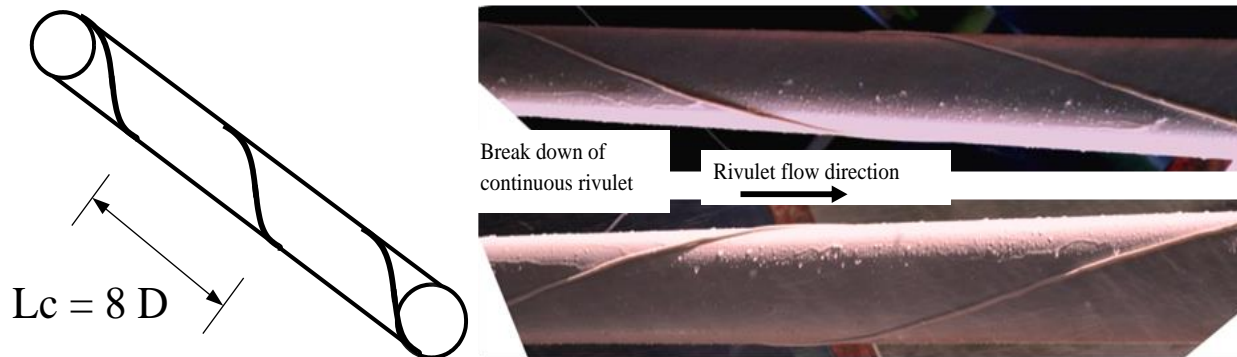


Figure 3.33 Cable with a thin wire of  $L_c=8D$

Figure 3.34 Breakdown of continuous rivulet ( $\alpha=25^\circ \beta=35^\circ$ )

In order to study the efficiency of the helical wire mitigation, the spacing between two rings ( $L_c$ ) were varied to  $8D$ ,  $10D$  and  $12D$  ( $D=15.5 \text{ cm}$ , i.e., Diameter of the cable) as and tested under  $10 \text{ mm/hr}$  rainfall condition and the results are shown in figure 3.35. It is also seen that vibration disappeared using the wires around the cable as it breaks the continuous rivulet.

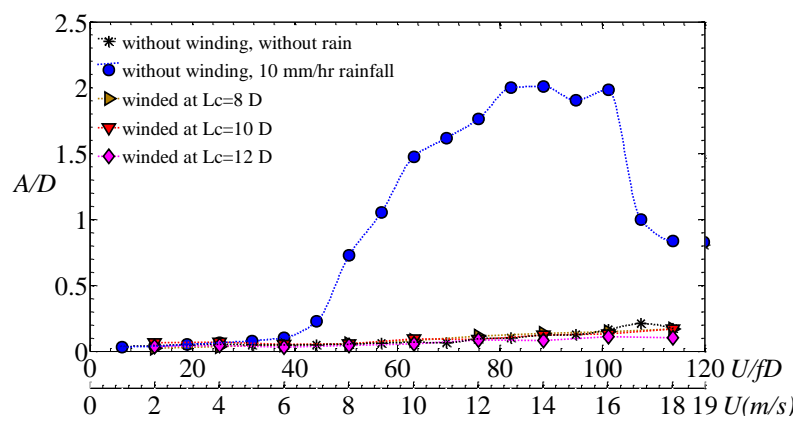
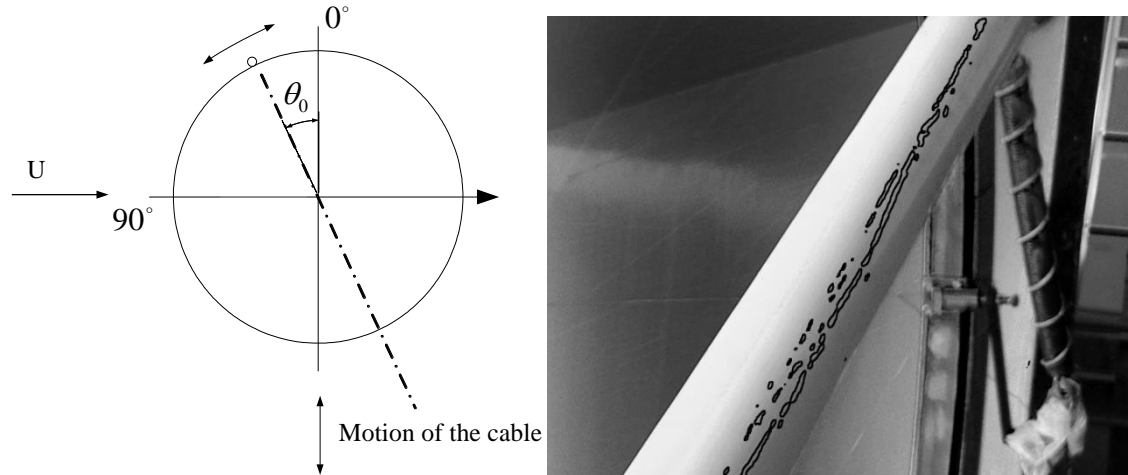


Figure 3.35 Comparison of vibration amplitudes with and without mitigation at 10 mm/hr rainfall condition ( $\alpha=25^\circ\beta=35^\circ$ )

**3.14 Evaluation of Rivulet position from the Experiment**

The rivulet positions were evaluated from the images and videos captured during the experiment. There are two markings on either side of the cable model, which facilitates the real-time evaluation of the position and motion of the rivulet. Figure 3.5 (section 3.10) shows the marking made at the ends of the cable model. Figure 3.36 (a) shows the direction of motion of the cable and static position of the rivulet. A sample picture of the processed image from the experiment for the case is shown in figure 3.36 (b).



(a) Static position of the rivulet

(b) Processed image –Evaluation of rivulet position for cable with  $\alpha=30^\circ \beta=30^\circ U=9 \text{ m/s}$

Figure 3.36 Evaluation of static position of the Experimental cable model

Figures 3.37, 3.38, 3.39 and 3.40 show the measured mean position of the rivulet with respect to the wind speed. The measured position is then fitted using a cubic polynomial and thus interpolation and extrapolation can be done to estimate the unknown variables. It is observed that during low rainfall, the rivulet appeared to be a very thin and appears at wind speeds of about 7 m/s and above. Since, the rivulet is thin under low rainfall and thus the circumferential motion of the rivulet varies for larger angles. Whereas during moderate and higher rainfall (40 mm/hr and 70 mm/hr) condition, the rivulet appears to be thick and also can vibrate for smaller circumference. When the wind speed is increased to 16 m/s, the rivulet gets washed away from the cable and a kind of buffeting response is observed.

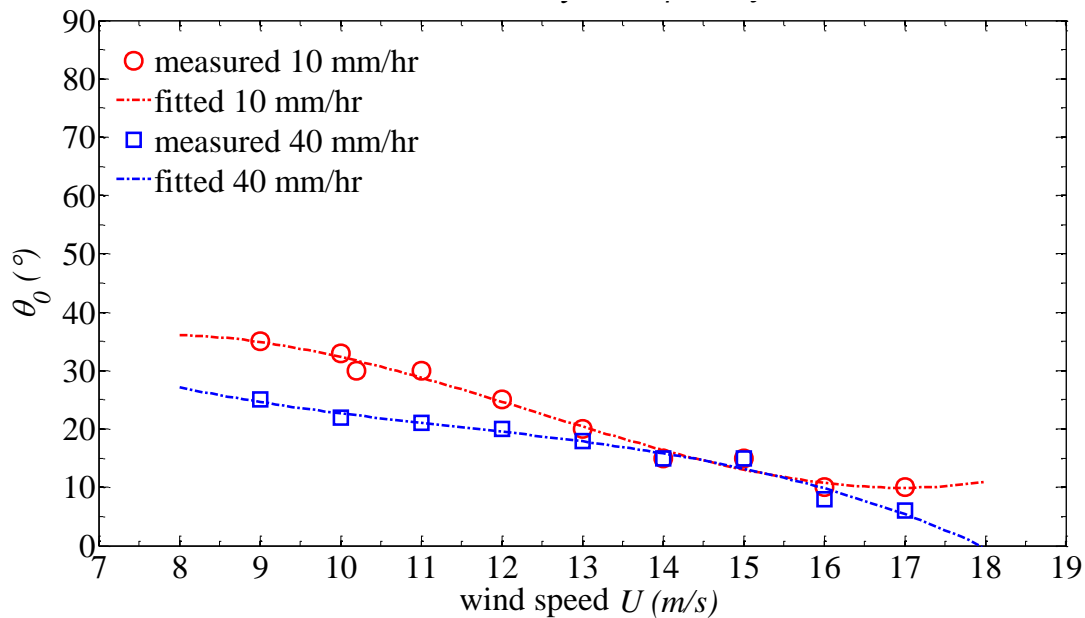


Figure 3.37 Mean wind speed versus position of the rivulet ( $\alpha=35^\circ, \beta=30^\circ, R=10,40$  mm/hr)

Figure 3.37 shows the observed mean position with respect to mean wind speed, in which the position of the rivulet under 10 m/hr is found to be  $36^\circ$  (8 m/s) and when the wind speed is 17 m/s, the circumferential mean position of the rivulet goes over the top of the cable due to the approaching wind and is found to be  $12^\circ$ . The measured observations were found for different cable inclination, wind yaw angle and the rainfall intensity.

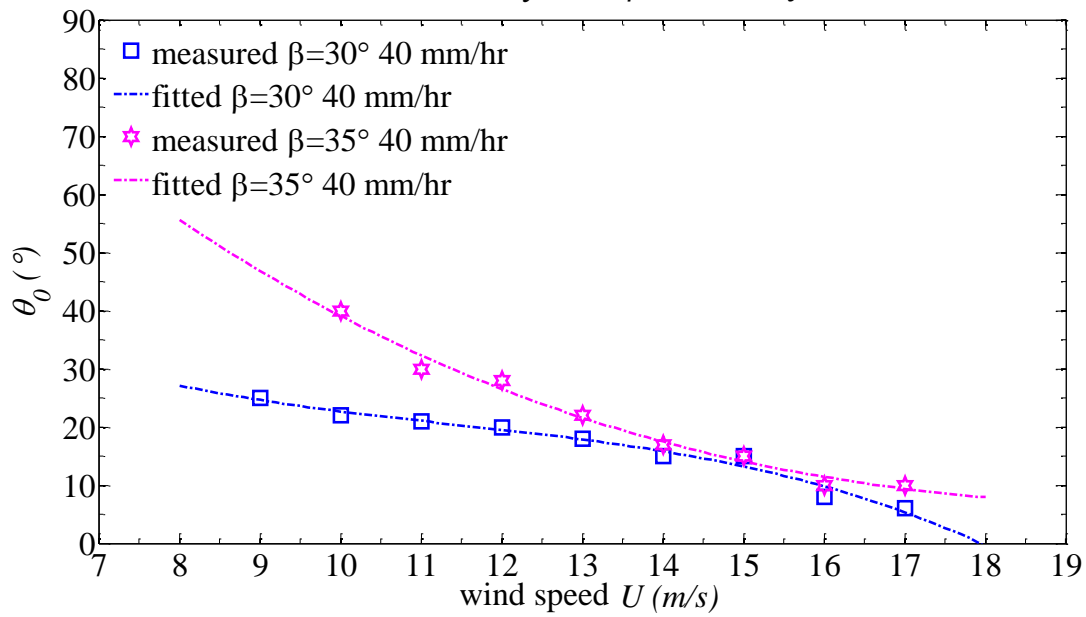


Figure 3.38 Mean wind speed versus position of the rivulet ( $\alpha=35^\circ, \beta=30^\circ$  and  $35^\circ$ )

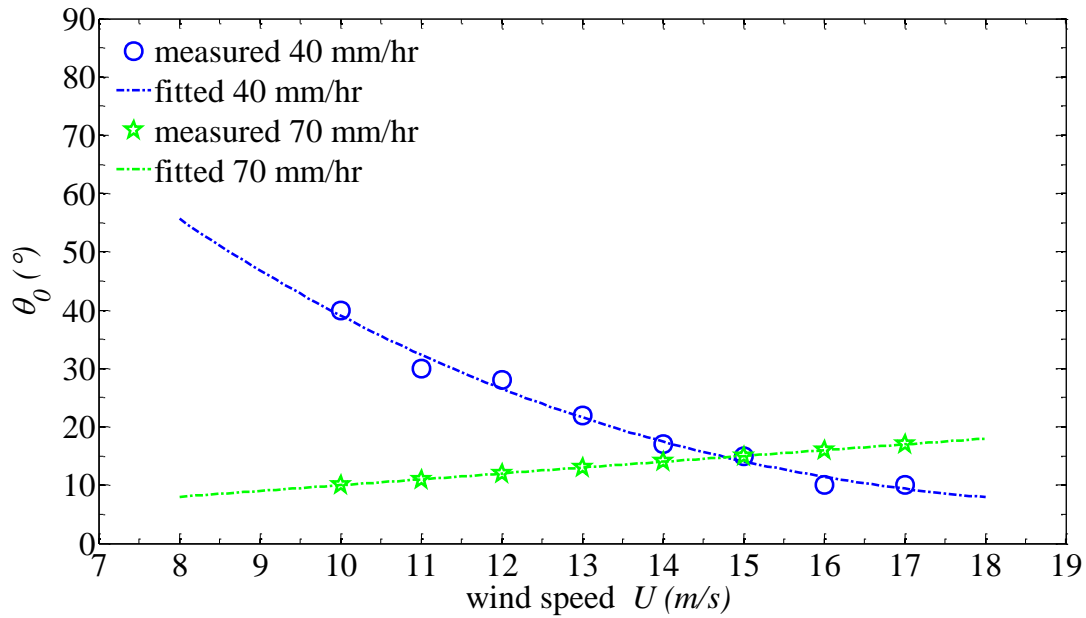


Figure 3.39 Mean wind speed versus position of the rivulet ( $\alpha=35^\circ, \beta=35^\circ, R=40, 70$  m/hr)

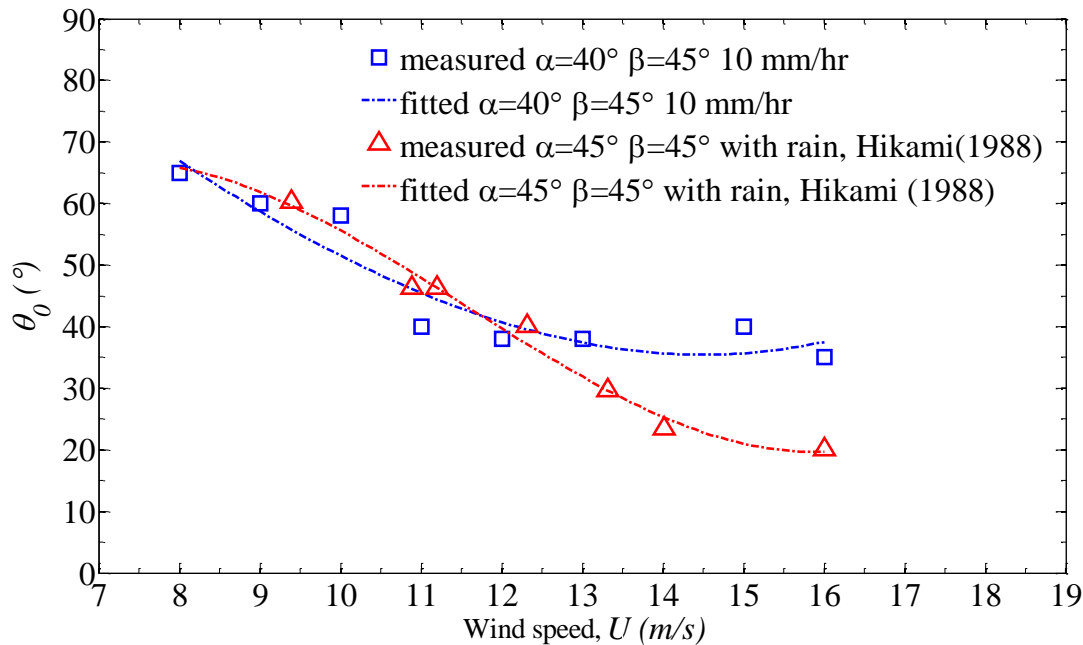


Figure 3.40 Mean wind speed versus position of the rivulet ( $\beta=45^\circ$ )

It is found that the position of the rivulet is a main function of wind speed, direction, rainfall and the turbulent intensity. Figure 3.40 shows the observed mean position of the rivulet under  $45^\circ$  wind yaw angle which also precisely matches with the results of Hikami (1988).

### 3.15 Concluding remarks

A new experimental setup was developed that can test cables under conditions of wind and rain-wind for a large variety of cable inclination and wind yaw angles. This setup was used to conduct a series of tests on cables to understand the phenomena of rain-wind-induced vibrations, and the effects of rainfall intensity, wind speed, inclination angle, and wind yaw angle on the vibration amplitude of the cables were studied. The results seem to be close to those of past studies and field investigations. The main conclusions and observations on rain-wind-induced vibrations are listed below.

- 1) Rain-wind-induced vibration is found to be a velocity-restricted vibration as well as to be guided by rainfall intensity.
- 2) An upper rivulet and a lower rivulet appeared on the cable. The formation of these rivulets depends on wind speed, cable inclination angle, wind yaw angle and the rainfall

intensity. Thin rivulets were formed over the upper surface during 10 mm/hr rainfall and thick ones during 40 mm/hr and 70 mm/hr rainfall. Also, the angular displacement of the upper rivulet over the cable was proportional to the cable vibration amplitude, which demonstrates that the cable vibration frequency must be the same as that of the rivulet.

- 3) Observations showed that the low-rainfall condition used in this experiment, i.e., 10 mm/hr, causes very large amplitude vibrations for several combinations of inclination and wind yaw angles. Also, the authors perceived that the cable vibration amplitude may be even more than  $2D$  when the rainfall is from 6-10 mm/hr.
- 4) For every case, the maximum vibration amplitude and the range of wind speeds causing the vibration, decreases as the rainfall intensity increases. The cable vibrates in most cases (i.e.,  $\alpha=25^\circ$  to  $40^\circ$  and  $\beta=25^\circ$  to  $50^\circ$ ), but the amplitude is very large for the combination of cable inclination and wind yaw angles, i.e.,  $\alpha=25^\circ$ ,  $30^\circ$  and  $\beta=30^\circ$ ,  $35^\circ$ , under 10 mm/hr of rainfall. The maximum amplitude was found to be 31.5 cm, which is  $2.03 D$  (2.03 times the Diameter of the cable) for  $\alpha=25^\circ$ ,  $\beta=35^\circ$ .
- 5) The ranges of critical reduced wind speeds causing vibrations fall between 56.9 and 107.5 (9-17 m/s) for 10 mm/hr rainfall, and 63.25-94.87 (10-15 m/s) for 40 mm/hr and 70 mm/hr rainfall conditions. Especially during 10 mm/hr rainfall, when the cable is positioned at  $\alpha=25^\circ$  and  $\beta=35^\circ$ , the range of critical wind speeds ( $U_{crit}$ ) causing vibration is from 37.9 to 107.52 (6-17 m/s) and when  $\alpha=30^\circ$  and  $\beta=30^\circ$ ,  $U_{crit}$  is from 56.9 to 101.2 (9-16 m/s) and for  $\alpha=30^\circ$  and  $\beta=35^\circ$ ,  $U_{crit}$  is from 50.6-94.87 (8-15 m/s)
- 6) It is also found that the maximum vibration amplitude and the range of wind speeds causing vibration decreases for wind yaw angles of  $35^\circ$ ,  $40^\circ$ ,  $45^\circ$  and  $50^\circ$  when the cable is inclined at  $25^\circ$  to  $40^\circ$ .
- 7) Similarly, for cable inclination angles of  $25^\circ$ ,  $30^\circ$ ,  $35^\circ$  and  $40^\circ$ , the cable vibration amplitude decreases with increase in wind yaw angle and is suppressed for certain combinations of angles, i.e.,  $\alpha=35^\circ$   $\beta=45^\circ$ ,  $\alpha=35^\circ$   $\beta=50^\circ$  and  $\alpha=40^\circ$   $\beta=45^\circ$ .
- 8) The effect of damping, Scruton number, and diameter were studied. The increase in damping from 0.04% to 0.1% doesn't suppress the vibration whereas it can reduce the amplitude level of the vibration. And the cable with diameter 0.128m causes vibrations for a short range of wind speeds whereas the increase in diameter (0.155m) cause

vibrations for a longer range of wind speeds. The larger diameter cable is more susceptible to large amplitude vibrations.

- 9) The images and videos captured during the experiments are processed and the mean positions of the rivulet with respect to the wind speed are obtained. The observations can be used in Chapter IV for evaluating the response of the cable for various conditions.
- 10) The rain-wind induced cable vibration can be mitigated by breaking down the rivulet by twining the helical wire around the cable.

### **3.16 References**

1. Y. Hikami and N. Shirashi, Rain-Wind induced vibrations of cables in cable stayed bridges, *Journal of Wind Engineering and Industrial Aerodynamics*, 29 (1988) 409-418.
2. M. Matsumoto, N. Shiraishi, Aerodynamic behavior of inclined circular cylinders-cable aerodynamics, *Journal of Wind Engineering and Industrial Aerodynamics*, 33 (1990) 63-72
3. M. Matsumoto, N. Shiraishi and H. Shirato, Rain-wind induced vibration of cables of cable-stayed bridges, *Journal of Wind Engineering and Industrial Aerodynamics*, 41-44 (1992) 2011-2022
4. Masaru Matsumoto, Tohru Saitoh, Masahiko Kitazawa, Hiromichi Shirato, Takayuki Nishizaki, Response characteristics of rain-wind induced vibration of stay-cables of cable-stayed bridges, *Journal of Wind Engineering and Industrial Aerodynamics* 57 (1995) 323-333.
5. Oliver Flamand, 'Rain-wind induced vibration of cables, *Journal of Wind Engineering and Industrial Aerodynamics* 57 (1995) 353-362.
6. Bosdogianni, D.Olivari, 'Wind and rain- induced oscillations of cables of stayed bridges', *Journal of Wind Engineering and Industrial Aerodynamics* 64 (1996) 79-95.
7. C.Verwiebe, H.Ruscheweyh, 'Recent research results concerning the exiting mechanisms of rain-wind-induced vibrations', *Journal of Wind Engineering and Industrial Aerodynamics* 74-76 (1998) 1005-1013.
8. Ming Gu, Xiaoqin Du, 'Experimental investigation on rain-wind-induced vibration of

- cables in cable-stayed bridges and its mitigation’, *Journal of Wind Engineering and Industrial Aerodynamics* 93 (2005) 79-95.
9. D.Zuo, N.P.Jones, J.A.Main, Field observation of vortex- and rain-wind-induced stay cable vibrations in a three dimensional environment, *Journal of Wind Engineering and Industrial Aerodynamics*, 96 (2008) 1124-1133.
  10. S. Zhan, Y.L. Xu, H.J. Zhou, K.M. Shum, ‘Experimental study of wind-rain-induced vibration using a new model setup scheme’, *Journal of Wind Engineering and Industrial Aerodynamics* 96 (2008) 2438-2451.
  11. Lin-Shan Xu, Yao-Jun Ge, Lin Zhao, ‘Experimental Investigation on Rain-Wind-Induced Vibration of Stay Cables based on High precision raining machine’, *The Seventh Asia Pacific Conference on Wind Engineering*, November 8-12, 2009, Taipei, Taiwan.
  12. Hui Li, Wen-Li Chen, Feng Xu, Feng-Chen Li, Jin Ping Ou, A numerical and experimental hybrid approach for the investigation of aerodynamic force on stay cables suffering from rain-wind induced vibration, *Journal of Fluids and Structures* 26 (2010) 1195-1215.
  13. Y.Q. Ni, X.Y. Wang, Z.Q. Chen, J.M. Ko, Field observations of rain-wind-induced cable vibration in cable-stayed Dongting Lake Bridge, *Journal of Wind Engineering and Industrial Aerodynamics*, 95 (2007) 303-328.
  14. D.Zuo, N.P.Jones, J.A.Main, Field observation of vortex- and rain-wind-induced stay cable vibrations in a three dimensional environment, *Journal of Wind Engineering and Industrial Aerodynamics*, 96 (2008) 1124-1133.
  15. Phelan, S. C., Sarkar, P. P. and Mehta, K.C. (2006), Full-Scale Measurements to Investigate Rain-Wind Induced Cable-Stay Vibration and its Mitigation, *Journal of Bridge Engineering*, ASCE, Vol. 11, p. 293 – 304.
  16. H. Yamaguchi, Analytical study of growth mechanism of Rain vibration of cables, *Journal of Wind Engineering and Industrial Aerodynamics*, 33 (1990) 73-80.
  17. Y.L. Xu, L.Y. Wang, Analytical study of wind-rain-induced cable vibration: SDOF model, *Journal of Wind Engineering and Industrial Aerodynamics*, 91 (2003) 27-40.

18. Krzysztof wilde, Wojciech Witkowski, Simple model of rain-wind induced vibrations of strayed cables, *Journal of Wind Engineering and Industrial Aerodynamics*, 91 (2003) 873-891.
19. Chen-Wen-Li, Li Hui, Xu Feng., Li-Feng Chen, Ou Jin-Ping, Study of aerodynamic forces on stay cables under rain-wind induced vibration by a hybrid method of test combining with computation, *The Fifth International symposium on Computational Wind Engineering* (May 23-27, 2010: CWE 2010).
20. Cecile Lemaitre, Emmanuel de Langre, Pascal Hemon, 'Rainwater rivulets running on a stay cable subject to wind', *European Journal of Mechanics B/Fluids* 29 (2010)251-258.
21. D.Q.Cao, R.W.Tucker, C.Wang, 'A stochastic approach to cable dynamics with moving rivulets', *Journal of Sound and Vibration* 268 (2003) 291-304
22. LIU Qingkuan, Zhang Feng, Ma Wenyong, Wang Yi. 'Experimental study on Reynolds number effect and dry cable galloping of stay cables', *Proceedings of the 13th International Conference on Wind Engineering*. Amsterdam, Netherlands, July 10-15, 2011



## **CHAPTER IV**

# **SDOF: ANALYTICAL MODEL ON RAIN-WIND INDUCED STAY CABLE VIBRATIONS**

### **4.1 Introduction**

Analytical methods had been developed by Yamanguchi (1990), Y.L.Xu (2003), M. Gu (209), Wilde (203) and many more. Most of the methods were coupled with Experimental results or with the aid of computational methods. In the previous chapter, it is explained that the presence of rivulet would cause the stay cable to vibrate and thus it is necessary to study the aerodynamic forces and the pressure distributions over the cylinder. The aerodynamic co-efficients or the pressure distributions obtained through experimental methods are believed to be more reliable as the problem involves any kind of complex vortices and thus most of the researchers relay on experimental results. Many researchers relay on computational fluid dynamics in order to eliminate the capitation cost and also to provide qualitative results in a short time.

Here in this Chapter IV, a detailed study had been done by evaluating the analytical model developed by Y.L.Xu(2003). The analytical model was also checked by considering the static position of the rivulet on a horizontal cylinder, then on to the yawed cylinder and then to the inclined cylinder. The inclined cylinder case considers the motion of the rivulet as a sinusoidal function. And the result of the inclined cable model was compared with the experimental results and a validation was also done.

In this study the analytical model of Xu (2003) is explained and the experimental data's

from the images taken during the experiment was used. And the analytical model was modified accordingly and the results were plotted.

#### 4.2 Modeling of rain-wind induced stay cable vibration

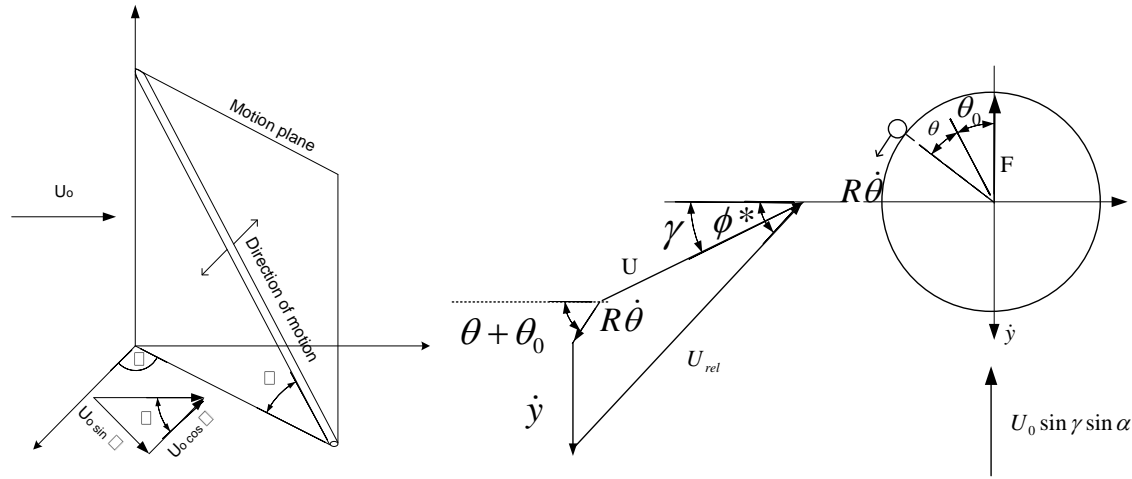


Figure 4.1 Modeling of rain-wind induced cable vibration (a) orientation of the cable and (b) relative velocity of the cable with moving rivulet

Let us consider a inclined stay cable as shown in figure 4.1 in which  $\alpha$  be the cable inclination angle,  $\beta$  be the wind yaw angle,  $U$  be the mean wind speed perpendicular to the plane of the inclined cable and  $\gamma^*$  be the angle of attack with respect to mean wind component  $U$ .

The mean wind perpendicular to the cable is given by,

$$U = U_0 \sqrt{\cos^2 \beta + \sin^2 \alpha \sin^2 \beta} \quad (4.1)$$

The angle of attack with respect to mean wind component  $U$  is given by,

$$\gamma^* = \varepsilon \sin^{-1} \left( \frac{\sin \alpha \sin \beta}{\sqrt{\cos^2 \beta + \sin^2 \alpha \sin^2 \beta}} \right) \quad (4.2)$$

Since there is no experimental results available to find the stagnation point of the wind

on to the cable with a rivulet and thus a influence factor called  $\varepsilon$  is multiplied with the angle of attack. The value of  $\varepsilon$  can be assumed to 0.3.

The relative wind speed  $U_{rel}$  is given by,

$$U_{rel} = \sqrt{(U \cos \gamma + R\dot{\theta} \cos(\theta + \theta_o))^2 + (U \sin \gamma + R\dot{\theta} \sin(\theta + \theta_o) + \dot{y})^2} \quad (4.3)$$

The relative wind speed determines the wind speed relative to the moving rivulet and thus it becomes a function of  $\dot{y}$ ,  $\theta$ ,  $\dot{\theta}$ , where  $\dot{y}$  be the transverse vibration velocity of the cable,  $\theta$  be the static initial position of the rivulet on the cable, and  $\dot{\theta}$  be the angular velocity of the upper rivulet. The angle between the relative velocity  $U_{rel}$  and the horizontal is given by  $\phi^*$ ,

$$\phi^* = \tan^{-1} \frac{(U \sin \gamma + R\dot{\theta} \sin(\theta + \theta_o) + \dot{y})}{(U \cos \gamma + R\dot{\theta} \cos(\theta + \theta_o))} \quad (4.4)$$

where R is the radius of the cylinder and the size of the rivulet is considered small compared with the diameter of the cylinder and thus  $\phi^*$  can be given as,

$$\phi = \phi^* - \theta - \theta_o = \tan^{-1} \frac{(U \sin \gamma + R\dot{\theta} \sin(\theta + \theta_o) + \dot{y})}{(U \cos \gamma + R\dot{\theta} \cos(\theta + \theta_o))} - \theta - \theta_o \quad (4.5)$$

The total vertical force acting on the cylinder can be given by,

$$F = \frac{\rho D U_{rel}^2}{2} [C_L(\phi) \cos \phi^* + C_D(\phi) \sin \phi^*] \quad (4.6)$$

where  $\rho$  is the air density, D is the diameter of the cross-section of the cylinder,  $C_D$  is the drag coefficient, and  $C_L$  is the lift coefficient. The aerodynamic coefficients of the cylinder with rigid rivulet measured from the wind tunnel tests is expressed as the function of the angle  $\phi$  defined in Fig. 4.2 (Gu et. al, 1999).

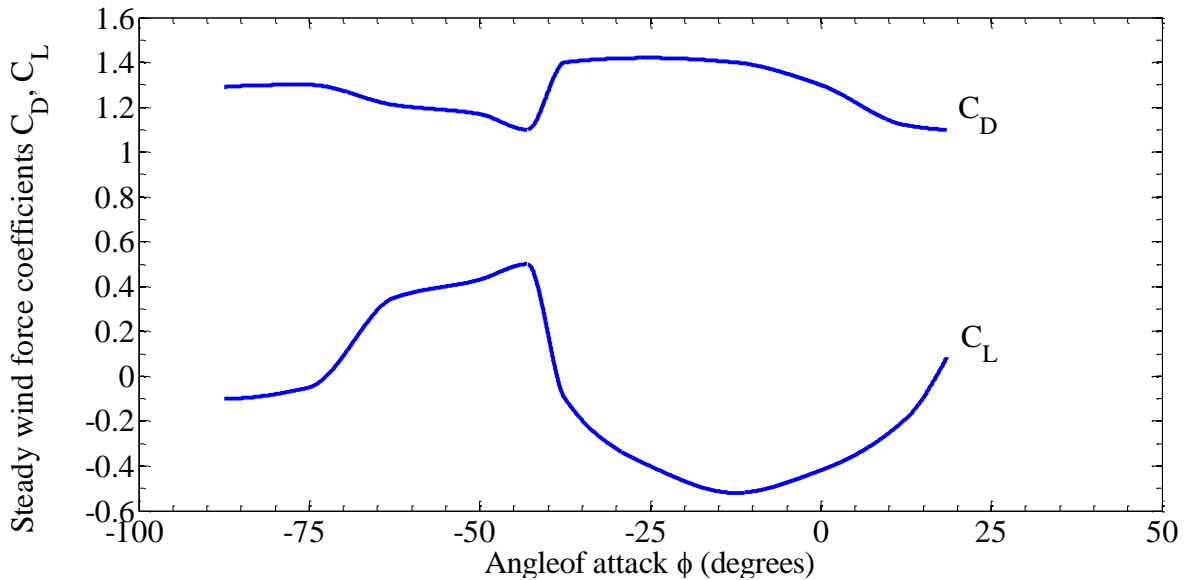


Figure 4.2 Aerodynamic co-efficients of a horizontal cylinder

The steady wind force co-efficients were fitted using Taylor series with respect to  $\phi$ . The first three terms of the Taylor's series are given below for lift and drag coefficients.

$$C_L(\phi) = A_0 + \frac{A_1\phi}{1!} + \frac{A_2\phi^2}{2!} + \frac{A_3\phi^3}{3!} + \dots, \quad -\infty < \phi < \infty \quad (4.7)$$

$$C_D(\phi) = B_0 + \frac{B_1\phi}{1!} + \frac{B_2\phi^2}{2!} + \frac{B_3\phi^3}{3!} + \dots, \quad -\infty < \phi < \infty \quad (4.8)$$

$A_0, A_1, A_2$  and  $A_3$  were the coefficients obtained by fitting the lift as a function of  $\phi$  and  $B_0, B_1, B_2$  and  $B_3$  were the coefficients of the drag which is also a function of  $\phi$ .

The substitution of Equation (9) and (10) into Equation (6) and then the expansion of the sine and cosine functions in Eq. (6) with respect to  $\phi$  and the use of the first two terms of the power series yield the vertical force acting on the cylinder per unit length of the form.

$$F = \frac{\rho D U_{rel}^2}{2} \left[ \left( A_0 + \frac{A_1 \phi}{1!} + \frac{A_2 \phi^2}{2!} + \frac{A_3 \phi^3}{3!} \right) \left( 1 - \frac{\phi^{*2}}{2} \right) + \left( B_0 + \frac{B_1 \phi}{1!} + \frac{B_2 \phi^2}{2!} + \frac{B_3 \phi^3}{3!} \right) \left( \phi^* - \frac{\phi^{*3}}{6} \right) \right] \quad (4.9)$$

The substitution of Eqs. 4.3 – 4.8 into Eq. (4.9) leave the following by leaving the linear terms of  $\dot{y}$ ,  $\theta$  and  $\dot{\theta}$  leads to the following force term.

$$F(x, t) = \frac{\rho D U(x)}{2} [R\dot{\theta}(x, t)\Gamma_1(x, t) + \dot{y}(x, t)\Gamma_2(x, t) + U(x)\theta(x, t)\Gamma_3(x, t)] \quad (4.10)$$

Where  $\Gamma_1, \Gamma_2$  and  $\Gamma_3$  are given in Xu (2003). Substitution of the force term (equation 12) in to the equation of motion (equation) leads to the following,

$$\ddot{y} + \omega^2 y + 2\hat{\xi}\omega\dot{y} = -\frac{\rho D a}{2m} (\Gamma_1 R U \cos \omega_r t + \Gamma_3 R U^2 \sin \omega_r t) = \check{F}(t) \quad (4.11)$$

Based on the observations done by Xu (2003), Hikami and also the explanations in chapter III of section, it can be assumed that the motion of the upper and the bottom rivulet as harmonic. But the bottom rivulet is almost static and thus the motion of the bottom rivulet is eliminated and motion of the upper rivulet is considered.

The motion of the upper rivulet is given by,

$$\theta = a \sin \omega_r t \quad (4.12)$$

Where  $a$  and  $\omega_r$  are the amplitude and natural frequency of the rivulet.

The aerodynamic damping is a function of  $\Gamma_2$  and is given by,

$$\hat{\xi} = \xi_s + \frac{\rho D \Gamma_2 U}{4m\omega} = \xi_s + \xi_a \quad (4.13)$$

### 4.3 Horizontal cylinder with fixed rivulet

It is assumed that the rivulet is static on the cable at the horizontal position and the wind yaw angle is  $0^\circ$  as shown in figure 4.3. When the rivulet is fixed, the dynamic motion  $\theta(t)$  of the rivulet relative to the cylinder is equal to zero and the static position of the rivulet  $\theta_0$  is no longer the function of the mean wind speed.

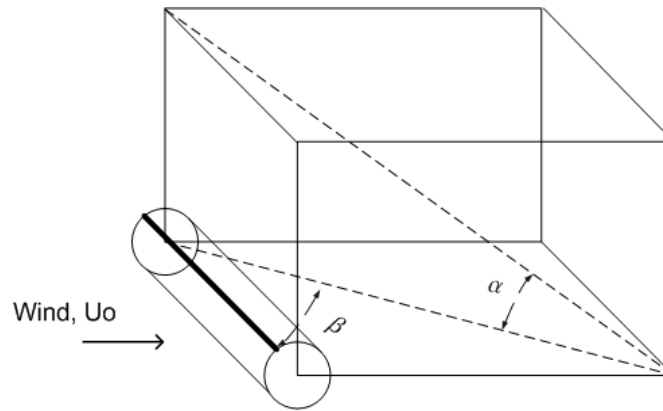


Figure 4.3 Horizontal cylinder with fixed rivulet

The equation of vertical motion of the horizontal cylinder becomes

$$\ddot{y} + \omega^2 y + 2\xi\omega\dot{y} = 0 \quad (4.14)$$

$\Gamma_2$  can be expressed by the following equation for the horizontal cylinder with zero wind yaw angle  $\beta$

$$\Gamma_2 = B_0 - B_1\theta_0 + \frac{B_2}{2}\theta_0^2 - \frac{B_3}{6}\theta_0^3 + A_1 - A_2\theta_0 + \frac{A_3}{2}\theta_0^3 \quad (4.15)$$

For the cylinder with fixed rivulet, the coefficients  $A_i$  and  $B_i$  (where  $i=1, 2, 3, 4$ ) may change with the angle  $\varphi$  that in turn depends on the cylinder velocity  $\dot{y}$  and the angle  $\varphi_n$ . Eq. (4.15) is a nonlinear differential equation and can be solved by Runge–Kutta method using MATLAB. A trial problem explained by Xu was adopted for the verification study and later on the analytical model was adopted for the experimental conditions, as explained in chapter III.

#### 4.4 Application of the analytical model (Horizontal cylinder with a fixed rivulet)

In order to evaluate the analytical model the parameters used in the experimental cable model is considered. The stay cable with inclinations  $30^\circ$  and yaw angle  $30^\circ$  was first considered. The parameters of the cable model were shown in the figures. The aerodynamic co-efficients of horizontal cylinder with fixed is listed in table 4.1.

Table 4.1 Aerodynamic co-efficients of a horizontal cylinder with fixed rivulet

Range	A0	A1	A2	A3	B0	B1	B2	B3
$\phi \geq -43^\circ$	-0.475	0.84	4.7	0.86	1.25	-0.65	-0.08	6.81
$\phi < -43^\circ$	2.19	5.89	14.06	17.53	-0.86	-5.97	-11.94	-12.18

At first the problem explained by Xu was carried out and the results are plotted in figures 4.4 and 4.5. The parameters of the cable model are displayed in the figures. Later on the same model was applied to the experimental model and the figure 4.6 shows the vibration amplitude of the cable for different static position of the rivulet.

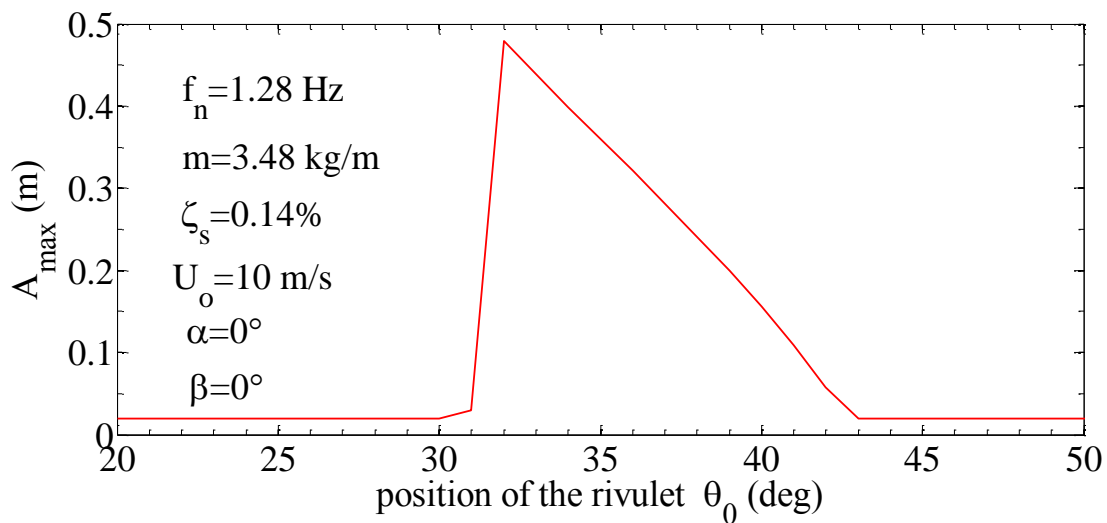


Figure 4.4 position of the rivulet vs Maximum vibration amplitude of the stay cable

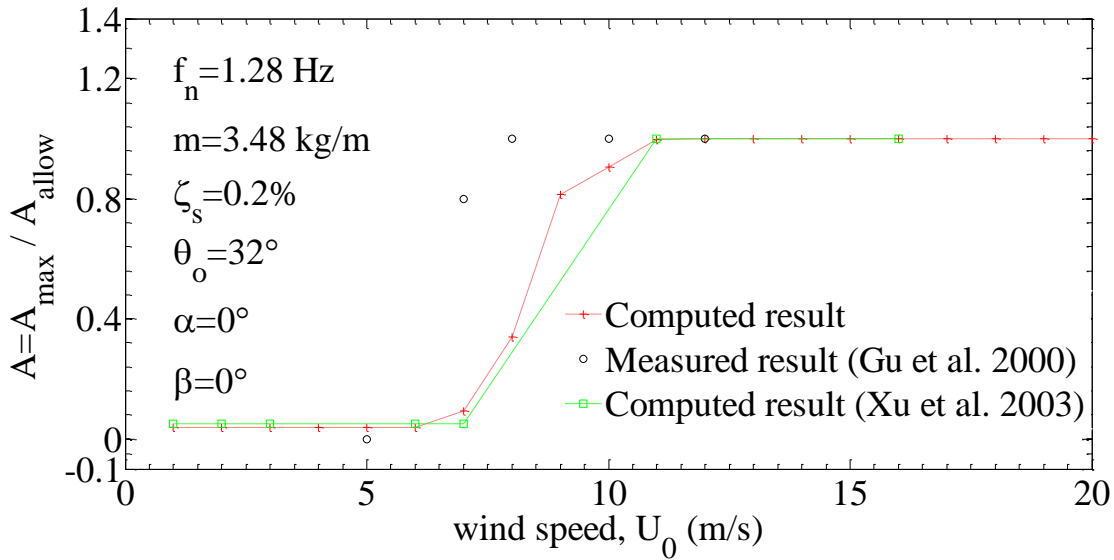


Figure 4.5 Wind speed vs normalized vibration amplitude of the stay cable

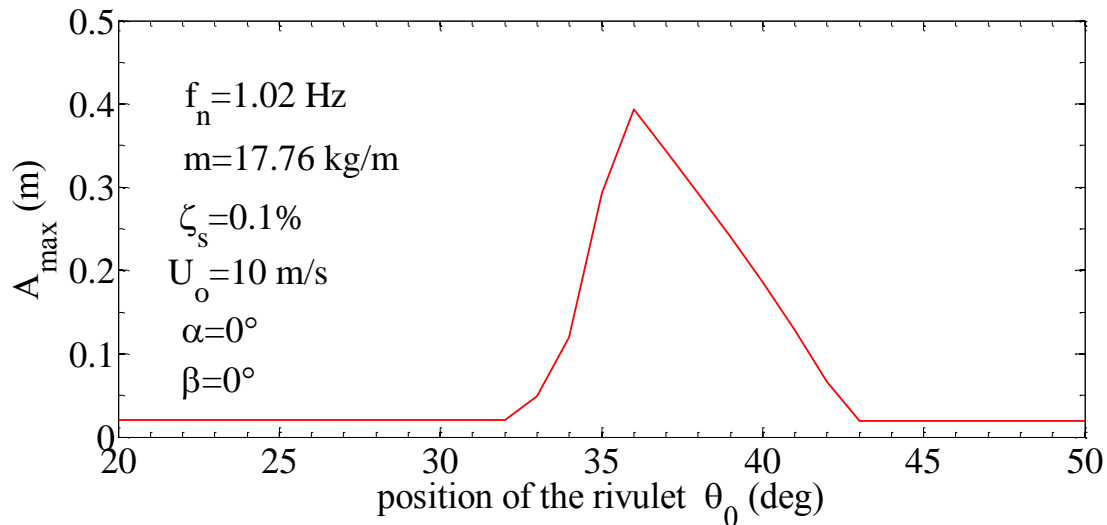


Figure 4.6 Position of the rivulet  $\theta_0$  vs Maximum vibration amplitude  $A_{\max}$  of the stay cable

#### 4.5 Inclined cylinder with moving rivulet

The following explains the SDOF analytical model for the inclined cable. The inclination angle, wind yaw angles, wind speeds with the rivulet were shown in the figure 4.7. The equation of motion is derived in the equation 4.11.

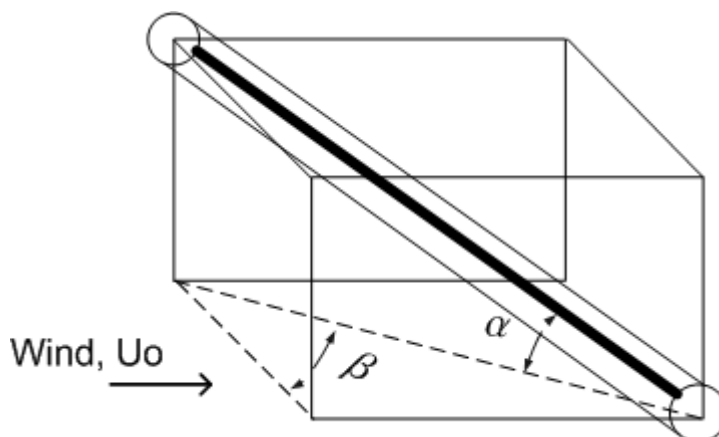


Figure 4.7 Inclined stay cable model

The aerodynamic coefficients of an inclined cylinder with a fixed rivulet are shown in figure 4.8. It can be seen at an angle of  $-55^\circ$ , there is drastic change in both the aerodynamic coefficients.

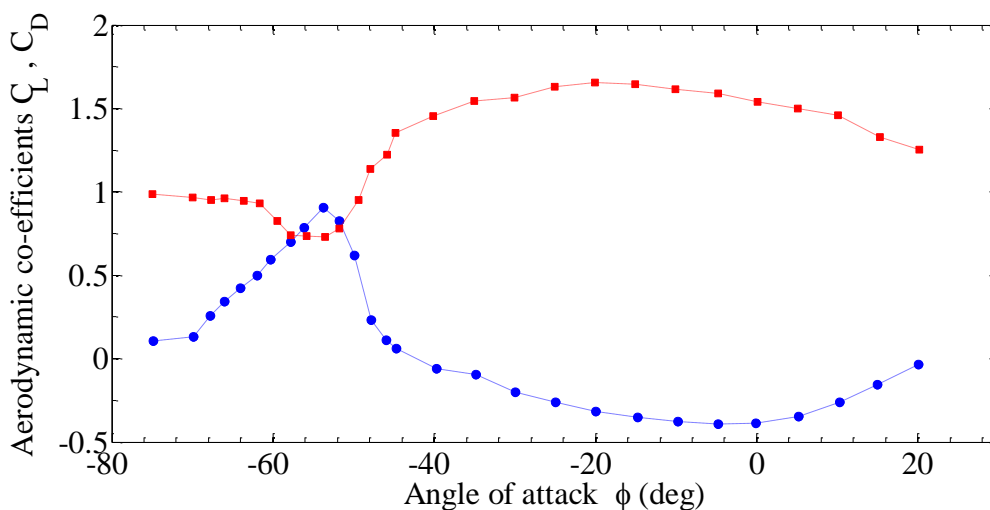


Figure 4.8 Aerodynamic co-efficient of a inclined cylinder (Hikami and shiraishi, 1988)

The motion of the rivulet is obtained from Hikami (1998) and is shown in figure 4.9 and 4.10. Figure 4.9 shows the variation of the upper rivulet with respect wind speed. It can be seen that as the approaching wind speed increases the static position of the rivulet moves upwards. Figure 4.10 shows the lower rivulet being almost static.

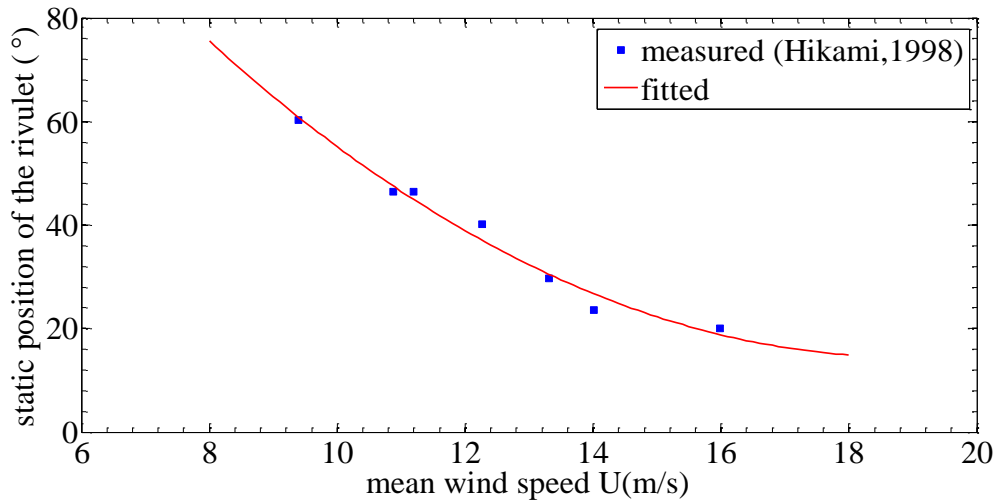


Figure 4.9 Mean wind speed vs. static position of the upper rivulet on an inclined cylinder

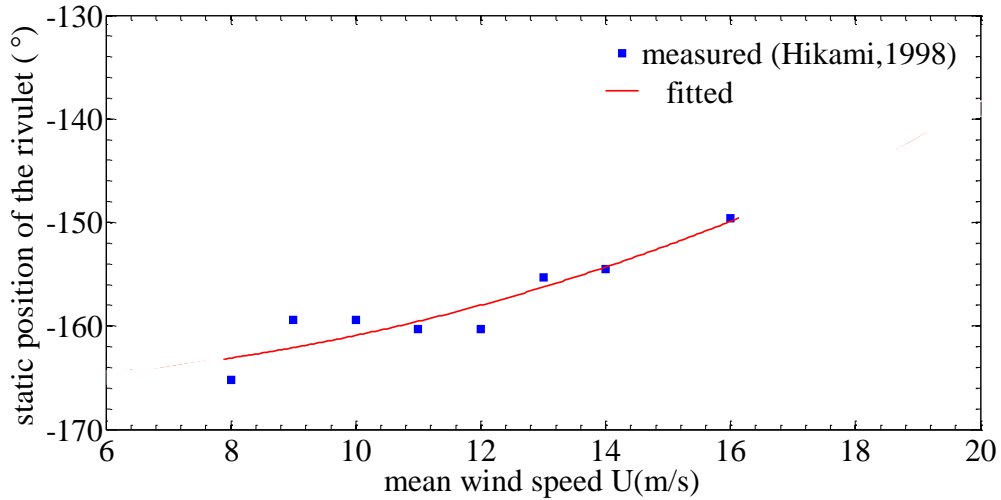


Figure 4.10 Mean wind speed vs. static position of the lower rivulet on an inclined cylinder

The motion of the upper rivulet is depicted in figure 4.11. From experiments and literature (Hikami 1998, Zhou 2007) it is found that the motion of the lower rivulet is static and is thus the effects of lower rivulet is neglected. By visual, it can be assumed that the motion of the rivulet is sinusoidal and vibration at the same frequency of the stay cable. The assumed motion of the stay cable is of the form,

$$\theta = a \sin \omega_r t \quad (4.16)$$

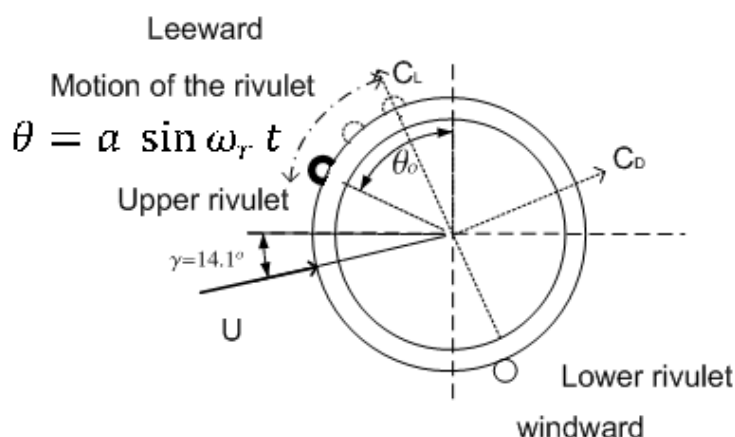


Figure 4.11 Motion of the upper rivulet on an inclined stay cable

In equation 4.16,  $a$  is the amplitude of the rivulet which is assumed by trial and error method. The analysis was carried out by solving the equation of motion equation and the response are plotted in figures 4.12 and 4.13.

#### 4.6 Application of the analytical model (inclined cable with moving rivulet)

The obtained aerodynamic coefficients are fitted using Taylor series as shown in equation 4.7 and 4.8 and the values of the fitted coefficients are shown in table 4.2. At first the model is tested with the example problem of Xu (2003) and Ohshima (1987). The initial conditions such as static position of the rivulet, motion of the rivulet were given and the analysis was run. Figure 4.12 shows the comparison of vibration amplitudes for different amplitudes of the rivulet.

Table 4.2 Aerodynamic coefficients of an inclined cylinder

Range	A0	A1	A2	A3	B0	B1	B2	B3
$\phi \geq -55^\circ$	-0.42	0.64	3.46	-2.29	1.53	-0.72	-1.07	7.16
$\phi < -55$	2.03	1.4	0	0	-5.08	-9.98	-8.12	0

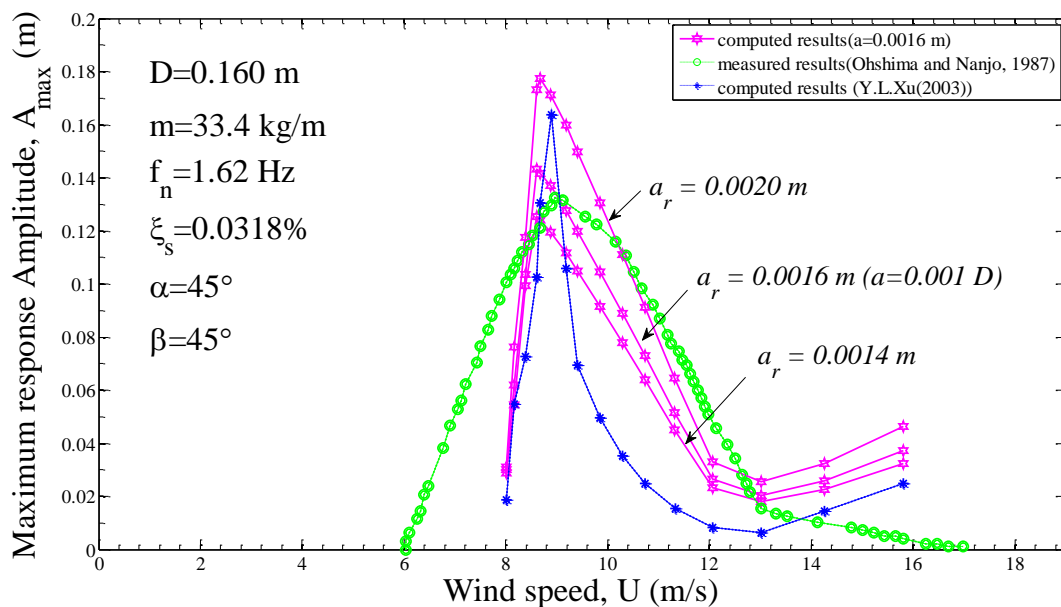


Figure 4.12 Comparison of vibration amplitudes for different rivulet amplitudes

Figure 4.13 shows the comparison of vibration amplitudes for experimental and analytical model. The amplitude of the rivulet was changed to match the response of the stay cable in different rainfall conditions.

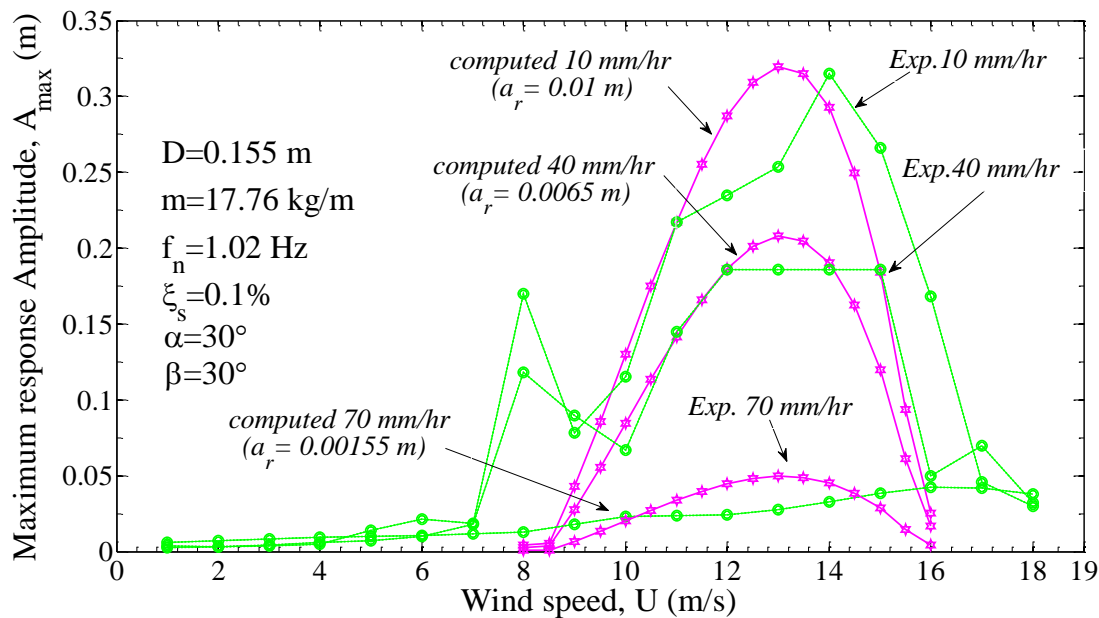


Figure 4.13 Comparison of experimental and analytical response

#### 4.7 Scruton number of the Stay cable

In general it is difficult to model large Scruton number in wind tunnel experiments and thus most of the researchers increase the frequency rather than altering the Scruton number. The cable model assumed in the previous section has very low Scruton number and thus large amplitude is observed, whereas the prototype has a large Scruton number. Table 4.3 shows the comparison of Scruton number for various models. The Scruton number of the cable model is assumed to be 4.61, which is same as that of the cable in the Fred-hartman bridge and the Scruton number of the assumed cable is also larger than the Scruton number of the Meikonishi bridge but slightly less than the Dongting lake bridge. The Scruton number is expressed from can be derived from equation 4.16.

$$S_c = \frac{m\xi}{\rho D^2} \quad (4.16)$$

The Scruton number for the cables are compared and shown in table 1. The Scruton number for the experiment is 0.6. Table 4.3 shows the Scruton number for the cables of the existing bridges and also the comparison with the experimental value.

Table 4.3 Comparison of Scruton number for different bridge cables

	Prototypes	Prototype / Exp.
Meikonishi bridge	1.7	2.81
Fredhartman bridge	4.61	7.64
Dongting lake bridge	5.31	8.8
Assumed for Megmai bridge	4.61	7.64
M.Gu's (2005) Prototype	6.86	11.3

Using the information provided in the table 4.3, it is decided to increase the Scruton number either by altering the mass or damping. Thus the damping of the cable model is assumed to be 0.1 %, so as to obtain the required Scruton number of about 4.61. The response was also estimated for the stay cable which is inclined and yawed at 45° with a Scruton number of 4.61,

making use of the aerodynamic coefficients along with the measured position of the rivulet as explained in section 3.14 of Chapter III.

#### 4.8 Response estimation for the stay cables C12 and D12

The main properties of the stay cable are assumed to be same as explained in section 5, except that the damping, Length and inclination angle and damping. Damping is increased to 0.1%, in order to increase the Scruton number of the stay cable. The response is estimated using analytical model assuming the motion of the rivulet is a function of wind speed, by interpolating the results shown in figures 3.37, 3.38, 3.39 and 3.40. The physical properties of the stay cable are shown in table 4.4. Table 4.5 shows the structural properties of the stay cable

Table 4.4 Properties of stay cable C12 and D12

Cable id.	Inclination angle $\alpha$ ( $^{\circ}$ )	Length (m)	Tension (kN)	Scruton number	Cross-sectional Area ( $m^2$ )
C12, D12	7152.2	82.7	4114.6	4.61	0.0118

Since rain-wind induced vibrations are restricted to wind yaw angles, wind speed and rainfall intensity and thus the analytical model explained in section 4.5 is applied for the cable with  $47^{\circ}$  inclination angle. More details about the cables of the Megami Bridge (Nagoya) is given in the Appendix II.

Table 4.5 Structural properties of stay cable C12 and D12

Cable id.	Density ( $kg/m^3$ )	Moment of inertia ( $m^4$ )	Young's modulus ( $N/m^2$ )	Frequency $f_n$ (Hz)	Damping $\xi$ (%)
C12, D12	7152.2	1.10E-5	$1.896058 \times 10^{11}$	1.35	0.1

It is also a well know fact that vibration amplitude of a cable is not only a function of wind speed but also a function of wind yaw angle, rainfall intensity and inclination angles (Chapter III) or it can be simulated using analytical the analytical model explained in section 4.5 by using the position of the rivulet and assuming the motion as sinusoidal. The amplitude of the

rivulet is approximated in section 4.6, which shows for the low rainfall case, the amplitude of the rivulet can be approximated as 0.003, for moderate rainfall (R40) case the amplitude of the rivulet is assumed as 0.002 and for higher rainfall (R70) case it is assumed to be 0.001. The aerodynamic coefficients of an inclined cylinder with a fixed rivulet are shown in figure 4.8. It can be seen at an angle of  $-55^\circ$ , there is drastic change in both the aerodynamic coefficients and thus it is discredited at  $-55^\circ$  and fitted using Taylor series. The coefficients are obtained and are shown in table 4.2.

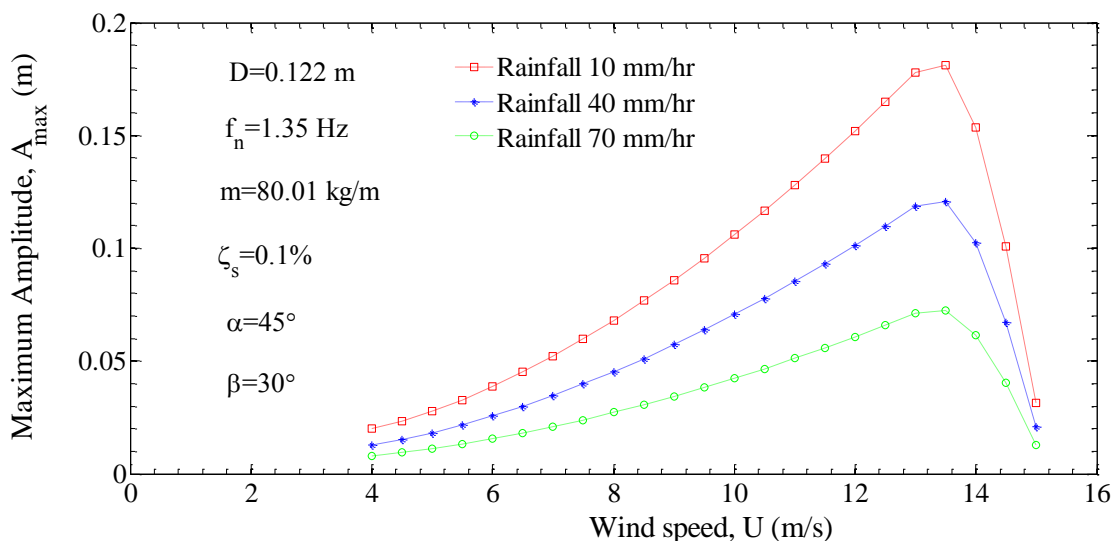


Figure 4.14 mean wind speed Vs. vibration amplitude of the cable ( $\alpha=45^\circ$ ,  $\beta=30^\circ$ )

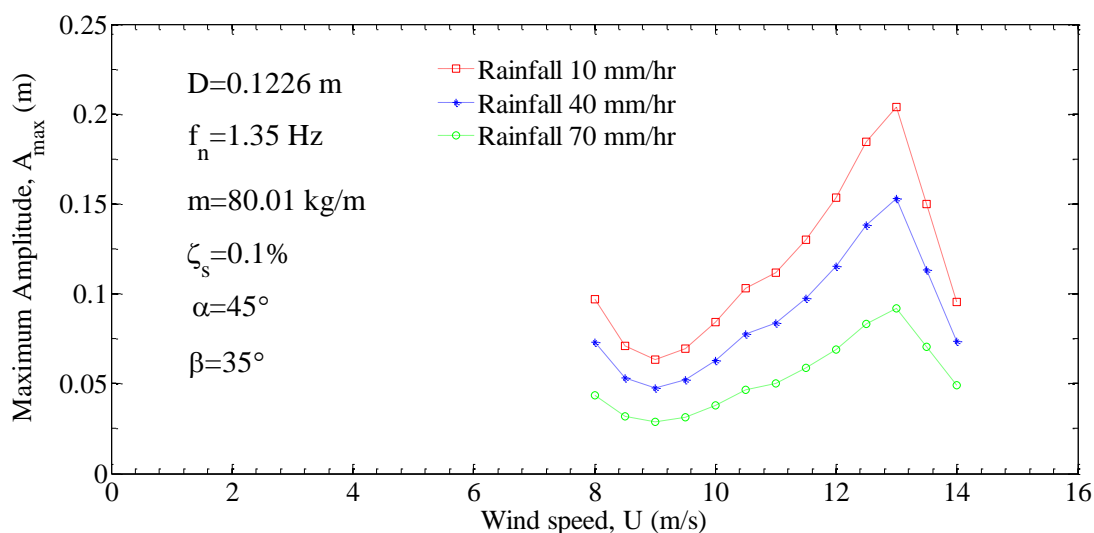


Figure 4.15 mean wind speed Vs. vibration amplitude of the cable ( $\alpha=45^\circ$ ,  $\beta=35^\circ$ )

By using the Cable parameters given in table 4.3 and table 4.4 the response of the cable structure is estimated. Since rain-vibration is limited to wind yaw angle and thus the static position of the rivulet is obtained in section 3.14 of chapter III and is used to evaluate the response. The response was estimated for three different rainfall conditions by altering the amplitude of the rivulet.

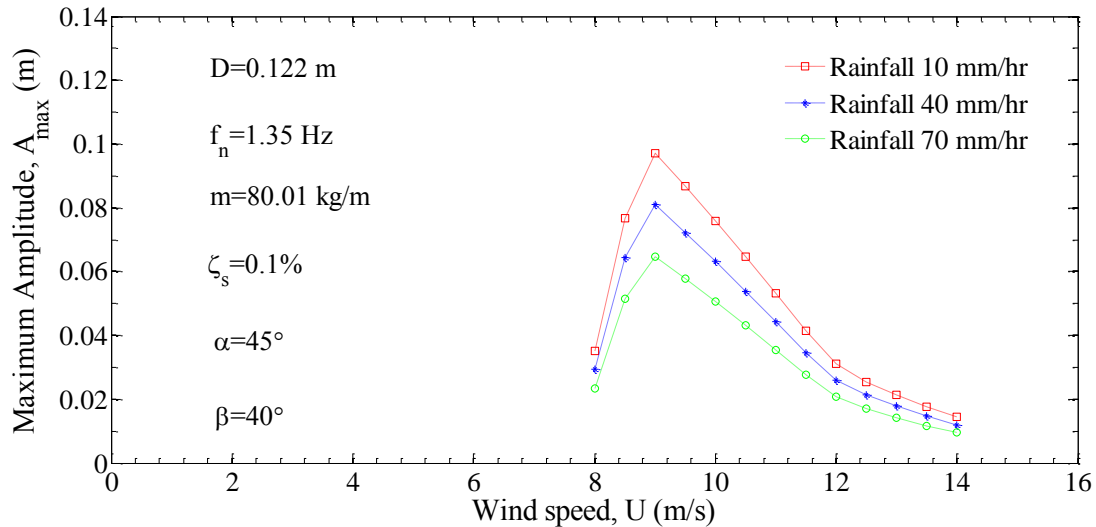


Figure 4.16 mean wind speed Vs. vibration amplitude of the cable ( $\alpha=45^\circ$ ,  $\beta=40^\circ$ )

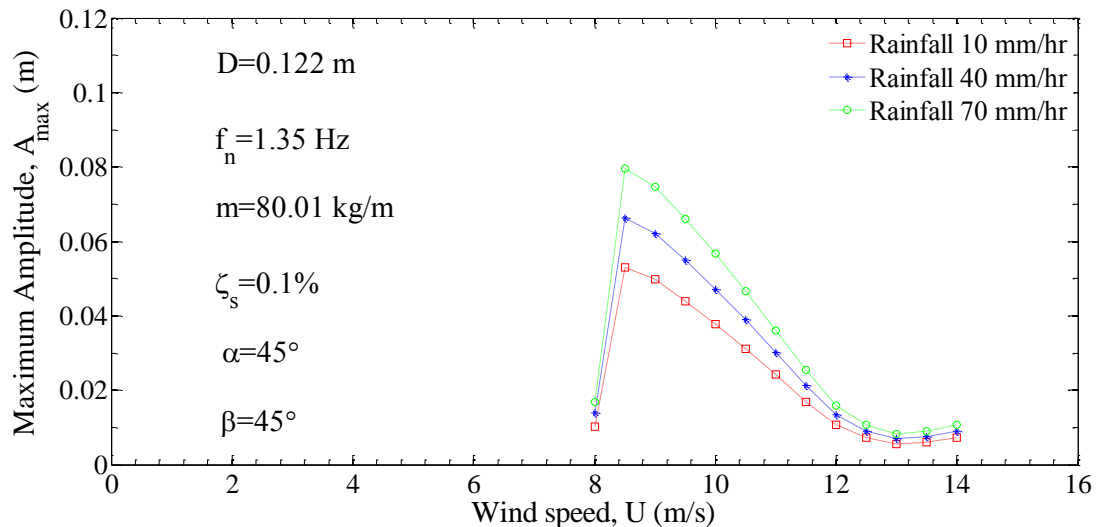


Figure 4.17 mean wind speed Vs. vibration amplitude of the cable ( $\alpha=45^\circ$ ,  $\beta=45^\circ$ )

The response was estimated for the cable inclined at  $47^\circ$  with yaw angle varying from

30° - 45°. Figure 4.13 shows the response of the stay cable inclined at 45° and yaw angle 30°, which shows maximum vibration amplitude of about 0.2 m at 13.5 m/s under 10 mm/hr rainfall conditions, altering the amplitude of the rivulet the response were estimated for 40 mm/hr and 70 mm/hr rainfall case. Similarly the response of the stay cable inclined at 45° and yaw angle 35° were also obtained as shown in figure 4.14, the peak amplitude was found to 0.21 m at 13 m/s. Further increasing the wind yaw angle to 40°, the vibration amplitude at 10 mm/hr reduced to 0.01 m as shown in figure 4.15, which is much less than vibration amplitudes of wind yaw angles 30° and 35°. Further increasing the wind yaw angle to 45° the vibration amplitudes decreases to 0.8 m at 8.3 m/s.

#### **4.9 GUI for Experimental and Analytical results**

In order to make the results user friendly to the designers and researchers, a Graphic User Interface was done in MATLAB. The results obtained in experiments as explained in Chapter III and analytical results explained in Chapter IV are feeded in to MATLAB and made use for the researchers. Matlab program was made to provide the user friendly results. The flow chart and the steps for accessing the results of the is explained in the Appendix III of the thesis. The Matlab program developed to carry out the response analysis and is also provided in Appendix IV.

#### **4.10 Conclusion**

Using the aerodynamic coefficients obtained from the literature, an modified analytical model was made predict the response of the stay cable. For a horizontal cylinder, the vibration amplitude was estimated using Taylor's series by assuming that the rivulet in a static condition. The results show that the critical positions of the rivulet are from 32° to 45°. Whereas in an inclined cylinder, the rivulet is meandering due to the opposing wind and thus by assuming the motion of the rivulet to be sinusoidal, the amplitude of the rivulet is varied according to rainfall intensity and the response analysis was carried out. The relation between the wind speed and position of the rivulet was obtained and the result of the analytical model is to validate the experimental results with a Scruton number.

In order to extend the results for a large Scruton number, the properties of the stay cable assumed in Chapter V is modified according to the bridge specifications (Appendix II) provided

of the Magami bridge. The Scruton number of the stay cable is 4.61 and also found that the vibration response is very low, whereas in real condition the observed amplitude is still high. Using the observations made during the experiments, the mean position of the rivulet with respect to wind speed is obtained and is produced in Chapter III, and is used in the analytical model to evaluate the response of the stay cable with large Scruton number. The obtained results will be further used in Chapter VI to evaluate the fatigue of the cable structures, under rain-wind induced vibrations.

#### 4.11 References

1. Ming Gu, 2009, "On wind-rain induced vibration of cables of cable-stayed bridges based on quasi-steady assumption", *Journal of Wind Engineering and Industrial Aerodynamics*, 97(7):381-391. DOI:10.1016/j.jweia.2009.05.004
2. H. J. Zhou, Y. L. Xu, 2007, "Wind-rain-induced vibration and control of stay cables in a cable-stayed bridge", *Journal of Structural Control and Health Monitoring*, 14, pp 1013-1033.
3. Krzysztof Wilde, Wojciech Witkowski, 2003, "Simple model of rain-wind-induced vibrations of stayed cables", *Journal of Wind Engineering and Industrial Aerodynamics*, Vol. 91,7, pp 873-891
4. Xu. Y.L., 2003, Analytical study of wind-rain-induced cable vibration: SDOF model, *Journal of Wind Engineering and Industrial Aerodynamics*, 91, 27-40
5. D.Q.Cao, R.W. Tucker and C. Wang, 2003, "A stochastic approach to cable dynamics with moving rivulets", *Journal of Sound and Vibration*, 268, pp. 291-304.
6. M. Gu, Q. Lu., 2001, "Theoretical analysis of wind-rain induced vibration of cables of cable-stayed bridges", *Journal of Wind Engineering*, 89, pp. 125-128.
7. Yamanguchi. H., 1990, Analytical study of growth mechanism of Rain vibration of Cables, *Journal of Wind Engineering and Industrial Aerodynamics*, 33, 73-80.
8. Y. Hikami, N. Shiraishi, 1988, Rain-wind induced vibrations of cables in cable stayed bridges, *Journal of Wind Engineering and Industrial Aerodynamics*, 29, pp. 409-418.

9. Ohshima, K., Nanjo, M., 1987. Aerodynamic stability of the cables of a cable-stayed bridge subjected to rain, In: Proc. US–Japan Joint Seminar on Natural Resources, Japan, 324–336.



## CHAPTER V

# DYNAMIC CHARACTERIZATION AND STRESS EVALUATION ON STAY CABLES

### 5.1 Introduction

In general, the stay cables acts as tension elements between the pylon and the bridge deck and carries a large amount of tensile force. In order to carry a large amount of tension forces, the stay cables posses very small amount of damping which makes the cable vulnerable to the wind and rain-wind induced vibrations. Since the cable if found to vibrate at very large amplitudes (explained in chapter 3 and 4) under the action of rain and wind. And thus these vibrations may affect the fatigue life of the cable. This chapter deals with cable-beam behavior cables, free vibration of stay cables and the stress evaluation due to rain-wind induced vibrations. Usually stay cables can be approximately considered as a taut string as it carries a large amount of axial tension. But the approximation may be valid for the cables with minimum flexural rigidity and the sag. But in order to study the effect of bending stiffness, mode shapes a taut string and a beam with clamped ends were considered in the study. And then using mode super position the bending moments on the cable is obtained.

### 5.2 Free-vibration of a taut string

Consider a discrete element of a string with length  $ds$  with an axial tension of  $T$  and  $T+dT$  on the ends, with a Bending moment  $M$ . Let  $\phi$  be the inclination angle at  $dx$ ,  $\phi + \frac{\partial\phi}{\partial x} dx$  be the inclination angle at  $X+dx$ . The forces acting on the string is pictured out in figure 5.1.

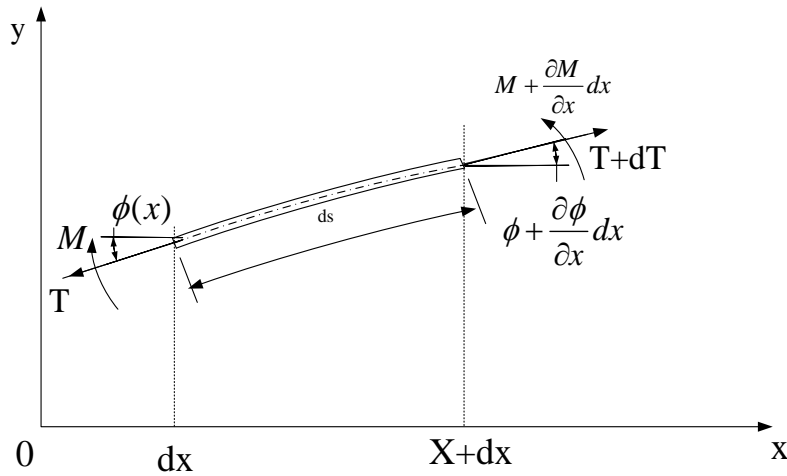


Figure 5.1 Discretized element of a string

The equation of motion of a string element considering bending is given by,

$$EI \frac{\partial^4 x}{\partial x^2} + m \frac{\partial^2 y}{\partial t^2} - T \frac{\partial^2 y}{\partial x^2} = 0 \quad 5.1$$

For a taut string, flexural rigidity is not considered and thus equation 5.1 becomes,

$$\frac{\partial^2 y}{\partial t^2} = C^2 \frac{\partial^2 y}{\partial x^2} \quad 5.2$$

where,  $C = \frac{T}{m}$

The natural frequency of the taut string is given by

$$f_n = \frac{n}{2L} \sqrt{\frac{T}{m}} \quad 5.3$$

where n is the mode number. And T is the axial tension along the string, L is the length of the string, m is the mass per unit length,  $f_n$  is the nth order frequency of the string.

Tension force in the string is given by,

$$T = \frac{4 m L^2 f_n^2}{n^2} \quad 5.4$$

Tension force in the first mode is given by,

$$T_1 = 4 m L^2 f_1^2 \quad 5.5$$

The frequency is distributed at the same interval and the interval is same as the fundamental or the 1<sup>st</sup> mode frequency. And can be seen by deducing the n<sup>th</sup> order term (equation 5.3) from the (n-1)<sup>th</sup> order term.

$$f_n - f_{n-1} = \left( \frac{n}{L} \sqrt{\frac{T}{4m}} \right) - \left( \frac{(n-1)}{L} \sqrt{\frac{T}{4m}} \right) = \frac{1}{L} \sqrt{\frac{T}{4m}} \quad 5.6$$

For a taut string, the Tension force T as a function of frequency in different modes is given in table 5.1

### 5.2.1. Application of string theory

A stay cable model of the Fred Hartman Bridge which was exposed to fatigue is considered as a sample example problem for the present study.

Table 5.1 Properties of stay cable (Aaron, 2005)

Cable id.	Density (kg/m <sup>3</sup> )	Moment of inertia (m <sup>4</sup> )	Young's modulus (N/m <sup>2</sup> )	Cross-sectional Area (m <sup>2</sup> )	Tension (kN)
C04, D04	7152.2	9.960481×10 <sup>-6</sup>	1.896058 × 10 <sup>11</sup>	0.01187	4114.604

The properties of the cable #24 of the Fred Hartman Bridge were reproduced from Aaron(2005) is shown in table 1 and it is assumed that the material properties of the stay cables are same for all the cables that exist in the Megami bridge, Nagasaki. The position of the cables C1 to C13 and D1 to D13 are shown in figure 2.4 of chapter II.

Application of string theory to the above cable yields the following results as shown in table 5.2 and 5.3. The frequencies of the cable were found using the equation 5.3 and are tabulated in table 5.2. Table 5.4 elaborates the tension force of the cable at different modes, calculated using the equation 5.5. The axial tensile stresses in the cable can be found using equation 5.6 through string approximation (Zhang Ping). But an ideal cable has no flexural rigidity and is capable of carrying tensile forces and no bending stress along its length. (Gimsing, 1998). Since the string theory neglects the bending stiffness and thus bending stresses are not available. The deviation at the edges can also be found by finding the deviation angle from which bending stresses can be found (Winkler Jan 2011, Sunichi Nakamura, 1989).

Table 5.2 Free vibration analysis of the cable #C03– string theory

Mode no.	1	2	3	4	5	6	7	8	9	10
Frequency (Hz)	0.57	1.15	1.72	2.29	2.87	3.44	4.02	4.59	5.16	5.74

Table 5.3 Axial stress in the stay cable #C03– string theory

	Tension at different modes (kN)	Axial stress (MN/m <sup>2</sup> )
$T_1 = 4 m L^2 f_1^2$	4214.3	0.376714
$T_2 = m L^2 f_2^2$	4214.3	0.376714
$T_3 = 4 m L^2 f_3^2 /9$	4160	0.37186
$T_4 = m L^2 f_1^2 /4$	4178	0.373469

Axial stress in the nth order natural frequency is given by,

$$\sigma_{a,n} = \frac{T_n}{A} = \frac{4 m L^2 f_n^2}{n^2} \quad (5.7)$$

In the design process of the bridge, for the simplicity sake, the cable can be modeled as pin connections with no flexural rigidity. But in a real condition of a stay cable hanging between the pylon and the anchorage does have an amount of stiffness causes a bending stress of negligible magnitude as there are no significant changes in the curvature of the cable. The stay

cables carry a large amount of tension forces along the cross-section of the cable in a static condition. Even at normal condition or due to the traffic in the bridge deck, the shape of influence lines of cable tension has both positive and negative areas which cause large stress amplitudes. While during the action of wind/rain-wind induced vibrations the stays are subjected to quite very large-amplitude vibrations in the direction perpendicular to the cable plane induced bending stresses leading to bending fatigue of the stay cables (H. J. Zhou, 2007) Bending stresses are even generated due to the sag, where the sag defines the curvature of the cable. The higher the sag, higher the bending stress and vice versa. It is known fact that the clamping the edges of the cable would give more bending stresses than pin joints. Since the stay cables are being influenced by the bending stress induced fatigue, it is decided to fix the edges of the cable. But researchers doing experimental fatigue analysis assume pin joints at the edges (John C. Eggers, 2003)

### 5.3 Free vibration analysis of a stiffed string or stay cable – continuous system

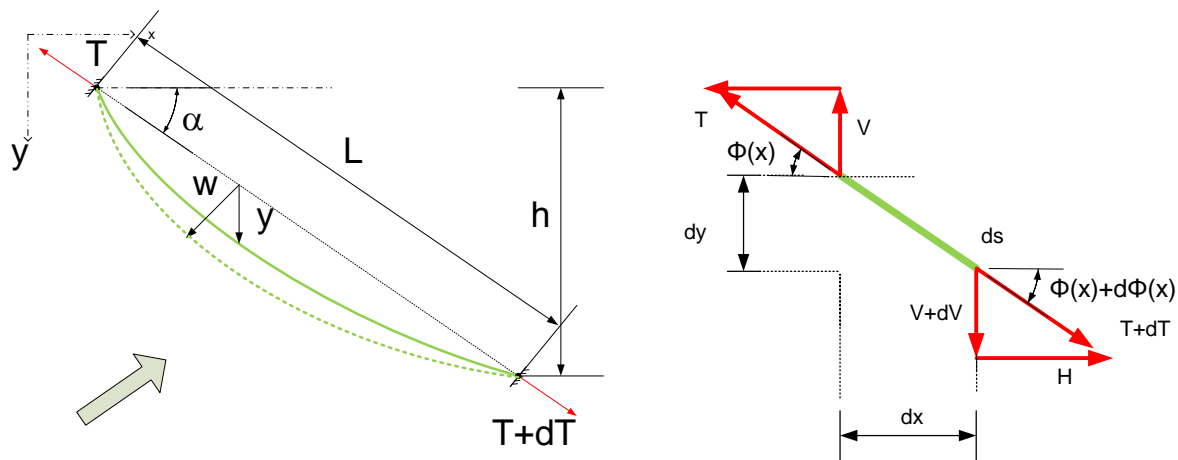


Figure 5.2 Forces acting on a Stay cable - Equations of Motion of a stay cable

Figure 5.2 shows the nomenclature of stay cable fixed at both ends. The top end of the cable is connected to the pylon and the bottom end of the cable be anchored to the bridge deck. And thus assuming both ends to be fixed, and tension force  $T$  acts on to the pylon, whereas a tension force of  $T + dT$  acts towards the anchorage.

In static condition, the cable is deflected away from the axis of the cable due to the sag. And  $y$  is the vertical distance from axis to the deflected profile of the cable, whereas  $w$  is the deflection of the cable and is perpendicular direction to  $y$ .

The deflected static profile (Hiroshi Zui 1996, Armin B. Mehrabi 1998) of the cable is given by

$$y = x(L - x) \frac{4d}{L^2} \quad (5.8)$$

Equations of motion of a stay cable considering bending stiffness can be written as,

$$\frac{\partial^2}{\partial x^2} EI \frac{\partial^2 w}{\partial x^2} - T \frac{\partial^2 w}{\partial x^2} - h \frac{d^2 y}{dx^2} + m \frac{\partial^2 w}{\partial t^2} + c \frac{\partial w}{\partial t} = 0 \quad (5.9)$$

where,

$T =$  Tension force,

$I =$  Second moment of inertia

$A =$  Cross sectional area

$m =$  mass per unit length

$L_e =$  Cable effective length

$L =$  Overall length

$E =$  Young's modulus

$d =$  Sag in the stay cable

$$\frac{\partial^2}{\partial x^2} EI \frac{\partial^2 w}{\partial x^2} - T \frac{\partial^2 w}{\partial x^2} - h \frac{d^2 y}{dx^2} + m \frac{\partial^2 w}{\partial t^2} + c \frac{\partial w}{\partial t} = 0 \quad (5.10)$$

Separation of variables  $W(x, t) = w(x)Y(t)$

$$EI \frac{w(x)^{IV} Y(t)}{w(x) Y(t)} - T \frac{w(x)^{II} Y(t)}{w(x) Y(t)} + h_t \frac{m g Y(t)}{T w(x) Y(t)} + m \frac{\ddot{Y}(t) w(x)}{Y(t) w(x)} + c \frac{\dot{Y}(t) w(x)}{Y(t) w(x)} = 0 \quad (5.11)$$

$Y(t)$  represents the time dependent and  $w(x)$  represents the space dependent,

$$EI \frac{w^{IV}}{w} Y(t) - T \frac{w^{II}}{w} Y(t) + h_t \frac{m g}{T} Y(t) + m \frac{\ddot{Y}(t)}{Y(t)} + c \frac{\dot{Y}(t)}{Y(t)} = 0$$

$$EI \frac{w(x)^{IV}}{w(x)} - T \frac{w(x)^{II}}{w(x)} + h_t \frac{m g}{T w(x)} = - \left( m \frac{\ddot{Y}(t)}{Y(t)} + c \frac{\dot{Y}(t)}{Y(t)} \right) = a^{IV} \quad (5.12)$$

<u>Space dependent</u>	<u>Time dependent</u>
$EI \frac{w(x)^{IV}}{w(x)} - T \frac{w(x)^{II}}{w(x)} + h_t \frac{m g}{T w(x)} = a^{IV}$	$- \left( m \frac{\ddot{Y}(t)}{Y(t)} + c \frac{\dot{Y}(t)}{Y(t)} \right) = a^{IV}$
$EI \frac{w(x)^{IV}}{w(x)} - T \frac{w(x)^{II}}{w(x)} + h_t \frac{m g}{T w(x)} = a^{IV}$	$\ddot{Y}(t) + \frac{c}{m} \dot{Y}(t) + \frac{a^{IV}}{m} Y(t) = 0$
$EI w(x)^{IV} - T w(x)^{II} - a^{IV} w(x) = -h_t \frac{m g}{T}$	$\lambda = \frac{c}{m}; \quad \omega^2 = \frac{a^{IV}}{m}$
$w(x)^{IV} - \frac{T}{EI} w(x)^{II} - \frac{a^{IV}}{EI} w(x) = -h_t \frac{m g}{TEI}$	$\ddot{Y}(t) + \lambda \dot{Y}(t) + \omega^2 Y(t) = 0$

Damping in the cable is negligible and thus can be neglected. Sag of cable can be eliminated for the sake of simplicity.

$w(x)^{IV} - \frac{T}{EI} w(x)^{II} - \frac{a^{IV}}{EI} w(x) = 0$	$\ddot{Y}(t) + \frac{a^{IV}}{m} Y(t) = 0$
---	---

$$w(x)^{IV} - \left(\frac{\gamma}{L}\right)^2 w(x)^{II} - \frac{a^{IV}}{EI} w(x) = 0 \quad (5.13)$$

$\gamma = L\sqrt{\frac{T}{EI}}$ , where  $\gamma$  is called as non-dimensioned Bending – Tension Parameter. In other words, it can also be said as the parameter that governs the cable-beam action.

$$\alpha = L \sqrt{\sqrt{\left(\frac{\gamma^2}{2L^2}\right)^2 + \frac{a^{IV}}{EI}} - \frac{\gamma^2}{2L^2}} \quad (5.14)$$

$$\beta = L \sqrt{\sqrt{\left(\frac{\gamma^2}{2L^2}\right)^2 + \frac{a^{IV}}{EI}} + \frac{\gamma^2}{2L^2}} \quad (5.15)$$

Substitute  $a^{IV} = m\omega^2$  leads to,

$$\alpha = L \sqrt{\sqrt{\left(\frac{\gamma^2}{2L^2}\right)^2 + \frac{m\omega^2}{EI}} - \frac{\gamma^2}{2L^2}} \quad (5.16)$$

$$\beta = L \sqrt{\sqrt{\left(\frac{\gamma^2}{2L^2}\right)^2 + \frac{m\omega^2}{EI}} + \frac{\gamma^2}{2L^2}} \quad (5.17)$$

$$w(x) = A_1 \cos(\alpha x) + A_2 \sin(\alpha x) + A_3 \cosh(\beta x) + A_4 \sinh(\beta x) \quad (5.18)$$

$$w'(x) = -A_1 \alpha \sin(\alpha x) + A_2 \alpha \cos(\alpha x) + A_3 \sinh(\beta x) + A_4 \beta \cosh(\beta x) \quad (5.19)$$

Imposing the boundary conditions as fixed-fixed end conditions,

$$\text{At } (x = 0); \quad W(0) = 0; \quad W'(0) = 0;$$

$$\text{At } (x = L); \quad W(L) = 0; \quad W'(L) = 0;$$

$$A_1 + A_3 = 0 \quad (5.20)$$

$$A_2 \alpha + A_4 \beta = 0 \quad (5.21)$$

$$\alpha A_1 \cos \alpha L + \alpha A_2 \sin \alpha L + \beta A_3 \cosh \beta L + \beta A_4 \sinh \beta L = 0 \quad (5.22)$$

$$-\alpha A_1 \sin \alpha L + \alpha A_2 \cos \alpha L + \beta A_3 \sinh \beta L + \beta A_4 \cosh \beta L = 0 \quad (5.23)$$

$$\begin{bmatrix} 1 & 0 & 1 & 0 \\ 0 & \alpha & 0 & \beta \\ \alpha \cos \alpha & \alpha \sin \alpha & \beta \cosh \beta & \beta \sinh \beta \\ -\alpha \sin \alpha & \alpha \cos \alpha & \beta \sinh \beta & \beta \cosh \beta \end{bmatrix} \begin{bmatrix} A_1 \\ A_2 \\ A_3 \\ A_4 \end{bmatrix} = \begin{bmatrix} 0 \\ 0 \\ 0 \\ 0 \end{bmatrix}$$

$$= 2(\cos \alpha \cosh \beta - 1) = \frac{(\beta^2 - \alpha^2)}{\alpha\beta} \sin \alpha \sinh \beta$$

$$\Rightarrow 2(\cos \alpha \cosh \beta - 1) - \left(\frac{\beta}{\alpha} - \frac{\alpha}{\beta}\right) \sin \alpha \sinh \beta = 0$$

$$2(\cos \alpha \cosh \beta) - \left(\frac{\beta}{\alpha} - \frac{\alpha}{\beta}\right) \sin \alpha \sinh \beta - 2 = 0 \quad (5.24)$$

$\alpha$  and  $\beta$  are functions of  $T$  and  $\omega$ .

In order to obtain the frequencies one has to solve the bi-linear transcendental equation (5.24) to obtain the values of  $\alpha$  and  $\beta$ . This can be done by plotting the equations graphically or by some interpolation methods. The equation 5.24 is plotted in figure 5.3. The contour plot of equation 5.4 shows the values zero at specific  $\alpha$  and  $\beta$ . The values of  $\alpha$  and  $\beta$  can be found by solving the equation to be  $10E-3$  and is shown in figure 5.4. There exists another interpolation method, which is used to verify the values of  $\alpha$  and  $\beta$ .

The parameters of the application problem explained in section 5.2.1 are again used considering the stiffness term via continuous system approach. The equation of motion (equation 5.10) considering the Tension and Bending stiffness is considered and thus the equation leaves ‘ $\gamma$ ’, the Bending – Tension Parameter, which can define the dominant action of cable or a beam behavior. For the present application problem  $\gamma$  read 42448.53.

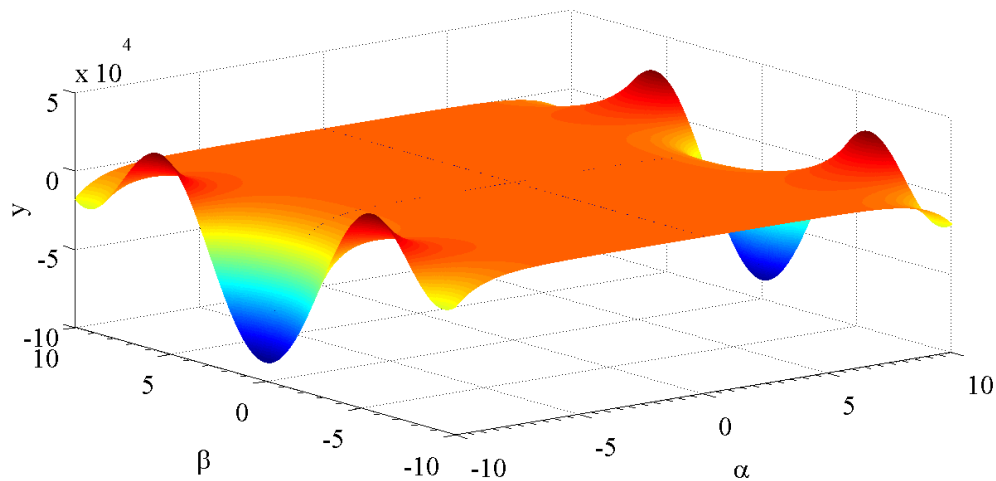


Figure 5.3 3-Dimensional plot of equation 5.24

The frequencies of the stay cable are found by considering the cable as a continuous system. Table 5.2 shows the comparison of natural frequency obtained through string theory, Continuous system-stiffed cable with the ANSYS results. The results show that the frequencies are very near to each other. Figure 5.8 shows the mode shapes for first three modes obtained through Analytical solution.

In order to study the effects of Tension-Bending parameter or the action of beam-cable, the application problem was again used in which the Tension-bending parameter was altered by changing the applied Tension force. The analysis was carried out using both the methods i.e., Continuous system solution (stiffed cable assumption) and the ANSYS solution.

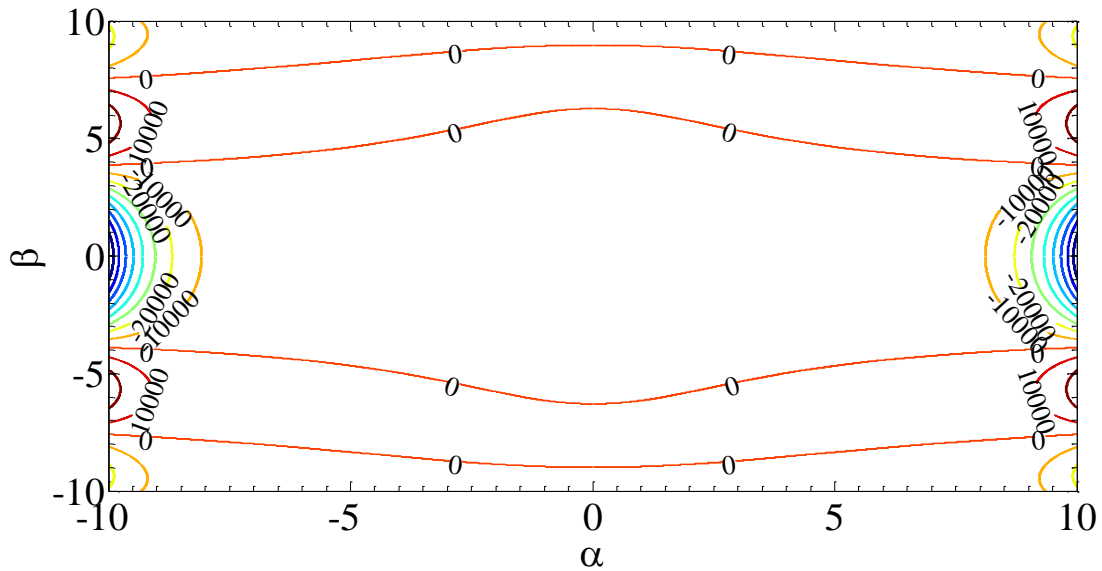


Figure 5.4 Contour plot of  $\alpha$  and  $\beta$  (Equation 5.24)

Table 5.4 Frequency of the stay cable- #C03– String theory and Euler Bernoulli (Analytical and ANSYS solution)

Mode no.	Frequency (Hz)					
	String theory		Continuous system-solution		ANSYS solution (1400 Elements)	
	Symmetric	Asymmetric	Symmetric	Asymmetric	Symmetric	Asymmetric
1	0.57	1.15	0.58	1.16	0.58	1.15
2	1.72	2.29	1.73	2.31	1.73	2.31
3	2.87	3.44	2.89	3.47	2.89	3.47
4	4.02	4.59	4.06	4.64	4.05	4.63
5	5.16	5.74	5.22	5.81	5.22	5.80

A sample MATLAB and ANSYS algorithm which was used to estimate the frequency and mode shapes are given in Appendix V.

### 5.3.1 Cable-beam behavior

$$\frac{\partial^2}{\partial x^2} EI \frac{\partial^2 w}{\partial x^2} - T \frac{\partial^2 w}{\partial x^2} + m \frac{\partial^2 w}{\partial t^2} = 0$$

$$\frac{\partial^4 w}{\partial x^4} - \frac{T}{EI} \frac{\partial^2 w}{\partial x^2} + \frac{m}{EI} \frac{\partial^2 w}{\partial t^2} = 0$$

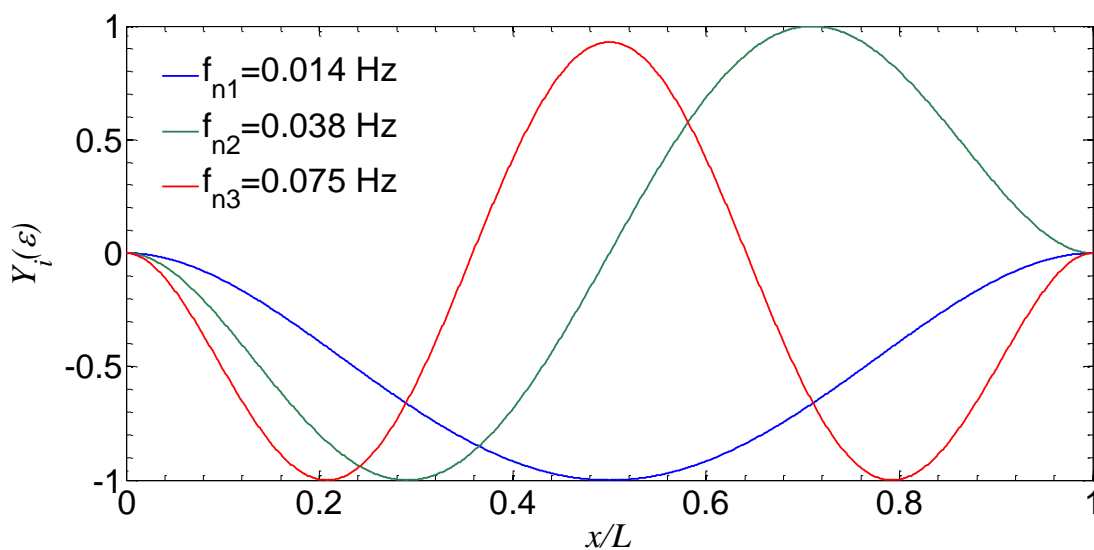


Figure 5.5 Mode shapes of the Euler-Bernoulli beam with  $T/EI=0$

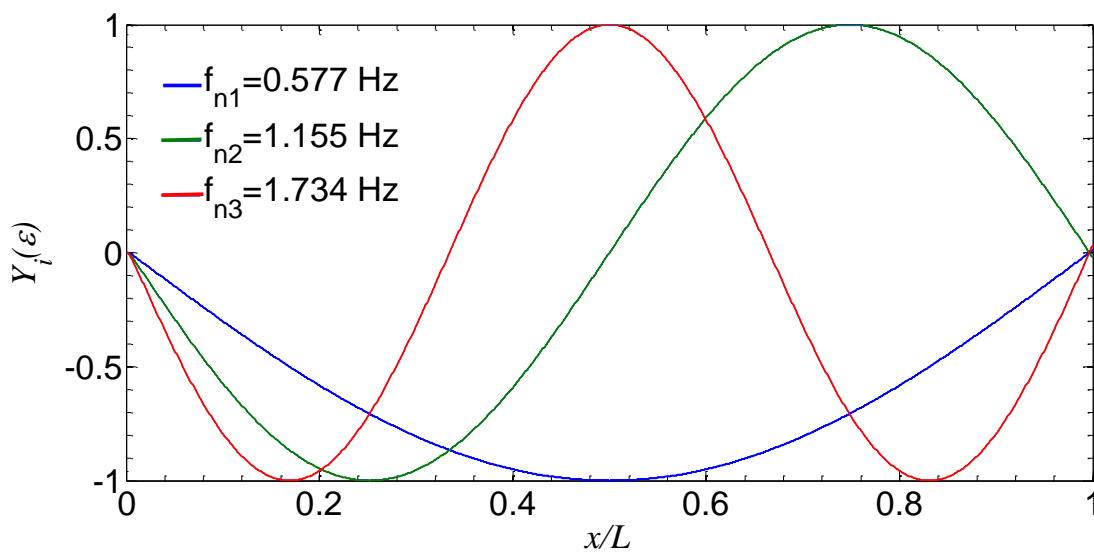


Figure 5.6 Mode shapes of the Euler-Bernoulli beam with  $T/EI=42637$

The equation of motion explained in 5.6 is solved by changing several parameters namely the tension force  $T$  and the aspect ratio  $L/D$  to understand the cable-beam behavior. The following conclusions were derived by varying the Tension and the aspect ratio.

- i) When the dimensional Tension- bending parameter ( $\gamma_d=T/EI$ ) is small  $<50$  the mode shape are of similar to clamped-clamped. When the  $T/EI$  is larger the mode shapes is like a taut string:  $\sin(\omega t)$ .
- ii)  $D/L=0.01$ . The mode shapes is like clamped-condition as shown in figure 5.5,  $D/L=0.001$  the mode shape deviation at the ends is little more between clamped & string.  $D/L=0.0006$  it looks like a string.
- iii) When the axial tension,  $T=0$ , then  $T/EI=0$  and the natural frequency is 0.013 Hz (exact clamped condition as shown in figure 5.5), whereas increasing the ratio  $T/EI=42$ ,  $f_n=0.024$  Hz and further increasing,  $T/EI$  to 42637, natural frequency increases to 0.57 HZ (as shown in figure 5.6).

### 5.3.2. Importance of sag and Bending in stay cables

There were lot of study which assumes the cable as a beam, and some assumes cable as a string. In reality the cable is a main tension element and carries a large amount of axial forces and thus assuming string will be appropriate. But including the sag, the behavior of the cable is neither a string nor a cable. Thus the Importance of sag and bending is discussed below.

$$\text{Axial stiffness or Hookean stiffness} = \frac{EA}{L} \quad 5.25$$

$$\text{Gravitational effect of pulling the sag by means of Tension} = \frac{12T}{L} \left( \frac{mgL}{T} \right)^2 \quad 5.26$$

Irvine parameter of sag extensibility given by Irvine (1992),

$$\text{Irvine Parameter, } \lambda^2 = \left( \frac{mgL}{T} \right)^2 \frac{EAL}{T L_e} \quad 5.27$$

A suspended cable behaves like a taut string when,  $\frac{12}{\lambda^2} > 0.5$

For the application problem,

$$\frac{12}{\lambda^2} = 16343.9 \times 10^3$$

The natural frequency of a taut string,  $\omega_{is} = \frac{i\pi}{l} \sqrt{\frac{T}{m}}$  5.28

And the natural frequency of the beam,  $\omega_{ib} = \sqrt{\frac{EI}{m} \left(\frac{i\pi}{l}\right)^4 + \frac{T}{m} \left(\frac{i\pi}{l}\right)^4}$  5.29

The ratio of these two gives the relative importance of the bending stiffness,

$$\gamma = \frac{T}{EI} \left(\frac{1}{i\pi}\right)^2$$
 5.30

where 'i' is the mode number.

For the application problem,  $\gamma = 206.03$

In other words, non-dimensionalised Tension-Bending parameter is,  $\gamma = L \sqrt{\frac{T}{EI}}$

$$d' = \frac{mgL^2}{8T}$$

Effect of Tension force on Tension-Bending parameter  $\gamma$  is shown in figure 5.7 and the effect of Axial tension force on sag is shown in figure 5.8.

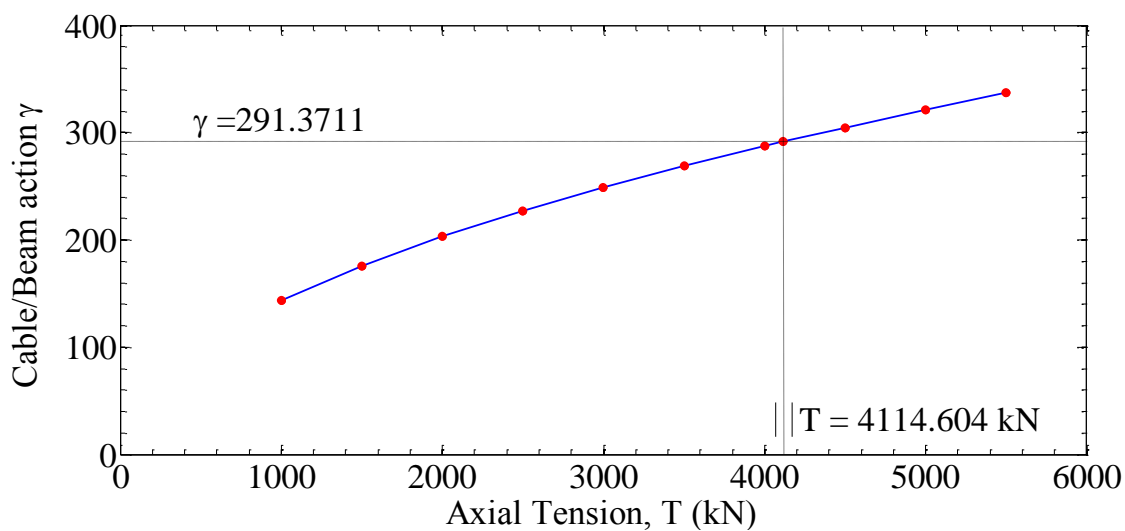


Figure 5.7 Effect of Tension force on Tension-Bending parameter

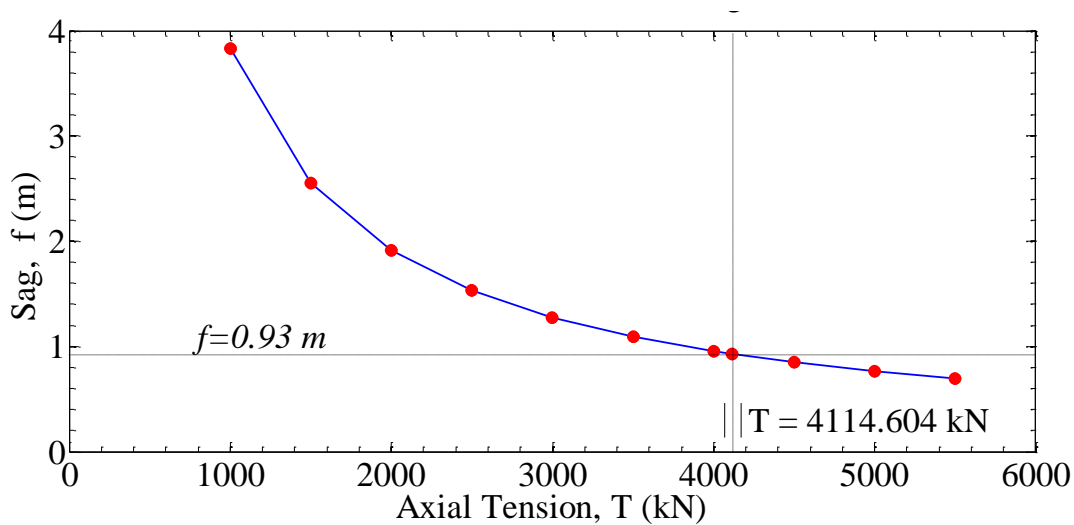


Figure 5.8 Effect of Axial tension force on sag parameter

#### 5.4 Evaluation of Bending stresses

In order to obtain the desired bending moment, a transient non-linear analysis was carried out by matching the displacement obtained in the wind tunnel experiment. A similar method was also done in the past by Aaron James Pebley, (2005). The vibration amplitude obtained from the experiment is used as the peak displacement of the stay cable. And the

dynamic characterization of the cable was done via Analytical solution and also by Finite Element Methods using ANSYS. The following will explain the methodology carried out for estimation of bending stresses for the application stay cable. This method can be applied to any other stay cable.

#### 5.4.1 Finite Element modeling of the cable

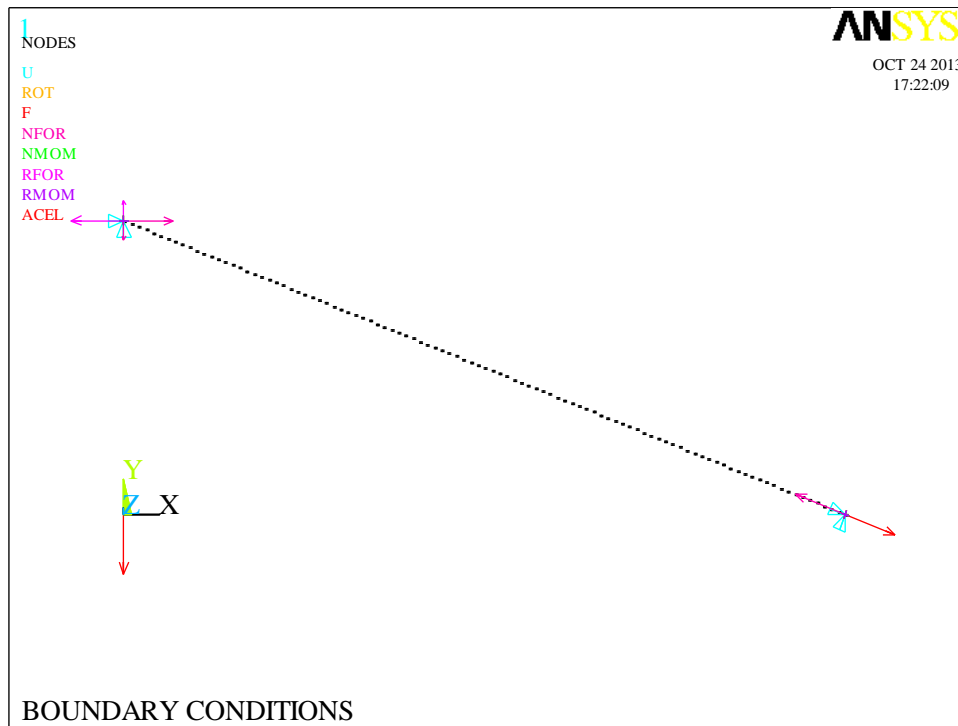


Figure 5.9 Boundary conditions and forces acting on the stay cable

The goal of the following analysis is to match the dynamic behavior of the cable obtained through the analytical methods and thus further a response analysis can be carried out to estimate the bending moment by matching the vibration amplitude of the cable.

The stay cable was modeled using BEAM3 Element. There were 1400 Elements and the size of each element is about 0.1 m. The tension force can be added either by direct method or through the real constant. To accommodate the tension force of 4114.6 kN a initial strain of 0.00194 can be added or the tension force can be applied directly by removing the UX constraint.

Both the methods will induce pre-stress effects on to the cable after running a static analysis. In ANSYS the pre-stress effects can be applied by making the PSTRESS to ON condition and it will be effective once after a static analysis. At first a static analysis and modal response was carried out and the mode shapes were normalize. Then the peak amplitude of the stay cable model is obtained from chapter III and is then multiplied with the modal co-ordinates. Again a static analysis was carried out to find the bending moments in different modes. Figure 5.9 shows the boundary conditions for modal and static analysis.

#### 5.4.2 Free vibration analysis of a stay cable – Finite Element Methods (ANSYS)

The modal response of the cable was carried out to ensure/validate the solution obtained through the analytical methods. In ANSYS it's a mandatory to carry out a static test for any pre-stress problem in which pre-stresses has to be effective. The following conditions were assumed based on the experimental condition and the knowledge in cable structures. The mode shapes and frequencies were calculated using block lanczos method, allowing Ansys to assume non-linear geometry (NLGEOM ON) and large deformation.

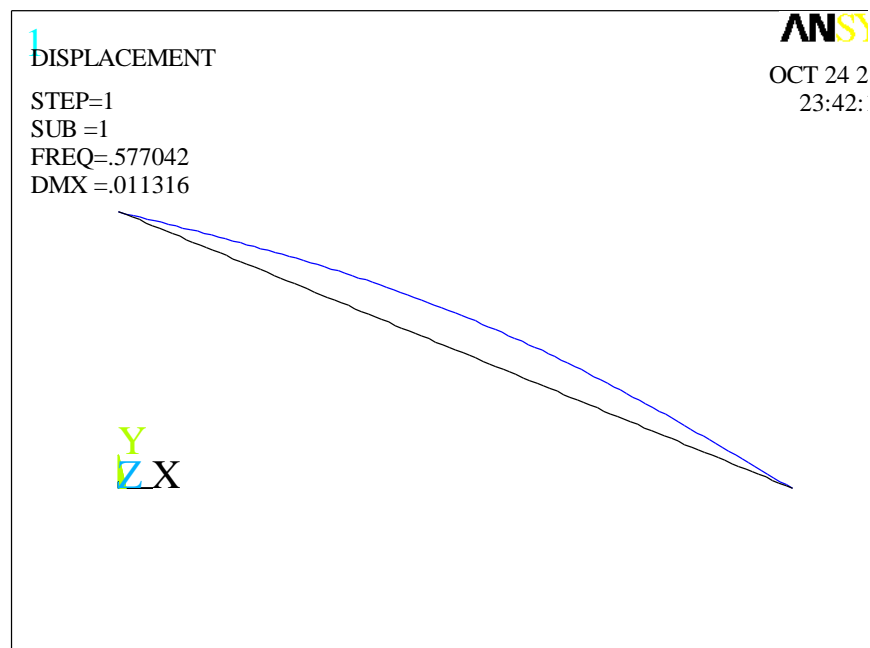
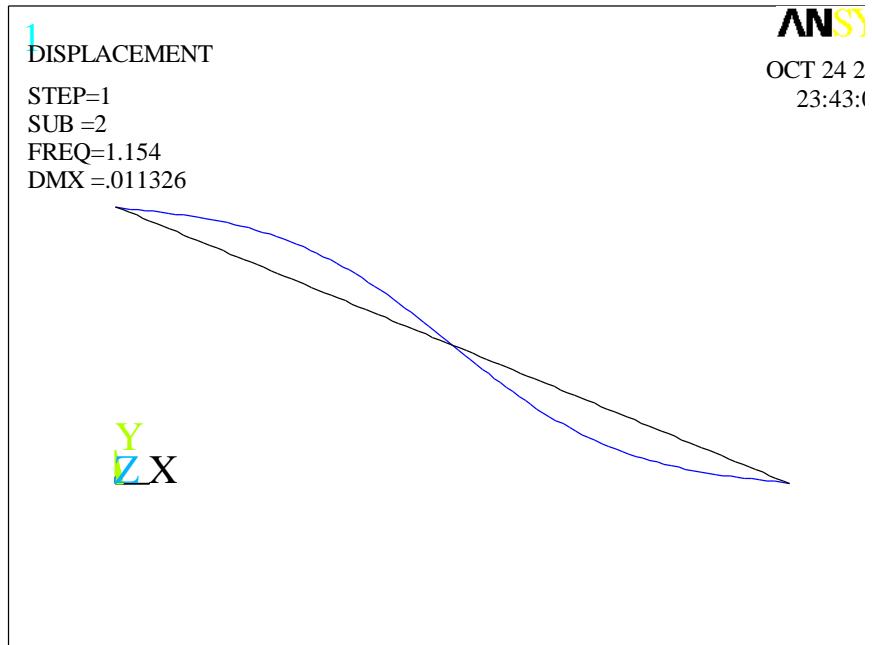
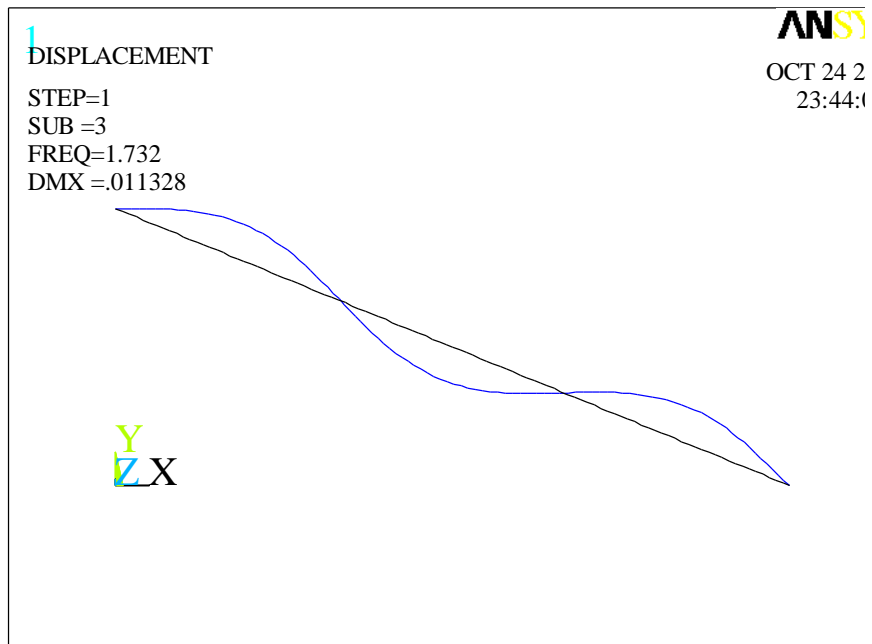
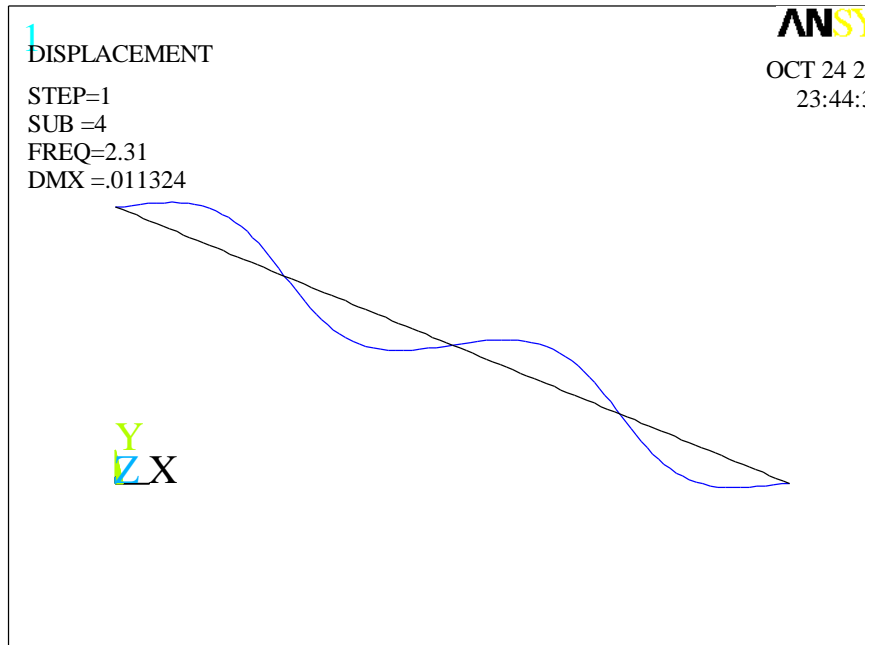


Figure 5.10 1<sup>st</sup> Symmetric mode of the stay cable

Figure 5.11 1<sup>st</sup> Anti-Symmetric of the stay cableFigure 5.12 2<sup>nd</sup> Symmetric mode of the stay cable

Figure 5.13 2<sup>nd</sup> Anti-symmetric mode of the stay cableFigure 5.14 3<sup>rd</sup> Symmetric mode of the stay cable

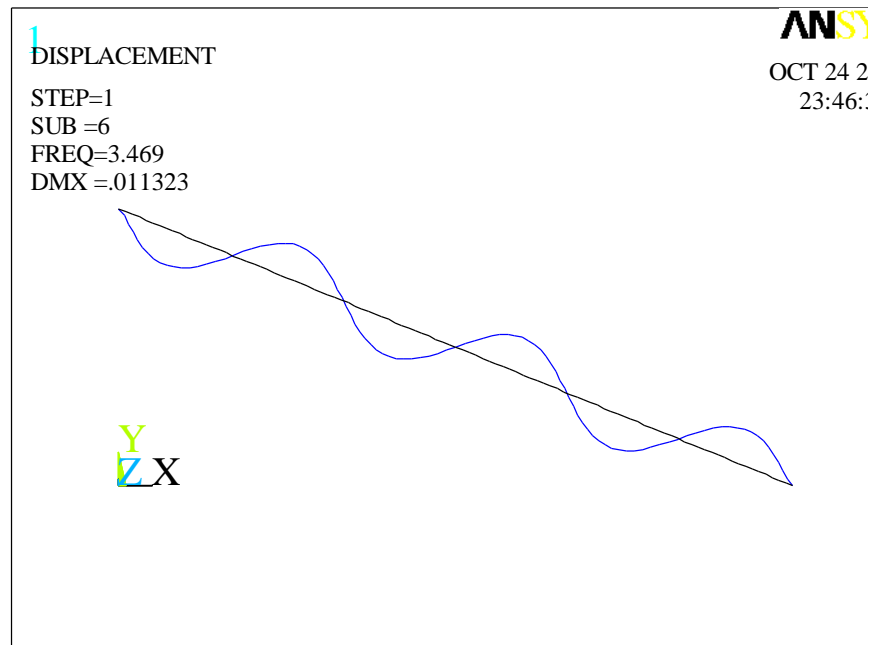


Figure 5.15 3<sup>rd</sup> Anti-Symmetric mode of the stay cable

The table 5.5 shows the comparison of natural frequencies of the application problem using ANSYS with analytical solutions. Figures 5.9-5.15 shows the first 3 symmetric and anti-symmetric mode shapes obtained using ANSYS.

### 5.4.3 Evaluation of Bending Moment and Bending stresses in the stay cable

The normalized vibration amplitudes of the cable model obtained in the experiment is listed in chapter III. After normalization, the vibration amplitude was found for the application problem explained in section 5.1. The stay cable bending moment was evaluated by inducing the modal displacements on to nodes of the structure.

The experimental results show that the peak vibration amplitude ranges from 0.001 m to 2 m. And thus the bending moment was checked for different vibration amplitudes ranging from 0.001m to 2 m. The bending moment profiles of the stay cable for different modes were obtained and are explained below.

#### 5.4.4 Deflected mode shapes, bending moments and stresses

The deflected mode shapes represents the deformable behavior of the structure vibrating in its frequency range. Since the mode shape of the cable is normalized to unity, it could be easily multiplied with the multiplication factor (the multiplication factor here is the peak displacement of the stay cable). It is assumed to consider the first six modes for the analysis, as the mode participation factor seems to be very less. The following will explain the evaluation of bending moments, bending stresses, axial stresses and the overall stress at the ends of the cable. The tensile force is calculated based on string theory and is shown in table of section 6.2. Axial stresses can be found from the tensile force using equation 5.7. Bending stresses were found from bending moments from equation. The equation for overall stress is given by .

$$\sigma_{bending} = \frac{Mc}{I} \quad (5.31)$$

where  $c = \frac{D}{2}$ , in which D is the Diameter of the application stay cable.

Overall stress in the cable can be found by summing up the bending and axial stresses and is given in equation

$$\sigma_{overall} = \frac{MD}{2I} + \frac{T}{A} \quad (5.32)$$

#### 5.5 Stresses in symmetric modes

The normalized mode shape co-ordinates were multiplied by the peak displacement and the displacement load is again applied on the pre-stressed structure at 100 nodes equally spaced along the length of the structure. Finally a static analysis was run to obtain the bending moments of the cable model. The bending moment profile for different symmetric modes is plotted in the following figures. Figure 5.16 shows the bending moments of the cable at a peak displacement of 0.5 m. It is also seen that the bending moment profile looks same for other peak displacements

i.e., 1 m, 1.5 m and 2 m. In mode 1, both the moments act in the same direction and is shown in figure 5.16. Table 1 shows the bending stress evaluated from the bending moment using the relation given in equation 6.88. The tensile force is calculated based on string theory and is shown in table of section 5.2. Table 6.88 also shows the calculation of axial stresses and overall stress. The relation between the axial force and stress is given in equation. The overall stress equation is given by equation 5.32.

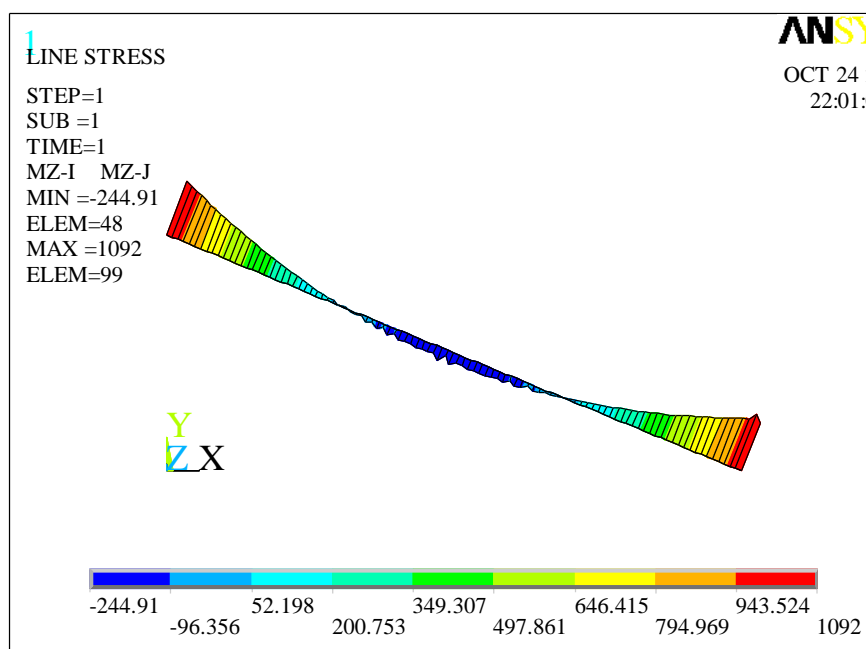


Figure 5.16 Bending stress in 1<sup>st</sup> symmetric mode for 0.5 m peak displacement

Table 5.5 Evaluation of stresses in 1<sup>st</sup> symmetric mode

Mid-span deflection (m)	Location	Bending moment $M$ Nm	Bending stress $\sigma_{bending}$ (MN/m <sup>2</sup> )	Axial stress $\sigma_{axial}$ (MN/m <sup>2</sup> )	Overall stress in the cable $\sigma_{overall}$ (MN/m <sup>2</sup> )
0.5	Pylon end	1067.6	6.38	3.76E+02	382.7071
	Mid-span	244.9	1.46	3.76E+02	377.7926
	Deck end	1092.1	6.52	3.76E+02	382.8535

1	Pylon end	1899.3	1.13	3.76E+02	387.6754
	Mid-span	725.71	4.34	3.76E+02	380.6648
	Deck end	1948.27	11.6	3.76E+02	387.9679
1.5	Pylon end	2731	16.3	3.76E+02	392.6437
	Mid-span	1206.5	7.21	3.76E+02	383.5369
	Deck end	2804.5	16.8	3.76E+02	393.0828
2	Pylon end	3562.7	21.3	3.76E+02	397.612
	Mid-span	1687.3	10.1	3.76E+02	386.409
	Deck end	3660.7	21.9	3.76E+02	398.1974

Figure 5.17 shows the bending moment profile of 2<sup>nd</sup> symmetric mode. It can be seen that the bending moment is quite large in comparison with the 1<sup>st</sup> symmetric mode but the moments at the ends are large and in the same direction. Table 5.6 shows the bending moment of the stay cable for different peak displacements in 2<sup>nd</sup> symmetric mode.

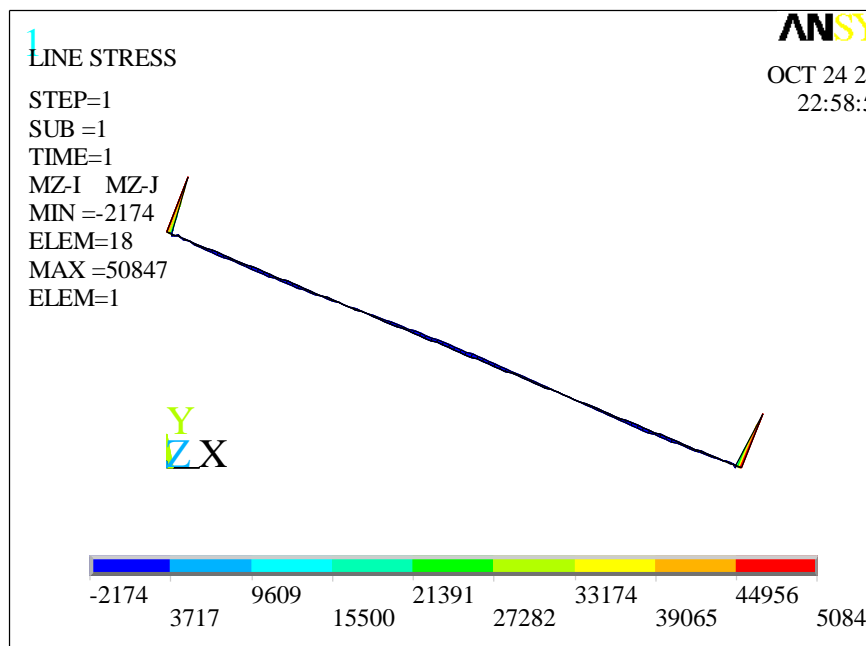


Figure 5.17 Bending stress in 2<sup>nd</sup> symmetric mode for 0.5 m peak displacement

Bending moment profile for 3<sup>rd</sup> symmetric mode is shown in figure 5.18. It can be seen

that the bending moment is quite large in comparison with the 1<sup>st</sup> and 2<sup>nd</sup> symmetric modes and also the moments at the ends are large and in opposite direction to that of the 1<sup>st</sup> and 2<sup>nd</sup> symmetric mode. Bending moments at different locations of the stay cable were tabulated in the table 5.7 for 3<sup>rd</sup> symmetric mode. It can be seen from the figures that the moments and the stresses at the deck and pylon are in same direction.

Table 5.6 Evaluation of stresses in 2<sup>nd</sup> symmetric mode

Mid-span deflection (m)	Location	Bending moment $M$ N-m	Bending stress $\sigma_{bending}$ (MN/m <sup>2</sup> )	Axial stress $\sigma_{axial}$ (MN/m <sup>2</sup> )	Overall stress in the cable $\sigma_{overall}$ (MN/m <sup>2</sup> )
0.5	Pylon end	50847.00	303.74	372.40	676.14
	Mid-span	2560.70	15.30	372.40	387.69
	Deck end	50503.00	301.69	372.40	674.08
1	Pylon end	101460.00	606.09	372.40	978.48
	Mid-span	4885.50	29.18	372.40	401.58
	Deck end	100770.00	601.96	372.40	974.36
1.5	Pylon end	152070.00	908.41	372.40	1280.81
	Mid-span	7210.30	43.07	372.40	415.47
	Deck end	151040.00	902.26	372.40	1274.66
2	Pylon end	202680.00	1210.74	372.40	1583.14
	Mid-span	9535.20	56.96	372.40	429.36
	Deck end	201310.00	1202.55	372.40	1574.95

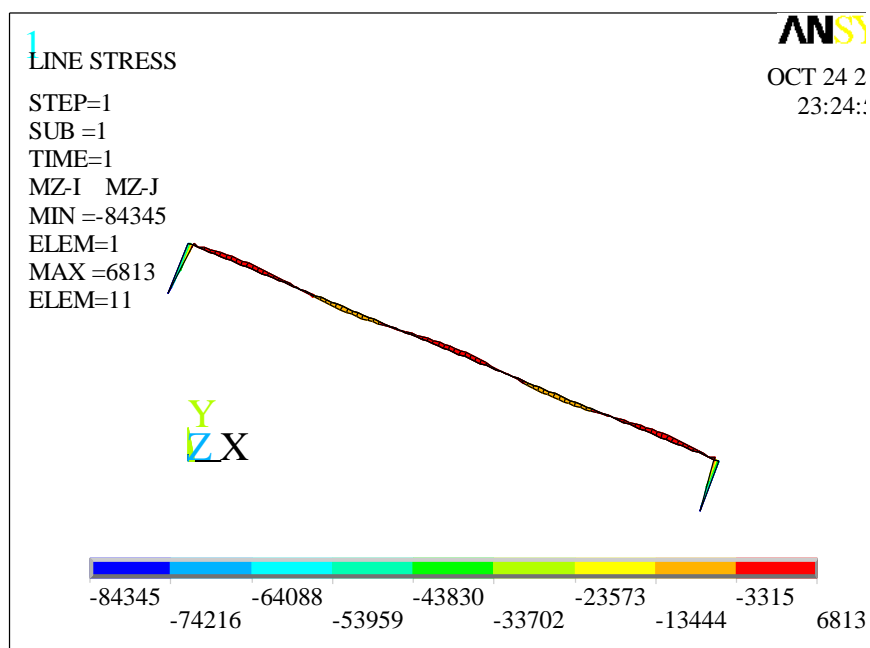


Figure 5.18 Bending stress in 2<sup>nd</sup> symmetric mode for 0.5 m peak displacement

Table 5.7 Evaluation of stresses in 3<sup>rd</sup> symmetric mode

Mid-span deflection (m)	Location	Bending moment $M$ N-m	Bending stress $\sigma_{bending}$ (MN/m <sup>2</sup> )	Axial stress $\sigma_{axial}$ (MN/m <sup>2</sup> )	Overall stress in the cable $\sigma_{overall}$ (MN/m <sup>2</sup> )
0.5	Deck end	84345.00	503.85	374.11	877.96
	Mid-span	6690.50	39.97	374.11	414.08
	Pylon end	83773.00	500.43	374.11	874.54
1	Deck end	168930.00	1009.13	374.11	1383.24
	Mid-span	13145.00	78.52	374.11	452.64
	Pylon end	167780.00	1002.26	374.11	1376.37
1.5	Deck end	253510.00	1514.38	374.11	1888.49
	Mid-span	19600.00	117.08	374.11	491.20
	Pylon end	251790.00	1504.10	374.11	1878.22

2	Deck end	338090.00	2019.63	374.11	2393.74
	Mid-span	26054.00	155.64	374.11	529.75
	Pylon end	335800.00	2005.95	374.11	2380.06

## 5.6 Stresses in Asymmetric modes

For stresses in 1<sup>st</sup> asymmetric mode, the displacement profile shown in figure 5.19 is normalized and loaded on to the structure. The static solution shows that the maximum bending moment occur at the edges and are opposite in direction, which is different from the 1<sup>st</sup> symmetric mode. The bending moment at the deck in 1<sup>st</sup> asymmetric mode is of 30.45 times that of 1<sup>st</sup> symmetric mode, whereas the bending moment at the pylon end is about 31.8 times of model. The bending moment profile for the 1<sup>st</sup> asymmetric mode for 0.5 m maximum displacement is shown in figure 5.19.

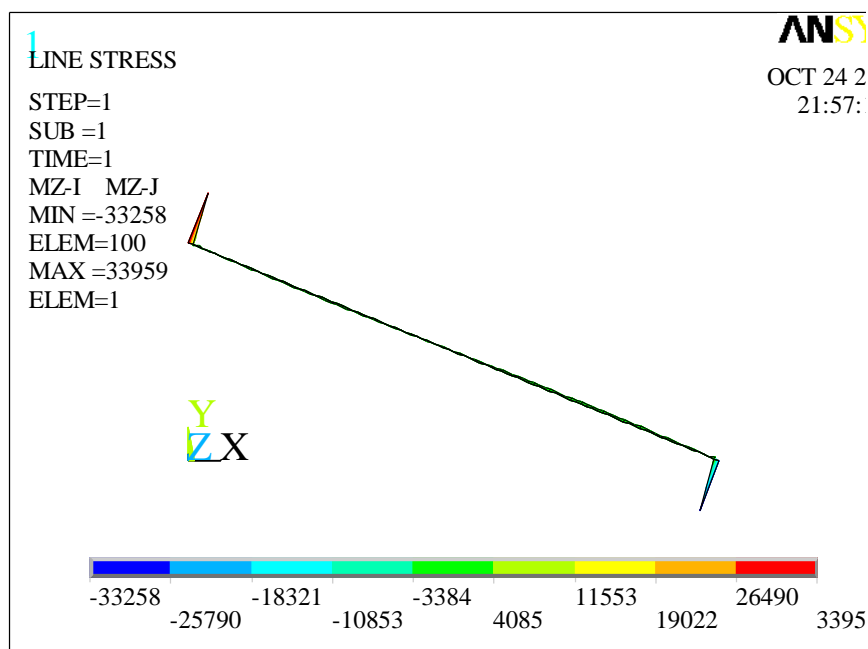


Figure 5.19 Bending stress in 1<sup>st</sup> asymmetric mode for 0.5 m peak displacement

Figures 5.20 and 5.21 shows the Bending moment profile for 2<sup>nd</sup> and 3<sup>rd</sup> Anti-symmetric modes. It can be seen that the bending moment is increases as the mode number increases. It

must be noted that the bending moments at the ends of the stay cables were opposite in direction, whereas the moments and the stresses at the deck and pylon are in same direction in case of symmetric modes.

Table 5.8 Evaluation of stresses in 1<sup>st</sup> Anti-symmetric mode

Mid-span deflection (m)	Location	Bending moment $M$ Nm	Bending stress $\sigma_{bending}$ (MN/m <sup>2</sup> )	Axial stress $\sigma_{axial}$ (MN/m <sup>2</sup> )	Overall stress in the cable $\sigma_{overall}$ (MN/m <sup>2</sup> )
0.5	Pylon end	33959.00	202.86	376.71	579.57
	Mid-span	242.42	1.45	376.71	378.16
	Deck end	33258.00	198.67	376.71	575.39
1	Pylon end	67682.00	404.31	376.71	781.02
	Mid-span	248.95	1.49	376.71	378.20
	Deck end	66753.00	398.76	376.71	775.47
1.5	Pylon end	101410.00	605.79	376.71	982.50
	Mid-span	255.49	1.53	376.71	378.24
	Deck end	100250.00	598.86	376.71	975.57
2	Pylon end	135130.00	807.22	376.71	1183.93
	Mid-span	262.02	1.57	376.71	378.28
	Deck end	133740.00	798.92	376.71	1175.63

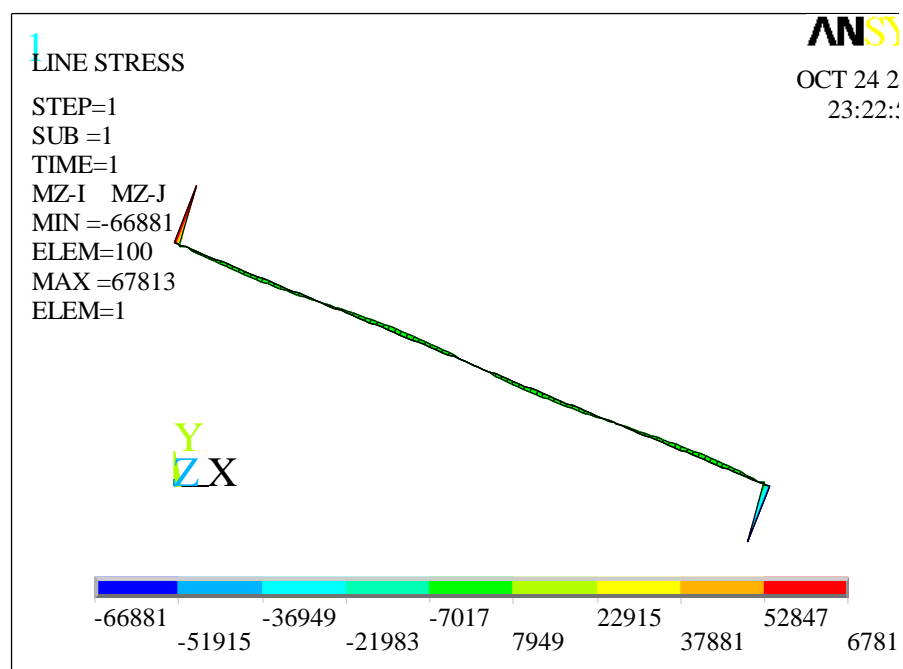


Figure 5.20 Bending stress in 2<sup>nd</sup> Asymmetric mode for 0.5 m peak displacement

Table 5.9 Evaluation of stresses in 2<sup>nd</sup> Anti-symmetric mode

Mid-span deflection (m)	Location	Bending moment $M$ N-m	Bending stress $\sigma_{bending}$ (MN/m <sup>2</sup> )	Axial stress $\sigma_{axial}$ (MN/m <sup>2</sup> )	Overall stress in the cable $\sigma_{overall}$ (MN/m <sup>2</sup> )
0.5	Deck end	67813.00	405.09	373.47	778.56
	Mid-span	187.91	1.12	373.47	374.59
	Pylon end	66881.00	399.52	373.47	772.99
1	Deck end	135390.00	808.77	373.47	1182.24
	Mid-span	139.92	0.84	373.47	374.31
	Pylon end	134000.00	800.47	373.47	1173.94
1.5	Deck end	202970.00	1212.47	373.47	1585.94
	Mid-span	91.94	0.55	373.47	374.02
	Pylon end	201100.00	1201.30	373.47	1574.77

2	Deck end	270540.00	1616.11	373.47	1989.58
	Mid-span	43.96	0.26	373.47	373.73
	Pylon end	268230.00	1602.31	373.47	1975.78

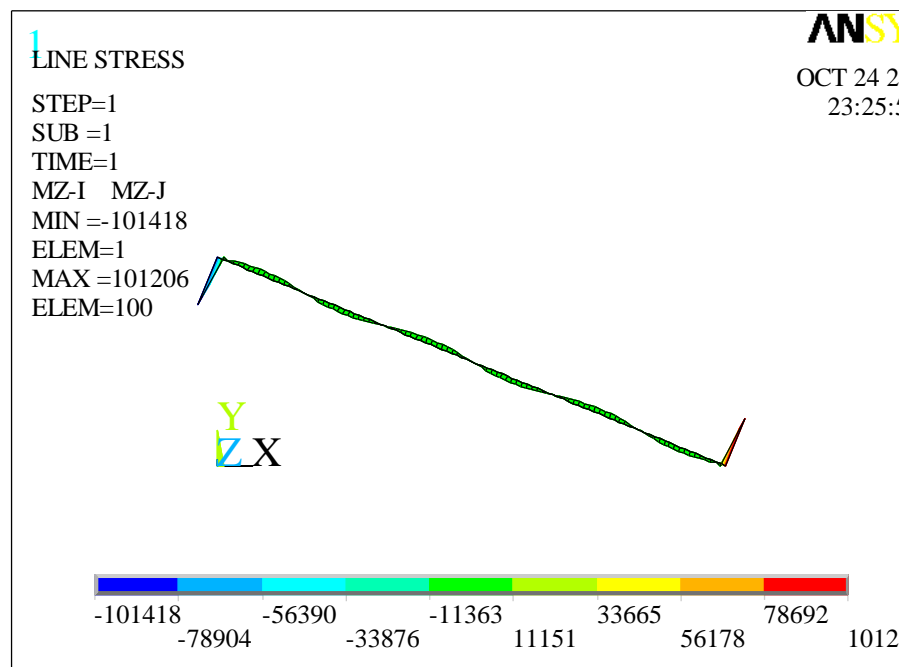


Figure 5.21 Bending stress in 3<sup>rd</sup> Asymmetric mode for 0.5 m peak displacement

Table 5.10 Evaluation of stresses in 3<sup>rd</sup> Anti-symmetric mode

Mid-span deflection	Location	Bending moment	Bending stress	Tension force	Axial stress	Overall stress in the cable
(m)		N-m	(MN/m <sup>2</sup> )	kN	(MN/m <sup>2</sup> )	(MN/m <sup>2</sup> )
0.5	Deck end	101420	605.8471	6033.7	539.3492	1145.196
	Mid-span	73.424	0.438609	6033.7	539.3492	539.7879
	Pylon end	101210	604.5926	6033.7	539.3492	1143.942
1	Deck end	203070	1213.068	6033.7	539.3492	1752.417
	Mid-span	89.038	0.531881	6033.7	539.3492	539.8811
	Pylon end	202180	1207.752	6033.7	539.3492	1747.101

1.5	Deck end	304720	1820.289	6033.7	539.3492	2359.638
	Mid-span	251.5	1.502372	6033.7	539.3492	540.8516
	Pylon end	303150	1810.91	6033.7	539.3492	2350.26
2	Deck end	406380	2427.57	6033.7	539.3492	2966.919
	Mid-span	413.96	2.47285	6033.7	539.3492	541.8221
	Pylon end	404120	2414.069	6033.7	539.3492	2953.419

The obtained stresses were plotted and a linear relationship between the displacement and the moments were found for different modes and are shown in the table. The obtained results will be used in the next chapter to estimate the fatigue life of the stay cable.

Table 5.11 Relationship between vibration amplitude of the cable and Bending moments at the ends

	Pylon End	Deck End
1st Symmetric	$1827.2*Y_{s1}$	$1869.7*Y_{s1}$
2nd Symmetric	$101380*Y_{s2}$	$100694*Y_{s2}$
3rd Symmetric	$169006*Y_{s3}$	$167860*Y_{s3}$
1st Anti-symmetric	$67605*Y_{as1}$	$66832*Y_{as1}$
2nd Anti-symmetric	$135311*Y_{as2}$	$134073*Y_{as2}$
3rd Anti-symmetric	$203149*Y_{as3}$	$202100*Y_{as3}$

## 5.7 Stresses in Stay cable C12 and D12 of Megami Bridge

There are cables that possess large Scruton numbers as shown in table 4.3 and thus it was decided to consider the cable C12 and D12, which is inclined at  $47^\circ$  is considered as explained in table 4.3 of Chapter IV. A similar procedure as explained in section 5.4 is adopted to estimate the stresses in stays C12 and D12. The model details are shown in table of Chapter IV.

Figure 5.22 shows the Boundary conditions of the stay cable C12 and D12. Table shows the vibration frequency of the cable in different modes. The obtained stresses were plotted and a linear relationship between the displacement and the moments were found for different modes

and are shown in the table. The obtained results will be used in the next chapter to estimate the fatigue life of the stay cable.

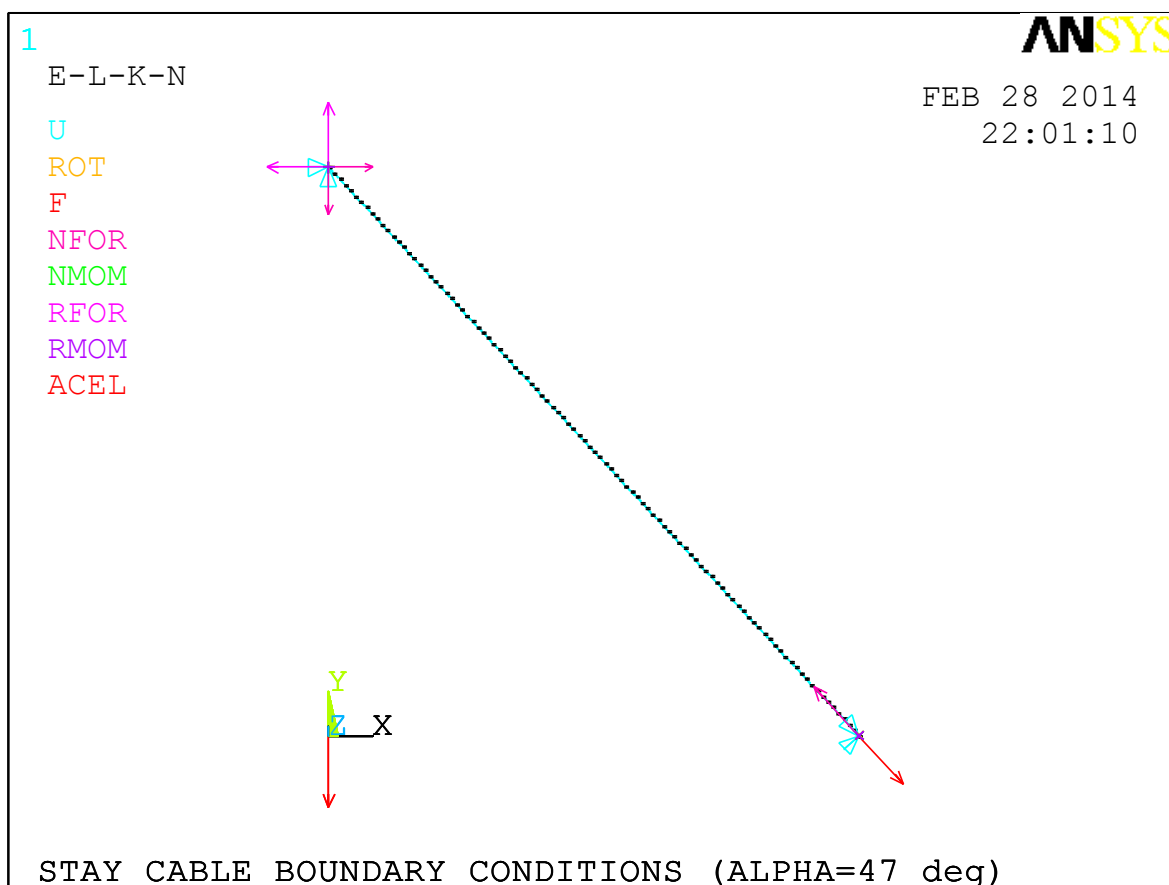


Figure 5.22 Boundary conditions of the stay cable inclined at 47° - C12 and D12

The mode shapes and its frequencies are obtained and shown in the table 5.12. The Tension forces and the axial stresses are obtained using string theory and are shown in table 5.12.

Table 5.12 Free vibration analysis of the cable C12 and D12 – string theory

Mode no.	1	2	3	4	5	6
Frequency (Hz)	1.35	2.71	4.07	5.44	6.82	8.22

Table 5.13 Tension force and axial stresses in stay cable C12 and D12

	Tension at different modes (kN)	Axial stress (MN/m <sup>2</sup> )
$T_1 = 4 m L^2 f_1^2$	3.99E+03	2.25E+04
$T_2 = m L^2 f_2^2$	4.02E+03	2.27E+04
$T_3 = 4 m L^2 f_3^2 / 9$	4.03E+03	2.27E+04
$T_4 = m L^2 f_1^2 / 4$	4.05E+03	2.28E+04

The axial stresses and bending stresses were estimated using the same procedure as explained in Chapter 5.4. The bending moment were estimated for different displacements levels from 0.5 m to 2m, for different modes and is shown in tables 5.14-5.19. Table 5.20 shows the relationship between peak vibration amplitude and bending moment.

Table 5.14 Evaluation of stresses in 1<sup>st</sup>-symmetric mode

Mid-span deflection (m)	Location	Bending moment $M$ N-m	Bending stress $\sigma_{bending}$ (MN/m <sup>2</sup> )	Axial stress $\sigma_{axial}$ (MN/m <sup>2</sup> )	Overall stress in the cable $\sigma_{overall}$ (MN/m <sup>2</sup> )
0.5	Deck end	7.2E+04	4.0E+02	2.2E+04	2.3E+04
	Mid-span	2.0E+03	1.1E+01	2.2E+04	2.2E+04
	Pylon end	7.1E+04	3.9E+02	2.2E+04	2.3E+04
1	Deck end	1.4E+05	7.9E+02	2.2E+04	2.3E+04
	Mid-span	4.1E+03	2.3E+01	2.2E+04	2.3E+04
	Pylon end	1.4E+05	7.9E+02	2.2E+04	2.3E+04
1.5	Deck end	2.1E+05	1.2E+03	2.2E+04	2.4E+04
	Mid-span	6.2E+03	3.4E+01	2.2E+04	2.3E+04
	Pylon end	2.1E+05	1.2E+03	2.2E+04	2.4E+04
2	Deck end	2.9E+05	1.6E+03	2.2E+04	2.4E+04
	Mid-span	8.2E+03	4.5E+01	2.2E+04	2.3E+04

	Pylon end	2.9E+05	1.6E+03	2.2E+04	2.4E+04
--	-----------	---------	---------	---------	---------

Table 5.15 Evaluation of stresses in 1<sup>st</sup> anti-symmetric mode

Mid-span deflection (m)	Location	Bending moment $M$ N-m	Bending stress $\sigma_{bending}$ (MN/m <sup>2</sup> )	Axial stress $\sigma_{axial}$ (MN/m <sup>2</sup> )	Overall stress in the cable $\sigma_{overall}$ (MN/m <sup>2</sup> )
0.5	Deck end	1.44E+05	7.94E+02	2.27E+04	2.34E+04
	Mid-span	8.31E+01	4.59E-01	2.27E+04	2.27E+04
	Pylon end	1.43E+05	7.90E+02	2.27E+04	2.34E+04
1	Deck end	2.87E+05	1.59E+03	2.27E+04	2.42E+04
	Mid-span	1.34E+02	7.41E-01	2.27E+04	2.27E+04
	Pylon end	2.86E+05	1.58E+03	2.27E+04	2.42E+04
1.5	Deck end	4.31E+05	2.38E+03	2.27E+04	2.50E+04
	Mid-span	1.85E+02	1.02E+00	2.27E+04	2.27E+04
	Pylon end	4.29E+05	2.37E+03	2.27E+04	2.50E+04
2	Deck end	5.74E+05	3.17E+03	2.27E+04	2.58E+04
	Mid-span	2.36E+02	1.30E+00	2.27E+04	2.27E+04
	Pylon end	5.72E+05	3.16E+03	2.27E+04	2.58E+04

Table 5.16 Evaluation of stresses in 2<sup>nd</sup> symmetric mode

Mid-span deflection (m)	Location	Bending moment $M$ N-m	Bending stress $\sigma_{bending}$ (MN/m <sup>2</sup> )	Axial stress $\sigma_{axial}$ (MN/m <sup>2</sup> )	Overall stress in the cable $\sigma_{overall}$ (MN/m <sup>2</sup> )
0.5	Deck end	2.16E+05	1.19E+03	2.27E+04	2.39E+04
	Mid-span	1.86E+04	1.03E+02	2.27E+04	2.28E+04
	Pylon end	2.15E+05	1.19E+03	2.27E+04	2.39E+04
1	Deck end	4.32E+05	2.39E+03	2.27E+04	2.51E+04

	Mid-span	3.71E+04	2.05E+02	2.27E+04	2.29E+04
	Pylon end	4.30E+05	2.38E+03	2.27E+04	2.51E+04
1.5	Deck end	6.48E+05	3.58E+03	2.27E+04	2.63E+04
	Mid-span	5.57E+04	3.08E+02	2.27E+04	2.30E+04
	Pylon end	6.45E+05	3.57E+03	2.27E+04	2.63E+04
2	Deck end	8.64E+05	4.77E+03	2.27E+04	2.75E+04
	Mid-span	7.42E+04	4.10E+02	2.27E+04	2.31E+04
	Pylon end	8.60E+05	4.76E+03	2.27E+04	2.75E+04

Table 5.17 Evaluation of stresses in 2<sup>nd</sup> anti-symmetric mode

Mid-span deflection (m)	Location	Bending moment $M$ N-m	Bending stress $\sigma_{bending}$ (MN/m <sup>2</sup> )	Axial stress $\sigma_{axial}$ (MN/m <sup>2</sup> )	Overall stress in the cable $\sigma_{overall}$ (MN/m <sup>2</sup> )
0.5	Deck end	2.89E+05	1.60E+03	2.28E+04	2.44E+04
	Mid-span	3.44E+02	1.90E+00	2.28E+04	2.28E+04
	Pylon end	2.88E+05	1.59E+03	2.28E+04	2.44E+04
1	Deck end	5.79E+05	3.20E+03	2.28E+04	2.60E+04
	Mid-span	7.20E+02	3.98E+00	2.28E+04	2.28E+04
	Pylon end	5.76E+05	3.19E+03	2.28E+04	2.60E+04
1.5	Deck end	8.68E+05	4.80E+03	2.28E+04	2.76E+04
	Mid-span	1.10E+03	6.05E+00	2.28E+04	2.28E+04
	Pylon end	8.64E+05	4.78E+03	2.28E+04	2.76E+04
2	Deck end	1.16E+06	6.40E+03	2.28E+04	2.92E+04
	Mid-span	1.47E+03	8.13E+00	2.28E+04	2.28E+04
	Pylon end	1.15E+06	6.37E+03	2.28E+04	2.92E+04

Table 5.18 Evaluation of stresses in 3<sup>rd</sup> symmetric mode

Mid-span deflection (m)	Location	Bending moment $M$ N-m	Bending stress $\sigma_{bending}$ (MN/m <sup>2</sup> )	Axial stress $\sigma_{axial}$ (MN/m <sup>2</sup> )	Overall stress in the cable $\sigma_{overall}$ (MN/m <sup>2</sup> )
0.5	Deck end	3.64E+05	2.01E+03	2.86E+04	2.86E+04
	Mid-span	5.17E+04	2.86E+02	2.86E+04	2.86E+04
	Pylon end	3.63E+05	2.01E+03	2.86E+04	2.86E+04
1	Deck end	7.28E+05	4.03E+03	2.86E+04	2.86E+04
	Mid-span	1.03E+05	5.72E+02	2.86E+04	2.86E+04
	Pylon end	7.25E+05	4.01E+03	2.86E+04	2.86E+04
1.5	Deck end	1.09E+06	6.04E+03	2.86E+04	2.86E+04
	Mid-span	1.55E+05	8.58E+02	2.86E+04	2.86E+04
	Pylon end	1.09E+06	6.02E+03	2.86E+04	2.86E+04
2	Deck end	1.46E+06	8.05E+03	2.86E+04	2.86E+04
	Mid-span	2.07E+05	1.14E+03	2.86E+04	2.86E+04
	Pylon end	1.45E+06	8.02E+03	2.86E+04	2.86E+04

Table 5.19 Evaluation of stresses in 3<sup>rd</sup> anti-symmetric mode

Mid-span deflection (m)	Location	Bending moment $M$ N-m	Bending stress $\sigma_{bending}$ (MN/m <sup>2</sup> )	Axial stress $\sigma_{axial}$ (MN/m <sup>2</sup> )	Overall stress in the cable $\sigma_{overall}$ (MN/m <sup>2</sup> )
0.5	Deck end	4.40E+05	2.43E+03	3.45E+04	2.86E+04
	Mid-span	1.07E+03	5.93E+00	3.45E+04	2.86E+04
	Pylon end	4.38E+05	2.42E+03	3.45E+04	2.86E+04
1	Deck end	8.79E+05	4.86E+03	3.45E+04	2.86E+04
	Mid-span	2.11E+03	1.17E+01	3.45E+04	2.86E+04

	Pylon end	8.76E+05	4.84E+03	3.45E+04	2.86E+04
1.5	Deck end	1.32E+06	7.29E+03	3.45E+04	2.86E+04
	Mid-span	3.15E+03	1.74E+01	3.45E+04	2.86E+04
	Pylon end	1.31E+06	7.26E+03	3.45E+04	2.86E+04
2	Deck end	1.76E+06	9.72E+03	3.45E+04	2.86E+04
	Mid-span	4.19E+03	2.32E+01	3.45E+04	2.86E+04
	Pylon end	1.75E+06	9.68E+03	3.45E+04	2.86E+04

Table 5.20 Relationship between Peak vibration amplitude and Bending moment

	Pylon End	Deck End
1st Symmetric	$143320 \times Y_{s1}$	$142754 \times Y_{s1}$
2 <sup>nd</sup> Symmetric	$431920 \times Y_{s2}$	$430235 \times Y_{s2}$
3 <sup>rd</sup> Symmetric	$728208 \times Y_{s3}$	$725456 \times Y_{s3}$
1st Anti-symmetric	$287075 \times Y_{as1}$	$285920 \times Y_{as1}$
2 <sup>nd</sup> Anti-symmetric	$578548 \times Y_{as2}$	$576249 \times Y_{as2}$
3 <sup>rd</sup> Anti-symmetric	$879291 \times Y_{as3}$	$875939 \times Y_{as3}$

## 5.8 Conclusion

In General stay cables carries a large amount of tension forces and bending stiffness and thus it leads to a debate that the cable can either assumed as neither a string nor a beam. In order to study the effects of cable-beam behavior, a cable from the Fredhartman Bridge was considered in this study. The frequencies and modes shapes of the stay cable were obtained according to string theory, Euler-beam with axial tension (assumed as a cable model). And later on the finite element model was created for the cable model (Beam with axial tension) and a modal analysis was carried out using ANSYS. The frequencies and mode shapes obtained in all the three are closer, but the string theory is less precise than the other two methods.

The cable-beam behavior and the importance of bending stiffness were explained by the cable model which was developed using vibration of continuous system. The behavior of cables was well explained by  $\gamma_d$  (Tension-Bending parameter), which decides the behavior of stays. It

is also observed that  $\gamma_d$  is small then the mode shapes are similar to clamped-beam conditions. Increasing  $\gamma_d$  makes the mode shapes like a taut string. The effect of aspect ratio D/L was also studied, confirming that the increase in D/L changes the mode shapes from a clamped beam to a string. The effect of tension force on natural frequency was also studied. The importance of bending stiffness and sag was once again explained by  $\gamma_d$ .

Chapter III explains the non-dimensional vibration amplitudes for different conditions of the stay cable. The non-dimensional vibration amplitudes were made dimensional according to the conditions such as modal frequencies and wind speed. At first a modal analysis was carried out using ANSYS and the modal co-ordinates were obtained manually. The obtained modal displacement was normalized and multiplied with dimensional vibration peak displacement obtained in the chapter III. The bending moments and the stresses were evaluated by inducing the modal displacements on to the nodes. A total of 3 symmetric and 3 anti-symmetric modes were considered for the analysis. The relation between the bending moments and the displacements were also obtained and which is required for the fatigue analysis explained in the chapter V. Axial stresses were estimated using string theory.

The response estimated for large Scruton number cable C12 and C14 in Chapter IV is considered in this Chapter, so as evaluate the stresses in stay cable. The properties of the cable are obtained from table 4.4 and table 4.5, and the free vibration analysis along with a static analysis was done to evaluate the stresses in different modes.

## 5.9 References

1. Aaron James Pebley, B.S., 2005, Bending Stresses in Stay-Cables During Large-Amplitude Vibrations - A Fred Hartman Bridge Case Study, The University of Texas at Austin
2. Niels J. Gimsing, Cable supported bridges-concept and design (1983), John Wiley and sons, New York

3. Zhang Ping, 2008, Design and Research of Structural Health Monitoring system for Stayed Cable Bridge based on Lab windows/CVI, M.S. Thesis, Blekinge Institute of Technology, Sweden.
4. Winkler Jan., Fischer Gregor., Georgakis Christos T., Agnieszka Kotas, 2011, A Preliminary Bending fatigue spectrum for steel monostrand cables”,*Journal of the International Association for Shell and Spatial Structures*, Vol. 52 (4) pp 249-255.
5. Shunichi Nakamura, Hajime Hosokawa, 1989, “A study on the fatigue design of parallel wire strands on Cable-stayed bridges”, *Japan Society of Civil Engineers (Proc. Of JSCE No. 410/I-12)*, pp. 327s-336s.
6. H. J. Zhou, Y. L. Xu, 2007, “Wind-rain-induced vibration and control of stay cables in a cable-stayed bridge”, *Journal of Structural Control and Health Monitoring*, 14, pp 1013-1033.
7. John C. Eggers, 2003, Cable Stay Fatigue Analysis for the Fred Hartman Bridge, M.S. Thesis, The University of Texas at Austin.
8. Hiroshi Zui, Tohru Shinke, Yoshio Namita, 1996, “Practical formulas for estimation of Cable Tension by Vibration method”, *Journal of Structural Engineering*, Vol. 122, pp. 651-656.
9. Armin B. Mehrabi, Habib Tabatabai P.E., 1998, Unified Finite Difference Formulation for Free vibration of cables, *Journal of Structural Engineering*, Vol. 124, No.11, pp: 1313-1322.
10. Sharon L. Wood, Marcel Poser, Karl H. Frank, Matthew J. Bean, Joseph A. Dowd, 2008, ‘Bending Fatigue Response of Grouted Stay Cables’, Texas department of Transportation, Report No. FHWA/TX-0-1401-1
11. Marcel Poser, 2001, Full-Scale Bending Fatigue Tests on Stay Cables, M.S. Thesis, The University of Texas at Austin
- Irvine, H.M., 1981, “Cable Structures”, 1st ed. New York: Dover Publications.
12. Irvine, H.M., 1993, “Local Bending Stresses in Cables”, *International Journal of Offshore and Polar Engineering* 3: 172-175.
13. Irvine, H.M., and T.K. Caughey, 1974, “The Linear Theory of Free Vibrations of a Suspended Cable” *Proceedings of the Royal Society* 341 (1974): 299-315.



## **CHAPTER VI**

# **FATIGUE ESTIMATION OF STAY CABLES UNDER THE ACTION OF WIND AND RAIN**

### **6.1. Introduction**

In general, the stay cables acts as tension elements between the pylon and the bridge deck and carries a large amount of tensile force. In order to carry a large amount of tension forces, the stay cables posses very small amount of damping which makes the cable vulnerable to the wind and rain-wind induced vibrations. Since the cable found to vibrate at very large amplitudes (explained in chapter 3 and 4) under the action of rain and wind, thus these vibrations are dangerous and thus expected to induce fatigue due to bending.

Previously, there are some remarkable works done on static fatigue of stay cables in experimental conditions, considering bending and axial fatigue. Federico Clunci (2007) presented a parametric investigation of the axial fatigue performance of suspended cables subjected to lateral wind-induced vibrations. The turbulent wind field is simulated as a multivariate mono-dimensional Gaussian process. A stochastic analysis of the cable responses under different wind loads is also proposed to discuss the hypothesis of Gaussian distribution. A similar procedure was followed in this Chapter for stay cables to estimate the axial fatigue. Maria Pia Repetto (2001) studied the dynamic along wind fatigue of slender vertical structures with an application problem for slender structures. Vanessa A. Pino (2010) and Christopher (2008) had studied the fatigue damage of signal structures using the stochastic models. Brent M. Phares (2007) developed a fatigue procedure to estimate the fatigue life of slender structures like traffic

Signals being subjected to Wind-Induced Excitations such as Vortex Shedding and Buffeting”. These above fatigue methodology in turn help the author to derive a new methodology for estimating the fatigue damage of the stay cable.

This chapter introduces a new methodology to evaluate fatigue using the joint probability models, as explained in chapter II. The methodology for fatigue is explained with its application models. Fatigue damage was estimated for three different joint probability models, which is explained in this chapter II and a comparison of the results were done. The purpose of evaluating fatigue for three possible probability models is to study the effect of meteorological/environmental parameters on fatigue damage of stay cables. Usually stay cables can be approximately considered as a taut string as it carries a large amount of axial tension. But the approximation may be valid for the cables with minimum flexural rigidity and the sag. But in order to study the effect of bending stiffness, mode shapes a taut string and a beam with clamped ends were considered in the study. And then using mode super position the bending moments on the cable is obtained. The methodology proposed by Christopher (2008) was modified in this Chapter and used to estimate the fatigue life of the stay cables.

The statistical analysis explained in chapter II was used to estimate the fatigue life of the cable. The general procedure for estimating fatigue explained has 6 main steps. In chapter II, three forms of joint probability densities were considered. The developed methodology is suitable for the entire three models I, which considers the Joint probability of wind speed and wind direction as dependent event and rainfall as independent event. In the second probability, wind speed, direction and rainfall is considered as dependent events. Whereas in the third model it is assumed assumes that the all wind comes through the most unfavorable direction.

## **6.2. Methodology followed for Fatigue estimation for the probability models**

The procedure for evaluating fatigue is discredited in to six main steps and is explained below.

1. The meteorological records collected at the bridge site are used to obtain the joint occurrence of wind speed, direction and rainfall intensity. The Joint occurrence matrix is called as W-matrix or the wind speed matrix and is of the following form,

$$[W] = \begin{bmatrix} W_{1,1} & W_{1,2} & \cdots & W_{1,\theta} \\ W_{2,1} & W_{2,2} & \cdots & W_{2,\theta} \\ \vdots & \vdots & \ddots & \vdots \\ W_{v,1} & W_{v,2} & \cdots & W_{v,\theta} \end{bmatrix} \quad (6.1)$$

And considering the rainfall intensity in to the W-matrix can be called as W-matrix for specified rainfall condition.

2. For the probability model I and III, the W-matrix can be obtained for different rainfall intensity using equation 6.2 and for probability model II, W-matrix is directly obtained in Chapter II.

$$[W]_R = P_r \begin{bmatrix} W_{1,1} & W_{1,2} & \cdots & W_{1,\theta} \\ W_{2,1} & W_{2,2} & \cdots & W_{2,\theta} \\ \vdots & \vdots & \ddots & \vdots \\ W_{v,1} & W_{v,2} & \cdots & W_{v,\theta} \end{bmatrix} \quad (6.2)$$

Where  $W_{i,j}$ - is the probability of the wind blowing in the  $i^{\text{th}}$  direction range and in the  $j^{\text{th}}$  speed range,  $v,\theta$ - number of discrete categories for wind speed and direction,  $P_r$ - Probability of Rainfall intensity.

3. The number of vibrations that the cable will experience in a specific period of time for joint conditions of wind speed, direction and rainfall can be estimated by multiplying the wind speed matrix with the natural frequency of the structure.

$$[n]_R = f_0 t [W]_R = \begin{bmatrix} n_{1,1} & n_{1,2} & \cdots & n_{1,\theta} \\ n_{2,1} & n_{2,2} & \cdots & n_{2,\theta} \\ \vdots & \vdots & \ddots & \vdots \\ n_{v,1} & n_{v,2} & \cdots & n_{v,\theta} \end{bmatrix}_R \quad (6.3)$$

Where  $n_{i,j}$  is the number of vibrations at  $i^{\text{th}}$  wind direction range and  $j^{\text{th}}$  wind speed range,

$f_0$  is the vertical fundamental frequency of the cable, and  $t$  is the length of the time period.

4. The vibration amplitude obtained from the experiment is used in the present analysis to estimate the fatigue life of the stay cables. The response matrix for different inclination, wind yaw angles and rainfall intensity can be obtained from the chapter III. A sample interpretation of the matrix for the case  $\alpha=30^\circ$ ,  $\beta=45^\circ$ ,  $R=0-30$  mm/hr is shown below:

$$[A]_R = \begin{bmatrix} Y_{1,1} & Y_{1,2} & \cdots & Y_{1,\theta} \\ Y_{2,1} & Y_{2,2} & \cdots & Y_{2,\theta} \\ \vdots & \vdots & \ddots & \vdots \\ Y_{v,1} & Y_{v,2} & \cdots & Y_{v,\theta} \end{bmatrix}_R \quad (6.4)$$

in which  $\{A_{i,j}\}_R$  is the peak to peak amplitudes of transverse vibrations for the combinations of wind speed, wind direction. The relation between displacement  $Y$  and bending moments is obtained in chapter IV and is shown in the table 5. The stresses were then obtained using the equation 5.

5. Evaluation of bending and axial stresses

- 5.1 The bending and the tensile stresses obtained for different displacements are used in the present study. The BS-matrix or the Bending stress matrix is evaluated for the equivalent Amplitude matrix (6.4) using equation 5 and 5.

$$[BS]_R = \begin{bmatrix} BS_{1,1} & BS_{1,2} & \cdots & BS_{1,\theta} \\ BS_{2,1} & BS_{2,2} & \cdots & BS_{2,\theta} \\ \vdots & \vdots & \ddots & \vdots \\ BS_{v,1} & BS_{v,2} & \cdots & BS_{v,\theta} \end{bmatrix}_R \quad (6.5)$$

Where  $BS_{i,j}$  is the stress range for the wind speed been blowing at  $i^{\text{th}}$  wind direction range and  $j^{\text{th}}$  wind speed range, in a specified rainfall ( $R$ ) condition.

- 5.2. The axial stresses were estimated for each mode using string theory and it is also assumed to be a singular matrix as the rain-vibration didn't contribute much on the in plane vibration. The AS-matrix or the axial stress matrix is evaluated for the equivalent

Amplitude matrix in equation 6.5.

$$[AS]_R = \begin{bmatrix} AS_{1,1} & AS_{1,2} & \cdots & AS_{1,\theta} \\ AS_{2,1} & AS_{2,2} & \cdots & AS_{2,\theta} \\ \vdots & \vdots & \ddots & \vdots \\ AS_{v,1} & AS_{v,2} & \cdots & AS_{v,\theta} \end{bmatrix}_R \quad (6.6)$$

Using S-N curve, transformation from the BS-Matrix to give the number of cycles  $N_{i,j}$  to failure at a constant stress range for different wind and rain conditions.

$$[N_B] = \begin{bmatrix} N_{1,1} & N_{1,2} & \cdots & N_{1,\theta} \\ N_{2,1} & N_{2,2} & \cdots & N_{2,\theta} \\ \vdots & \vdots & \ddots & \vdots \\ N_{v,1} & N_{v,2} & \cdots & N_{v,\theta} \end{bmatrix} \quad (6.7)$$

Where  $N_{i,j}$  is the number of cycles at constant amplitude bending stress range  $S_{i,j}$  that it would take for the cable to fail.

6. Making use of n-matrix in equation 6.2 and the N-matrix in equation 6.6, the bending fatigue damage can be estimated for the specified time period. From which the fatigue life of the stay cable can be estimated.

$$D = \sum \left( \frac{n_{i,j}}{N_{B_{i,j}}} \right) \quad (6.8)$$

For more information, a sample flow-chart for evaluating the fatigue is provided in Appendix VI.

### 6.3. Application of the Fatigue methodology for the probability model I

#### 6.3.1. Joint occurrence probability of wind speed, direction and rainfall-W matrix

The Statistical analysis of the wind speed, wind direction and rainfall is explained in the Chapter II. The joint occurrence table for wind speed, wind direction and rainfall intensity was used to estimate the fatigue life of the stay cable. The general occurrence probability table consists of all the wind speeds falling in to the 16 direction sectors as explained in Chapter II.

The Probability of rainfall intensity was considered to be an independent parameter for the first probability model. The rainfall intensity was divided in to three main categories such as 1-30 mm/hr, 30-60 mm/hr and above 60 mm/hr. The Probability of these rainy events can be obtained by dividing the rainy event to the total event and is shown in table 6.1.

Table 6.1 Distribution of rain events only

	Events without rain $P_r(WR))$	Total rainy events $(P_r(R))$	0-30 mm/hr $P_r(R10)$	30-60 mm/hr $P_r(R40)$	>60 mm/hr $P_r(R70)$
Events	695552	24017	23526	419	72
$P_r(R)$	0.97	0.03	0.03	0	0

Since the vibration amplitude of the stay cable under rain-wind induced vibration is not only velocity restricted but also dependent on rainfall intensity (Vinayagamurthy et. al, 2013, S. Zhan, 2008) and thus it is necessary to include the effect of rainfall intensity in to the relative frequency of wind. Table 6.3 shows the distribution of rainy events from the collected rainfall data, whereas the total probability of rainy events can be found by dividing the probability of rainy events to the probability of total events.

$$P_r(T) = \text{Total number of rainy events} = 24017$$

$$P_r(R10) = \text{Probability of 10 mm/hr rainfall} = 0.03$$

Similarly  $P_r(R40)$  and  $P_r(R70)$  were obtained. The vibration amplitude obtained for three different categories of rainfall conditions namely 10, 40 and 70 mm/hr. And thus it is assumed that 1-30 mm/hr rainfall can be grouped to 10 mm/hr, 30-60 mm/hr to 40 mm/hr and anything above 60 mm/hr to 70 mm/hr rainfall intensity of the experimental conditions and this will be dealt in the step 3

The W-matrix is shown in table 2.2 of chapter II and when multiplied by the Probability of rainfall events gives the Occurrence probability of wind speed, wind direction and rainfall

intensity. The table 6.2 shows the occurrence probability of wind speed, direction and rainfall for 0-30 mm/hr rainfall or  $W_{10}$  matrix. The probability density of rainfall intensities of 40 and 70 mm/hr is very low in comparison with 10 mm/hr rainfall condition and without any rainfall condition.

### **6.3.2. Evaluation of n-matrix**

The n-matrix or the number of vibrations that the cable had experienced during a particular time period for different rainfall intensity is obtained, so as to estimate the fatigue damage in the stay cables.

At first, it is assumed that the stay cable vibrates in 1<sup>st</sup> symmetric or its fundamental mode. The fundamental frequency was found in table 5.4 of Chapter V. The n-matrix can be obtained using the equation 6.5. From table 6.1, it is found that there are 1601.3 (10 minute events) occur every year. The fundamental frequency was found to be 0.58 Hz and is multiplied with the time length (for 1 year i.e.,  $1601.3 \times 10 \times 60$  seconds) to give the number of vibrations occurred per wind speed, direction under an assumed rainy event on an average year. The assumed design life of a stay cable is 100 years, and thus the n-matrix (R10 condition, i.e., 10 mm/hr rainfall condition) is obtained for 100 years (i.e.,  $1601.3 \times 10 \times 60 \times 100$  seconds) and is shown in Table 6.3. Table 6.3 can also be called as the number of vibrations occurs in the cable for 100 years in 10 mm/hr rainfall in the first mode. Similar steps were followed to obtain n-matrix for different modes.

Table 6.2  $W_{10}$ -matrix for 0-30 mm/hr rainfall condition ( $W_{10}$  matrix)

U (m/s)	Wind direction ( $\theta$ )															
	N	NNE	NE	ENE	E	ESE	SE	SSE	S	SSW	SW	WSW	W	WN W	NW	NW W
0-3	0.13 %	0.17%	0.18%	0.18%	0.09%	0.05%	0.03%	0.03%	0.03%	0.03%	0.02%	0.03%	0.04%	0.03%	0.03%	0.07%
3-6	0.16 %	0.08%	0.02%	0.02%	0.03%	0.03%	0.02%	0.02%	0.03%	0.06%	0.05%	0.04%	0.03%	0.04%	0.04%	0.10%
6-9	0.09 %	0.02%	0.00%	0.00%	0.00%	0.01%	0.01%	0.01%	0.03%	0.11%	0.06%	0.04%	0.04%	0.05%	0.04%	0.10%
9-12	0.03 %	0.01%	0.00%	0.00%	0.00%	0.00%	0.00%	0.00%	0.02%	0.10%	0.03%	0.03%	0.04%	0.04%	0.02%	0.07%
12-15	0.01 %	0.00%	0.00%	0.00%	0.00%	0.00%	0.00%	0.00%	0.02%	0.06%	0.02%	0.02%	0.06%	0.02%	0.01%	0.05%
15-18	0.00 %	0.00%	0.00%	0.00%	0.00%	0.00%	0.00%	0.00%	0.00%	0.01%	0.00%	0.01%	0.01%	0.00%	0.00%	0.00%
18-21	0.00 %	0.00%	0.00%	0.00%	0.00%	0.00%	0.00%	0.00%	0.00%	0.00%	0.00%	0.00%	0.01%	0.00%	0.00%	0.00%
>21	0.00 %	0.00%	0.00%	0.00%	0.00%	0.00%	0.00%	0.00%	0.00%	0.00%	0.00%	0.00%	0.01%	0.00%	0.00%	0.00%

Table 6.3 n-matrix for the first symmetric mode under 10 mm/hr rainfall

U (m/s)	N	NNE	NE	ENE	E	ESE	SE	SSE	S	SSW	SW	WSW	W	WNW	NW	NWW
0-3	7E+4	9E+4	1E+5	1E+5	5E+4	3E+4	2E+4	2E+4	2E+4	2E+4	1E+4	2E+4	2E+4	1E+4	2E+4	4E+4
3-6	9E+4	5E+4	1E+4	1E+4	2E+4	1E+4	1E+4	1E+4	2E+4	3E+4	3E+4	2E+4	2E+4	2E+4	2E+4	6E+4
6-9	5E+4	1E+4	6E+2	7E+2	2E+3	3E+3	4E+3	6E+3	1E+4	6E+4	4E+4	2E+4	2E+4	3E+4	2E+4	5E+4
9-12	2E+4	3E+3	7E+1	9E+1	4E+2	8E+2	2E+3	2E+3	1E+4	5E+4	2E+4	2E+4	2E+4	2E+4	9E+3	4E+4
12-15	7E+3	1E+3	3E+0	3E+1	5E+1	3E+2	8E+2	1E+3	1E+4	3E+4	9E+3	1E+4	3E+4	1E+4	3E+3	3E+4
15-18	5E+2	6E+1	0E+0	0E+0	3E+0	2E+1	4E+1	7E+1	3E+3	6E+3	2E+3	3E+3	8E+3	7E+2	6E+1	3E+3
18-21	3E+2	3E+1	0E+0	0E+0	0E+0	1E+1	3E+0	1E+1	1E+3	3E+3	9E+2	1E+3	5E+3	1E+2	5E+0	6E+2
>21	3E+2	2E+1	0E+0	0E+0	0E+0	5E+0	2E+1	5E+0	5E+2	2E+3	6E+2	1E+3	5E+3	6E+1	8E+0	4E+2

### 6.3.3. Dimensionalised Amplitude matrix or (Y-matrix)

Chapter III of the thesis explains the results obtained from the experiments on rain-wind induced vibrations. The non-dimensional vibration amplitudes are made dimensional according to the modal frequency and diameter of the stay cable.

For the example problem listed in table of Chapter V is considered for the fatigue study. The response amplitude of the cable inclined at 25 can be obtained from the experimental cases of Chapter III. Table 6.4 shows that response or Y-matrix before transformation. The maximum amplitude of the stay cable is found for the every 3 m/s wind speed range such as the maximum amplitude exists in the wind speed range 0-3 m/s, 3-6 m/s, 3-9 m/s, 9-12 m/s, 12-15 m/s, 15-18 m/s and greater than 18 m/s. Since the assumed cable lies on the left side (megami end) of the bridge and the wind comes from all the 16 sectors of the rose plot shown in figure 6.1.

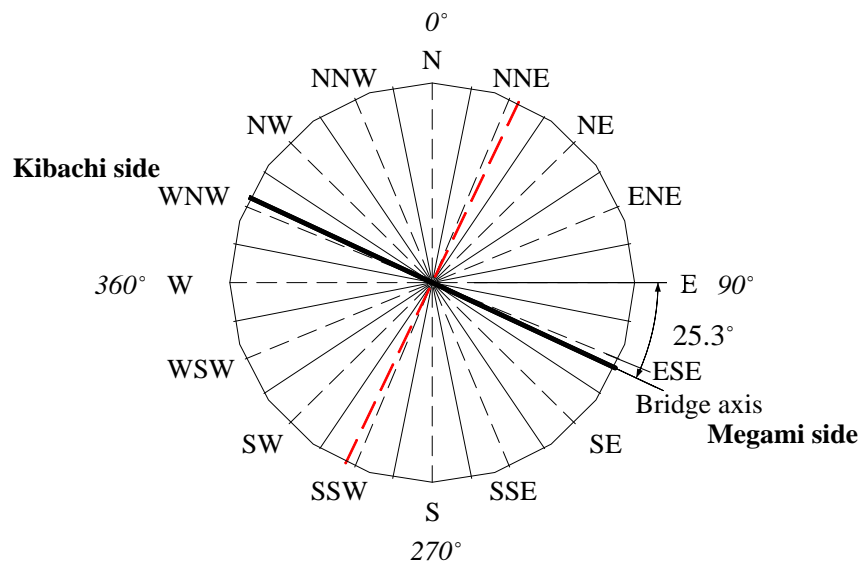


Figure 6.1 Bridge axis and the wind directions

The Y-matrix before transformation is tabulate in table 6.4. Since the bridge lies 25.3° to the East and thus a transformation has to be done for the wind direction to find the equivalent wind yaw angle. The transformation between wind yaw angle and the wind direction is given by,

$$Y(\beta) = Y(\theta) - 25.3^\circ \quad (6.9)$$

Table 6.4 Y-matrix before transformation

U (m/s)	wind yaw angle ( $\beta$ )					U	30	35	40	50
	30	35	40	50						
0.44	0.01	0.00	0.01	0.00	0-3	0.02	0.01	0.02	0.01	0.01
0.87	0.01	0.00	0.01	0.00						
1.31	0.01	0.01	0.01	0.00						
1.75	0.01	0.01	0.02	0.00						
2.18	0.01	0.01	0.02	0.01						
2.62	0.02	0.01	0.02	0.01						
3.06	0.02	0.03	0.01	0.01	3-6	0.21	0.24	0.22	0.02	
3.49	0.02	0.09	0.09	0.02						
3.93	0.02	0.13	0.04	0.01						
4.37	0.07	0.18	0.14	0.02						
4.80	0.17	0.19	0.21	0.02						
5.24	0.18	0.21	0.22	0.02						
5.68	0.21	0.24	0.19	0.02	6-9	0.17	0.24	0.19	0.06	
6.11	0.17	0.24	0.19	0.05						
6.55	0.05	0.23	0.17	0.06						
6.98	0.03	0.24	0.04	0.03						
7.42	0.03	0.12	0.03	0.02						
7.86	0.03	0.10	0.03	0.02						
8.29	0.03	0.10	0.03	0.02	9-12	0.03	0.10	0.03	0.02	
8.73	0.03	0.10	0.03	0.02						
9.17	0.03	0.10	0.03	0.02						
9.60	0.03	0.10	0.03	0.02						
10.04	0.03	0.10	0.03	0.02						
10.48	0.03	0.10	0.03	0.02						
10.91	0.03	0.10	0.03	0.02						

11.35	0.03	0.10	0.03	0.02						
11.79	0.03	0.10	0.03	0.02						
12.22	0.03	0.10	0.03	0.02	}	12-15	0.03	0.10	0.03	0.02
12.66	0.03	0.10	0.03	0.02						
13.10	0.03	0.10	0.03	0.02						
13.53	0.03	0.10	0.03	0.02						
13.97	0.03	0.10	0.03	0.02						
14.41	0.03	0.10	0.03	0.02						
14.84	0.03	0.10	0.03	0.02						
15.28	0.03	0.10	0.03	0.02	}	15-18	0.03	0.10	0.03	0.02
15.72	0.03	0.10	0.03	0.02						
16.15	0.03	0.10	0.03	0.02						
16.59	0.03	0.10	0.03	0.02						
17.03	0.03	0.10	0.03	0.02						
17.46	0.03	0.10	0.03	0.02						
17.90	0.03	0.10	0.03	0.02						
18.34	0.03	0.10	0.03	0.02		>18	0.03	0.10	0.03	0.02
18.77	0.03	0.10	0.03	0.02						

Y-matrix after transformation from the wind direction to the equivalent wind yaw angle is given by  $\beta^*$ . And the table 6.4 gives the transformed Y-matrix for the first symmetric mode.

Since rain-wind induced vibration is limited to certain wind yaw angles i.e., from 25° to 50° and thus only the directions which cause vibrations are only considered. The non-dimensional vibration response amplitude for different directions is dimensionalized and is shown in table 6.5.

Table 6.5 Displacement matrix for the 1<sup>st</sup> symmetric mode

U	N	NNE	NE	ENE	E	ESE	SE	SSE	S	SSW	SW	WSW	W	WNW	NW	NWW
$\beta$												59.0°-36.5°	36.5°-14°	14°-8.4°	8.4°-30.9°	30.9°-53.4°
0-3	0	0	0	0	0	0	0	0	0	0	0	1.61E-2	1.59E-2	0	1.59E-2	1.61E-2
3-6	0	0	0	0	0	0	0	0	0	0	0	2.19E-1	2.38E-1	0	2.11E-1	2.38E-1
6-9	0	0	0	0	0	0	0	0	0	0	0	1.90E-1	2.39E-1	0	1.70E-1	2.39E-1
9-12	0	0	0	0	0	0	0	0	0	0	0	2.92E-2	9.98E-2	0	2.92E-2	9.98E-2
12-15	0	0	0	0	0	0	0	0	0	0	0	2.92E-2	9.98E-2	0	2.92E-2	9.98E-2
15-18	0	0	0	0	0	0	0	0	0	0	0	2.92E-2	9.98E-2	0	2.92E-2	9.98E-2
>18	0	0	0	0	0	0	0	0	0	0	0	2.92E-2	9.98E-2	0	2.92E-2	9.98E-2
												Wind from sea			Wind from land	

\*Displacements are in meters

### 6.3.4. Evaluation of Stress matrixes (S-matrix)

The first part of the stress matrix discusses about the bending stress matrix and the later part discusses about the axial stress.

Section of the Chapter V of the thesis explains the evaluation of bending moment and stresses. Table 6.6 shows the relationship between the bending moment and the peak displacement, which was derived from the Chapter V. Using the table, bending stresses were found for different modes at the pylon and deck end.

Table 6.6 Relationship between vibration amplitude of the cable and Bending moments at the ends

	Pylon End	Deck End
1st Symmetric	$1.83E+3 \times Y_{s1}$	$1.87E+3 \times Y_{s1}$
2nd Symmetric	$1.01E+5 \times Y_{s2}$	$1.01E+5 \times Y_{s2}$
3rd Symmetric	$1.69E+5 \times Y_{s3}$	$1.68E+5 \times Y_{s3}$
1st Anti-symmetric	$6.76E+4 \times Y_{as1}$	$6.68E+4 \times Y_{as1}$
2nd Anti-symmetric	$1.35E+5 \times Y_{as2}$	$1.34E+5 \times Y_{as2}$
3rd Anti-symmetric	$2.03E+5 \times Y_{as3}$	$2.02E+5 \times Y_{as3}$

\*Bending moments are in N-m

$Y_{s1}, Y_{s2}, Y_{s3}$  are the Peak displacements in symmetric modes 1, 2 and 3.

$Y_{as1}, Y_{as2}, Y_{as3}$  are the Peak displacements in anti-symmetric modes 1, 2 and 3.

Bending stresses were evaluated for all the first 3 symmetric and anti-symmetric modes. Table 6.7 and 6.8 shows the bending stresses at the pylon and deck end for the 1st symmetric mode. The stress values in tables are given in terms of MPa (Mega Pascal). Axial stresses were evaluated using string theory and are explained in section of Chapter V. It is assumed that the axial stresses are not influenced by the bending of the cable. And it is predominant only if the cable vibrates and thus table becomes a constant stress matrix and is shown in table 6.9.

Table 6.7 Bending stresses (in Mpa) at the Pylon end in 1st symmetric mode

U (m/s)	N	NNE	NE	ENE	E	ESE	SE	SSE	S	SSW	SW	WSW	W	WNW	NW	NWW
												59.0°-36.5° (β)	36.5°-14° (β)	14°-8.4° (β)	8.4°-30.9° (β)	30.9°-53.4° (β)
0-3	0	0	0	0	0	0	0	0	0	0	0	1.78E-1	1.76E-1	0	1.76E-1	1.78E-1
3-6	0	0	0	0	0	0	0	0	0	0	0	2.42E+0	2.63E+0	0	2.33E+0	2.63E+0
6-9	0	0	0	0	0	0	0	0	0	0	0	2.10E+0	2.64E+0	0	1.88E+0	2.64E+0
9-12	0	0	0	0	0	0	0	0	0	0	0	3.22E-1	1.10E+0	0	3.22E-1	1.10E+0
12-15	0	0	0	0	0	0	0	0	0	0	0	3.22E-1	1.10E+0	0	3.22E-1	1.10E+0
15-18	0	0	0	0	0	0	0	0	0	0	0	3.22E-1	1.10E+0	0	3.22E-1	1.10E+0
>18	0	0	0	0	0	0	0	0	0	0	0	3.22E-1	1.10E+0	0	3.22E-1	1.10E+0

Table 6.8 Bending stresses (in Mpa) at the Deck end in 1st symmetric mode

U	N	NNE	NE	ENE	E	ESE	SE	SSE	S	SSW	SW	WSW	W	WNW	NW	NWW
												36.5°-59.0°	14°-36.5°		8.4°-30.9°	30.9°-53.4°
0-3	0	0	0	0	0	0	0	0	0	0	0	1.82E-01	1.80E-01	0	1.80E-01	1.82E-01
3-6	0	0	0	0	0	0	0	0	0	0	0	2.48E+00	2.69E+00	0	2.39E+00	2.69E+00
6-9	0	0	0	0	0	0	0	0	0	0	0	2.15E+00	2.70E+00	0	1.93E+00	2.70E+00
9-12	0	0	0	0	0	0	0	0	0	0	0	3.30E-01	1.13E+00	0	3.30E-01	1.13E+00
12-15	0	0	0	0	0	0	0	0	0	0	0	3.30E-01	1.13E+00	0	3.30E-01	1.13E+00
15-18	0	0	0	0	0	0	0	0	0	0	0	3.30E-01	1.13E+00	0	3.30E-01	1.13E+00
>18	0	0	0	0	0	0	0	0	0	0	0	3.30E-01	1.13E+00	0	3.30E-01	1.13E+00

Table 6.9 Axial stresses (in Mpa) at the Pylon and Deck end in 1st symmetric mode

U	N	NNE	NE	ENE	E	ESE	SE	SSE	S	SSW	SW	WSW	W	WNW	NW	NWW
(m/s)												36.5°-59.0°	14°-36.5°		8.4°-30.9°	30.9°-53.4°
0-3	0	0	0	0	0	0	0	0	0	0	0	376.33	376.33	0	376.33	376.33
3-6	0	0	0	0	0	0	0	0	0	0	0	376.33	376.33	0	376.33	376.33
6-9	0	0	0	0	0	0	0	0	0	0	0	376.33	376.33	0	376.33	376.33
9-12	0	0	0	0	0	0	0	0	0	0	0	376.33	376.33	0	376.33	376.33
12-15	0	0	0	0	0	0	0	0	0	0	0	376.33	376.33	0	376.33	376.33
15-18	0	0	0	0	0	0	0	0	0	0	0	376.33	376.33	0	376.33	376.33
>18	0	0	0	0	0	0	0	0	0	0	0	376.33	376.33	0	376.33	376.33

### 6.3.5. Evaluation of N-matrix

The fatigue life of the stay cables is often represented by S-N curve. These curves give the relation between stresses and the number of cycles to failure. Since the stay cables carries a large amount of tension forces, FIB (2005) and PTI (2000) doesn't address the fatigue issues related to transverse vibration of stay cables and therefore bending fatigue is not considered in their guidelines. Still there are cable stayed bridges which have been severely affected by rain-wind induced vibrations. But the presence of bending stiffness will contribute more to the bending fatigue as explained in Chapter V, bridges such as Fred Hartman, Meiko-nishi have been severally influenced by transverse vibrations and thus considering bending fatigue is a must for the design phase of the stay cable. There are few researchers who carried out the static fatigue analysis under laboratory conditions assuming both the ends of the cable are pinned. Winkler, J.(2010), Wood S.(2010), Hobbs R.E.(1996), carried out experimental fatigue test on stay cables.

Shunichi Nakamura (1989) had carried out fatigue damage estimation of stay cables due to bending stresses in which the bending stresses were found based on the deviation at the end of the stay cable, whereas fatigue damage was estimated assuming the equation 6.5. The fatigue spectrum of Winkler's test considers the bending stresses and thus it is used in this study to calculate the Number of cycles that could cause the stress fluctuations. The  $\sigma$ -N equation for bending spectrum is plotted in figure 6.8 (Winkler Jan, 2011).The fitted equation is found to be,

$$\log N_{bending} = 9.74 - 1.88 \log \sigma_{bending} \quad (6.10)$$

Equation can also reduced to

$$N_{bending} \sigma_{bending}^{1.88} = 5.5 \times 10^9 \quad (6.11)$$

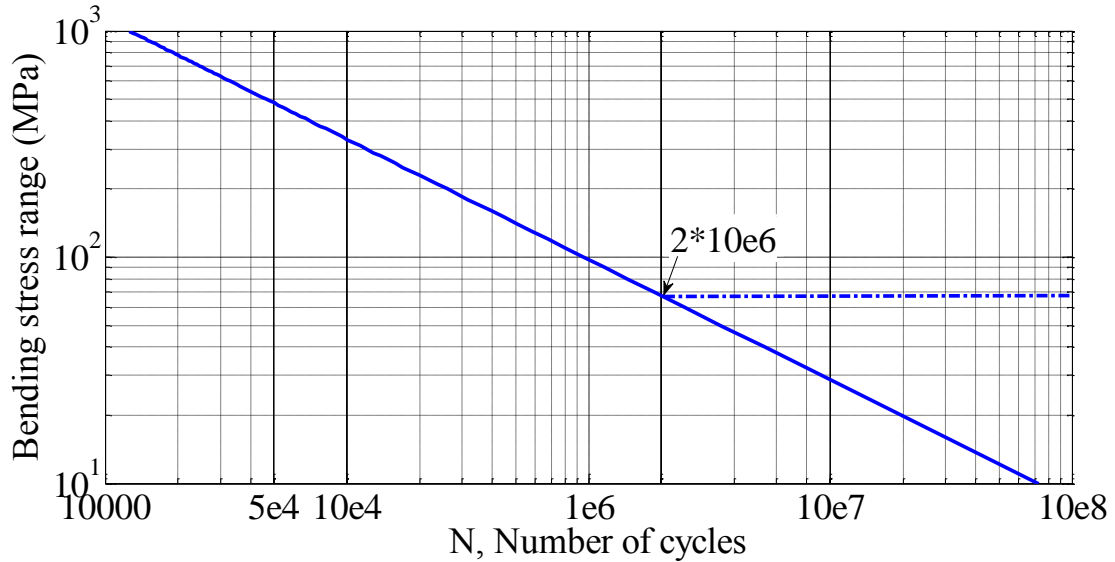


Figure 6.2 Preliminary bending spectrum for monostrand (Winkler Jan, 2011)

The N-matrix was derived from equation 6.11 and is shown in tables 6.10 and 6.11. Table 6.10 shows the N-matrix for Rainfall 10 mm/hr at the Pylon end in 1st symmetric mode and table 6.11 N-matrix for Rainfall 10 mm/hr at the Deck end in 1st symmetric mode. There is a small difference in the  $N_{bending}$  matrix at deck and pylon end, because the stresses at the deck end are larger than the pylon end, and the  $N_{bending}$  matrix for the Pylon and Deck end in 1st symmetric mode is shown in table 6.10 and table 6.11. Using string theory the axial stresses were evaluated in chapter V. Using the equation for fatigue life given by PTI (1986), the axial fatigue life can be found using equation 6.12.

The total number of cycles is given by,

$$N_{axial} = \frac{A}{0.75 * \sigma_{axial}} \quad (6.12)$$

Assuming a constant stress in each mode leaves a specific number of cycles in each mode and is shown in table 6.12.

Table 6.10 N-matrix at the Pylon end in 1st symmetric mode

U (m/s)	WSW	W	WNW	NW	NWW
	36.5°-59.0°	14°-36.5°		8.4°-30.9°	30.9°-53.4°
0-3	1.41E+11	1.45E+11	∞	1.45E+11	1.41E+11
3-6	1.04E+09	8.94E+08	∞	1.12E+09	8.94E+08
6-9	1.36E+09	8.84E+08	∞	1.67E+09	8.84E+08
9-12	4.62E+10	4.58E+09	∞	4.62E+10	4.58E+09
12-15	4.62E+10	4.58E+09	∞	4.62E+10	4.58E+09
15-18	4.62E+10	4.58E+09	∞	4.62E+10	4.58E+09
18-21	4.62E+10	4.58E+09	∞	4.62E+10	4.58E+09
>21	4.62E+10	4.58E+09	∞	4.62E+10	4.58E+09
sum	3.75E+11	1.70E+11	∞	3.79E+11	1.66E+11

Table 6.11 N-matrix at the Deck end in 1st symmetric mode

U (m/s)	WSW	W	WNW	NW	NWW
	36.5°-59.0°	14°-36.5°		8.4°-30.9°	30.9°-53.4°
0-3	1.35E+11	1.39E+11	∞	1.39E+11	1.35E+11
3-6	9.99E+08	8.56E+08	∞	1.07E+09	8.56E+08
6-9	1.30E+09	8.47E+08	∞	1.60E+09	8.47E+08
9-12	4.43E+10	4.39E+09	∞	4.43E+10	4.39E+09
12-15	4.43E+10	4.39E+09	∞	4.43E+10	4.39E+09
15-18	4.43E+10	4.39E+09	∞	4.43E+10	4.39E+09
18-21	4.43E+10	4.39E+09	∞	4.43E+10	4.39E+09

>21	4.43E+10	4.39E+09	$\infty$	4.43E+10	4.39E+09
sum	3.59E+11	1.62E+11	$\infty$	3.63E+11	1.59E+11

Table 6.12 N-matrix for axial stresses

Mode no.	symmetric modes	Anti-symmetric modes
1	1.75E+05	1.74E+05
2	1.80E+05	1.79E+05
3	1.80E+05	5.94E+04

### 6.3.6. Miner's Rule

The fatigue damage is found from the Miner's rule as in equation 6.13. The damage matrix for 1<sup>st</sup> symmetric mode under 10 mm/hr is shown in table and the cumulative fatigue damage in any particular direction can be found by summing up and is tabulated in table.

$$D_I^* = \sum_u \sum_{\theta} \sum_k \left( \frac{n_{i,j,k}}{N_{i,j,k}} \right)_R \quad (6.13)$$

Where  $D_I^*$  is the damage calculated for ith wind speed, jth direction at kth mode shape.

Where  $n_{i,j,k}$  is the n-matrix obtained in step 2 and is also called as number of vibrations at ith wind speed and jth wind direction,  $N_{i,j,k}$  is the N-matrix obtained in step 5 (shown in table 6.10, table 6.11 and table 6.12) or the number of constant amplitude stress ranges (Bending or axial) that it would take the cable to fail, D is the total fatigue damage for different rainfall intensity R.

### **6.3.7. Fatigue Estimation of stay cables using the probability model I**

Previously, Willox (2000) approximated that rain-wind induced vibration were found to happen at 3rd symmetric, in the absence of any deck/tower movement. This approach was based on the reports described earlier (Poston, 1998) for the video in question, which suggests, as already described, the presence of a standing wave (possibly first anti-symmetric mode). Since the stay cables are being influenced by first order and third order modes, and thus its must to consider the fatigue life of stay cables vibrating at different modes.

#### **6.3.7.1. Bending fatigue of stays (C04, Model I)**

From the table 6.1, it is found that there are 1601 (10 minute events) rainy events occur every year. Using the information in the table 6.1, the cumulative fatigue damage estimated at the deck end was estimated for 100 years. The fatigue damage matrix of the cable at its deck end under 10 mm/hr rainfall condition for the 1<sup>st</sup> symmetric mode is estimated for 100 years and is shown in table 6.14. The fatigue damage in all the three rainfall regimes were added together and the cumulative fatigue in different directions for 100 years of service were estimated for different rainfall conditions, and are shown in table 6.15. It can also be seen that the fatigue damage during 40 mm/hr and 70 mm/hr rainfall conditions were minimal when compared with low-rainfall region.

The table 6.16 shows the 1<sup>st</sup> symmetric, 1<sup>st</sup> anti-symmetric and 2<sup>nd</sup> symmetric mode doesn't cause serious damage whereas a higher second order mode causes fatigue damage. It can be said that the higher order symmetric and anti-symmetric modes contribute more to the fatigue damage of the stays, whereas the 1<sup>st</sup> order modes doesn't cause fatigue in the assumed service period (100 years) of the stay cable. But it can be seen from the table 6.15, that fatigue could occur in North-West-West direction in 2<sup>nd</sup> anti-symmetric mode or in the 3<sup>rd</sup>

symmetric and anti-symmetric mode at both pylon and deck end. Table 6.16 shows the bending fatigue life of stay cables if vibrated in different modes of vibration. From table 6.17, the fatigue life acquired by the stay cable in 1<sup>st</sup> symmetric, 1<sup>st</sup> anti-symmetric and 2<sup>nd</sup> symmetric is larger than the design life of the cable. But for 2<sup>nd</sup> anti-symmetric and higher order modes are subjected to fatigue below the design life of the stay cable.

Table 6.13 n-matrix for 1<sup>st</sup> symmetric mode at Deck end under 10 mm/hr rainfall conditions for 100 years (C04, Model I)

U (m/s)	WSW	W	WNW	NW	NWW
	36.5°-59.0°	14°-36.5°		8.4°-30.9°	30.9°-53.4°
0-3	2.E+04	2.E+04	1.E+04	2.E+04	4.E+04
3-6	2.E+04	2.E+04	2.E+04	2.E+04	6.E+04
6-9	2.E+04	2.E+04	3.E+04	2.E+04	5.E+04
9-12	2.E+04	2.E+04	2.E+04	9.E+03	4.E+04
12-15	1.E+04	3.E+04	1.E+04	3.E+03	3.E+04
15-18	3.E+03	8.E+03	7.E+02	6.E+01	3.E+03
18-21	1.E+03	5.E+03	1.E+02	5.E+00	6.E+02
>21	1.E+03	5.E+03	6.E+01	8.E+00	4.E+02
sum	9.E+04	1.E+05	1.E+05	7.E+04	2.E+05

Table 6.14 Estimated Fatigue Damage for 1st symmetric mode at Deck end under 10 mm/hr rainfall conditions for 100 years (C04, Model I)

U (m/s)	WSW	W	WNW	NW	NWW
	36.5°-59.0°	14°-36.5°		8.4°-30.9°	30.9°-53.4°
0-3	1.E-07	2.E-07	0.E+00	1.E-07	3.E-07

3-6	2.E-05	2.E-05	0.E+00	2.E-05	7.E-05
6-9	2.E-05	3.E-05	0.E+00	1.E-05	6.E-05
9-12	3.E-07	5.E-06	0.E+00	2.E-07	8.E-06
12-15	3.E-07	7.E-06	0.E+00	6.E-08	7.E-06
15-18	7.E-08	2.E-06	0.E+00	1.E-09	6.E-07
18-21	3.E-08	1.E-06	0.E+00	1.E-10	1.E-07
>21	2.E-08	1.E-06	0.E+00	2.E-10	9.E-08
sum	4.E-05	7.E-05	0.E+00	4.E-05	1.E-04

Table 6.15 Estimated Bending Fatigue Damage for 1st Symmetric mode at Deck end under three rainfall conditions for 100 years (C04, Model I)

Rainfall (mm/hr)	WSW	W	WNW	NW	NWW
10 mm/hr	4.E-05	7.E-05	0	4.E-05	1.E-04
40 mm/hr	6.E-07	6.E-07	0	1.E-07	2.E-06
70 mm/hr	5.E-08	8.E-08	0	2.E-08	2.E-07
	4.E-05	7.E-05	0	4.E-05	1.E-04

Table 6.16 Estimated Cumulative Bending Fatigue Damage at deck end for symmetric and anti-symmetric modes for 100 years (C04, Model I)

Mode no.	symmetric modes					anti-symmetric modes				
	WSW	W	WNW	NW	NWW	WSW	W	WNW	NW	NWW
1	4.E-5	7.E-5	0	4.E-5	1.E-4	0.06	0.08	0	0.06	0.22
2	0.21	0.27	0	0.19	0.70	0.49	0.86	0	0.43	<b>1.79</b>
3	0.94	1.65	0	0.82	<b>3.42</b>	<b>1.60</b>	<b>2.81</b>	0	<b>1.40</b>	<b>5.82</b>

$\sum_1^3 k$	1.15	1.92	0	1.01	4.12	2.16	3.75	0	1.88	7.83
--------------	------	------	---	------	------	------	------	---	------	------

Table 6.17 Estimated Bending Fatigue life of stay cable (C04, Model I)

	Bending Fatigue life in years	
Mode no.	Symmetric modes	Asymmetric modes
1	>500	464
2	143	<b>56</b>
3	<b>29</b>	<b>17</b>

### 6.3.7.2. Axial fatigue of stays (C04, Model I)

The axial stresses were evaluated based on the assumption that stresses developed are irrespective of the vibration amplitude. And thus the credibility of the results for axial fatigue estimation is unknown. But for the study it gives an overall idea about the importance of axial stress and fatigue damage. The axial fatigue damage estimated in deck end of the cable during the service period is obtained and is shown in table 6.18. Table 6.19 shows the bending fatigue life of stay cables vibrating in different modes of vibration. It can be seen from table 6.17 and 6.19, that the axial fatigue damage is much larger than the bending fatigue.

Table 6.18 Estimated Cumulative Axial Fatigue Damage at deck end for symmetric and anti-symmetric modes for 100 years (C04, Model I)

mode no.	symmetric modes					anti-symmetric modes				
	WSW	W	WNW	NW	NWW	WSW	W	WNW	NW	NWW
1	0.54	0.79	0	0.42	1.26	1.09	1.58	0	0.85	<b>2.52</b>

2	<b>1.56</b>	<b>2.28</b>	0	<b>1.22</b>	<b>3.63</b>	<b>2.11</b>	<b>3.07</b>	0	<b>1.64</b>	<b>4.89</b>
3	<b>2.61</b>	<b>3.81</b>	0.00	<b>2.04</b>	<b>6.06</b>	<b>9.53</b>	<b>13.89</b>	0.00	<b>7.44</b>	<b>22.12</b>

Table 6.19 Estimated Axial Fatigue life of stay cable (C04, Model I)

Mode no.	Axial Fatigue life in years	
	Symmetric modes	Asymmetric modes
1	<b>79.7</b>	<b>40.0</b>
2	<b>28.3</b>	<b>21.0</b>
3	<b>17.4</b>	<b>4.7</b>

#### 6.4. Application of the Fatigue methodology for the probability model II

The procedure adopted in section 6.2 and section 6.3 was followed to estimate the fatigue damage and life of the stay cable. For any structure, it is a must to consider the most unfavorable environment conditions that may occur and thus the present probability model may be ideal, by considering the relative frequency of all winds blown in most unfavorable condition. The steps 1-6 explained 6.2 is again repeated.

And the W-matrix is shown in table 2.5 in which West South West and West direction specifies wind from sea side whereas North West and North West West denotes the wind from land side. The n-matrix was obtained by considering rainfall as an independent event. Table 6.1 shows the distribution of rainy events from the collected rainfall data, whereas the total probability of rainy events can be found by dividing the probability of rainy events to the probability of total events.

$$P_r(T) = \text{Total number of rainy events} = 24017$$

$$P_r(R10) = \text{Probability of 10 mm/hr rainfall} = 0.03$$

Similarly  $P_r(R40)$  and  $P_r(R70)$  were obtained. Using these information, the n-matrix was found for different rainfall intensities by using the probability of the particular rainy event with the relative frequency table and the vibrating frequency of the structure as given by equation 6.3. A sample n-matrix is shown in table 6.20 for 10 mm/hr rainfall condition at 1<sup>st</sup> symmetric mode.

Table 6.20 n-matrix for 1st Symmetric mode under 10 mm/hr rainfall conditions for 100 year (Model II)

U (m/s)	WSW	W	WNW	NW	NWW
	36.5°-59.0°	14°-36.5°		8.4°-30.9°	30.9°-53.4°
0-3	631107.9	631107.9	631107.9	0	631107.9
3-6	437247.2	437247.2	437247.2	0	437247.2
6-9	337453.2	337453.2	337453.2	0	337453.2
9-12	213325.6	213325.6	213325.6	0	213325.6
12-15	155064.8	155064.8	155064.8	0	155064.8
15-18	25593.71	25593.71	25593.71	0	25593.71
18-21	12116.29	12116.29	12116.29	0	12116.29
>21	9810.713	9810.713	9810.713	0	9810.713
sum	631107.9	631107.9	631107.9	0	631107.9

The fatigue damage is found from the Miner's rule as in equation 6.13. The damage matrix for different rainfall conditions, mode shapes were obtained by dividing  $n_{u,k}$

(n-matrix- table 6.20, number of applied load cycles) to the  $N_{u,k}$  (refer table 6.11, pertinent fatigue life).

$$D_{II}^* = \sum_u \sum_{\theta} \sum_k \left( \frac{n_{u,k}}{N_{u,k}} \right)_R \quad (6.17)$$

where  $D_{II}^*$  is the damage calculated for  $u^{\text{th}}$  wind speed,  $k^{\text{th}}$  mode shape, n and N-matrix are obtained using the methods explained in sections 6.25 and 6.11.

#### 6.4.1 Bending fatigue of stays (C04, Model II)

The cumulative fatigue damage estimated at the deck end was estimated for 100 years and is shown in table 6.21. The fatigue damage in all the three rainfall regimes were added together and the cumulative fatigue in different directions for 100 years of service were estimated for different rainfall conditions, and are shown in table 6.22. It can also be seen that the fatigue damage during 40 mm/hr and 70 mm/hr rainfall conditions were minimal when compared with low-rainfall region, which is similar to other two models. The table 6.23 shows the 1<sup>st</sup> symmetric mode doesn't cause serious damage whereas a higher second order mode causes fatigue damage. It can be said that the higher order symmetric and anti-symmetric modes contribute more to the fatigue damage of the stays, whereas the 1<sup>st</sup> order symmetric mode doesn't cause fatigue in the assumed service period (100 years) of the stay cable. But it can be seen from the table 6.23, that fatigue damage could occur in West-South-West, West, North-West and North-West-West direction in 1<sup>st</sup> anti-symmetric mode or in 2<sup>nd</sup> or 3<sup>rd</sup> symmetric and anti-symmetric mode at both pylon and deck end. Table 6.24 shows the bending fatigue life of stay cables vibrating in different modes of vibration.

It is a must to note that, the possible mode of vibration is assumed to be the 1<sup>st</sup> anti-symmetric mode and thus there is a possibility of fatigue damage in the considered

service period of the cable, and therefore it is important to consider the bending fatigue due to rain-wind induced vibrations.

Table 6.21 Estimated Fatigue Damage for 1st Symmetric mode at Deck end under 10 mm/hr rainfall conditions for 100 years (C04, Model II)

U (m/s)	WSW	W	WNW	NW	NWW
	36.5°-59.0°	14°-36.5°		8.4°-30.9°	30.9°-53.4°
0-3	4.E-06	4.E-06	0.E+00	4.E-06	5.E-06
3-6	4.E-04	4.9 E-04	0.E+00	4.E-04	5.E-04
6-9	2.4 E-04	3.8 E-04	0.E+00	2.E-04	4.E-04
9-12	5.E-06	5.E-05	0.E+00	5.E-06	5.E-05
12-15	3.E-06	3.E-05	0.E+00	3.E-06	3.E-05
15-18	6.E-07	6.E-06	0.E+00	6.E-07	6.E-06
18-21	3.E-07	3.E-06	0.E+00	3.E-07	3.E-06
>21	2.E-07	2.E-06	0.E+00	2.E-07	2.E-06
sum	7.1 E-04	1 E-03	0.E+00	6.3 E-04	1 E-03

Table 6.22 Estimated Bending Fatigue Damage for 1st Symmetric mode at Deck end under three rainfall conditions for 100 years (C04, Model II)

Rainfall (mm/hr)	WSW	W	WNW	NW	NWW
10 mm/hr	7.1E-04	1E-03	0	6.3E-04	1E-03
40 mm/hr	9.7E-06	9.81E-06	0	2.1E-06	1.1E-05
70 mm/hr	7.8E-07	1E-06	0	3.2E-07	1.1E-06
sum	7.1E-04	1E-03	0	6.3E-04	1E-03

Table 6.23 Estimated Cumulative Bending Fatigue Damage at deck end for symmetric and anti-symmetric modes for 100 years (C04, Model II)

Mode no.	symmetric modes					anti-symmetric modes				
	WSW	W	WNW	NW	NWW	WSW	W	WNW	NW	NWW
1	0	0	0	0	0	1.2	1.5	0	1.0	1.5
2	3.8	4.9	0	3.3	5	8.8	12.6	0	7.7	12.6
3	16.8	24.0	0	14.7	24.0	28.6	40.8	0	25.1	40.9
$\sum_1^3 k$	20.6	28.9	0	18.0	29.0	38.5	54.9	0	33.8	55.0

Table 6.24 Estimated Bending Fatigue life of stay cable (C04, Model II)

Mode no.	Bending Fatigue life in years	
	Symmetric modes	Asymmetric modes
1	>500	65.30
2	20.15	8.03
3	4.16	2.45

#### 6.4.2 Axial fatigue of stays (C04, Model II)

The axial fatigue life estimated in a similar manner at the deck end of the cable, vibrating in different modes of vibration and is shown in table 6.25. It can be seen from table 6.24 and 6.25, that the axial fatigue damage is much larger than the bending fatigue. The axial fatigue life estimated is not reliable as bending fatigue, because of the assumption that the axial stresses are independent of the vibration amplitude. Table 6.26 shows the estimated axial fatigue due to rain-wind induced vibrations considering the relative frequency of all windblown in the most unfavorable direction to rain-wind induced vibration.

Table 6.25 Estimated Cumulative Axial Fatigue Damage at deck end for symmetric and anti-symmetric modes for 100 years (C04, Model II)

Mode no.	symmetric modes					anti-symmetric modes				
	WSW	W	WNW	NW	NWW	WSW	W	WNW	NW	NWW
1	0.21	0.21	0	0.21	0.21	0.11	0.11	0	0.11	0.11
2	0.41	0.41	0	0.41	0.41	0.31	0.31	0	0.31	0.31
3	1.87	1.87	0	1.87	1.87	0.51	0.51	0	0.51	0.51

Table 6.26 Estimated Axial Fatigue life of stay cable (C04, Model II)

Mode no.	Axial Fatigue life in years	
	Symmetric modes	Asymmetric modes
1	9.40	4.73
2	3.27	2.43
3	1.96	0.54

### 6.5. Application of the Fatigue methodology for the probability model III (Rainfall : dependent events)

For the probability model-II, the joint occurrence of wind speed, direction and rainfall are considered as dependent events. The W-matrix for different rainfall condition is obtained from tables 2.6, table 2.7 and table 2.8 in chapter II. The n-matrix can be obtained using equation 6.14,

$$n\text{-matrix} = W\text{-matrix} \times \text{time period} * \text{frequency}(\text{hz}) \quad (6.14)$$

In order to obtain n-matrix for 10 mm/hr rainfall condition in first symmetric mode, the above

can be written as in the equation 6.15

$$n_{10} - matrix = W_{10} - matrix \times \text{time period} * \text{frequency( Hz)} \quad (6.15)$$

where  $W_{10}$  is the obtained from table 2.6 explained chapter II, time period is the service or the assumed design life of stay cable, which 100 years. From table 6.1, it can be said that an average rainfall in a year would be 1601.3 (10 minute events). And thus for 100 years the total time period would be  $9.61 \times 10^7$  seconds. For first mode, the frequency of the stay cable is found to be 0.58 Hz and from these, the  $n_{10}$ -matrix is obtained for 10 mm/hr rainfall for the first mode and is shown in table 6.27.

Table 6.27 n-matrix for 1st Symmetric mode under 10 mm/hr rainfall conditions for 100 year (C04, Model III)

U (m/s)	WSW	W	WNW	NW	NWW
	36.5°-59.0°	14°-36.5°		8.4°-30.9°	30.9°-53.4°
0-3	3.E+05	4.E+05	4.E+05	5.E+05	1.E+06
3-6	4.E+05	3.E+05	3.E+05	4.E+05	1.E+06
6-9	3.E+05	2.E+05	2.E+05	2.E+05	1.E+06
9-12	3.E+05	2.E+05	2.E+05	7.E+04	5.E+05
12-15	2.E+05	2.E+05	1.E+05	3.E+04	2.E+05
15-18	1.E+05	2.E+05	7.E+04	1.E+04	9.E+04
18-21	2.E+05	3.E+05	3.E+04	1.E+04	2.E+05
>21	9.E+04	1.E+05	3.E+04	2.E+03	1.E+05
sum	2.E+06	2.E+06	1.E+06	1.E+06	5.E+06

Except the evaluation of n-matrix (step 2), all other steps explained in sections 6.2 or

6.3 is again repeated so as to evaluate the fatigue damage of the cable in the service period and also the expected fatigue life of the stay cable.

The fatigue damage is found from the Miner's rule as in equation 6.13, in which n-matrix is obtained in table 6.27 and the  $N_{\text{bending}}$ -matrix remains same for all the probability models (shown in table 6.11).

### 6.5.1. Bending fatigue of stays (C04, Model III)

The cumulative fatigue damage estimated at the deck end was estimated for 100 years and is shown in table 6.28. The fatigue damage in all the three rainfall regimes were added together and the cumulative fatigue in different directions for 100 years of service were estimated for different rainfall conditions, and are shown in table 6.29. Similar to probability model I, the fatigue damage estimated during 40 mm/hr and 70 mm/hr rainfall conditions were minimal, when compared with low-rainfall region. Table 6.30 shows the estimated cumulative bending fatigue damage acquired at the cable end in 100 years of service. Table 6.32 and 6.33 shows the estimated bending and axial fatigue life of the stay cable, the estimated fatigue life is very low when the cable vibrates in any mode other than the primary symmetric mode.

Table 6.28 Estimated Fatigue Damage for 1st Symmetric mode at Deck end under 10 mm/hr rainfall conditions for 100 years (C04, Model III)

U (m/s)	WSW	W	WNW	NW	NWW
	36.5°-59.0°	14°-36.5°		8.4°-30.9°	30.9°-53.4°
0-3	5.E-07	3.E-06	0.E+00	4.E-06	9.E-06
3-6	5.E-06	3.E-04	0.E+00	4.E-04	2.E-03
6-9	3.E-05	3.E-04	0.E+00	1.E-04	1.E-03

9-12	2.E-06	5.E-05	0.E+00	2.E-06	1.E-04
12-15	2.E-06	5.E-05	0.E+00	6.E-07	6.E-05
15-18	1.E-06	4.E-05	0.E+00	3.E-07	2.E-05
18-21	1.E-06	6.E-05	0.E+00	3.E-07	5.E-05
>21	8.E-07	3.E-05	0.E+00	5.E-08	2.E-05
sum	4.E-05	8.E-04	0.E+00	5.E-04	3.E-03

Table 6.29 Estimated Bending Fatigue Damage for 1st Symmetric mode at Deck end under three rainfall conditions for 100 years (C04, Model III)

Rainfall (mm/hr)	WSW	W	WNW	NW	NWW
10 mm/hr	4.E-05	8.E-04	0.E+00	5.E-04	3.E-03
40 mm/hr	9.E-05	6.E-04	0.E+00	8.E-05	2.E-03
70 mm/hr	6.E-05	6.E-04	0.E+00	2.E-04	6.E-04
sum	2.E-04	2.E-03	0.E+00	7.E-04	6.E-03

Table 6.30 Estimated Cumulative Bending Fatigue Damage at deck end for symmetric and anti-symmetric modes for 100 years (C04, Model III)

Mode no.	symmetric modes					anti-symmetric modes				
	WSW	W	WNW	NW	NWW	WSW	W	WNW	NW	NWW
1	0	0.00	0	0	0.01	0	1.75	0	0.76	7.63
2	0	8.45	0	2.47	28.61	0	24.00	0	5.67	77.97
3	0	50.25	0	14.29	148.84	1.32	85.54	0	28.73	253.35
$\sum_1^3 k$	0	59	0	17	177	1	111	0	35	339

Table 6.31 Estimated Bending Fatigue life of stay cable (C04, Model III)

Modes	Bending	
	Symmetric	anti-symmetric
1	<500	13.11
2	3.50	1.28
3	0.67	0.39

### 6.5.2. Axial fatigue of stays (C04, Model III)

The axial fatigue life estimated in a similar manner at the deck end and is shown in table 6.33 which shows the bending fatigue life of stay cables vibrating in different modes of vibration. It can be seen from table 6.33 and 6.31, that the axial fatigue damage is much larger than the bending fatigue. The axial fatigue life estimated is not reliable as bending fatigue, because of the assumption that the axial stresses are independent of the vibration amplitude.

Table 6.32 Estimated Cumulative Axial Fatigue Damage at deck end for symmetric and anti-symmetric modes for 100 years (C04, Model III)

Mode no.	symmetric modes					anti-symmetric modes				
	WSW	W	WNW	NW	NW W	WSW	W	WN W	NW	NWW
1	59	42	0	28	64	118	85	0	57	128
2	170	122	0	82	185	229	164	0	111	249
3	284	203	0	137	309	1037	742	0	501	1127
sum	513	367	0	248	558	1384	991	0	669	1505

Table 6.33 Estimated Axial Fatigue life of stay cable (C04, Model III)

Modes	Axial	
	Symmetric	anti-symmetric
1	1.56	0.78
2	0.54	0.40
3	0.32	0.09

### 6.6. Fatigue damage comparison between the three probability models (Cables C04,D04)

Fatigue damage and life estimated in section 6.3, 6.4 and 6.5 using the three probability models developed in chapter II were compared in this section.

Table 6.34 and 6.35 shows the accumulated bending fatigue damage in symmetric and anti-symmetric modes for 100 years using different probability models. In table 6.34, 6.35, 6.36 and 6.37, the value exceeds 1 indicates the possibility of fatigue damage. It is known from the table 6.34, that there is no fatigue damage in first symmetric mode whereas higher modes causes fatigue damage. The probability model I predicts a low value of bending fatigue life as the probability model assumes the rainfall intensity is independent of wind speed and direction, whereas the estimation based on the probability model II and III shown in table 6.32 shows a large amount of bending fatigue damage in 2<sup>nd</sup> and 3<sup>rd</sup> symmetric modes.

Table 6.33 shows the bending fatigue damage in anti-symmetric modes during the assumed life time of the cable. The probability model I predicts axial fatigue in 2<sup>nd</sup> anti-symmetric mode in the North-West-West direction and in 3<sup>rd</sup> anti-symmetric modes in

West-South-West, West, North-West and North-West-West direction, whereas the probability models II and III predicts fatigue in 1<sup>st</sup> anti-symmetric mode.

The credibility of the axial fatigue estimation is unknown because of the assumption made in Chapter V and VI, i.e., the stresses developed in the cable ends to the maximum irrespective of the vibration amplitude. Table 6.36 and 6.37 shows the axial fatigue damage in symmetric and anti-symmetric modes. The estimation shows that there is possibility of fatigue in all the symmetric and anti-symmetric modes for all the three probability models.

The total bending and axial fatigue life of the cable was estimated in table 6.38 and 6.39, in which the values below 100 shows the fatigue could occur during the assumed life of the cable (100 years). For bending, the cable has a large fatigue life or can serve for more than 500 years of service when vibrated in 1<sup>st</sup> mode as estimated by all the three models. But it can be seen that model I predicts earlier fatigue in 2<sup>nd</sup> anti-symmetric mode, whereas the model II and III predicts fatigue in 1<sup>st</sup> anti-symmetric mode and eventually higher modes causes less fatigue life and vulnerable to rain-wind induced vibrations. All the three probability models predict axial fatigue in 1<sup>st</sup> symmetric mode. The fatigue life prediction made by model I is quite small in comparison with the probability models II and III.

Table 6.34 Accumulated bending fatigue damage in symmetric obtained for 100 years using different probability models (Cables: C04, D04)

Mode no.	Probability model I (R independent)					Probability model II (R independent)					Probability model III (R dependent)				
	WSW	W	WNW	NW	NWW	WSW	W	WNW	NW	NWW	WSW	W	WNW	NW	NWW
1	4E-05	7E-05	0	4E-05	1E-04	0	0	0	0	0	0	0	0	0	0.01
2	0.21	0.27	0	0.19	0.7	<u>3.8</u>	<u>4.9</u>	0	<u>3.3</u>	<u>5</u>	0	<u>8.45</u>	0	<u>2.47</u>	<u>28.61</u>
3	0.94	<u>1.65</u>	0	0.82	<u>3.42</u>	<u>16.8</u>	<u>24</u>	0	<u>14.7</u>	<u>24</u>	0	<u>50.25</u>	0	<u>14.29</u>	<u>148.84</u>

Table 6.35 Accumulated bending fatigue damage in anti-symmetric obtained for 100 years using different probability models (Cables: C04, D04)

Mode no.	Probability model I (R independent)					Probability model II (R independent)					Probability model III (R dependent)				
	WSW	W	WNW	NW	NWW	WSW	W	WNW	NW	NWW	WSW	W	WNW	NW	NWW
1	0.06	0.08	0	0.06	0.22	0	<u>1.75</u>	0	0.76	<u>7.63</u>	<u>1.2</u>	<u>1.5</u>	0	<u>1</u>	<u>1.5</u>
2	0.49	0.86	0	0.43	<u>1.79</u>	0	<u>24</u>	0	<u>5.67</u>	<u>77.97</u>	<u>8.8</u>	<u>12.6</u>	0	<u>7.7</u>	<u>12.6</u>
3	<u>1.6</u>	<u>2.81</u>	0	1.4	<u>5.82</u>	<u>1.32</u>	<u>85.54</u>	0	<u>28.73</u>	<u>253.35</u>	<u>28.6</u>	<u>40.8</u>	0	<u>25.1</u>	<u>40.9</u>

Table 6.36 Accumulated axial fatigue damage in symmetric modes for 100 years using different probability models (Cables: C04, D04)

Mode no.	Probability model I (R independent)					Probability model II (R independent)					Probability model III (R dependent)				
	WSW	W	WNW	NW	NWW	WSW	W	WNW	NW	NWW	WSW	W	WNW	NW	NWW
1	0.54	0.79	0	0.42	<b><u>1.26</u></b>	<b><u>59</u></b>	<b><u>42</u></b>	0	<b><u>28</u></b>	<b><u>64</u></b>	<b><u>10.6</u></b>	<b><u>10.6</u></b>	0	<b><u>10.6</u></b>	<b><u>10.6</u></b>
2	<b><u>1.56</u></b>	<b><u>2.28</u></b>	0	<b><u>1.22</u></b>	<b><u>3.63</u></b>	<b><u>170</u></b>	<b><u>122</u></b>	0	<b><u>82</u></b>	<b><u>185</u></b>	<b><u>30.8</u></b>	<b><u>30.8</u></b>	0	<b><u>30.8</u></b>	<b><u>30.8</u></b>
3	<b><u>2.61</u></b>	<b><u>3.81</u></b>	0	<b><u>2.04</u></b>	<b><u>6.06</u></b>	<b><u>284</u></b>	<b><u>203</u></b>	0	<b><u>137</u></b>	<b><u>309</u></b>	<b><u>51.4</u></b>	<b><u>51.4</u></b>	0	<b><u>51.4</u></b>	<b><u>51.4</u></b>

Table 6.37 Accumulated axial fatigue damage in anti-symmetric modes for 100 years using different probability models (Cables: C04, D04)

Mode no.	Probability model I (R independent)					Probability model II (R independent)					Probability model III (R dependent)				
	WSW	W	WNW	NW	NWW	WSW	W	WNW	NW	NWW	WSW	W	WNW	NW	NWW
1	<b><u>1.09</u></b>	<b><u>1.58</u></b>	0	0.85	<b><u>2.52</u></b>	<b><u>118</u></b>	<b><u>85</u></b>	0	<b><u>57</u></b>	<b><u>128</u></b>	<b><u>21.3</u></b>	<b><u>21.3</u></b>	0	<b><u>21.3</u></b>	<b><u>21.3</u></b>
2	<b><u>2.11</u></b>	<b><u>3.07</u></b>	0	<b><u>1.64</u></b>	<b><u>4.89</u></b>	<b><u>229</u></b>	<b><u>164</u></b>	0	<b><u>111</u></b>	<b><u>249</u></b>	<b><u>41.4</u></b>	<b><u>41.4</u></b>	0	<b><u>41.4</u></b>	<b><u>41.4</u></b>
3	<b><u>9.53</u></b>	<b><u>13.89</u></b>	0	<b><u>7.44</u></b>	<b><u>22.12</u></b>	<b><u>1037</u></b>	<b><u>742</u></b>	0	<b><u>501</u></b>	<b><u>1127</u></b>	<b><u>187.4</u></b>	<b><u>187.4</u></b>	0	<b><u>187.4</u></b>	<b><u>187.4</u></b>

Table 6.38 Estimated bending fatigue life (in years) of stay cable using different probability models (Cables: C04, D04)

Mode no.	Probability model I (R independent)		Probability model II (R independent)		Probability model III (R dependent)	
	symmetric	anti-symmetric	symmetric	anti-symmetric	symmetric	anti-symmetric
1	>500	464	>500	<b><u>65.3</u></b>	>500	<b><u>13.11</u></b>
2	143	<b><u>56</u></b>	<b><u>20.15</u></b>	<b><u>8.03</u></b>	<b><u>3.5</u></b>	<b><u>1.28</u></b>
3	<b><u>29</u></b>	<b><u>17</u></b>	<b><u>4.16</u></b>	<b><u>2.45</u></b>	<b><u>0.67</u></b>	<b><u>0.39</u></b>

Table 6.39 Estimated axial fatigue life (in years) of stay cable using different probability models (Cables: C04, D04)

Mode no.	Probability model I (R independent)		Probability model II (R independent)		Probability model III (R dependent)	
	symmetric	anti-symmetric	symmetric	anti-symmetric	symmetric	anti-symmetric
1	<b><u>79.7</u></b>	<b><u>40</u></b>	<b><u>9.4</u></b>	<b><u>4.73</u></b>	<b><u>1.56</u></b>	<b><u>0.78</u></b>
2	<b><u>28.3</u></b>	<b><u>21</u></b>	<b><u>3.27</u></b>	<b><u>2.43</u></b>	<b><u>0.54</u></b>	<b><u>0.4</u></b>
3	<b><u>17.4</u></b>	<b><u>4.7</u></b>	<b><u>1.96</u></b>	<b><u>0.54</u></b>	<b><u>0.32</u></b>	<b><u>0.09</u></b>

### 6.7. Fatigue Evaluation of Stay cables C23, D23

A similar procedure for fatigue analysis was carried out for the cable positioned on the either side of the bridge i.e., C23 and D23 (refer Figure 2.5 and Appendix II). The results of the fatigue analysis of cables C23 and D23 are given in the Appendix VII. The results shows similar tendency as the Cable C04 as considered above. The accumulated bending fatigue damage in symmetric modes is shown in table 1A. The results shows that there is no possibility of fatigue damage in 1<sup>st</sup> symmetric mode under probability model I (Rainfall is assumed as independent event) and III (Rainfall is assumed as dependent event).

From table 1A it can be seen that there is a possible fatigue damage in 2<sup>nd</sup> Symmetric mode and higher. The damage in E and SSE direction are predominant for the probability model I, whereas the model III shows large damage in East direction. Table 2A shows the bending fatigue damage in anti-symmetric modes, which shows that there is possibility of fatigue in first anti-symmetric mode under both the probability models I and III. Table 3A and 4A shows the accumulated axial fatigue damage in symmetric and anti-symmetric modes. The cumulative bending fatigue life for symmetric and antisymmetric modes are shown in table 6.40 and 6.41. It is observed that there is no bending fatigue in first symmetric mode under the probability model I and II during the service period of the cable. The probability model-III finds earlier fatigue in its 1<sup>st</sup> anti-symmetric mode after 23 years of service, whereas the probability model I predicts it in 65.3 years of service.

The cumulative axial fatigue life for symmetric and anti-symmetric modes are shown in table 6.42 and 6.43. The axial fatigue is obvious and the service period is less than 10 years, but the credibility of the axial fatigue life is unknown as the methodology assumes

that the stresses developed in the cable are irrespective of the vibration amplitude.

Table 6.40 Estimated bending fatigue life (in years) of stay cable using different probability models-Symmetric modes (C23, D23)

Mode no.	Probability model I (R independent)					Probability model III (R dependent)				
	ENE	E	ES E	SE	SSE	ENE	E	ES E	SE	SSE
1	1.4E5	<b>9.8E4</b>	∞	1.6E5	<b>9.8E4</b>	9E4	4.6E4	∞	7.3E4	<b>2.4E4</b>
2	2.6E1	<b>2 E1</b>	∞	3.0E1	<b>2E1</b>	1.7E1	1.1E0	∞	2.1E1	<b>5.3</b>
3	6	<b>4.2</b>	∞	6.8	<b>4.2</b>	3.9	2	∞	3.5	<b>1.0</b>

Table 6.41 Estimated bending fatigue life (in years) of stay cable using different probability models-Antisymmetric modes (C23, D23)

Mode no.	Probability model I (R independent)					Probability model III (R dependent)				
	ENE	E	ESE	SE	SSE	ENE	E	ESE	SE	SSE
1	85.65	<b>65.44</b>	∞	97.23	<b>65.34</b>	92.99	34.81	∞	68.14	<b>22.97</b>
2	11.41	7.96	∞	13.00	7.95	7.43	3.93	∞	9.24	2.13
3	3.50	2.45	∞	3.99	2.45	2.29	1.16	∞	1.73	0.60

Table 6.42 Estimated axial fatigue life (in years) of stay cable using different probability models-Symmetric modes (C23, D23)

Mode no.	Probability model I (R independent)					Probability model III (R dependent)				
	ENE	E	ESE	SE	SSE	ENE	E	ESE	SE	SSE
1	9.40	9.40	∞	9.40	9.40	4.68	4.68	∞	4.68	4.68
2	3.25	3.25	∞	3.25	3.25	2.41	2.41	∞	2.41	2.41

3	1.95	1.95	$\infty$	1.95	1.95	0.53	0.53	$\infty$	0.53	0.53
---	------	------	----------	------	------	------	------	----------	------	------

Table 6.43 Estimated axial fatigue life (in years) of stay cable using different probability models-Antisymmetric modes (C23, D23)

Mode no.	Probability model I (R independent)					Probability model III (R dependent)				
	ENE	E	ESE	SE	SSE	ENE	E	ESE	SE	SSE
1	4.72	2.68	$\infty$	1.99	1.65	2.35	1.33	$\infty$	0.99	0.82
2	1.63	0.93	$\infty$	0.69	0.57	1.21	0.69	$\infty$	0.51	0.42
3	0.98	0.55	$\infty$	0.41	0.34	0.27	0.15	$\infty$	0.11	0.09

## 6.8. Fatigue Evaluation of Stay cable using Analytical model

The above evaluated fatigue considers the stay cable using the response estimated via experiments, whereas here, in this section the Fatigue Damage and life of the cable is estimated using the analytical model as discussed Chapter IV. The vibration amplitudes are obtained using the analytical model (as explained in Chapter IV) and dynamic characteristics and stresses evaluated in different modes are explained in section of Chapter V. The methodology explained in section 6.2 of this Chapter is considered and the application model is same as explained in sections 6.3-6.5 of this Chapter. The application explained in section 6.3, 6.4 and 6.5 is repeated so as to evaluate the fatigue using the analytical model results.

### 6.8.1. Fatigue evaluation of stay cable using the probability model I (Cables -C12, D12, C15 and D15, JPD Model-I)

Using the methodology explained in section 6.2 and 6.3, the bending fatigue for the stay cables C12, C15, D12 and D15 were estimated. The W-matrix is obtained from the

Chapter II and the n-matrix is evaluated using the equation 6.18, in which the probability of rainfall is considered as the independent event.

$$n\text{-matrix} = P_r(R) \times W\text{-matrix} \times \text{time period} \times \text{frequency (hz)} \quad (6.18)$$

Table 6.44, 6.45 and 6.46 shows the n-matrix for three different rainfall categories i.e., R10, R40 and R70 and the displacement matrix is given in table 6.47. The displacement matrix and stress matrix is same for all the three models as the stay cable material is the same. Figure 6.3 shows the position of the assumed stay cable C12, D12, C15 and D15 are shown on the Megami bridge. Since, the stay cable arrangements are assumed to be parallel on either side of the bridge, thus the results of cables C12 is more or less same as that of D12, whereas the cable C15 located on the opposite side will have the equivalent wind from East North East (ENE) direction to South South East (SSE) which is depicted in figure 6.3.

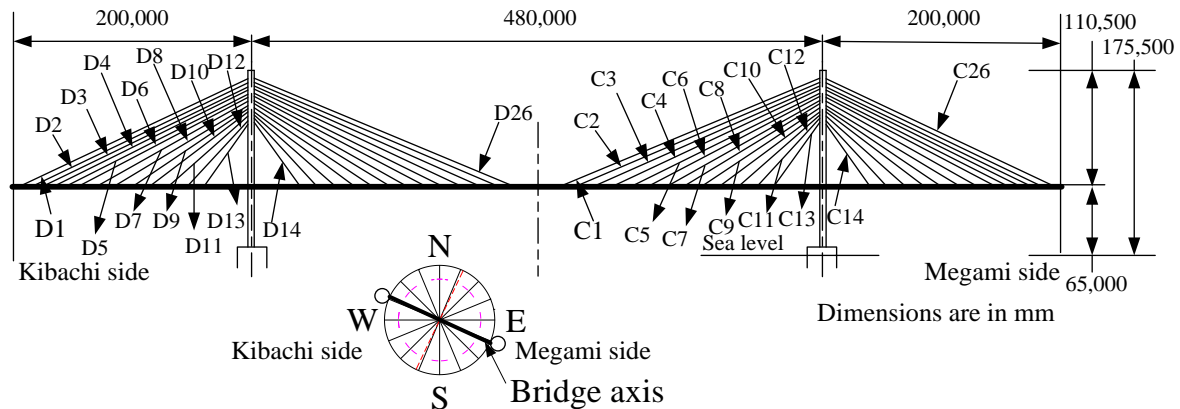


Figure 6.3 Stay cable positions on the Megami birdge

The Y-matrix after transformation from the wind direction to the equivalent wind yaw angle is given by  $\beta^*$ . And the table 6.47 shows the Y-matrix or the amplitude matrix evaluated in Chapter IV, which is normalized for the first symmetric mode. Since rain-wind induced vibration is limited to certain wind yaw angles i.e., from  $25^\circ$  to  $50^\circ$  and thus only the directions which cause vibrations are only considered. Using the information provided in the

table 5.20, the relationship between the bending moment and the peak displacement, the bending moments and bending stresses were estimated for different modes at the pylon and deck end. Table 6.48 and table 6.49 shows the estimated bending stresses in stay cables C12, D12, C15 and D15. It can be seen that for the cable with an inclination  $\alpha=47^\circ$  shows bending moment at the Pylon end is slightly larger than that of the cable inclined at  $\alpha=21.9^\circ$ . The stresses at the pylon end of the cable are larger than the deck end and the mid-span of the cable and thus the results of stresses at the pylon end is considered for the fatigue estimation.

Table 6.44 n-matrix for the first symmetric mode under 10 mm/hr rainfall ( $\alpha=47^\circ$ ,  $S_c=4.61$ , Cables -C12, D12,C15 and D15, JPD model I)

U (m/s)	N	NNE	NE	ENE	E	ESE	SE	SSE	S	SSW	SW	WSW	W	WNW	NW	NWW
0-3	1.6E+5	2.2E+5	2.4E+5	2.3E+5	1.2E+5	6.0E+4	4.0E+4	4.3E+4	4.1E+4	4.4E+4	3.1E+4	3.6E+4	4.9E+4	3.5E4	3.7E+4	8.5E+4
3-6	2.1E+5	1.1E+5	2.9E+4	3.1E+4	4.4E+4	3.4E+4	2.4E+4	3.1E+4	4.1E+4	7.7E+4	5.8E+4	4.9E+4	4.4E+4	5.3E4	5.6E+4	1.3E+5
6-9	1.2E+5	2.9E+4	1.4E+3	1.6E+3	5.7E+3	6.7E+3	8.6E+3	1.4E+4	3.3E+4	1.4E+5	8.3E+4	5.3E+4	5.2E+4	6.8E4	4.6E+4	1.2E+5
9-12	4.1E+4	7.3E+3	1.6E+2	2.1E+2	8.8E+2	1.9E+3	3.5E+3	5.2E+3	2.6E+4	1.2E+5	4.5E+4	3.5E+4	5.2E+4	4.8E4	2.2E+4	8.5E+4
12-15	1.6E+4	2.5E+3	5.9	5.9E+1	1.1E+2	7.9E+2	1.9E+3	2.3E+3	2.9E+4	8.0E+4	2.2E+4	3.0E+4	7.5E+4	2.7E4	6.7E+3	6.8E+4
15-18	1.2E+3	1.4E+2	0	0	5.9E	4.1E+1	8.8E+1	1.6E+2	6.0E+3	1.4E+4	4.1E+3	7.1E+3	1.9E+4	1.7E3	1.5E+2	6.1E+3
18-21	6.0E+2	5.9E+1	0	0	0	2.4E+1	5.9	2.4E+1	2.6E+3	6.3E+3	2.1E+3	3.2E+3	1.1E+4	2.8E2	1.2E+1	1.5E+3
>21	7.0E+2	3.5E+1	0	0	0	1.2E+1	4.7E+1	1.2E+1	1.2E+3	4.0E+3	1.4E+3	2.5E+3	1.2E+4	1.5E2	1.8E+1	8.9E+2

Table 6.45 n-matrix for the first symmetric mode under 40 mm/hr rainfall ( $\alpha=47^\circ$ ,  $S_c=4.61$ , Cables -C12, D12, C15 and D15, JPD model I)

N	NNE	NE	ENE	E	ESE	SE	SSE	S	SSW	SW	WSW	W	WNW	NW	NWW
2.9E+3	3.9E+3	4.3E+3	4.1E+3	2.1E+3	1.1E+3	7.2E+2	7.7E+2	7.4E+2	7.8E+2	5.5E+2	6.3E+2	8.8E+2	6.1E+2	6.7E+2	1.5E+3
3.7E+3	1.9E+3	5.2E+2	5.6E+2	7.9E+2	6.1E+2	4.3E+2	5.6E+2	7.2E+2	1.4E+3	1.0E+3	8.7E+2	7.9E+2	9.5E+2	1.0E+3	2.3E+3
2.1E+3	5.2E+2	2.4E+1	2.9E+1	1.0E+2	1.2E+2	1.5E+2	2.6E+2	5.8E+2	2.6E+3	1.5E+3	9.4E+2	9.2E+2	1.2E+3	8.2E+2	2.2E+3
7.3E+2	1.3E+2	2.8	3.7	1.6E+1	3.4E+1	6.3E+1	9.3E+1	4.6E+2	2.2E+3	8.0E+2	6.2E+2	9.3E+2	8.5E+2	3.8E+2	1.5E+3
2.9E+2	4.5E+1	1E-1	1	2	1.4E+1	3.3E+1	4.1E+1	5.1E+2	1.4E+3	3.9E+2	5.4E+2	1.3E+3	4.8E+2	1.2E+2	1.2E+3
2.2E+1	2.4	0	0	1.0E-1	7.3E-1	1.6E	2.9	1.1E+2	2.5E+2	7.3E+01	1.3E+2	3.4E+2	3.0E+1	2.6	1.1E+2
1.1E+1	1	0	0	0	4.2E-1	1.0E-1	4.2E-1	4.6E+1	1.1E+2	3.8E+1	5.7E+1	2.0E+2	4.9	2.1E-1	2.7E+1
1.2E+1	6.3E-1	0	0	0	2.1E-1	8.4E-1	2.1E-1	2.1E+1	7.1E+1	2.4E+1	4.5E+1	2.1E+2	2.6	3.1E-1	1.6E+1

Table 6.46 n-matrix for the first symmetric mode under 70 mm/hr rainfall ( $\alpha=47^\circ$ ,  $S_c=4.61$ , Cables -C12, D12, C15 and D15, JPD model I)

N	NNE	NE	ENE	E	ESE	SE	SSE	S	SSW	SW	WSW	W	WNW	NW	NWW
5E+2	6.7E+2	7.3E+2	7.0E+2	3.5E+2	1.8E+2	1.2E+2	1.3E+2	1.3E+2	1.3E+2	9.4E+1	1.1E+2	1.5E+2	1.1E+2	1.1E+2	2.6E+2
6.3E+2	3.3E+2	9E+1	9.6E+1	1.4E+2	1.0E+2	7.4E+1	9.6E+1	1.2E+2	2.4E+2	1.8E+2	1.5E+2	1.4E+2	1.6E+2	1.7E+2	4.0E+2
3.6E+2	8.9E+1	4.2	5	1.7E+1	2.0E+1	2.6E+1	4.4E+1	1E+2	4.4E+2	2.5E+2	1.6E+2	1.6E+2	2.1E+2	1.4E+2	3.8E+2
1.2E+2	2.2E+1	4.9E-1	6.3E-1	2.7	5.9E	1.1E+1	1.6E+1	7.9E+1	3.8E+2	1.4E+2	1.1E+2	1.6E+2	1.5E+2	6.6E+1	2.6E+2
5.0E+1	7.8	1.8E-2	1.8E-1	3.4E-1	2.4E	5.7	7.1	8.7E+1	2.5E+2	6.7E+1	9.3E+1	2.3E+2	8.2E+1	2.0E+1	2.1E+2
3.8	4.1E-1	0	0	1.8E-2	1.3E-1	2.7E-1	5E-1	1.8E+1	4.2E+1	1.3E+1	2.2E+1	5.8E+1	5.2	4.5E-1	1.9E+1
1.8	1.8E-1	0	0	0	7.2E-2	1.8E-2	7.2E-2	7.9	1.9E+1	6.5	9.8	3.5E+1	8.5E-1	3.6E-2	4.6
2.1	1.1E-1	0	0	0	3.6E-2	1.4E-1	3.6E-2	3.6	1.2E+1	4.2	7.7	3.6E+1	4.5E-1	5.4E-2	2.7

Table 6.47 Y-matrix for 1<sup>st</sup> symmetric mode ( $\alpha=47^\circ$ ,  $Sc=4.61$ , Cables -C12, D12, C15 and D15)

ENE	E	ESE	SE	SSE
WSW	W	WNW	NW	NWW
36.5°-59°( $\beta$ )	36.5°-14°( $\beta$ )	14°-8.4°( $\beta$ )	8.4°-30.9°( $\beta$ )	30.9°-53.4°( $\beta$ )
1.6E-02	1.6E-02	0	1.6E-02	1.6E-02
2.2E-01	2.4E-01	0	2.1E-01	2.4E-01
1.9E-01	2.4E-01	0	1.7E-01	2.4E-01
2.9E-02	1.0E-01	0	2.9E-02	1.0E-01
2.9E-02	1.0E-01	0	2.9E-02	1.0E-01
2.9E-02	1.0E-01	0	2.9E-02	1.0E-01
2.9E-02	1.0E-01	0	2.9E-02	1.0E-01
2.9E-02	1.0E-01	0	2.9E-02	1.0E-01

\*Displacement are in meters

Table 6.48 Bending stresses (in Mpa) at the Pylon end in 1st symmetric mode ( $\alpha=47^\circ$ ,  $Sc=4.61$ , Cables -C12, D12,C15 and D15)

U (m/s)	Bending stresses (in Mpa)				
	WSW	W	WNW	NW	NWW
	59.0°-36.5° ( $\beta$ )	36.5°-14° ( $\beta$ )	14°-8.4° ( $\beta$ )	8.4°-30.9° ( $\beta$ )	30.9°-53.4° ( $\beta$ )
0-3	5.2E+02	3.4E+02	0	4.1E+01	5.2E+02
3-6	5.2E+02	3.4E+02	0	4.1E+01	5.2E+02
6-9	6.3E+02	5.0E+02	0	6.1E+01	6.3E+02
9-12	8.4E+02	9.0E+02	0	1.1E+02	9.0E+02
12-15	1.3E+03	1.2E+03	0	1.4E+02	1.3E+03
15-18	6.6E+02	8.5E+02	0	1.0E+02	8.5E+02
>18	6.3E+02	8.5E+02	0	1.0E+02	8.5E+02

Table 6.49 Bending stresses (in Mpa) at the Deck end in 1st symmetric mode ( $\alpha=47^\circ$ ,  $Sc=4.61$ , Cables -C12, D12,C15 and D15)

U (m/s)	Bending stresses (in Mpa)				
	WSW	W	WNW	NW	NWW
	59.0°-36.5° ( $\beta$ )	36.5°-14° ( $\beta$ )	14°-8.4° ( $\beta$ )	8.4°-30.9° ( $\beta$ )	30.9°-53.4° ( $\beta$ )
0-3	5.1E+02	3.4E+02	0	4.1E+01	5.1E+02
3-6	5.1E+02	3.4E+02	0	4.1E+01	5.1E+02
6-9	6.2E+02	4.9E+02	0	6.1E+01	6.2E+02
9-12	8.4E+02	9.0E+02	0	1.1E+02	9.0E+02
12-15	1.3E+03	1.2E+03	0	1.4E+02	1.3E+03
15-18	6.6E+02	8.5E+02	0	1.0E+02	8.5E+02
>18	6.2E+02	8.5E+02	0	1.0E+02	8.5E+02

In general, the fatigue life of the stay cables is often represented by  $\sigma$ -N curve. Section 6.3.5 explains the evaluation of N-matrix or the number of possible vibrations that any structure can withstand at a particular stress level can be evaluated using the Stress values produced in the table 6.48 and 6.49. The  $\sigma$ -N equation for bending spectrum is plotted in figure 6.8 (Winkler Jan, 2011) is given by the equation 6.19.

$$N_{bending} \sigma_{bending}^{1.88} = 5.5 \times 10^9 \quad (6.11)$$

Table 6.50 shows the N-matrix for the Pylon end in its 1<sup>st</sup> symmetric mode. It was also found that the N-matrix appears approximately same as that at the deck end, because of the stress difference at the deck and pylon are minimal.

Table 6.50 N-matrix at the Pylon end in 1st symmetric mode ( $\alpha=47^\circ$ ,  $Sc=4.61$ , Cables -C12, D12,C15 and D15)

U (m/s)	WSW	W	WNW	NW	NWW
	59.0°-36.5° ( $\beta$ )	36.5°-14° ( $\beta$ )	14°-8.4° ( $\beta$ )	8.4°-30.9° ( $\beta$ )	30.9°-53.4° ( $\beta$ )
0-3	4.4E+04	9.7E+04	0	5.0E+06	4.4E+04
3-6	4.4E+04	9.7E+04	0	5.0E+06	4.4E+04
6-9	3.0E+04	4.7E+04	0	2.4E+06	3.0E+04
9-12	1.7E+04	1.5E+04	0	7.9E+05	1.5E+04
12-15	7.5E+03	9.4E+03	0	4.8E+05	7.5E+03
15-18	2.7E+04	1.7E+04	0	8.8E+05	1.7E+04
18-21	3.0E+04	1.7E+04	0	8.8E+05	1.7E+04
>21	3.0E+04	1.7E+04	0	8.8E+05	1.7E+04
sum	2.3E+05	3.2E+05	0	1.6E+07	1.9E+05
>21	3.0E+04	1.7E+04	$\infty$	8.9E+05	1.7E+04
sum	2.3E+05	3.2E+05	$\infty$	1.7E+07	1.9E+05

After evaluating the N-matrix, fatigue damage was found using Miner's rule as given in equation 6.13. Table 6.51 shows the fatigue damage for 1st symmetric mode at Pylon end under R10 (or 10 mm/hr) conditions, similarly fatigue damage for Pylon end in different modes and rainfall conditions were evaluated. Table 6.52 shows the cumulative fatigue damage in 1<sup>st</sup> mode under three different rainfall conditions. The summation of all three conditions are found for different modes and the Cumulative bending fatigue damage at pylon end for symmetric and anti-symmetric modes are shown in table 6.53 for the cable C12 and D12 whereas table 6.54 shows the Cumulative bending fatigue damage at pylon end for

the cables C15 and D15. Table 6.55 shows the fatigue life of stay cables C12, D12, C15 and D15 using the Probability model considering the rainfall as an dependent event. The fatigue of the cable decreases as the vibration mode progresses and the fatigue life estimated is very low for the stay cables. Since the relative frequency of wind is more in ENE and NWW, and thus majority of possible failure may occur in ENE direction for the cables C12 and D12, and NWW directions for C15 and D15 cables.

Table 6.51 Estimated Fatigue Damage for 1st symmetric mode at Pylon end under R10 conditions (Cables -C12, D12, C15 and D15, JPD Model-

D)

U (m/s)	N	NNE	NE	ENE	E	ESE	SE	SSE	S	SSW	SW	WSW	W	WNW	NW	NWW
0-3	0	0	0	5.2E+0	1.2E+0	0	7.9E-3	9.8E-1	0	0	0	8.1E-1	5.0E-1	0	7.4E-3	1.9
3-6	0	0	0	7.1E-1	4.5E-1	0	4.8E03	7.2E-1	0	0	0	1.1E+0	4.5E-1	0	1.1E-2	3
6-9	0	0	0	5.4E-2	1.2E-1	0	3.5E-3	4.7E-1	0	0	0	1.7E+0	1.1	0	1.9E-2	4.1
9-12	0	0	0	1.2E-2	5.7E-2	0	4.5E-3	3.4E-1	0	0	0	2.0E+0	3.4	0	2.7E-2	5.5
12-15	0	0	0	7.8E-3	1.2E-2	0	3.8E-3	3.1E-1	0	0	0	4.0E+0	7.9	0	1.4E-2	9
15-18	0	0	0	0	3.4E-4	0	9.9E-5	9.6E-3	0	0	0	2.6E-1	1.1	0	1.7E-4	3.5E-1
18-21	0	0	0	0	0	0	6.6E-6	1.4E-3	0	0	0	1.0E-1	6.7E-1	0	1.3E-5	8.7E-2
>21	0	0	0	0	0	0	5.3E-5	6.9E-4	0	0	0	8.3E-2	6.9E-1	0	2.0E-5	5.2E-2
sum	0	0	0	6.1	1.8	0	2.5E-2	2.8	0	0	0	1.0E+1	1.6E+1	0	7.8E-2	2.4E+1

Table 6.52 Estimated Bending Fatigue Damage for 1st Symmetric mode at Pylon end under three rainfall conditions for 100 years (Cables -C12, D12, C15 and D15, JPD Model-I)

Rainfall (mm/hr)	ENE	E	ESE	SE	SSE	WSW	W	WNW	NW	NWW
10	6.1	1.8	0	2.5E-2	2.9	1.0E+01	1.6E+1	0	7.9E-02	2.4E+01
40	3.4E-4	1.2E-3	0	2.1E-4	8.9E-4	1.4E-03	4.4E-3	0	6.5E-04	6.6E-03
70	3.8E-5	3.4E-5	0	1.4E-5	4.4E-5	1.3E-04	2.3E-4	0	4.3E-05	4.3E-04
Sum	6.1	1.8	0	2.5E-2	2.9	1.0E+01	1.6E+1	0	7.9E-02	2.4E+01

Table 6.53 Estimated Cumulative Bending Fatigue Damage at Pylon end for symmetric and anti-symmetric modes for 100 years (Cables -C12, D12, JPD Model-I)

Mode no.	symmetric modes					anti-symmetric modes				
	ENE	E	ESE	SE	SSE	ENE	E	ESE	SE	SSE
1	6.1	1.8	0	2.5E-2	2.8	4.5E+1	1.3E+1	0	1.8E-1	2.1E+1
2	1.4E+2	4.4E+1	0	6.0E-1	6.8E+1	3.3E+2	1.0E+2	0	1.4	1.6E+2
3	6.5E+2	2 E+2	0	2.7	3.0E+2	1.1E+3	3.4E+2	0	4.6	5.2E+2

Table 6.54 Estimated Cumulative Bending Fatigue Damage at Pylon end for symmetric and anti-symmetric modes for 100 years (Cables -C15, D15, JPD Model-I)

Mode no.	symmetric modes					anti-symmetric modes				
	WSW	W	WNW	NW	NWW	WSW	W	WNW	NW	NWW
1	1E1	1.6E1	0	7.9E-2	2.4E1	7.5E1	1.2E2	0	5.8E-1	1.8E2
2	2.5E2	3.9E2	0	1.9	5.8E2	5.8E2	9.1E2	0	4.4	1.3E3
3	1.1E3	1.8E3	0	8.5	2.6E3	1.9E3	3.0E3	0	1.5E1	4.4E3

Table 6.55 Bending Fatigue life of stays (Cables -C12, D12, C15 and D15, JPD Model-I)

Mode no.	(Cables -C12, D12, JPD Model-I)		(Cables -C15, D15, JPD Model- I)	
	symmetric	anti-symmetric	symmetric	anti-symmetric
1	16.60	2.24	4.17	0.56
2	6.92E-01	2.99E-01	1.73E-01	7.49E-02
3	1.55E-01	9.00E-02	3.88E-02	2.26E-02

### 6.8.2. Fatigue evaluation of stay cable using the probability model II (Cables -C12, D12, C15 and D15, JPD Model-II)

The steps explained section 6.2 and 6.5 are again repeated to evaluate fatigue in the most unfavorable direction, provided the probability of rainfall is assumed as independent event. Table 6.56 shows the total cumulative bending fatigue for the stay cable inclined at 47°. The following probability models assume the most unfavorable direction as a higher relative frequency and thus the fatigue evaluations remains same for all the cables i.e., C12, D12, C15 and D15 respectively.

Table 6.56 Estimated Cumulative Bending Fatigue Damage at Pylon end for symmetric and anti-symmetric modes (Cables –C12, D12, C15, D15, JPD Model-II)

Mode no.	symmetric mode					anti-symmetric mode				
	ENE	E	ES E	SE	SSE	ENE	E	ES E	SE	SSE
1	1.6E2	1.2E+2	0	2.3	1.7E+2	1.2E3	8.8E+2	0	1.7E+1	1.3E+3
2	4.0E3	2.9E+3	0	5.6E+1	4.1E+3	9.1E3	6.7E+3	0	1.3E+2	9.5E+3
3	1.8E4	1.3E+4	0	2.5E+2	1.8E+4	3.0E4	2.2E+4	0	4.3E+2	3.1E+4

Table 6.57 Bending Fatigue life of stays (Cables -C12, D12, C15 and D15, JPD Model-II)

Mode no.	C12, D12		C15, D15	
	symmetric	anti-symmetric	symmetric	anti-symmetric
1	0.59	0.08	0.59	0.08
2	2.44E-02	1.05E-02	2.44E-02	1.05E-02
3	5.46E-03	3.18E-03	5.46E-03	3.18E-03

From the table 6.57, It can be seen that there is a larger risk of bending fatigue in stay cables, when the cables are inclined at angles about 45°. The static and dynamic analysis

explained in Chapter V clearly shows that the stresses are more for cable with larger inclination than the small inclined long cables.

### **6.8.3. Fatigue evaluation of stay cable using the probability model III (Cables -C12, D12, C15 and D15, JPD Model-II)**

Using the methodology explained in section 6.2 and 6.4, the bending fatigue for the stay cables C12, C15, D12 and D15 were estimated. The W-matrix is obtained from the Chapter II and the n-matrix is evaluated using the equation 6.19, in which the probability of rainfall is considered as the dependent event.

The steps explained in section 6.2 and 6.3 were repeated to evaluate the fatigue. W-matrix is obtained in table 6.2, the n-matrix is obtained in the same manner as explained in section 6.4.

$$n_{10(Rd)}-matrix = W_{Rd} - matrix \times \text{time period} \times \text{frequency (hz)} \quad (6.19)$$

The n-matrix was evaluated for three different rainfall conditions using the equation 6.19, in which probability of wind in R10, R40 and R70 conditions are taken directly. Table 6.58, 6.59 and 6.60 shows the n-matrix for three different rainfall categories i.e., R10, R40 and R70 and the displacement matrix is given in table 6.43. The displacement matrix and stress matrix is same for all the three models as the stay cable material is the same. The Bending stresses and the number of stress equivalent cycles to cause failure is also given in table 6.48, 6.49 and 6.50. And using Miner's rule as stated in equation 6.17, using the n-matrix of R10, R40 and R70 and N-matrix will give the damage accumulated in the cable. Table 6.59 shows the fatigue damage for 1st symmetric mode at Pylon end under R10 (or 10 mm/hr) conditions, similarly fatigue damage for Pylon end in different modes and rainfall

conditions were evaluated. Table 6.60 shows the cumulative fatigue damage in 1<sup>st</sup> mode under three different rainfall conditions. The summation of all three conditions are found for different modes and the Cumulative bending fatigue damage at pylon end for symmetric and anti-symmetric modes are shown in table 6.61 for the cable C12 and D12 whereas table 6.62 shows the Cumulative bending fatigue damage at pylon end for the cables C15 and D15. Table 6.63 and 6.64 shows the estimated bending fatigue at the Pylon end in its service period for cables C12, D12, C15 and D15. Table 6.65 shows the fatigue life of stay cables C12, D12, C15 and D15 using the Probability model considering the rainfall as a dependent event. The fatigue of the cable decreases as the vibration mode progresses and the fatigue life estimated is very low for the stay cables. Since the relative frequency of wind is more in ENE and NWW, and thus majority of possible failure may occur in ENE direction for the cables C12 and D12, and NWW directions for C15 and D15 cables for both the probability models.

Table 6.58 n-matrix for the first symmetric mode under 10 mm/hr rainfall ( $\alpha=47$ ,  $S_c=4.61$ , Cables -C12, D12,C15 and D15, JPD Model III)

U (m/s)	N	NNE	NE	ENE	E	ESE	SE	SSE	S	SSW	SW	WSW	W	WNW	NW	NWW
0-3	6.4E 6	6.0E+ 06	3.4E+ 06	2.7E+ 06	2.6E+ 06	1.9E+ 06	1.3E+ 06	1.3E+ 06	1.2E+ 06	1.4E+ 06	9.6E+ 5	7.8E+ 05	9.6E+ 05	9.0E+ 05	1.2E+ 06	2.7E+ 06
3-6	1.0E 7	5.2E+ 06	1.2E+ 06	1.3E+ 06	1.9E+ 06	1.8E+ 06	1.4E+ 06	1.4E+ 06	1.4E+ 06	2.0E+ 06	1.1E+ 6	8.3E+ 05	6.2E+ 05	7.1E+ 05	8.8E+ 05	3.5E+ 06
6-9	5.7E 6	2.3E+ 06	1.8E+ 05	3.1E+ 05	8.1E+ 05	8.6E+ 05	1.1E+ 06	1.3E+ 06	1.5E+ 06	2.6E+ 06	1.1E+ 6	7.3E+ 05	5.3E+ 05	5.2E+ 05	4.0E+ 05	2.7E+ 06
9-12	1.9E 6	9.2E+ 05	5.5E+ 04	4.4E+ 04	1.7E+ 05	3.5E+ 05	7.9E+ 05	8.0E+ 05	1.2E+ 06	2.7E+ 06	6.6E+ 5	6.6E+ 05	5.4E+ 05	4.0E+ 05	1.7E+ 05	1.2E+ 06
12-15	5.6E 5	3.5E+ 05	5.5E+ 03	1.7E+ 04	4.4E+ 04	1.7E+ 05	4.1E+ 05	4.9E+ 05	1.3E+ 06	2.7E+ 06	6.3E+ 5	4.6E+ 05	5.6E+ 05	2.3E+ 05	6.6E+ 04	5.6E+ 05
15-18	3.3E 5	1.4E+ 05	0	0.0E+ 00	0.0E+ 00	9.4E+ 04	1.1E+ 05	1.6E+ 05	9.8E+ 05	1.9E+ 06	5E+5	3.3E+ 05	4.4E+ 05	1.7E+ 05	2.8E+ 04	2.2E+ 05
18-21	5.4E +5	1.3E+ 05	0	0.0E+ 00	5.5E+ 03	2.8E+ 04	1.7E+ 04	6.6E+ 04	1.3E+ 06	2.5E+ 06	6.2E+ 05	4.0E+ 05	6.3E+ 05	7.2E+ 04	2.8E+ 04	5.0E+ 05
>21	3.6E +05	3.3E+ 04	0.0E+ 00	0.0E+ 00	0.0E+ 00	0.0E+ 00	0.0E+ 00	0.0E+ 00	2.5E+ 05	8.2E+ 05	1.3E+ 05	2.2E+ 05	3.4E+ 05	7.2E+ 04	5.5E+ 03	2.3E+ 05

Table 6.59 n-matrix for the first symmetric mode under 40 mm/hr rainfall ( $\alpha=47$ ,  $S_c=4.61$ , Cables -C12, D12, C15 and D15, JPD Model III)

U (m/s)	N	NNE	NE	ENE	E	ESE	SE	SSE	S	SSW	SW	WSW	W	WNW	NW	NWW
0-3	2.9E3	3.9E+3	4.3E+3	4.1E+3	2.1E+3	1.1E+3	7.2E2	7.7E2	7.4E2	7.8E2	5.5E2	6.3E2	8.8E2	6.1E2	6.7E2	1.5E3
3-6	3.7E3	1.9E+3	5.2E+2	5.6E+2	7.9E+2	6.1E+2	4.3E2	5.6E2	7.2E2	1.4E3	1.0E3	8.7E2	7.9E2	9.5E2	1.0E3	2.3E3
6-9	2.1E3	5.2E+2	2.4E+1	2.9E+1	1.0E+2	1.2E+2	1.5E2	2.6E2	5.8E2	2.6E3	1.5E3	9.4E2	9.2E2	1.2E3	8.2E2	2.2E3
9-12	7.3E2	1.3E+2	2.8	3.7	1.6E+1	3.4E+1	6.3E1	9.3E1	4.6E2	2.2E3	8.0E2	6.2E2	9.3E2	8.5E2	3.8E2	1.5E3
12-15	2.9E2	4.5E+1	1E-1	1	2	1.4E+1	3.3E1	4.1E1	5.1E2	1.4E3	3.9E2	5.4E2	1.3E3	4.8E2	1.2E2	1.2E3
15-18	2.2E1	2.4	0	0	1.0E-1	7.3E-1	1.6	2.9	1.1E2	2.5E2	7.3E1	1.3E2	3.4E2	3.0E1	2.6	1.1E2
18-21	1.1E1	1	0	0	0	4.2E-1	1.0E-1	4.2E-1	4.6E1	1.1E2	3.8E1	5.7E1	2.0E2	4.9	2.1E-1	2.7E1
>21	1.2E1	6.3E-1	0	0	0	2.1E-1	8.4E-1	2.1E-1	2.1E1	7.1E1	2.4E1	4.5E1	2.1E2	2.6	3.1E-1	1.6E1

Table 6.60 n-matrix for the first symmetric mode under 70 mm/hr rainfall ( $\alpha=47$ ,  $S_c=4.61$ , Cables -C12, D12, C15 and D15, JPD Model III)

N	NNE	NE	ENE	E	ESE	SE	SSE	S	SSW	SW	WSW	W	WNW	NW	NWW
5E+2	6.7E+2	7.3E+2	7.0E+2	3.5E+2	1.8E+2	1.2E+2	1.3E+2	1.3E+2	1.3E+2	9.4E+1	1.1E+2	1.5E+2	1.1E+2	1.1E+2	2.6E+2
6.3E+2	3.3E+2	9E+1	9.6E+1	1.4E+2	1.0E+2	7.4E+1	9.6E+1	1.2E+2	2.4E+2	1.8E+2	1.5E+2	1.4E+2	1.6E+2	1.7E+2	4.0E+2
3.6E+2	8.9E+1	4.2	5	1.7E+1	2.0E+1	2.6E+1	4.4E+1	1E+2	4.4E+2	2.5E+2	1.6E+2	1.6E+2	2.1E+2	1.4E+2	3.8E+2
1.2E+2	2.2E+1	4.9E-1	6.3E-1	2.7	5.9E	1.1E+1	1.6E+1	7.9E+1	3.8E+2	1.4E+2	1.1E+2	1.6E+2	1.5E+2	6.6E+1	2.6E+2
5.0E+1	7.8	1.8E-2	1.8E-1	3.4E-1	2.4E	5.7	7.1	8.7E+1	2.5E+2	6.7E+1	9.3E+1	2.3E+2	8.2E+1	2.0E+1	2.1E+2
3.8	4.1E-1	0	0	1.8E-2	1.3E-1	2.7E-1	5E-1	1.8E+1	4.2E+1	1.3E+1	2.2E+1	5.8E+1	5.2	4.5E-1	1.9E+1
1.8	1.8E-1	0	0	0	7.2E-2	1.8E-2	7.2E-2	7.9	1.9E+1	6.5	9.8	3.5E+1	8.5E-1	3.6E-2	4.6
2.1	1.1E-1	0	0	0	3.6E-2	1.4E-1	3.6E-2	3.6	1.2E+1	4.2	7.7	3.6E+1	4.5E-1	5.4E-2	2.7

Table 6.61 Estimated Fatigue Damage for 1st symmetric mode at Pylon end under R10 conditions (Cables -C12, D12, C15 and D15, JPD Model-III)

U (m/s)	N	NNE	NE	ENE	E	ESE	SE	SSE	S	SSW	SW	WSW	W	WNW	NW	NWW
0-3	0	0	0	62	27	0	0	31	0	0	22	18	10	0	0	63
3-6	0	0	0	29	19	0	0	32	0	0	24	19	6	0	0	79
6-9	0	0	0	10	17	0	0	44	0	0	35	24	11	0	0	90
9-12	0	0	0	3	11	0	1	52	0	0	38	38	35	0	0	76
12-15	0	0	0	2	5	0	1	65	0	0	85	61	59	0	0	75
15-18	0	0	0	0	0	0	0	9	0	0	18	12	26	0	0	13
18-21	0	0	0	0	0	0	0	4	0	0	20	13	37	0	0	29
>21	0	0	0	0	0	0	0	0	0	0	4	7	20	0	0	13
sum	0	0	0	106	79	0	3	237	0	0	248	193	205	0	1	439

Table 6.62 Estimated Bending Fatigue Damage for 1st Symmetric mode at Pylon end under three rainfall conditions for 100 years (Cables -C12, D12, C15 and D15, JPD Model-III)

Rainfall (mm/hr)	ENE	E	ESE	SE	SSE	SW	WSW	W	WNW	NW	NWW
10	105.5	78.9	0	3	235.5	245.8	191.6	203.6	0	1	436.2
40	0.2	1.1	0	1.3	4.5	1.5	1.2	4.4	0	0.8	6.5
70	0.1	0.8	0	0.8	4.8	3.6	1.1	1.5	0	0.3	0.9
Sum	105.8	80.8	0	5.1	244.8	250.9	193.9	209.5	0	2.1	443.6

Table 6.63 Estimated Cumulative Bending Fatigue Damage at Pylon end for symmetric and anti-symmetric modes for 100 years (Cables -C12, D12, JPD Model-III)

Mode no.	symmetric modes					anti-symmetric modes				
	ENE	E	ESE	SE	SSE	ENE	E	ESE	SE	SSE
1	1.1E+02	8.1E+01	0	5.1E+00	2.4E+02	7.8E+02	6.0E+02	0	3.7E+01	1.8E+03
2	2.5E+03	1.9E+03	0	1.3E+02	5.9E+03	5.9E+03	4.5E+03	0	3.0E+02	1.4E+04
3	1.1E+04	8.7E+03	0	6.0E+02	2.6E+04	1.9E+04	1.5E+04	0	1.0E+03	4.5E+04

Table 6.64 Estimated Cumulative Bending Fatigue Damage at Pylon end for symmetric and anti-symmetric modes for 100 years (Cables -C15, D15, JPD Model-III)

Mode no.	symmetric modes					anti-symmetric modes				
	WSW	W	WNW	NW	NWW	WSW	W	WNW	NW	NWW
1	1.9E+02	2.1E+02	0	2.1E+00	4.4E+02	1.4E+03	1.6E+03	0	1.2E+01	3.3E+03
2	5.2E+03	5.4E+03	0	5.0E+01	1.1E+04	1.2E+04	1.3E+04	0	1.2E+02	2.6E+04
3	2.3E+04	2.4E+04	0	2.4E+02	5.0E+04	4.0E+04	4.2E+04	0	4.1E+02	8.5E+04

Table 6.65 Bending Fatigue life of stays (Cables -C12, D12, C15 and D15, JPD Model-III)

Mode no.	(Cables -C12, D12, JPD Model-III)		(Cables -C15, D15, JPD Model-III)	
	symmetric	anti-symmetric	symmetric	anti-symmetric
1	4.08E-01	5.51E-02	2.25E-01	3.04E-02
2	1.70E-02	7.35E-03	9.01E-03	3.89E-03
3	3.80E-03	2.22E-03	2.01E-03	1.17E-03

From table 6.51, 6.53 and 6.61, the probability model I (assuming the rainfall as a independent event) and the probability model III (assuming the rainfall as a dependent event) shows a large amount of possible fatigue and also very low fatigue life of the stay cable, whereas the model I (considering rainfall intensity as an independent event) results looks conservative.

## **6.9. Recommendations and Conclusions**

A new modified methodology was presented in this chapter which will allow the designers to calculate the fatigue damage of the stay cables. PTI and FIB doesn't address the bending fatigue due to high axial tension, whereas in the present study it was found that the bending fatigue must be considered and this paper recommends the designers to consider the bending fatigue due to presence of large stiffness and sag in the stay cable.

The following conclusions were derived based on the study.

1. Assuming stay cable as a stiff-string, the frequencies were evaluated and compared with string and the ANSYS solution (Pres-stressed beam). The frequencies are very close to each other.
2. Using the frequencies obtained from equation 7 and the assumed cable parameters, the vibration amplitudes were normalized. Bending moments and stresses on the stay cables were found for different vibration amplitudes (Obtained from the literature). The results show that the stresses in the deck end are larger than the pylon and mid-span position. The stress intensity increases as the mode progresses higher.
3. A statistical analysis of wind data was collected at a meteorological observatory near the bridge site. Three different probability models were developed namely,
  - i. Joint probability of wind speed, direction and rainfall as dependent events.
  - ii. Joint Probability of wind speed, direction and rainfall, assuming rainfall as a independent event.

- iii. Probability of wind in the most unfavorable condition, where the rainfall is assumed as a independent event
4. Using the probability models and the Stresses, fatigue damage and life was evaluated using miner's rule for the assumed life of the stay cable (100 years). Due to the relation between low-wind speed and light rain condition, the results shows that the low-rainfall causes more fatigue damage, whereas large rainfall conditions causes minimal fatigue.
5. All the three probability models show bending fatigue damage in higher modes other than the first symmetric mode. Fatigue damage increases as the assumed vibration mode increases.
6. The probability model I (considering the rainfall as dependent events) shows a large fatigue damage. The probability model II shows very low fatigue damage in comparison with the probability model I and III. Assuming the stay cable vibrates in the 1<sup>st</sup> Anti-symmetric mode (Poston, 1998, Pebley, 2005), the probability model I and III predicts bending fatigue damage after 13.1 and 65.3 years of service, whereas the model II didn't show fatigue damage in 1<sup>st</sup> anti-symmetric mode. The probability model II evaluates fatigue only in the 2<sup>nd</sup> anti-symmetric and higher modes.
7. Assuming the axial stresses are independent of the vibration amplitude, axial fatigue was evaluated and found that the axial fatigue damage is much higher than bending.

The bending life of the stay cable is assumed to be 100 years and it is also found that there is possibility of fatigue in higher modes other than the first symmetric mode. The credibility of axial fatigue life estimation is unknown and the results show that there is a possibility of axial fatigue in less than 10 years of service. And these results can give an outlook for the maintenance technicians to check the fatigue damage in the stays. If the stay cable is mitigated for the rain-wind induced vibration, the damage for the cable under rain-wind induced vibration can be eliminated.

In all the three probability models, the fatigue damage in North-West-west and West direction are higher which corresponds to a wind yaw angle ranging from 30.9° to 53.4° and

36.4° to 14°. The relative frequency of moderate wind in North-West-West direction is large, whereas the vibration amplitude between the yaw angles 14° and 35° is large and thus large fatigue damage in North-West-West and West direction.

Using the analytical results obtained in Chapter IV and combining the results of the Static and Dynamic analysis in Chapter V, fatigue damage was evaluated for the stay cable inclined at 47°. The results shows similar results as of the Cable C04, which was studied earlier in section 6.1 – 6.6. The fatigue damage of the stay cable C12,D12,C15 and D15 are large in compared with the cable C04.

The vibration amplitude is very much less than that of cable C04 whereas the stresses induced at those vibration levels are large and thus prominent fatigue is being found be in stay cables inclined at 45°.

## 6.10. References

1. Federico Cluni, Vittorio Gusella, Filippo Ubertini, 2007, “A parametric investigation of wind-induced cable fatigue”, *Engineering structures*, 29,3094-3405.
2. Maria Pia Repetto, Giovanni Solari, 2001, “Dynamic alongwind fatigue of slender vertical structures”, *Engineering structures*, 23, pp. 1622-1633.
3. Vanessa A. Pino, 2010, “Fatigue Life Prediction of Cantilevered Light Pole Structures”, M.S. Thesis, Virginia Polytechnic Institute and State University.
4. Christopher Letchford, Hector Cruzado, 2008, Risk Assessment Model for Wind-Induced Fatigue Failure of Cantilever Traffic Signal Structures, Report No. FHWA/TX -07-4586-4, Texas Department of Transportation Research and Technology Implementation

5. Brent M. Phares, Partha P. Sarkar, Terry J. Wipf, and Byungik Chang, 2007, “Development of Fatigue Design Procedures for Slender, Tapered Support Structures for Highway Signs, Luminaries, and Traffic Signals Subjected to Wind-Induced Excitation from Vortex Shedding and Buffeting”, MTC Project 2005-02, Iowa State University.
6. Walther R., Houriet B., Isler W., 1999, Cable stayed bridges, Thomas Telford Publishing, ISBN 0 7277 2773 7
7. Winkler J., Kotas A., 2010, “Fatigue Analysis of Steel Cables under Bending Load”, Master’s Thesis, Technical University of Denmark, DTU Byg
8. Wood S., Frank K.H., 2010, “Experimental investigation of bending fatigue response of grouted stay cables”, *Journal of Bridge Engineering*, Vol. 15, pp. 123-130, 2010.
9. Hobbs R.E., Raof M., 1996, “Behaviour of cables under dynamic or repeated loading”, *Journal of Constructional Steel Research*, Vol. 39, pp. 31–50.
10. Shunichi Nakamura, Hajime Hosokawa, 1989, “A study on the fatigue design of parallel wire strands on Cable-stayed bridges”, *Japan Society of Civil Engineers (Proc. Of JSCE No. 410/I-12)*, pp. 327s-336s.
11. Acceptance of Stay Cable Systems Using Prestressing Steels: Recommendation, 2005, International Federation for Structural Concrete (fib), ISBN 2-88394-070-3
12. Post-Tensioning Institute, 2000 “Recommendations for Stay-Cable Design, Testing and Installation.” PTI Guide Specification.
13. Winkler Jan., Fischer Gregor., Georgakis Christos T., Agnieszka Kotas, 2011, “A Preliminary Bending fatigue spectrum for steel monostrand cables”, *Journal of the International Association for Shell and Spatial Structures*, Vol. 52 (4) pp 249-255.

14. Cremona C., 2003, "A short note on cable fatigue", In: Proc. 5th international symposium on cable dynamics.
15. Jensen J.L., Bitsch N., Laursen E., "Fatigue Risk Assessment of Hangers on Great Belt Bridge", In: Proc. 7th International Symposium on Cable Dynamics, 2007.
16. Miki C., Endo T., Okukawa A., "Full-Size Fatigue Test of Bridge Cables", IABSE Reports, Length Effects on Fatigue of Wires and Strands, Vol. 66, pp. 167-178, 1992.
17. Gourmelon J.P., 2003, "Cable fatigue behavior as a major safety factor in cable-stayed bridges", Bulletin des Laboratoires des Ponts et Chaussees, pp. 53-71, Issue: 244-245.
18. Acceptance of Stay Cable Systems Using Prestressing Steels: Recommendation, 2005, International Federation for Structural Concrete (fib), ISBN 2-88394-070-3
19. J.D. Holmes, 2002, Fatigue life under along-wind loading –closed-form solutions, Engineering structures 24, pp. 109-114.
20. Dowd J., Poser M., Frank K. H., Wood S. L., Williamson E. B., 2001, Bending Fatigue of Cable stays,
21. Conrad Paulson, Jr., Karl H. Frank, 1983, "A fatigue study of Prestressing strand", Center for Transportation research, The University of Texas at Austin, Report No. FHWA/TX-82/54+300-1
22. Yan Li, Dagang Lv, Hongfei Sheng, 2011, Fatigue Reliability Analysis of the Stay Cables of Cable-stayed Bridge under Combined Loads of Stochastic Traffic and Wind, Key Engineering Materials Vol. 456, pp 23-35



## **CHAPTER VII**

### **DISCUSSION, CONCLUSION AND RECOMMENDATIONS**

#### **7.1. Discussion and Conclusions**

An Introduction to stay cables, cable-stayed bridges, rain-wind induced vibration was given in the chapter I. This chapter also explains the flow chart of the thesis. Further this chapter deals with the influence of rain-wind induced vibrations on fatigue life of the stay cable by comparing with the literature. Literatures on the Fatigue damage due to vibrations were also explained in the chapter.

Chapter II of the thesis elaborates the new framework developed for the Joint probability models. A statistical analysis was carried out for the data obtained near the bridge site. Three kinds of probability models were discussed. The first joint probability was developed for wind speed, wind direction and rainfall, assuming the rainfall as an independent event, whereas the second probability model it is assumed that all the wind blowing in the most unfavorable direction and the third model considers rainfall as dependent event. This probability model was used again in chapter VI for the fatigue estimation.

A new experimental setup was modeled using AutoCAD 2007 and the model was later manufactured in China. A series of experiments covering wide range of inclination and

yaw angles were conducted the multi-functional wind tunnel at Shijiazhuang Tiedao University. Chapter III of the thesis explains the rain-wind induced vibrations in detail by testing variety of parameters and also overcomes the limitations of the past research by testing a wide range  $\alpha$ ,  $\beta$ ,  $U$ , and  $R$ . Two cable models of different diameters were considered in the study. The first one is of small diameter (0.128 m) and the other with large diameter (0.155 m).

By varying inclination angle and wind yaw angle, a series of tests were conducted for different wind speed and rainfall conditions. The experimental results consist of qualitative and quantitative amount of information on the vibration response for large diameter cable. Based on the experimental results of the large diameter cable, the experiment was repeated for the small diameter cable. The effect of frequency and damping were also studied. A GUI framework was made to obtain the results by specifying the key parameters of the cable.

Photographic images and videos taken during the experiment is used to identify the static position and motion of the rivulet and further this chapter also explains the phenomenon of rain-wind induced vibration with the help of the images. Further simple calculations were done to compute the motion of the rivulet. Rain-wind induced vibrations were also mitigated by producing wires along the surface of the cable. The effectiveness of the rain-wind induced vibration was tested by varying the space between the wires.

Chapter IV of the thesis discusses about the analytical model for the rain-wind induced vibration. The analytical model for rain-wind induced vibration was used to validate the experimental results. The effects of various parameters such as wind speed, wind direction, damping, frequency, were also studied. Assuming the rivulet motion and position, the response was calculated and compared with the experimental results. An elaborate study was done covering the response of the horizontal and yawed cable with a static rivulet. The

response of the inclined cable assumed the motion to be a sinusoidal and the rivulet position is also a function of wind speed. Later the model was extended and the solutions were checked for Den-Hartog's Mechanism. A GUI was developed to produce the results by specifying the key parameters of the cable. And further this GUI is made to interconnect with the experimental GUI, so as to compare the response obtained in both the Experimental and analytical methods.

Stay cable carries a large amount of tension and thus can be assumed as a string. But rain-wind induced vibration is mostly concerned about the large amplitude that could occur along the out-of the plane direction of the cable and thus the considering the bending stiffness in the cable is a must. And thus, cable-behavior was studied in this chapter. Frequency analysis was carried out using analytical methods and ANSYS solution. The solution is then compared with the string theory. The mode shapes and frequencies were obtained for the cable with and without tension force and based on that the effect of Tension-Bending parameter and the aspect ratio were discussed. This chapter also explains the importance of sag and bending stiffness based on the results analytical methods. Further as an extension of the study a static and modal response analysis were carried out. The modal response results of ANSYS were compared with the analytical solutions. The displacements obtained were normalized and multiplied by the peak amplitudes obtained in the chapter III. Using matrix methods the displacements were feeded back to ANSYS using batch program. The static deformation was obtained for each mode and is tabulate in chapter IV. Finally the relation between the bending moment and displacement was obtained and using the moments stresses were obtained. Axial stresses were obtained using string theory. It is also assumed that the amplitude of the cable doesn't affect the axial stresses. Contributions of stresses in different modes were also studied.

The methodology used to estimate the fatigue life was introduced. Three Joint

probability models developed in the Chapter II was used for calculating the fatigue. A comparison study was also made between the three probability models for stay cables. The Bending stresses were then used to estimate the fatigue life of the cables. Since the Megami ohhashi bridge site receives rainy events of about 1601.3 (10 minute events) every year and thus it is recommended to consider the probability model based on the terrain and environmental conditions. And the author recommends that the stay cables can be checked every 15 years considering the fatigue caused by other vibrations such as traffic, wind, earthquake etc. Four cables namely C4, D4, C23, D23, C12, D12, C15 and D15 were tested for fatigue. Vibration amplitude of the cables C04, C23, D23 and D3 were estimated using the results obtained from the experiment, whereas the vibration of the cable C12 and D12 were estimated using the analytical method.

For the cable C04 and D04, it is also found that the lower rainfall, anti-symmetric modes, higher order modes causes large fatigue. The fatigue damage of the cable estimated using model I, II and III were then compared and shows that the cable fatigue damage is large for model III as it consider the rainfall as a dependent event. The probability model I and II assumes the rainfall as a independent event. The fatigue analysis was carried out for the stay cable under different rainfall conditions and it is a must to ensure that the location of the bridge site is not repeatedly influenced by large of amount slight rain conditions. In all the three models the maximum fatigue was caused by West (from sea side) and North West directions (from land side).

For the cable C23 and D23, it is also found that the lower rainfall, anti-symmetric modes, higher order modes causes large fatigue. The fatigue damage of the cable estimated using model I and III were then compared and shows that the cable fatigue damage is large for model II as it consider the rainfall as a dependent event.

For the stay cables C12 and C15 which is inclined at  $47^\circ$ , the fatigue damage and life was estimated using the three probability models (explained in Chapter III). It was then found the fatigue of the cables C12 and C15 are more vulnerable than C04 which is inclined at  $21.9^\circ$ , as the stress levels are higher. And thus, it is a must consider all the cables for the analysis, so as to ensure the safety of the bridge due to rain-wind induced vibrations. The fatigue result shows that the fatigue damage increases as the vibration mode progresses higher. The most unfavorable directions are found to be ENE and NWW directions for all the three probability models.

In Chapter VI, it is also found that higher rainfall intensity causes less fatigue damage and may be negligible, whereas lower rainfall regime causes severe fatigue damage. And it is known from the results that Fatigue life estimated in the anti-symmetric modes are severe than the Symmetric modes. The fatigue analysis was carried out for the stay cable under different rainfall conditions and it is a must to ensure that the location of the bridge site is not repeatedly influenced by large of amount slight rain conditions. In all the three models the maximum fatigue was caused by West (from sea side), North West directions (from land side).

The results obtained from the study are displayed in the tables 7.1 and 7.2. Three different probability models were used to evaluate the fatigue life of the cable. Cables C04, D04, C23 and D23 doesn't show fatigue in 1<sup>st</sup> symmetric mode, whereas in 1<sup>st</sup> anti-symmetric mode it shows a possible fatigue in all the three models. Cables C12, D12, C15, D15 were found to be vulnerable as large stresses have been developed in these cables even under small vibration amplitude and thus, the study ensures that the stay cables has to be considered for bending fatigue analysis before installation and also frequent checks can ensure the safety of the stay cable from fatigue damage.

Table 7.1 Bending Fatigue life of stay cables under three different probability models- 1<sup>st</sup>

Symmetric and anti-symmetric mode

Stay cable id.	JPD Model I		JPD Model II		JPD Model III	
	Sym..	Asym.	Sym..	Asym.	Sym..	Asym.
C04, D04	>500	464	>500	65.30	<500	13.11
C12, D12	16.60	2.24	0.59	0.08	4.08E-01	5.51E-02
C15, D15	4.17	0.56	0.59	0.08	2.25E-01	3.04E-02
C23, D23	9.8E4	65.34	-	-	2.4E4	22.97

Table 7.2 Axial Fatigue life of stay cables under three different probability models- 1<sup>st</sup>

Symmetric and anti-symmetric mode

Stay cable id.	JPD Model I		JPD Model II		JPD Model III	
	Sym..	Asym.	Sym..	Asym.	Sym..	Asym.
C04, D04	<b><u>79.7</u></b>	<b><u>40</u></b>	<b><u>9.4</u></b>	<b><u>4.73</u></b>	<b><u>1.56</u></b>	<b><u>0.78</u></b>
C23, D23	1.65	9.40		-	0.82	4.68

## 7.2. Recommendation to the designers

Since stay cables carries a large amount of tension forces guidelines and design manuals doesn't consider bending vibrations for fatigue. But the presence of high stiffness and sag makes it to a mixed kind of beam-cable behavior, which can be found by the tension-bending parameter (explained in chapter V). Thus it is necessary to consider the bending based on this parameter. Also for stay cables being severe to rain-wind induce vibrations it is a must to consider bending fatigue in to design. Based on the location of bridge, meteorological conditions either second or third probability model can be used to find

the fatigue. It is recommended for the stay cables to consider bending and axial fatigue to estimate the damage and life of the stay cables. Since apart from the rain-wind induced vibration, other vibrations such as vortex shedding, buffeting and galloping can also cause bending fatigue.

## Appendix I



Figure A1. Megami bridge and Nagasaki Marine Observatory 32.73° N, 129.86° E, 26.9m High

Distance between Megami Ohhashi and Nagasaki Marine Observatory 2.2km



Figure A2. Tataru Bridge and Meteorological stations: Ohmishima Amedas and Ikuchijima Amedas

Ohmishima Amedas 34.25° N, 133.0067° E, 3.0m high, Distance: 5.8km

Ikuchijima Amedas 34.27° N, 133.12° E, 3.0m high, Distance: 5.3km

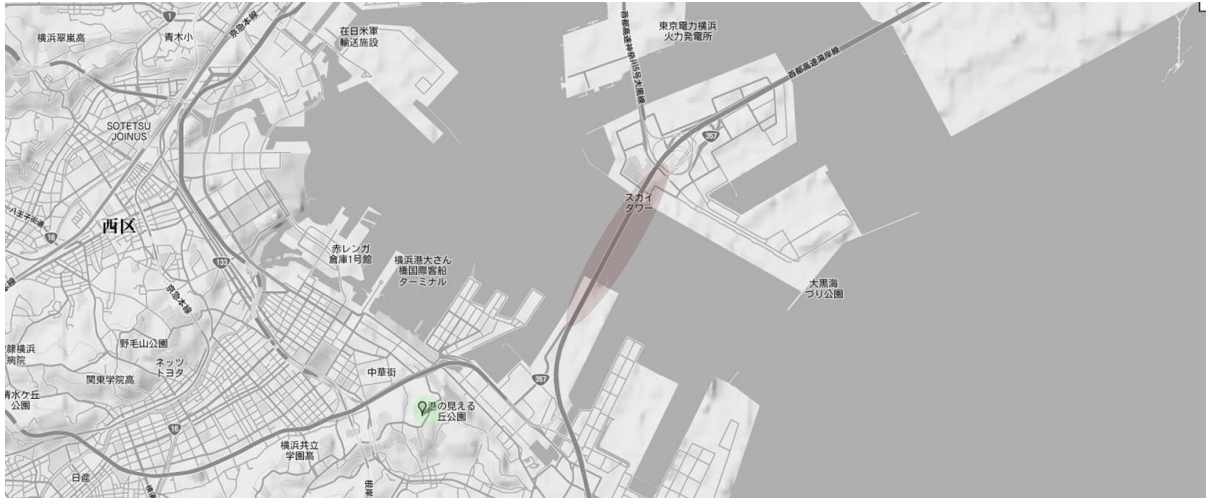


Figure A3. Yokohama Bay Bridge and Nagasaki Marine Observatory North Latitude : 35.02° N, 136.9° N, 39.1m high, Distance : 2.6km

Distance between Yokohama Bay Bridge and Nagasaki Marine Observatory 2.2km



Figure A4. Mihara Ohhashi and Meteorological stations: Ohmishima Amedas and Ikuchijima Amedas

Ohmishima Amedas 34.25° N, 133.0067° E, 3.0m high, Distance: 5.8km

Ikuchijima Amedas 34.27° N, 133.12° E, 3.0m high, Distance: 5.3km

## Appendix II

### Parameters of the Stay cables in Megami Bridge

Cable Id.	Estimated parameters				
	Inclination angle (deg)	Horizontal length (m)	Overall length (m)	Vertical length (m)	Frequency (Hz)
C01, D01	25.00	224.30	247.49	104.59	0.48
C02, D02	26.00	209.20	232.76	102.03	0.53
C03, D03	26.30	216.70	241.72	107.10	0.57
<b>C04, D04</b>	<b>26.50</b>	<b>-</b>	<b>197.84</b>	<b>-</b>	<b>0.58</b>
C05, D05	27.00	162.70	182.60	82.90	0.63
C06, D06	28.00	147.80	167.39	78.59	0.62
C07, D07	30.00	132.80	153.34	76.67	0.67
C08, D08	32.00	116.20	137.02	72.61	0.78
C09, D09	34.00	102.90	124.12	69.41	0.90
C10, D10	37.00	86.30	108.06	65.03	1.00
C11, D11	41.00	76.40	101.23	66.41	1.14
<b>C12, D12</b>	<b>47.00</b>	<b>56.40</b>	<b>82.70</b>	<b>60.48</b>	<b>1.35</b>
C13, D13	53.00	40.00	66.47	53.08	1.62
C14, D14	53.08	41.52	69.11	55.25	1.63
<b>C15, D15</b>	<b>46.79</b>	<b>56.47</b>	<b>82.48</b>	<b>60.12</b>	<b>1.36</b>
C16, D16	42.31	71.41	96.56	65.00	1.15
C17, D17	37.39	86.36	108.69	66.00	1.00
C18, D18	34.76	98.33	119.69	68.25	0.84
C19, D19	31.81	115.00	135.33	71.34	0.72
C20, D20	29.82	130.00	149.84	74.51	0.63
C21, D21	28.18	145.00	164.50	77.68	0.55
C22, D22	27.55	155.00	174.82	80.85	0.52
<b>C23, D23</b>	<b>27.42</b>	<b>165.00</b>	<b>185.89</b>	<b>85.61</b>	<b>0.57</b>
C24, D24	26.90	175.00	196.23	88.78	0.55
C25, D25	26.43	185.00	206.59	91.95	0.51
C26, D26	26.65	194.32	217.41	97.50	0.48

### Appendix III

#### Graphic User Interface for Experimental and Analytical results

##### Database for rain-wind induced cable vibration-analytical & experimental

Step 1

Enter the basic parameters of the stay cable

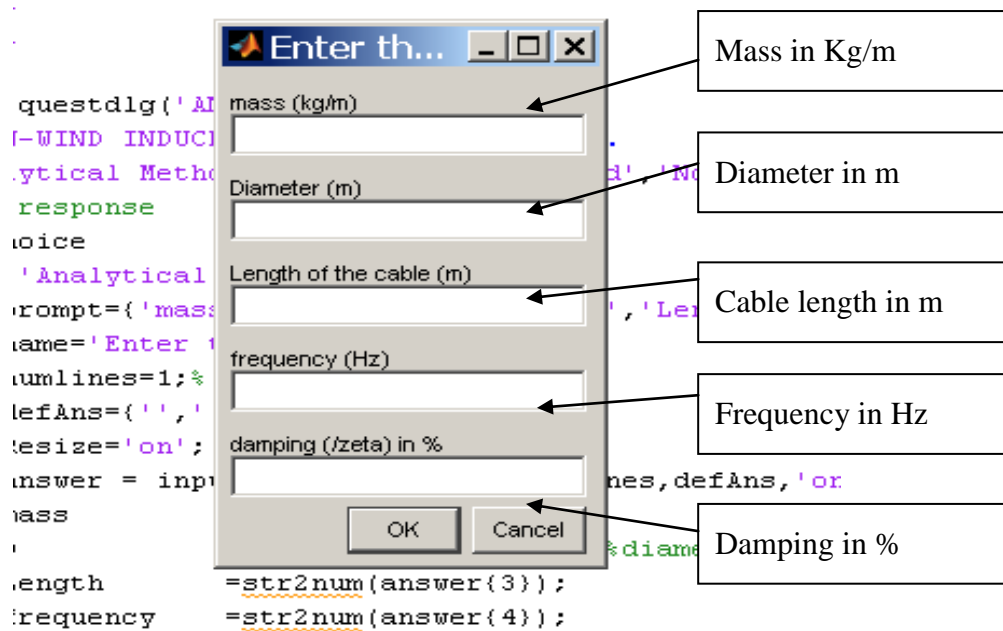


Figure 1B. Input parameters for stay cable vibration

Step 2

Specify the method of analysis either Experimental or Analytical

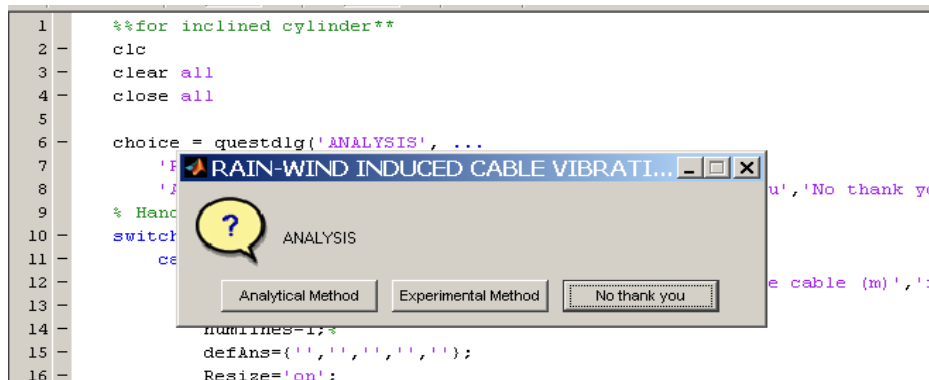


Figure 2B. Specify the method of analysis

### Step 3

If Experimental, Specify any of the required choices as shown in figure

The screenshot shows the MATLAB 'Results to display' dialog box. The 'EXPERIMENT' section is active, and three options are available:

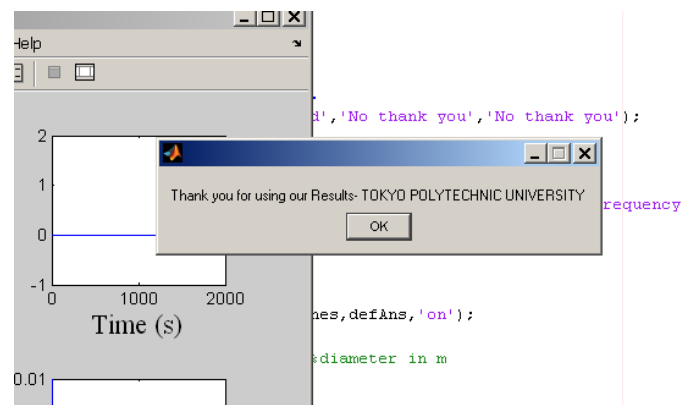
- Amplitude of the cable at particular wind speed and rainfall
- Effects of Wind speed and Rainfall intensity
- 3-D plot for the Joint effect of Rainfall Intensity

Arrows from these options point to the following text boxes:

- Amplitude of the cable at particular wind speed
- Effect of wind speed and rainfall intensity
- 3-D plot for the Joint effect of rainfall intensity, wind speed and direction.

### Step 4

Matlab will automatically display and save the results, which can also be printed.



## Appendix IV

### Algorithm – Analytical model: Response estimation of the stay cable

A sample program for evaluating the response of the Stay cable using Analytical methods is shown below. The lift and drag coefficients can be obtain from Chapter IV, position of the rivulet with respect to Wind speed can be obtained from Chapter III.

#### File name: cylvelovary\_mod

```
%% Program to estimate the response cable C12 AND D12 **
clear all
% close all
clc
global z U Uo to
fn=1.35;           %natural frequency in Hz
omega=2*pi*fn;    %Natural frequency in rad/s
m=80.016;         %mass, kg/m
rho=1.225;        %Density of air in kg/m3
D=0.1226;        %Diameter of the cable in m
R=D/2;           %Radius of the cable in m
alpha=45*(pi/180); %inclination angle
beta=30*(pi/180); %yaw angle
g=0.8*(asin(((sin(alpha)*sin(beta))/((sqrt(cos(beta)^2 + (sin(alpha)*sin(beta))^2)))))); %*(pi/180);
zs=0.001;
[num1,txt,row] = xlsread('trials_cubics');
    for j=1:length(num1);
        Uo=num1(j,13)
        to=num1(j,14)*(pi/180); %32*(pi/180); %static position of the rivulet when the cyliinder is
stationary
        a=num1(j,15)*10;
        U = Uo*(sqrt(cos(beta)^2 + (sin(alpha)*sin(beta)).^2))
        %Parameters-Forcing function
        c0=(cos(beta)^2 + (sin(alpha)*sin(beta)).^2);
        c1=(2-(g-to).^2)*(sqrt(c0));
        c2=2*(sin(g))*(sqrt(c0));
        c3=1/((sqrt(c0))*cos(g));
```

```

c4=(to-(to.^3)/6)/((sqrt(c0))*cos(g));
c5=tan(g);
c6=c5-to;
Aterm0=(c0*c4*(1-((c5.^2)/2))+c1*c5*(1-((c5).^2)/6));
Aterm1=(c0*c4*c5*(1-((c5.^2)/6))+c0*c4*c6*(1-((c5.^2)/2))+c1*c5*c6*(1-((c5).^2)/6));
Aterm2=(c0*c4*c5*c6*(1-((c5.^2)/6))+c0*c4*(c6.^2)/2*(1-((c5.^2)/2))+c1*c5*(c6.^2)/2*(1-((c5.^2)/6));
Aterm3=((c0*c4*c5*(c6.^2)/2*(1-((c5.^2)/6))+c0*c4*(c6.^3)/6*(1-((c5.^2)/2))+c1*c5*(c6.^3)/6*(1-((c5.^2)/6)));
Aterm4=(c1*(1-(c5.^2)/2)-c0*c4*c5);
Aterm5=(c0*c4*(1-(c5.^2)/2)+c1*c6*(1-(c5.^2)/2)-c0*c4*c5*c6);
Aterm6=(c0*c4*c6*(1-(c5.^2)/2)-(c0*c4*c5*c6.^2)/2)+(c1*(c6.^2)/2*(1-(c5.^2)/2));
Aterm7=((c0*c4*(c6.^2)/2*(1-(c5.^2)/2)-(c0*c4*c5*c6.^3)/6)+(c1*(c6.^3)/6*(1-(c5.^2)/2));

Bterm0=(c0*c3*(1-(c5.^2)/2)+(c2*c5*(1-((c5).^2)/6));
Bterm1=(c0*c3*c5*(1-((c5.^2)/6))+c0*c3*c6*(1-((c5.^2)/2))+c2*c5*c6*(1-((c5).^2)/6));
Bterm2=(c0*c3*c5*c6*(1-((c5.^2)/6))+c0*c3*(c6.^2)/2*(1-((c5.^2)/2))+c2*c5*(c6.^2)/2*(1-((c5.^2)/6));
Bterm3=((c0*c3*c5*(c6.^2)/2*(1-((c5.^2)/6))+c0*c3*(c6.^3)/6*(1-((c5.^2)/2))+c2*c5*(c6.^3)/6*(1-((c5.^2)/6)));
Bterm4=(c2*(1-(c5.^2)/2)-c0*c3*c5);
Bterm5=(c0*c3*(1-(c5.^2)/2)+c2*c6*(1-(c5.^2)/2)-c0*c3*c5*c6);
Bterm6=(c0*c3*c6*(1-(c5.^2)/2)-(c0*c3*c5*(c6.^2)/2)+(c2*(c6.^2)/2*(1-(c5.^2)/2));
Bterm7=((c0*c3*(c6.^2)/2*(1-(c5.^2)/2)-(c0*c3*c5*(c6.^3)/6)+(c2*(c6.^3)/6*(1-(c5.^2)/2));

% *****ODE SOLVER*****
pos=[0.0001;0];
time = [0 500];
ind=1;
options=odeset('RelTol',1e-4,'AbsTol',1e-4);
[t,p]=ode45(@vdvelovary_mod1,time,pos,options,ind,fn,omega,m,rho,D,R,alpha,beta,g,a,to,U,Uo,c0,c1,c2,c3,c4,c5,c6,Aterm0,Aterm1,Aterm2,Aterm3,Aterm4,Aterm5,Aterm6,Aterm7,Bterm0,Bterm1,Bterm2,Bterm3,Bterm4,Bterm5,Bterm6,Bterm7,zs);
theta=a*(sin(omega*t)); %*(pi/180); %dynamic angular displacement of the

```

rivulet as a cylinder vibrates is designated from to

```
tdot=a*omega*(cos(omega*t)); %*(pi/180);
```

```
phivec=[];
```

```
for i=1:length(t)
```

```
    phivec(i) = ((U*sin(g)+p(i,2)+R*tdot(i)*((theta(i)+to)-(1/6)*(theta(i)+to).^3))/(U*cos(g)) -  
theta(i) - to)*180/pi;
```

```
end
```

```
T2(1:length(phivec))=0;
```

```
for i=1:length(phivec)
```

```
if (phivec(i)>=(-55))
```

```
    B0 = 1.53;
```

```
    B1 = -0.72;
```

```
    B2 = -1.07;
```

```
    B3 = 7.16;
```

```
    A0 = -0.42;
```

```
    A1 = 0.64;
```

```
    A2 = 3.46;
```

```
    A3 = -2.29;
```

```
else
```

```
    B0 = -5.08;
```

```
    B1 = -9.98;
```

```
    B2 = -8.12;
```

```
    B3 = 0.00;
```

```
    A0 = 2.03;
```

```
    A1 = 1.40;
```

```
    A2 = 0.0;
```

```
    A3 = 0.0;
```

```
end
```

```
T1(i)=Aterm0*B0+Aterm1*B1+Aterm2*B2+Aterm3*B3+Aterm4*A0+Aterm5*A1+Aterm6*A2+Aterm7*A3;
```

```
T2(i)=Bterm0*B0+Bterm1*B1+Bterm2*B2+Bterm3*B3+Bterm4*A0+Bterm5*A1+Bterm6*A2+Bterm7*A3;
```

```

T3(i)=((-c0*c5)*((1-(c5.^2)/2))*(B1+B2*c6+(B3*(c6.^2)/2))-c0*(1-(c5.^2)/2)*(A1+A2*c6+((A3*c6.
^2)/2)));
F(i)=(rho*D*a/2*m)*(T1(i)*R*Uo*omega*cos(omega*t(i))+T3(i)*(Uo^2)*sin(omega*t(i)));
end
za=(rho*D*T2*Uo)/(4*m*omega);
z=zs+za;
Amax(j)=max(p(:,1))-min(p(:,1))
A(j)=Amax(j)
end
figure (1);
plot(num1(:,1),A,'m-h');
set(gca,'FontSize',16,'XMinorTick','on','YMinorTick','on');
axis([0 19 0.0 0.20]);
xlabel('Wind speed, U (m/s)','FontSize',28,'FontName','Times New Roman');
ylabel('Maximum response Amplitude, A_m_a_x (m)','FontSize',28,'FontName','Times New
Roman');

```

### **File name: vdvelovary\_mod**

#### **function**

```

pdot=vdvelovary_mod(t,p,ind,fn,omega,m,rho,D,R,alpha,beta,g,a,to,U,Uo,c0,c1,c2,c3,c4,c5,c6,Aterm
0,Aterm1,Aterm2,Aterm3,Aterm4,Aterm5,Aterm6,Aterm7,Bterm0,Bterm1,Bterm2,Bterm3,Bterm4,B
term5,Bterm6,Bterm7,zs)
theta=a*(sin(omega*t)); %(pi/180); %dynamic angular displacement of the rivulet
as a cylinder vibrates is designated from to
tdot=a*omega*(cos(omega*t)); %(pi/180);
% to=30*(pi/180); %static position of the rivulet when the cylinder is
stationary
phi = (U*sin(g)+p(2)+R*tdot*((theta+to)-(1/6)*(theta+to)^3))/(U*cos(g)) - theta - to;
if (phi>=(-55*pi/180))
    B0=1.53;
    B1=-0.72;
    B2=-1.07;
    B3=7.16;
    A0=-0.42;
    A1=0.64;

```

```

A2=3.46;
A3=-2.29;
else
B0=-5.08;
B1=-9.98;
B2=-8.12;
B3=0.00;
A0=2.03;
A1=1.40;
A2=0.0;
A3=0.0;
end
T1=Aterm0*B0+Aterm1*B1+Aterm2*B2+Aterm3*B3+Aterm4*A0+Aterm5*A1+Aterm6*A2+Aterm7*A3;
T2=Bterm0*B0+Bterm1*B1+Bterm2*B2+Bterm3*B3+Bterm4*A0+Bterm5*A1+Bterm6*A2+Bterm7*A3;
T3=((-c0*c5)*((1-(c5.^2)/2))*(B1+B2*c6+(B3*(c6.^2)/2))-c0*(1-(c5.^2)/2)*(A1+A2*c6+((A3*c6.^2)/2)));
za=(rho*D*T2*Uo)/(4*m*omega);
F=(rho*D*a/2*m)*(T1*R*Uo*omega*cos(omega*t)+T3*(Uo.^2)*sin(omega*t));
z=zs+za;
pdot(1)= p(2);
pdot(2)= - p(1)*(omega^2) - 2*(z)*omega*p(2)-F;
pdot= [pdot(1); pdot(2)];
end

```

## Appendix V

### 1 MATLAB program for Free vibration analysis and mode shape extraction

```

% C.6 Euler with tensile pretension
% Calculation of natural frequencies and eigenmodes without shear and
% with tensile axial pretension
% Variables
% x = position in x-direction [m] (x = 0 at left end of the beam)
% y = position in y-direction [m] (y = 0 at the middle of the beam)
% z = position in z-direction [m] (z = 0 at the middle of the beam)
% L = length of the beam [m]
% H = height of the beam [m]
% B = width of the beam [m]
% I = second moment of area [m^4]
% rho = density [kg.m^-3]
% E = Young's modulus [Pa]
% A = area of cross section [m^2]
% O, OMEGA = relative natural frequency [-]
% a = sqrt((EI)/(rho*A)) [m^2/s]
% U = relative axial force [-]
% ts = tensile pretension [Pa]
% T = axial tensile force [N]
% omega = natural frequency [rad/s]
% M, N = mode shape coefficient [-]
% ci (i=1,2,3,4) = mode schape coefficient [-]
% k = number of natural frequencies [-]
% ksi = dimensionless beam coordinate [-]
% set defaults
format long e;
clc;
clear all;
close all;
% values for various parameters
L = 197.4;
D = 0.119;
R = D/2;
w = 15830.37;

```

```

m = w/L;
v = (pi*R*R*L);
rho = w/v;
E = 1.8960582*(10^11)
I = 9.96041801*(10^-6)
A = 0.011187*(10^-6);
gr=9.81
T =4114.6*(10^3);
gamma = T*L^2 / (2*E*I);
% T=0;
d_L =
((m*gr*L)/(T*8))*(1-((8/((gamma*gamma)))*(1-(sech(gamma/2))))) %sag-Tens
ion ratio
Le= L*(1+8*((d_L)^2))
lambda= (((m*gr*L)/(T))^2)*((E*A*L)/(T*Le))
a = sqrt((E*I) / (m));
U = T*L^2 / (2*E*I);
k = 100;
% Solve the characteristic equation with O as unknown
OMEGA = [ ]; % make empty vector
for i = 1:k
O_i =
fzero(@(O)O+U*sinh(sqrt(U+sqrt(U^2+O^2)))*sin(sqrt(-U+sqrt(U^2+O^2)))-O*cos
h(sqrt(U+sqrt(U^2+O^2)))*cos(sqrt(-U+sqrt(U^2+O^2))),((i*pi)^2));
OMEGA = [OMEGA; O_i];
end
% calculate natural frequencies
f = OMEGA * a / (2 * pi * L^2)
omega_estimate = f * (2 * pi)
% for calculating the mode shapes some coefficients have to be
% determined: first M and N, thereafter c_i (i = 1,2,3,4) which are a
% function of M and N. These constants are different for each natural % frequency.
% Calculation of M en N
M = [ ]; % make empty vector for M
N = [ ]; % make empty vector for N
for i = 1:k
M_i = sqrt(U + sqrt(U^2 + OMEGA(i,1)^2));

```

```

Ni = sqrt(-U + sqrt(U^2 + OMEGA(i,1)^2));
M = [M ; Mi];
N = [N ; Ni];
end
% Calculation of ci (i = 1,2,3,4)
c1 = [ ];
c2 = [ ];
c3 = [ ];
c4 = [ ];
for i = 1:k
c1i = 1;
c2i = (M(i,1)*sin(N(i,1)) - N(i,1)*sinh(M(i,1))) / (N(i,1)*(cosh(M(i,1))
-cos(N(i,1))));
c3i = -M(i,1) / N(i,1);
c4i = -c2i;
c1 = [c1 ; c1i];
c2 = [c2 ; c2i];
c3 = [c3 ; c3i];
c4 = [c4 ; c4i];
end
% calculation of ksi
ksi = 0 : 0.001 : 1;
% calculation of the mode shapes
Y = [ ]; % make empty matrix for the mode shapes
for i = 1 : k
Yi = c1(i,1) * sinh(M(i,1) * ksi) + c2(i,1) * cosh(M(i,1) * ksi) + c3(i,1)
*sin(N(i,1) * ksi) + c4(i,1) * cos(N(i,1) * ksi);
Y = [Y ; Yi];
end
% Normalization of the mode shapes with max(Y) = 1
for i = 1 : k
Y(i,:) = Y(i,:) ./ max(abs(Y(i,:)));
end
% Plotting of the results
figure
grid
hold on

```

```

for i = 1 : k
plot(ksi,Y(i,:))
end

%%%%%%%%%%CREATE
% calculation of ksi
kpi = 0 : 0.05 : 1;
% calculation of the mode shapes
Y = [ ]; % make empty matrix for the mode shapes
for i = 1 : k
Yi = c1(i,1) * sinh(M(i,1) * kpi) + c2(i,1) * cosh(M(i,1) * kpi) + c3(i,1)
*sin(N(i,1) * kpi) + c4(i,1) * cos(N(i,1) * kpi);
Y = [Y ; Yi];
end
% Normalization of the mode shapes with max(Y) = 1
for i = 1 : k
Y(i,:) = Y(i,:) ./ max(abs(Y(i,:)));
end

```

## 2 ANSYS APDL program for Dynamic characterization

The APDL program for dynamic characterization of a pre-stressed beam is shown below and the

finish

/clear

/PMACRO

/FILNAM, 0m\_model

/TITLE, STAY CABLE BOUNDARY CONDITIONS (ALPHA=47 deg)

/CONFIG, NRES,100000

/PREP7

D =0.1226 ! Diameter of the cable

ET, 1, BEAM3 ! 2-D Beam element: beam3

KEYOPT, 1, 6, 1 ! KOPT(6)

KEYOPT, 1, 9, 0 ! KOPT(9)

```

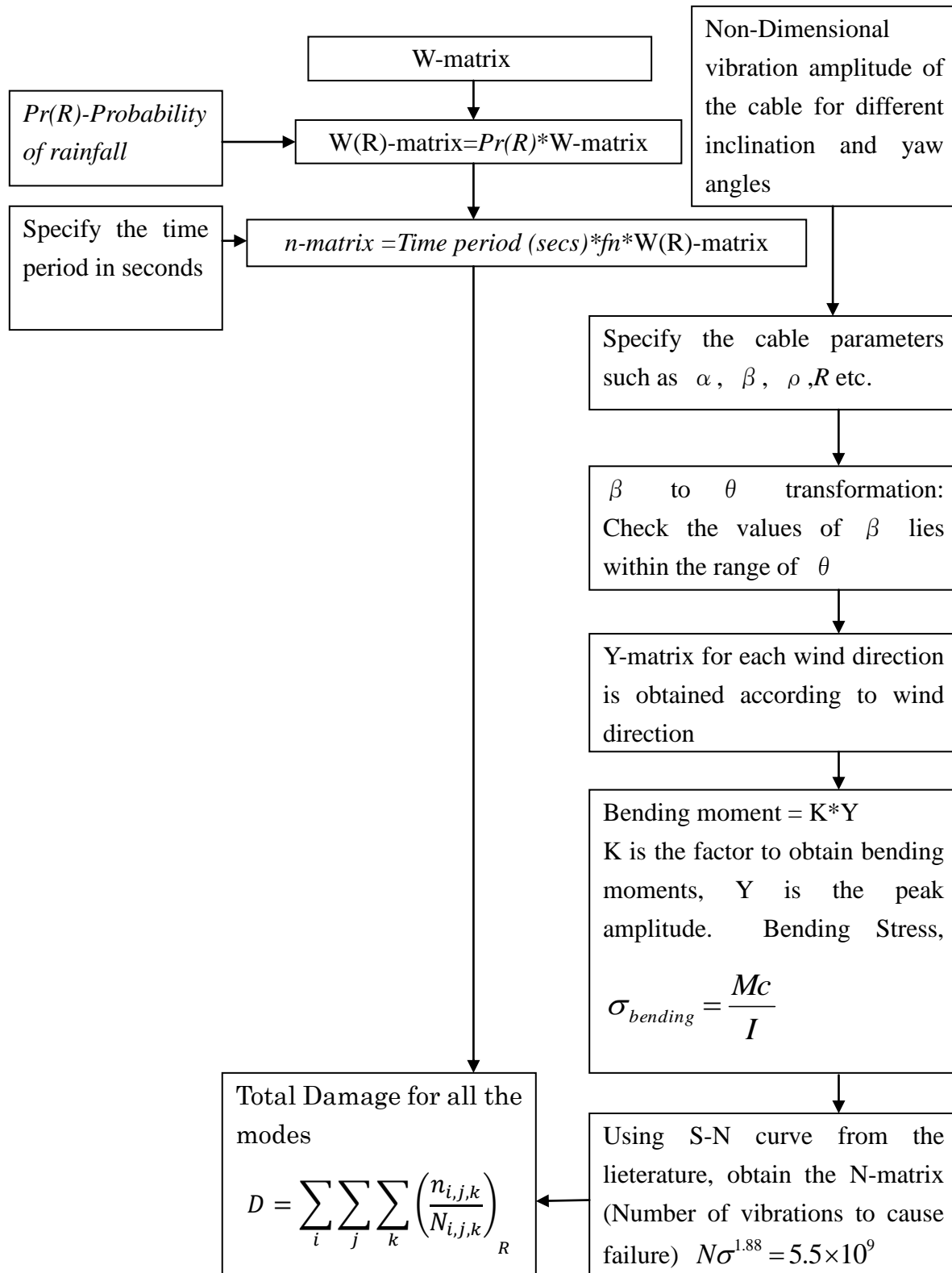
AREA = (3.14/4)*(D)*(D)          ! Cross-sectional area
IZZ = 9.960481E-6                ! Moment of inertia about z axis
R, 1, AREA, IZZ, D,              ! Real constant- R, id, Area, Moment of inertia,
Height=Diameter
MP, EX, 1, 1.8960582E11          ! Material properties- Young's Modulus
MP, DENS, 1, 7152.2              ! Density
MP, PRXY, 1, 0.3                 ! Poison's ratio
K,1,0,60.48                      ! keypoints-K,id,x,y,z
k,2,56.4,0                       ! keypoints-K,id,x,y,z
L,1,2
TYPE, 1
ESIZE,0, 100                     ! Meshing
LMESH, ALL                        ! Line Mesh
! Apply pretension force along the cable length
NMODIF,2, , , ,-47,0,0
F,2,Fx,4114604.98                ! Pre Tesnion Force
ACEL,,-9.81
/SOLU                             ! enters the solution phase
ANTYPE, STATIC
PSTRES, ON
EMATWRITE,YES                    ! write emat file, this is important, since it is required by
psolve
D,1,all
D,2,all
DDELE,2,ux
OUTRES,ALL,ALL                   !Resulting output frequency setting
SAVE
SOLVE
FINISH
!! Modal analysis
/solu
ANTYPE, MODAL

```

```
PSTRES, ON
D,2,ALL
MXPAND, 10, , ,
MODOPT,LANB,10,0,0, ,ON
SAVE
SOLVE
!/post1
!ETABLE,Mz-i,SMISC,6
!ETABLE,Mz-j,SMISC,12
! PLETAB
!/DEVICE, TIMES NEW ROMAN,1,400
!/DEVICE, TIMES NEW ROMAN,2,400
!PLLS,Mz-i,Mz-j,1,1
!PLETAB, Itlab, Avglab
/RGB,INDEX,100,100,100, 0
/RGB,INDEX, 80, 80, 80,13
/RGB,INDEX, 60, 60, 60,14
/RGB,INDEX, 0, 0, 0,15
```

## Appendix VI

### Flow chart for fatigue analysis



### Appendix VII

Fatigue damage evaluation on stay cables for the cable positioned a Megami side of the bridge. From figure 6.1, in the rose plot diagram of the cable is located at the megami side of the bridge towards East South East direction. A similar procedure explained in section 6.1-6.6 is repeated to estimate the fatigue damage and life of the stay cable which is inclined to 25°.

Table 1A. Accumulated bending fatigue damage in symmetric obtained for using different probability models

Mode no.	Probability model I (R independent)					Probability model III (R dependent)				
	ENE	E	ES E	SE	SSE	ENE	E	ES E	SE	SSE
1	7.21E-4	<b>1.02E-3</b>	0	6.35E-4	<b>1.02E-03</b>	1.11E-3	2.19E-3	0	1.36E-03	<b>4.21E-03</b>
2	3.79	<b>4.9</b>	0	3.31	<b>4.9</b>	5.89E+0	9.26	0	4.73E+00	<b>1.88E1</b>
3	1.68E1	<b>2.4E+1</b>	0	1.47E+1	<b>2.4E+1</b>	2.57E+1	5.07E+1	0	2.85E+01	<b>9.8E1</b>

Table 2A Accumulated bending fatigue damage in anti-symmetric obtained for 100 years using different probability models

Mode no.	Probability model I (R independent)					Probability model III (R dependent)				
	ENE	E	ESE	SE	SSE	ENE	E	ESE	SE	SSE
1	1.17E+00	1.53E+00	0.00E+00	1.03E+00	1.53E+00	1.08E+00	2.87E+00	0.00E+00	1.47E+00	4.35E+00
2	8.76E+00	1.26E+01	0.00E+00	7.69E+00	1.26E+01	1.35E+01	2.55E+01	0.00E+00	1.08E+01	4.70E+01
3	2.86E+01	4.08E+01	0.00E+00	2.51E+01	4.09E+01	4.37E+01	8.63E+01	0.00E+00	5.79E+01	1.67E+02

Table 3A Accumulated axial fatigue damage in symmetric modes for 100 years using different probability models

Mode no.	Probability model I (R independent)					Probability model III (R dependent)				
	ENE	E	ES E	SE	SSE	ENE	E	ES E	SE	SSE
1	1.06E+ 1	1.06 E+1	0	1.06E+ 1	1.06E+ 1	2.13E+ 1	2.13E+ 1	0	2.13E+ 1	2.13E+ 1
2	3.08E+ 1	3.08 E+1	0	3.08E+ 1	3.08E+ 1	4.14E+ 1	4.14E+ 1	0	4.14E+ 1	4.14E+ 1
3	5.14E+ 1	5.14 E+1	0	5.14E+ 1	5.14E+ 1	1.87E+ 2	1.87E+ 2	0	1.87E+ 2	1.87E+ 2

Table 4A Accumulated axial fatigue damage in anti-symmetric modes for 100 years using different probability models

Mode no.	Probability model I (R independent)					Probability model III (R dependent)				
	ENE	E	ESE	SE	SSE	ENE	E	ESE	SE	SSE
1	2.12E +01	3.74E +01	0.00E +00	5.01E +01	6.07E +01	4.25E +01	7.50E +01	0.00E +00	1.01E +02	1.22E +02
2	6.12E +01	1.08E +02	0.00E +00	1.45E +02	1.75E +02	8.25E +01	1.45E +02	0.00E +00	1.95E +02	2.36E +02
3	1.02E +02	1.80E +02	0.00E +00	2.42E +02	2.93E +02	3.73E +02	6.58E +02	0.00E +00	8.83E +02	1.07E +03

Table 5A Estimated bending fatigue life (in years) of stay cable using different probability models-Symmetric modes

Mode no.	Probability model I (R independent)					Probability model III (R dependent)				
	ENE	E	ES E	SE	SSE	ENE	E	ES E	SE	SSE
1	1.4E5	<b>9.8E4</b>	∞	1.6E5	<b>9.8E4</b>	9E4	4.6E4	∞	7.3E4	<b>2.4E4</b>
2	2.6E1	<b>2 E1</b>	∞	3.0E1	<b>2E1</b>	1.7E1	1.1E0	∞	2.1E1	<b>5.3</b>

3	6	4.2	$\infty$	6.8	4.2	3.9	2	$\infty$	3.5	1.0
---	---	-----	----------	-----	-----	-----	---	----------	-----	-----

Table 6A Estimated bending fatigue life (in years) of stay cable using different probability models-Antisymmetric modes

Mode no.	Probability model I (R independent)					Probability model III (R dependent)				
	ENE	E	ESE	SE	SSE	ENE	E	ESE	SE	SSE
1	85.65	65.44	$\infty$	97.23	65.34	92.99	34.81	$\infty$	68.14	22.97
2	11.41	7.96	$\infty$	13.00	7.95	7.43	3.93	$\infty$	9.24	2.13
3	3.50	2.45	$\infty$	3.99	2.45	2.29	1.16	$\infty$	1.73	0.60

Table 7A Estimated axial fatigue life (in years) of stay cable using different probability models-Symmetric modes

Mode no.	Probability model I (R independent)					Probability model III (R dependent)				
	ENE	E	ESE	SE	SSE	ENE	E	ESE	SE	SSE
1	9.40	9.40	$\infty$	9.40	9.40	4.68	4.68	$\infty$	4.68	4.68
2	3.25	3.25	$\infty$	3.25	3.25	2.41	2.41	$\infty$	2.41	2.41
3	1.95	1.95	$\infty$	1.95	1.95	0.53	0.53	$\infty$	0.53	0.53

Table 8A Estimated axial fatigue life (in years) of stay cable using different probability models-Antisymmetric modes

Mode no.	Probability model I (R independent)					Probability model III (R dependent)				
	ENE	E	ESE	SE	SSE	ENE	E	ESE	SE	SSE
1	4.72	2.68	$\infty$	1.99	1.65	2.35	1.33	$\infty$	0.99	0.82
2	1.63	0.93	$\infty$	0.69	0.57	1.21	0.69	$\infty$	0.51	0.42

3	0.98	0.55	$\infty$	0.41	0.34	0.27	0.15	$\infty$	0.11	0.09
---	------	------	----------	------	------	------	------	----------	------	------